Sheffield Hallam University

A Sheffield Hallam University thesis

Phosphonium-Functionalised Gold Nanoparticles for Mitochondria Targeted Therapeutics

Yu-Su Chen

A thesis submitted in partial fulfilment of the requirements of Sheffield Hallam University for the degree of Doctor of Philosophy

Sep 2014

Acknowledgments

Abstract

The work presented in this thesis demonstrates that triarylphosphoniopropyl-thiosulfate zwitterions and ω-thioacetylpropyl(triphenyl)phosphonium salts can be used to prepare cationic, water-soluble gold nanoparticles with mean core sizes in the range of 2.5-5 nm. Phosphonium-functionalised gold nanoparticles have been characterised by a number of techniques including NMR, LDI-MS, SIMS, XPS, TGA, ICP-MS, MALDI-MS and TEM.

Cytotoxicity studies illustrated that phosphonium ligands are relatively non-toxic to human prostate cancer cells and therefore can be used as a delivery vector to delivery gold nanoparticles specifically to the site of the mitochondria for other therapeutic applications such as photothermal therapy. Cellular uptake studies of phosphonium ligands by MALDI-MS showed that they are rapidly taken-up by cells within ten minutes.

Phosphonium-functionalised gold nanoparticles are soluble in biological media which is of great importance for cell biology studies. Initial photothermal therapy studies demonstrated that the gold nanoparticles responds specifically to a green light excitation source (510-550 nm) which overlaps the surface plasmon resonance band of the phosphonium-functionalised gold nanoparticles at 525 nm. Preliminary data also showed that phosphonium-functionalised gold nanoparticles can selectively induce apoptosis in cells followed by irradiation, this was confirmed by Hoechst and caspase-3 staining.

Quantification studies of phosphonium-functionalised gold nanoparticles by ICP-MS illustrated that these nanoparticle have good uptake in cells (above 75%). TEM data confirmed that phosphonium-functionalised gold nanoparticles are taken-up by human prostate cancer cells and are localised in the mitochondria.

Table of Contents

List of Figures

List of Tables

Appendices

Abbreviations

AIF	Apoptosis inducing factors
ANOVA	Analysis of variance
Anti-EGFR	Anti-epidermal growth factor receptor
Anti-HER2	Anti-human epidermal growth factor receptor 2
APAF1	Apoptotic–protease-activating factor-1
AuNPs	Gold nanoparticles
BaP	Benzo[a]pyrene
Bcl-2	B-cell lymphoma 2
BPDE	BaP-7,8-dihydrodiol-9,10-epoxide
CEB	Cytosol extraction buffer
CF	Cytosolic fraction
CHCA	α-Cyano-4-hydroxycinnamic acid
CIN	Chromosomal instability
CPDs	Cyclobutane dimmers
CW	Continous wave
CYP1A2	Cytochrome P450 1A2
DCM	Dichloromethane
DCTB	*Trans*-2-[3-(4-*tert*-butylphenyl)-2-methyl-2-propenylidene] malononitrile
DECA	Dequalinium choride
DHB	2,5-Dihydroxybenzoic acid
DIH$_2$O	Deionised water
DLCs	Delocalised lipophilic cations
DMSO	Dimethyl sulfoxide
DNA	Deoxyribonucleic acid
DPF	α, β-Diphenylfumaronitrile
DQAsomes	DeQuAlinium based liposome-like vesicles
ECM	Extracellular matrix
EGFR	Epidermal growth factor receptor
EMT	Epithelial-mesenchymal transition
EndoG	Endonuclease G
EPR	Enhanced permeability and retention
EPR	Enhanced permeability retention
ER	Estrogen receptor
ESI MS	Electrospray ionisation mass spectrometer
ETC	Experimental Technique Centre

EtOH	Ethanol
FADD	Fas associated death domain
FDA	Food and drug administration
FPPTA	(3-thioacetylpropyl)tris(4-fluorophenyl)phosphonium bromide
FPPTS	Tris(4-fluorophenyl)phosphoniopropylthiosulfate
FTIR	Fourier transform infrared
GF	Growth factor
HA	Hemagglutinin A
HCA	Heterocyclic amines
HEPES	4-(2-Hydroxyethyl)piperazine-1-ethanesulfonic acid
HER2	Human epidermal growth factor receptor 2
HERVs	Human endogenous retroviruses
HIF-1	Hypoxia-inducible factor 1
HPV	Human papilloma virus
ICP-OES	Inductively coupled plasma optical emission spectrometry
IS	Internal standard
LPCs	Lipophilic phosphonium compounds
MALDI	Matrix-assisted laser desorption ionisation
Mce_6	Mesochlorine e_6
MDM2	Murine double minute clone 2
MEB	Mitochondrial extraction buffer
MeCN	Acetonitrile
MeOH	Methanol
MERI	Materials and Engineering Research Institute
MF	Mitohcondria fraction
MMPs	Metalloproteinases
MOMP	Mitochondrial outer membrane permeabilisation
MPCs	Mixed monolyer protected clusters
MPT	Mitochondrial permeability transition
MS	Mass spectrometer
MSI	Microsatellite instability
NER	Nucleotide excision repair
NIR	Near-infrared
NMR	Nuclear magnetic resonance
NNK	Nitrosamine 4-(methylnitrosamino)-1-(3-pyridyl)-1-butanone

OMM	Outer mitochondrial membrane
p53	Tumor protein 53
PAH	Polycyclic aromatic hydrocarbons
P-AuNPs	Phosphonium-Functionalised Gold Nanoparticles
PBS	Phosphate-buffered saline
PC3	Human prostate cancer cells
PCD	Program cell death
PDT	Photodynamic therapy
PEG	Polyethylene glycol
PET	Positron emission tomography
PhIP	2-amino-1-methyl-6-phenylimidazo[4,5-*b*]pyridine
PI	Propidium iodide
PPTA	(3-thioacetylpropyl)triphenylphosphonim bromide salt
PPTS	3-triphenylphosphoniopropylthiosulfate
PTPC	Permeability transition pore complex
PTT	Photothermal therapy
QDs	Quantum dots
RB	Retinoblastoma protein
Rh 123	Rhodamine 123
RNA	Ribonucleic acid
ROS	Reactive oxygen species
R-point	Restrcition point
SERS	Surface enhanced Raman scattering
SIMS	Secondary ion mass spectrometry
Smac/DIABLO	Second mitochondria-derived activator of caspase/direct inhibitor of apoptosis-binding protein with low pI
SPECT	Single-photon emission computed tomography
SPR	Surface plasmon resonance
TEM	Transmission electron microscope
TetraPP	Tetraphenylphosphonium
TF	Transferrin
TFA	Trifluoroacetic acid
TGA	Thermogravimetric analyses
THF	Tetrahydrofuran
TLC	Thin layer chromatography
TNF	Tumour necrosis factor
TOF	Time-of-flight

TPMP	Methytriphenylphosphonium
TPP	Triphenylphosphine
TSP-1	Thrombospondin-1
UV	Ultraviolet
UVA	Ultraviolet A radiation
UVB	Ultraviolet B radiation
UV-Vis	Ultraviolet-visible
VDAC	Voltage-dependent anion channel
VEGF	Vascular endothelial growth factor
XPS	X-ray photoelectron spectroscopy
$\Delta\Psi_m$	Mitochondrial transmembrane potential
$\Delta\Psi_p$	Plasma membrane potential

Chapter 1.

Introduction

1.1 Nanoscience

Nanoscience is a multidisciplinary subject incorporating chemistry, physics, biology, engineering and medicine. Mainstream research has focused on synthesising novel nanomaterials and exploring new applications. Nanomaterials can be synthesised from a diverse range of materials including noble metals, metal oxides, semiconductors, polymers, magnetic compounds, liposomes, carbon and silica-based materials. The field of nanotechnology is rapidly advancing discipline and is continuously attracting immense interest from researchers worldwide across a wide array of industries including, electronics, catalysis, environmental remediation, textiles, cosmetics and pharmaceuticals (Daniel and Astruc, 2004). Amongst the most widely studied nanomaterials are gold nanoparticles.

1.1.1 Gold Nanoparticles

The production, characterisation and properties of gold nanoparticles (AuNPs) has gained momentum in recent years, particularly with a view to their applications in the field of biotechnology and biomedical science (Boisselier and Astruc, 2009, Cobley *et al.*, 2011, Sperling *et al.*, 2008). This interest stems not least because of their apparent non-toxicity, inertness, biocompatibility, ease of synthesis and, most remarkably, their tuneable optical properties.

1.1.2 Synthesis of Gold Nanoparticles

Since Faraday published the first report on the preparation of colloidal gold in 1857 (Faraday, 1857) a plethora of books, research and review articles have been published on this topic. The most well-known methods for synthesising gold nanoparticles include the Turkevich method (Turkevich *et al.*, 1953), using sodium citrate to reduce $AuCl_4^-$ salts in boiling water producing AuNPs ~20nm; the Frens method (Frens, 1973) which is modified from the Turkevich method to produce AuNPs size between 16-147nm by varying the ratio between trisodium citrate and gold, and the Brust-Schiffrin two-phase method (Brust *et al.*, 1994, Brust *et al.*, 1995) to produce monolayer protected clusters (MPCs) with smaller gold core size between 1.5-6nm. $AuCl_4^-$ salts are reduced by sodium borohydride ($NaBH_4$) in the presence of a thiol capping ligand, in a biphasic system (water-toluene) using tetraoctylammonium bromide as a phase transfer reagent to transfer $AuCl_4^-$ to the organic phase. Different core sizes can be

achieved by fine-tuning the thiol to gold ratio, the larger thiol/gold mole ratios leads to smaller average core sizes. Mixed monolayer protected clusters can be synthesised either directly or by post-functionalisation of MPCs using the Murray place-exchange method (Templeton *et al.*, 2000).

Interestingly not only gold nanospheres can be synthesised, other geometries of gold nanoparticles can also be synthesised using appropriate methods, these include nanorods (Huang *et al.*, 2009, Vigderman *et al.*, 2012), nanocages (Chen *et al.*, 2005, Skrabalak *et al.*, 2008), nanoshells (Hirsch *et al.*, 2003) nanoprisms (Shankar *et al.*, 2004) and nanostars (Barbosa *et al.*, 2010, Khoury and Vo-Dinh, 2008). Extensive research in this area has enabled scientists to synthesis AuNPs with precise shapes and sizes and narrow size distributions. The reason for the synthesis of different shapes of gold nanomaterials is that their morphology is strongly related to their properties which will influence the end application (Kanaras *et al.*, 2011).

1.1.3 Surface Functionality and Gold Nanoparticles' Cytotoxicity

Surface properties of AuNPs play a significant role in dictating their interactions with biological systems, these interactions determine the efficacy and cytotoxicity of AuNPs (Kim *et al.*, 2013). The surface charge is a crucial factor; Goodman and colleagues have investigated the cytotoxicity of AuNPs functionalised with anionic and cationic side chains in monkey kidney cells (COS-1), the results indicated that cationic AuNPs were moderately toxic compared to anionic AuNPs (Goodman *et al.*, 2004). Surface hydrophobicity is another important parameter to consider, Chompoosor and colleagues have examined the cytotoxicity of AuNPs functionalised with quaternary ammonium group with varied hydrophobic alkyl chains in HeLa cells and the results showed that an increase in the hydrophobicity of the surface ligands induces higher cytotoxicity in cells (Chompoosor *et al.*, 2010).

1.1.3.1 Surface Ligands

Common strategies for synthesising AuNPs involve a surface coating of some form, usually a ligand, surfactant or polymer to encapsulate the growing particle, providing stability, preventing uncontrolled aggregation and imparting functionality for specific applications; suitable receptor groups for sensor or

diagnostic purposes and appropriate targeting moieties for delivery applications (Wang and Ma, 2009, Agasti *et al.*, 2010, Ghosh *et al.*, 2008).

The surface of AuNP is very versatile and can be coated with a variety of organic ligands such as thiols, sulfate, phosphine, phosphine oxide, ammonium, amine, carboxylate, selenide and isocyanide; among all ligands organic thiolates derived from thiols or disfuldies are most widely used (Daniel and Astruc, 2004, Love *et al.*, 2005). Furthermore thiol-protected AuNPs can undergo biological modification; various biological cargoes including nucleic acids, amphiphilic polymers, short peptide sequences, proteins, lipids, antibodies and drugs have been successfully attached to the surface of nanoparticles via the strong Au-S bond (Giljohann *et al.*, 2010, Shan and Tenhu, 2007, Ghosh *et al.*, 2008, Giljohann *et al.*, 2009, Rana *et al.*, 2012, Wang and Ma, 2009, Pissuwan *et al.*, 2011).

1.1.3.2 Neutral Gold Nanoparticles

AuNPs can be coated with neutral species such as polyethylene glycol (PEG) to minimise protein adsorption and prevent uptake by macrophages through the protection of AuNPs from the mononuclear phagocyte system (Wang and Thanou, 2010, Larson *et al.*, 2012, Walkey *et al.*, 2012). However PEGylation can also diminish cellular interaction, however it can be highly desirable to produce AuNPs that do not interact with cells for certain applications such as negative control experiments (Arnida *et al.*, 2010, Larson *et al.*, 2012). An alternative way for producing uncharged AuNPs is by coating the nanoparticles with zwitterionic ligands which are electrically neutral as the ligands incorporate both a positive and negative charge (Rouhana *et al.*, 2007).

1.1.3.3 Negatively Charged Gold Nanoparticles

There is evidence in the literature suggesting that negatively charged AuNPs are taken-up by cells despite their unfavourable interaction with the negatively charged cell membrane. Cho and co-workers (Cho *et al.*, 2009) have demonstrated that citrate coated gold nanospheres are taken up slightly more by breast cancer cells (SK-BR-3) compared to neutral AuNPs, but are taken up significantly less compared to positively charged AuNPs. Arvizo and colleagues (Arvizo *et al.*, 2010) have shown that the intracellular uptake of AuNPs is

4

influenced by the cellular membrane potential, and the perturbation of the membrane potential is dependent on the surface charge of the nanoparticles. While negatively charged and neutral AuNPs have negligible effect on the membrane potential, positively charged AuNPs depolarize the membrane considerably. Overall, negatively charged AuNPs are not readily taken up by cells and have little cellular interaction, as the negatively charged membrane repelling each other would prevent the AuNPs from entering the cells (Chithrani *et al.*, 2006, Verma and Stellacci, 2010).

1.1.3.4 Positively Charged Gold Nanoparticles

In comparison to the low level of cellular uptake and interaction by neutral and negatively charged AuNPs, positively charged AuNPs have a higher affinity for negatively charged species on the cell surface resulting in higher level of cellular interaction and uptake efficiencies (Verma and Stellacci, 2010). Zhu and co-workers have used mass spectrometry (LDI-MS and ICP-MS) to quantify uptake of AuNPs in monkey kidney cells (COS-1 cells). The results showed that all cationic AuNPs (secondary amine species with different alkyl chains) were readily taken up compared to neutral AuNPs, however all four cationic AuNPs exhibited different uptake efficiencies (Zhu *et al.*, 2008). It is well known that positively charged AuNPs are capable of binding to negatively charged groups on the cell surface and translocate cross the cellular membrane thus making positively charged AuNPs attractive scaffold for drug and gene delivery (Bilensoy, 2010).

1.1.4 Phosphonium Functionalised Nanoparticles

While there have been many reports on the use of organophosphorus ligands, notably phosphines Figure 1.1 (a) (Shem *et al.*, 2009) and phosphine oxides (e) (Green and O'Brien, 2000) for passivating the surface of metal nanoparticles, there have been far fewer studies on the use of phosphorus ligands to impart functionality to nanoparticles. The phosphonium ionic liquid trihexyl(tetradecyl)phosphonium bis(2,4,4-trimethylpentyl phosphinate) (d) has been used in the production of luminescent cadmium selenide quantum dots (Green *et al.*, 2007). Phosphinophosphonic acids (b) have been used to prepare water soluble rhodium and platinum nanoparticles (Richter *et al.*, 2012, Glöckler *et al.*, 2007). Tris(hydroxymethyl)phosphine capped AuNPs have been formed

5

through the reduction of $HAuCl_4$ with tetrakis(hydroxymethyl)phosphonium chloride (c) (Harnack *et al.*, 2002).
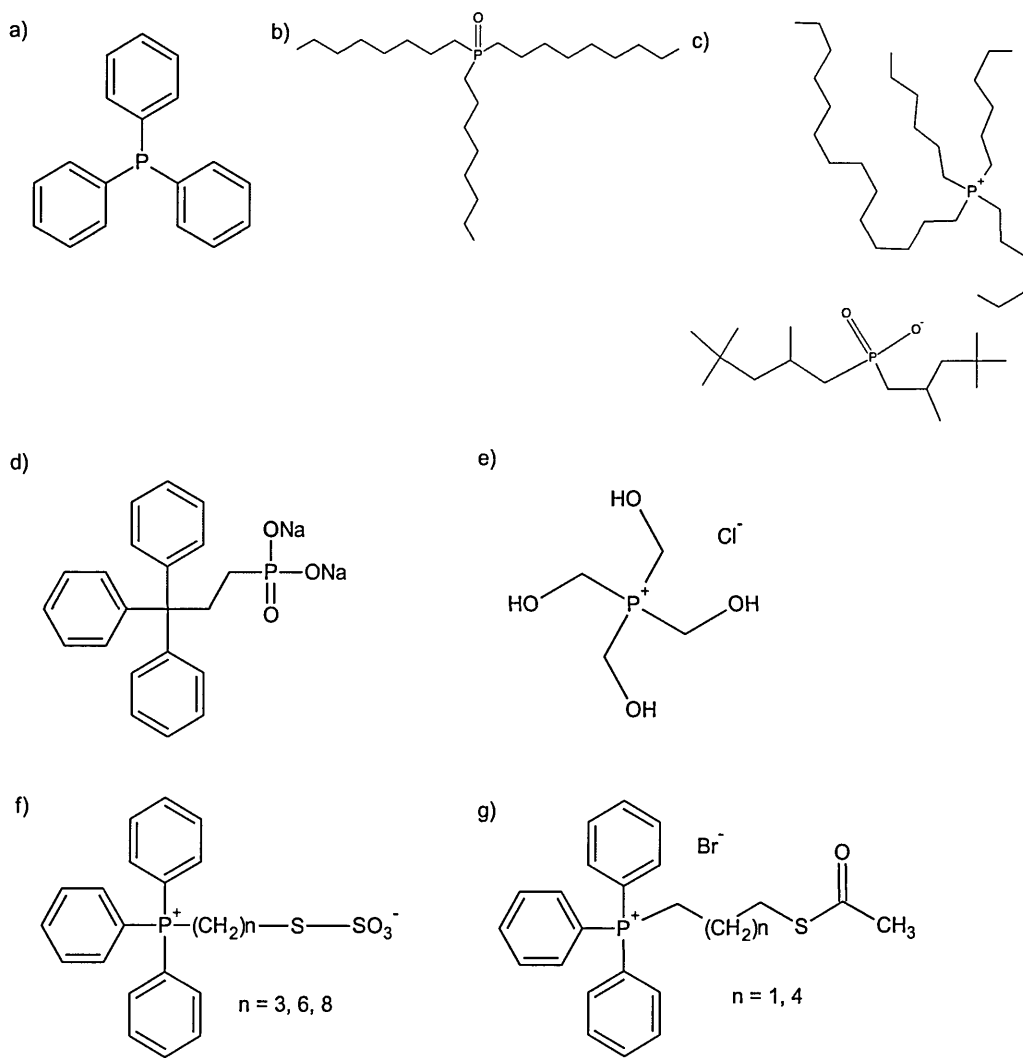
Figure 1.1 Chemical structure of phosphonium ligands used for the synthesis of functionalised nanoparticles: a) triphenylphosphine, b) tri-*n*-octylphosphine oxide, c) trihexyl(tetradecyl)phosphonium bis(2,4,4-trimethylpentyl phosphonate, d) tetrakis(hydroxymethyl)phosphonium chloride, e) diethyl(3,3,3-triphenylpropyl) phosphonate, f) phosphonioalkylthiosulfate zwitterions and g) ω-thioacetylalkylphosphonium salts.

Previously, Bricklebank and co-workers have investigated the use of an alternative system based on the phosphonium moiety; they have successfully synthesised a family of novel cationic phosphonium thiol precursor ligands (f and g) which can be used to produce phosphonium-functionalised AuNPs (P-AuNPs) (Ju-Nam *et al.*, 2008, Ju-Nam *et al.*, 2006).

1.1.5 The Surface Plasmon Resonance of Gold Nanoparticles

One of the exciting properties of AuNPs is their unique optical property which is due to the phenomenon of the surface plasmon resonance (SPR) effect; according to Mie theory, free electrons on the surface of a spherical nanoparticles (if smaller than the light wavelength) oscillate in response to an electromagnetic frequency (Moores and Goettmann, 2006). This localised SPR enhances the electromagnetic field at the AuNP surface which results in AuNPs having a high-scattering cross section with astonishing high extinction co-efficient of the SPR bands up to 10^{11} M^{-1} cm^{-1} (which is several orders of magnitude higher compared to organic dyes) (Jain *et al.*, 2006, Du *et al.*, 1998).

The SPR band of nanoparticles is very sensitive to the particle size, shape, composition and the surrounding environment (dielectric environment) (Dreaden *et al.*, 2011, Jain *et al.*, 2008, Kelly *et al.*, 2003, Liz-Marzán, 2004). Therefore this property can be selectively fine-tuned to engineer AuNPs with the desired properties for specific purposes. For example spherical AuNPs of 5 nm have an SPR band located at 520 nm, an simple increase in size to 99 nm induces a slight shift in the SPR band from 520 nm to ~560 nm, whereas with a change in the shape from sphere to rod the SPR band shifts significantly from the visible to the near-infrared (NIR) region (Chen *et al.*, 2008, Link and El-Sayed, 1999).

1.1.6 Biomedical Applications of Gold Nanoparticles

Tailorable surface chemistry for biological modification along with tuneable optical properties has made AuNPs attractive candidates for biomedical applications. As mentioned above, the SPR effect is sensitive to the dielectric environment, therefore any changes to the environment such as aggregation, refractive index of the medium and surface modification can all result in a shift in the SPR band and this property has been exploited for a range of biomedical applications ranging from diagnostic through to therapeutics (Rosi and Mirkin,

2005, Cobley *et al.*, 2011, Sperling *et al.*, 2008, Kumar *et al.*, 2013b). Immunostaining was the first biomedical application of AuNPs which began in the early 1970s when Faulk and Taylor discovered immunogold labeling (Faulk and Taylor, 1971) and since then the use of AuNPs in this field has expanded.

1.1.6.1 Biosensing

The SPR band changes when the mean distance between gold particles are reduced forming small aggregates, a visual colour change can be observed and this property has been utilised in colorimetric sensor applications. One of the most renowned gold-based sensors was developed by Mirkin and co-workers which was used to detect DNA, the colloidal solution changed from red to blue in the presence of DNA (Mirkin *et al.*, 1996, Elghanian *et al.*, 1997). AuNPs have been used as biosensors to detect analytes such as microalbumin in urine (Wiwanitkit *et al.*, 2007), glucose (Zeng *et al.*, 2012) and human chorionic gonadotropin for pregnancy tests (Rojanathanes *et al.*, 2008) which all rely on the change of colour due to aggregation of particles. Infectious pathogens (gonorrhoea, syphilis, malaria parasite and hepatitis B have been detected with the use of custom made MNAzyme-linker-AuNPs, for example MNAzyme$_{Mal}$ containing substrate arms specific to Linker$_{Mal}$ has been used to detect the malaria parasite (Zagorovsky and Chan, 2013).

Raman spectroscopy enables the detection and identification of molecules, however the signals are relatively weak and a high analyte concentration is required for a decent signal. The SPR can dramatically improve the Raman signals of molecules near the surface of AuNPs by several orders of magnitude with a technique known as surface-enhanced Raman spectroscopy (SERS) allowing ultrasensitive detection of analytes. SERS has been applied to the detection of DNA and RNA in fingerprints (Cao *et al.*, 2002), DNA in cells (Kneipp *et al.*, 2002) and two-photon excitation (Kneipp *et al.*, 2010).

1.1.6.2 Imaging and Visualising

AuNPs unusual high-scattering cross section (4-5 orders of magnitude more intensive compared to the most efficient Rhodamine 6G dye molecule) (Jain *et al.*, 2006, Du *et al.*, 1998) in conjugation with their superior photostability, unlike organic dyes AuNPs do not suffer from photobleaching, has resulted in the

utilisation of the light-scattering properties of AuNPs for cellular imaging, particularly cancer imaging which has advanced in recent years (Sokolov *et al.*, 2003a, Sokolov *et al.*, 2003b, El-Sayed *et al.*, 2005, Huang *et al.*, 2006).

Single particle tracking has been achieved by conjugating AuNPs with antibodies against the molecules on the cell surface; the binding of the molecules to the antibodies on the surface of AuNPs induces a change in the SPR frequency, since AuNPs absorb and scatter light intensively this change can be observed by dark-field microscopy (Khlebtsov and Dykman, 2010, Anker *et al.*, 2008, Eustis and El-Sayed, 2006, Wilson, 2008, Raschke *et al.*, 2003). AuNPs have also been investigated as contrast agents for *in vivo* X-ray imaging, since the gold core provides a strong X-ray absorption thereby facilitating computed tomography imaging (Alric *et al.*, 2008, Hainfeld *et al.*, 2006).

1.1.6.3 Delivering of Biomolecules

A common trait of all nanomaterials is their high surface-area-to-volume ratio which enables the attachment of copious drug molecules onto the surface for drug delivery applications, for example AuNPs with a core diameter of 2nm can be loaded with approximately 100 ligands per particle (Kim *et al.*, 2009). Nanocarriers provide a novel platform for site-specific delivery of therapeutic agents into cells. Different strategies have been utilised for the intracellular delivery of nanomaterials, these include 1) the use of cationic coatings for strong interaction with the negatively charged cellular membrane, 2) attachment of ligands onto the surface of nanoparticles for ligand-mediated internalisation and 3) cell-penetrating peptides to facilitate the translocation of nanocarriers across the membrane and to target specific organelles (Chou *et al.*, 2011).

A variety of nano-scale vehicles have been employed including dendrimers, liposomes and AuNPs (Ghosh *et al.*, 2008, Wang *et al.*, 2012), the latter has been extensively studied due to their apparent non-toxicity, easy of synthesis and versatility for further functionalisation through thiol-linkages. Furthermore, functionalised or tagged AuNPs are readily taken-up by cells making them an ideal carrier system for transporting drugs, biomolecules or other therapeutic agents into cells. A variety of biological cargoes including oligonucleotides, amphiphilic polymers, short peptide sequences, proteins, lipids, carbohydrates,

antibodies and drugs have been successfully attached to the surface of GNPs (Giljohann *et al.*, 2010, Rana *et al.*, 2012).

1.1.6.4 Photothermal Therapy

For metal nanoparticles such as AuNPs with size much smaller than the wavelength of the incident light, the free electrons on the surface will oscillate in respond to an electromagnetic field at a specific wavelength, also known as the SPR effect. As a result of the SPR effect, the particle absorbs and scatters the electromagnetic radiation intensely to a high degree (Li and Gu, 2010).

AuNPs have the unique ability to convert absorbed light into heat on a picosecond time-domain, the strong SPR absorption followed by rapid energy conversion and dissipation has been exploited for the heating of local environments by using a light source with a frequency that overlaps the SPR band of the AuNPs (Huang *et al.*, 2007). This unique property has resulted in AuNPs being promising candidates for photothermal therapy (PTT) applications (Huang *et al.*, 2008, Vauthier *et al.*, 2011, Cherukuri *et al.*, 2010, Dreaden *et al.*, 2011).

The first use of AuNPs for PTT was reported by Pitsillides and co-workers, who treated peripheral blood lymphocyte cells with spherical AuNPs (d = 20 nm) conjugated to IgG antibodies that target CD8 receptor on lymphocytes and irradiated with the short laser pulses at 565 nm (Pitsillides *et al.*, 2003). Since then the use AuNPs in this field has been widely investigated and has the potential in revolutionising cancer therapeutics in the future (Kennedy *et al.*, 2011, Dreaden *et al.*, 2011, Akhter *et al.*, 2012).

1.2 Cancer

Cancer is a collective term for a group of diseases characterised by invasive abnormal cell growth, and is a common terminology for describing a malignant tumour (Hesketh, 2013). While the origin of the word cancer is credited to the Greek physician Hippocrates who described tumours as *karkinos* and *karkinona*, it was Galen who described the appearance of a tumour as similar to the legs of a crab, and this resemblance lead to the name of the disease - *karkinos* (cancer) which means crab in Greek (Papavramidou *et al.*, 2010).

Cancer is the major cause of death in economically developed countries; this is predominantly driven by increasing average life-span, in addition to unhealthy lifestyle choices including smoking, lack of physical activity and adopting westernised diets. In 2008 approximately 12.7 million cancer cases were diagnosed with 7.6 million deaths globally, however more than half the cases and deaths (56% and 64% respectively) occurred in economically developing countries, despite being the second leading cause of death in developing countries (Jemal *et al.*, 2011). In the UK alone, 325,000 people were diagnosed with cancer in 2010 and someone is diagnosed with cancer every two minutes (CancerResearch UK).

1.2.1 Causes of Cancer

Cancer is perceived as a genetic disease involving a series of irreversible genetic changes, encompassing single point mutations, gene amplification and the loss of large regions of the genome (Tlsty and Coussens, 2006). The concept of cancer being a genetic disease of somatic cells was proposed in 1914 by Theodor Boveri (Knudson, 2001). Alterations in genetics may result in the gene no longer functioning normally and can acquire new cellular phenotypes that are beneficial to the cells such as resistance to cell death and many others which are also known as the hallmarks of cancer (Hanahan and Weinberg, 2011). The transition of normal cell into malignant phenotype is facilitated through the accumulation of genetic mutation, which can be induced by a variety of chemical, physical and biological agents.

1.2.1.1 Chemical Carcinogens

Chemical carcinogens refers to a group of chemicals that are generally genotoxic and are able to induce DNA damage either through deletions, amplifications, single point mutations or re-arrangements. To date a large number of chemical carcinogens that lead to cancer have been identified (Wogan *et al.*, 2004, Cohen and Arnold, 2011). However not all cancer causing agents result in DNA damage; phorbol esters are a class of tumour promoters which induce cellular proliferation but are not mutagenic themselves (Goel *et al.*, 2007).

The role of cigarette smoking as a cause of cancer is unquestionable, with more than 60 carcinogens from cigarette smoke having been verified to be carcinogenic in either animals or humans, nevertheless the majority of tobacco carcinogens requires metabolic activation in order to trigger their carcinogenic effects. (Pfeifer *et al.*, 2002, Peto *et al.*, 2000). Among all tobacco carcinogens tobacco-specific nitrosamine 4-(methylnitrosamino)-1-(3-pyridyl)-1-butanone (NNK) and polycyclic aromatic hydrocarbons (PAH) have shown to be predominately involved in the induction of lung cancer (Hecht, 1999).

Within the PAH family benzo[a]pyrene (BaP) has been the most extensively studied compound (Pfeifer *et al.*, 2002). BaP is activated by cytochrome P450 enzymes by oxidising BaP into an epoxide (BaP-7,8-epoxide) followed by detoxification by epoxide hydrolase converting the epoxide into a dihydrodiol (BaP-7,8-dihydrodiol). This intermediate is further metabolised to BaP-7,8-dihydrodiol-9,10-epoxide (BPDE) a highly reactive species which can interact with DNA, forming adducts favourably at guanine residues inducing double strand breakages (Moserova *et al.*, 2009, Kim *et al.*, 1998, Schwarz *et al.*, 2001).

It is widely accepted that the main cause of colon cancer is associated to dietary carcinogens; heterocyclic amines (HCA) are a group of carcinogens which are formed as pyrolysis products when protein-rich food is cooked above 180°C for long periods of time, these chemicals are commonly found when meat or fish have been over-cooked or flame-grilled (Layton *et al.*, 1995, Sugimura *et al.*, 2004). Similar to other chemical carcinogens, HCA needs to be metabolic activated by cytochrome P450 enzymes to chemically reactive electrophiles before reacting with DNA to exert their genotoxicity (Wogan *et al.*, 2004).

One of the most abundant chemicals found in cooked meats, 2-amino-1-methyl-6-phenylimidazo[4,5-*b*]pyridine (PhIP) is readily activated by the cytochrome P450 enzymes, particularly CYP1A2 producing a mutagenic and non-mutagenic product (Crofts *et al.*, 1998). The mutagenic metabolite 2-hydroxy-amino-PhIP can be further activated by undergoing acetylation or sulfation to form highly mutagenic products mainly at the C8 position of guanines (Schut and Snyderwine, 1999, Turesky *et al.*, 1991, Sugimura *et al.*, 2004).

1.2.1.2 Viruses

It has been estimated that 15% of all human cancers are caused by viruses, contributing to a substantial proportion of the cancer burden worldwide (Liao, 2006). Retroviruses cover a diverse class of ribonucleic acid (RNA) viruses which are small viruses containing only RNA in their genome, they are associated with an array of immunodeficiencies, neurological disorders and malignancies (D'Souza and Summers, 2005). Human T lymphotrophic virus type 1 and hepatitis C virus are two RNA viruses that have shown to contribute towards the development of cancers (Liao, 2006).

Retroviruses can either be non-transforming or transforming, depending on the absence or presence of an oncogene in their viral genome (Uren *et al.*, 2005). Although no human retroviruses have this ability, many viruses in other species do and these viruses produce an enzyme called reverse transcriptase enabling the host cell to make a replica of the viral genome and integrate into the host cell genome (Weinberg, 2013).

Other virus families such as DNA viruses are also linked to the development of a variety of malignancies; these include hepatitis B virus, Epstein-Barr virus, human herpes virus 8 and the human papilloma virus (HPVs) (Liao, 2006). HPV of the parpova family is the most common cause of certain skin cancers (Dubina and Goldenberg, 2009) and cervical cancers (zur Hausen, 2002). Currently more than 100 types of HPV have been discovered, type 16 and 18 being the most important as they cause the majority of cancers of the cervix, contributing for 12% of all cancers in women (zur Hausen, 2002). They encode for proteins (E6 and E7) that target p53 and retinoblastoma protein (RB) which regulates apoptosis (p53) and cell cycle (RB and p53) and thereby ablating two essential tumour suppressors (Liao, 2006, Narisawa-Saito and Kiyono, 2007).

1.2.1.3 Radiation

Acute or prolonged exposure to high doses of ionising radiation can lead to damaging consequences in humans including but not limited to cancer, in contrast at very low levels of radiation the after effects are unclear (Brenner *et al.*, 2003). The carcinogenic effect of radiation has been well documented and is undisputable; radiation exposure in Hiroshima and Nagasaki in Japan has been

associated with a number of different cancers predominately leukaemia, underground miners exposed to radon sources were prone to develop lung cancer and luminous dial painters exposed to radium have been linked with bone cancer (Gilbert, 2009).

DNA damage from ionising radiation can occur from either a direct interaction between DNA and radiation or via the creation of free radicals, which can result in cell death or non-lethal DNA modification including DNA cross-linking, mutations, chromosomal loss, single and double strand breaks (Wakeford, 2004, Cwikel et al., 2010). It is well known that UV radiation (UVR) present in sunlight is a potent carcinogen and chronic repeated exposure of UVR is the main cause of skin cancers. Both ultraviolet A radiation (UVA) (320-400 nm) and ultraviolet B radiation (UVB) (280-320nm) have important biological significances to the skin; UVA has a crucial role in the carcinogenesis of stem cells of the skin while UVB produces DNA damage and subsequently gene mutations, oxidative stress, immunosuppression and tumourigenesis (Narayanan et al., 2010). UVB induces DNA damage by forming dimeric photoproducts at "hot spots" of UV-induced mutations between adjacent pyrimidine bases on the same strand; pyrimidine-pyrimidone (6-4) photoproducts and cyclobutane dimers (CPDs) are the two most prevalent adducts formed (Ichihashi et al., 2003).

Although both lesions are potentially mutagenic, the latter is the major contributor to mutations in humans; CPDs are produced three times more often and has a slower repair rate compared to (6-4) photoproducts (Matsumura and Ananthaswamy, 2004). Furthermore, UVR creates mutations to p53 tumour suppressor genes which have critical roles in DNA repair and controlling apoptosis of cells with DNA damage. Therefore cells with mutated p53 genes no longer have the ability to repair DNA and result in dysregulation of apoptosis, therefore mutated keratinocytes increase and initiate skin cancer (Narayanan et al., 2010).

Xeroderma pigmentosum is a condition whereby individuals are unable to repair DNA damage as a result of UVR; it is an autosomal recessive defect with 100% penetrance and can be triggered from mutations in any one of the eight genes. Seven out of the eight genes (XP-A through to G) are critically involved in the

14

nucleotide excision repair (NER) mechanism which repair UV induced photoproducts in DNA. Therefore a defect in any one of those seven genes results in defective NER and the accumulation of mutations (Lehmann *et al.*, 2011).

1.2.2 Classification of Tumours

Tumours is a collective term for a group of disease characterised by excessive cell proliferation, the naming of tumours based on their cell type and tissue of origin is reasonable since tumours exhibit a wide spectrum of characteristics. Tumours can be categorised in a number of ways including tissue of origin, cell type, aetiology and biological behaviour (Weinberg, 2013, Underwood and Cross, 2009).

1.2.2.1 Biological Behaviour

An abnormal cell that grows and proliferates out of control will give rise to a tumour or neoplasm which can either be benign or malignant. (Hesketh, 2013). At the initial stages of primary tumour expansion the cells are neither invasive nor metastatic and are referred to as benign tumours, only tumours capable of invading surrounding tissues enabling the tumour to metastasise are defined as malignant cells (Yokota, 2000).

Metastases represent the outcome of the multistep invasion metastasis cascade, which involves the dissemination of cancer cells to distant organ sites, and is the central problem of malignant disease (Valastyan and Weinberg, 2011). The cascade comprises a long series of sequential, interconnected steps which all play a critical role, failure at any one of the steps can lead to the entire process being halted (Fidler, 2003). Since every event is driven by the recruitment of genetic and/or epigenetic alterations within tumour cells (Valastyan and Weinberg, 2011), it isn't surprising that highly metastatic cells accumulate more gene alterations compared to non-metastatic cells (Yokota, 2000). Although only a limited fraction of the cells in the primary neoplasm are highly metastatic (Yokota, 2000) they have an important impact on mortality rates associated with cancer, and is accountable for a staggering 90% of deaths from solid tumours (Gupta and Massague, 2006). Primary tumours can be treated surgically or by radiotherapy or chemotherapy, however once becoming

15

metastatic they become surgically unresectable and it is uncommon for long-term control of the disease by radio- or chemotherapy (Bogenrieder and Herlyn, 2003).

1.2.2.2 Nomenclature

Solid tumours are primarily categorised into benign and malignant type, benign tumours have the suffix of "oma" and malignant tumours have the suffix of carcinoma, epithelial or sarcoma if mesenchymal. Tumours are further categorised to their cell of origin and the tissue in which they arise. Carcinomas rising from epithelial tissues are by far the most common cancers in humans, accountable for more than 80% of cancer related deaths in the western world (King and Robins, 2006, Underwood and Cross, 2009).

For example a benign and malignant epithelial tumour with squamous cell organisation is termed squamous cell papilloma and squamous cell carcinoma respectively. Cells originated from mesenchymal tissues also follow the same pattern, for example benign and malignant tumour of smooth muscle is called leiomyoma and leiomyosarcoma respectively, benign and malignant tumour of the bone is called osteoma and osteosarcoma respectively. Neuroectodermal tumours refer to cells derived from the central and peripheral nervous system including gliboblastomas, neutroblastomas, schwannomas and medulloblastomas. There are exceptions where tumours do not fit into the major classifications these include melanomas, leukaemias and lymphomas (King and Robins, 2006, Underwood and Cross, 2009).

1.2.3 Cancer Genes

Normal human cells are continuously exposed to DNA damage by mutagens however they have efficient repair mechanisms to protect them against the potentially dangerous effects of cancer gene mutations and thus only a small proportion become somatically acquired mutations (Vogelstein and Kinzler, 2004). A substantial number of genes mutated in human cancers have the capacity to interrupt cellular homeostatic mechanisms causing additional mutations and/or alterations in gene expression, it has been established that individual tumours can contain up to 40 alterations (Bielas and Loeb, 2005).

Alterations in oncogenes, tumour suppressors and caretaker genes all contribute towards tumourigenesis; while oncogenes and tumour suppressor genes both behave similarly in driving the neoplasm process by increasing cell numbers through promoting cell birth, inhibiting cell-cycle arrest or cell death. Caretakers or DNA stability genes including the nucleotide-excision repair, base-excision repair and mismatch repair genes stimulate tumourigenesis differently when mutated, since stability genes keep genetic alterations to a minimum, when they become inactivated it causes higher mutation rates in other genes (Vogelstein and Kinzler, 2004).

1.2.3.1 Oncogenes

Proto-oncogenes encode for proteins that control cell proliferation, apoptosis, or both, and become oncogenes when mutated in a style that renders the gene constitutively active or active under circumstances in which the wild-type gene is not (Vogelstein and Kinzler, 2004).

Activation can occur through chromosomal translocations, gene amplifications or fusion gene, an active somatic mutation in one allele of an oncogene is sufficient to promote cell growth. For instance, the most widely activated mutation of *BRAF* in human cancers is at codon 600 where valine changes to a glutamate, which in turns activates BRAF kinase, which subsequently phosphorylates downstream targets such as extracellular signal regulated kinases and induces aberrant growth (Vogelstein and Kinzler, 2004). The major oncogenes can be classified into six broad groups: transcription factors, chromatin remodelers, growth factors, growth factor receptors, signal transducers, and apoptosis regulators (Croce, 2008).

1.2.3.2 Tumour Suppressor Genes

In contrast to oncogenes, tumour suppressor genes target the opposite direction by reducing the activity of the gene production via mutations, among all the regulators disrupted in malignant cells are the two tumour suppressors: retinoblastoma protein (pRb) and p53 transcription factor (Sherr and McCormick, 2002). RB has been regarded as the guardian of the restriction point (R-point) and can interact with many proteins particularly with E2F transcription factors which are key players in controlling the cell division cycle.

17

Under normal conditions E2Fs are sequestered by pRb in early G_1 phase, providing pRb remains hyophosphorylated the cell will not pass the R-point and remain in G_1. The interaction between pRb and E2F is regulated by phosphorylation and primarily by D-type cyclin-dependent kinases (Cyclin D); Cyclin D/cdk4 phosphorylate pRb to release E2Fs and alter its function and thus initiate cells to progress from G_1 into the S-phase (Nevins, 2001). pRb has been identified as a regulator of cell proliferation; it is a significant target of oncoproteins that are expressed by DNA tumour viruses including adenovirus E1A protein, SV40 T antigen and human papillomavirus E7 protein. Cells with overexpression of pRb undergo G_1 arrest while cells deficient in pRb leads to acceleration in G_1 transition (Classon and Harlow, 2002).

p53 is the guardian protein that preserves genomic stability in response to a variety of trauma including hypoxia, metabolic stress, DNA damage and oncogene activation response to DNA damage. p53 act as the defence mechanism against tumourigenesis by activating the following pathways: cell cycle arrest, DNA repair and apoptosis (Whibley et al., 2009). The levels of p53 in cells are tightly regulated, under normal conditions murine double minute clone 2 (MDM2) is a key negative regulator of p53, which binds to p53 and ubiquitylates the protein and ultimately degrades by the 26S proteasome.

This negative feedback maintain low levels of unphosphorylated p53 in normal cells, however in response to DNA damage p53 becomes active followed by phosphorylation and can no longer bind to MDM2 thus preventing MDM2-medaited degradation, resulting in p53 level rises leading to expression of p53-responsive genes (Momand et al., 2000). pRb and p53 pathways are disrupted in virtually all human tumours, and are found to be simultaneously inactivated in various types of cancer including small-cell lung carcinoma and osteosarcoma (Yokota and Sugimura, 1993).

1.2.4 Multistep Tumour Development

While various hypotheses have been proposed for the development of cancer, the majority of evidence indicates that carcinogenesis is a complex, multistep process also referred to as "somatic evolution". Carcinogenesis models are usually based on the Darwinian theory that new phenotypes are generated

through the evolution of genetic and/or epigenetic changes (Gatenby and Gillies, 2008, Vogelstein and Kinzler, 1993). A single mutation is inadequate for the development of cancer, cells requires sequential alterations in a number of different genes (oncogenes, tumour-suppressors or microRNA genes), usually 5-7 mutations are required for the transformation to carcinoma (Croce, 2008, Yokota and Sugimura, 1993).

Vogelstein and co-workers reported the first model (Vogelstein's model) depicting the sequence of genetic events leading to colorectal cancer (Fearon and Vogelstein, 1990) (Figure 1.2), other tumours follow a similar pathway but with different genes.
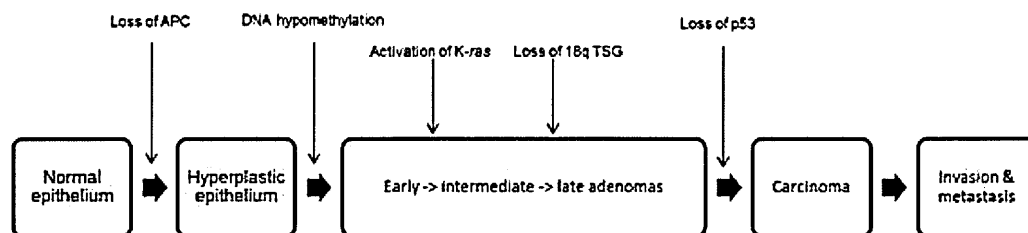
Figure 1.2 Vogelstein's multi-hit model showing the sequence of events how colorectal cancer developed from normal epithelium, this involved the alterations of tumour suppressor genes including adenomatous polyposis coli gene (APC), p53 and oncogenes such as K-ras. Diagram adapted from Fearon and Vogelstein 1990.

1.2.5 Hallmarks of Cancer

Hanahan and Weinberg summarised that cancer cell genotypes are a manifestation of several key alterations in cell physiology that influence malignant growth, which are also known as the hallmarks of cancer Figure 1.3. In 2000 they reported the six common traits that normal cells must acquire; each of these novel capabilities gained during the tumour development stage indicate the successful breaching of an anti-cancer defence mechanism present in cells (Hanahan and Weinberg, 2000). In 2011 the authors updated the hallmarks of cancer and incorporated four new emerging hallmarks (Hanahan and Weinberg, 2011), Figure 1.3.
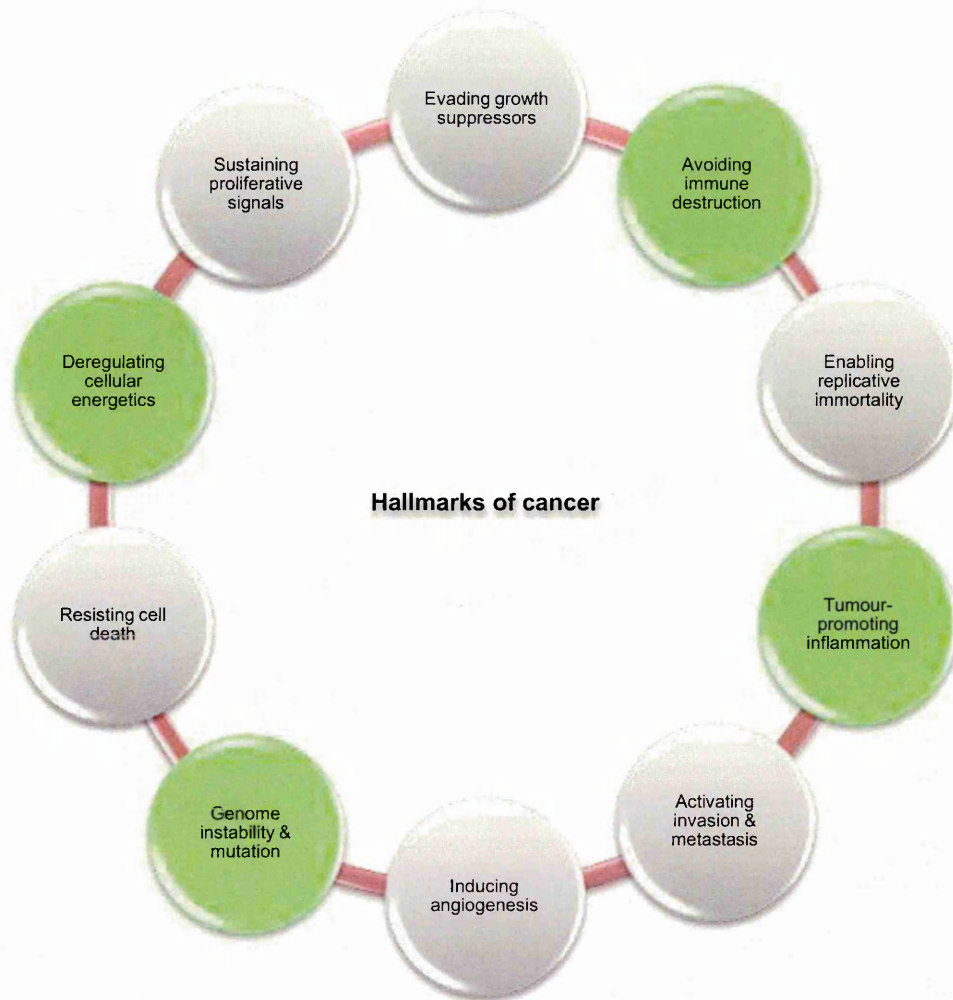
Figure 1.3 This diagram encompasses the six hallmark capabilities (pale grey) proposed by Hanahan and Weinberg in 2000 (evading growth suppressors, enabling replicative immortality, activating invasion and metastasis, inducing angiogenesis, resisting cell death and sustaining proliferative signals) and the emerging of new hallmarks updated by the same authors in 2011 as highlighted in green (avoiding immune destruction, tumour promoting inflammation, genome instability and mutation and deregulating cellular energetics) (diagram adapted from Hanahan and Weinberg 2000 and 2011).

1.2.5.1 Sustain Proliferative Signals

The ultimate trait of malignant cells is perhaps their ability to maintain chronic proliferation; in normal cells the production and release of growth factor (GF) signals for initiating the cell division cycle is vigilantly controlled ensuring tissue homeostasis for maintaining normal tissue architecture and function. Growth signals are a necessity for cells to transit from a quiescent state into an active proliferative state, no normal cells can proliferate in the absence of these stimulatory signals. Since the majority of oncogenes behave by mimicking normal growth signal by some means, tumour cells are not dependent on growth stimulation from their normal tissue microenvironment. Cancer cells can obtain the ability to sustain proliferative signalling either by producing GF themselves or sending signals to stimulate normal cells within the supporting tumour-associated stroma. For example glioblastomas and sarcomas both produce their own GF: platelet-derived growth factor and tumour growth factor α respectively (Witsch *et al.*, 2010, Perona, 2006).

The majority of GF receptors consist of tyrosine kinase activities in their domains are overexpressed in many cancers, overexpression of receptors on cancer cells could result in the cells becoming hyper-responsive to ambient levels of GF that would usually not trigger a proliferation response. For instance epidermal growth factor receptor is up-regulated in stomach, brain and breast cancer (Witsch *et al.*, 2010, Normanno *et al.*, 2006, Cheng *et al.*, 2008, Bhowmick *et al.*, 2004).

1.2.5.2 Evade Growth Suppressors

Numerous anti-proliferative signals are active within normal tissue to sustain cellular quiescence and tissue homeostasis. These signals can block proliferation by either forcing the cells out of the active proliferation state into the quiescent (G_0) state or prompting the cells to enter into post-mitotic states. Anti-proliferative signals are controlled by the tumour suppressor gene pRb (described previously) which inhibits proliferation by sequestering and altering the function of E2Fs that drives cells progression from G_1 into S-phase. Dysfunction in the pRb pathway make cells become insensitive to anti-growth signals, therefore cancer cells with defects in the pRb pathway are missing the crucial gatekeeper of cell-cycle progression thus enabling malignant cells to

flourish by evading anti-proliferative signals (Weinberg, 1995, Burkhart and Sage, 2008, Sherr and McCormick, 2002).

1.2.5.3 Tissue Invasion and Metastasis

The process of invasion and metastasis is very complicated and can be described as a sequence of events often termed the invasion-metastasis cascade (Talmadge and Fidler, 2010). For metastasis to occur in human cancers, primary tumour mass must spawn pioneer cells with the capacity to move and invade adjacent tissues and travel to distant sites forming new colonies, metastasis remains the majority cause of deaths from solid tumours. When cells possess invasive or metastatic capabilities their ability to adhere to one another decreases and an alteration in their shape, attachment to other cells and to the extracellular matrix (ECM) can be observed (Berx and van Roy, 2009). One of the key changes exhibited by carcinoma cells is the loss of cell-cell adhesion molecule notably the immunoglobulin and calcium-dependent cadherin families, both of which facilitate cell to cell interactions and integrins, which are involved in interactions between cells of the ECM. E-cadherin is a key player in cell-to-cell interactions, forming adherens junctions with adjacent epithelial cells aiding the assembly of epithelial sheets, as well as maintaining the quiescence of cells within the epithelial sheets. It has been well established that E-cadherin is a key suppressor for this hallmark; down-regulation of E-cadherin is frequently observed in human epithelial cancers, while up-regulation of E-cadherin inhibits tumour invasion (Cavallaro and Christofori, 2004, Gupta and Massague, 2006).

The degradation of the extra-cellular matrix and basement membranes is another important factor associated with cancer-cell invasion and metastasis; in general the activity of matrix metalloproteinases (MMPs) are tightly controlled through specific localization, autoinhibition, and secreted tissue inhibitors (Gupta and Massague, 2006) and there is usually an increase in expression and activity of MMPs in human cancers (Egeblad and Werb, 2002). MMPs are proteolytic enzymes that degrade the basement membrane which is a vital step during the metastatic cascade. MMPs (such as MMP7) originate from cancer cells, however in human tumours they are not the only source, other MMP (including MMP2 and MMP9) are predominantly synthesised by stromal cells

22

(Egeblad and Werb, 2002). An epithelial-mesenchymal transition (EMT) is a biological process that allows epithelial cells to undergo a series of multiple biochemical changes and behave as a mesenchymal cell phenotype, which comprises improved migratory ability, invasiveness, elevated resilience to apoptosis and increased production of ECM components (Kalluri and Weinberg, 2009). The EMT model has been perceived to transform epithelial cells to acquire the abilities to invade, to resist apoptosis and to disseminate, features of EMT have been observed in many different cancer models including colon, oesophageal, ovarian and breast. In general, EMT is characterised by a down-regulation of epithelial markers, predominantly E-cadherin and an up-regulation of mesenchymal markers particularly vimentin or fibronectin, complemented by an increase in cell migration and invasion (Micalizzi *et al.*, 2010).

1.2.5.4 Resisting Cell Death

Apoptosis is a form of programmed cell death and exists in latent form in almost all cell types through the body. Apoptosis is a highly regulated mechanism, when triggered by physiologic signals, cells undergo a precise sequence of events; disruption of cellular membrane, breakdown of cytoplasmic and nuclear skeletons, extrusion of the cytosol, degradation of the chromosomes and the fragmentation of nucleus, all in a time of 30-120 min. The apoptotic bodies are engulfed by nearby cells within 24 hours (Wyllie *et al.*, 1980).

The two main apoptotic pathways are the death receptor-mediated pathway (extrinsic) and the mitochondrial-mediated pathway (intrinsic) (Figure 1.4), though their initial method of activation differs, both cascades are mediated by a family of proteins called cysteinyl-aspartate-specific proteases (caspases) (Samali *et al.*, 1999, Wang and Lenardo, 2000). Caspases are synthesised as inactive pro-caspases and are generally classified into two groups: initiator (or apical) caspase (caspases-2, -8, -9 and -10) and executioner (or effector) caspase (caspases-3,-6 and -7) (Thornberry and Lazebnik, 1998, Bao and Shi, 2007, Gupta *et al.*, 2009). While the initiator caspases are different in the two apoptotic pathways; caspase-9 for the intrinsic pathway and caspase -8 and -10 for the extrinsic pathway, both pathways share the same executioner caspases (caspase-3, -6 and -7) which cleave cellular substrates and induce apoptotic cell death (Chen and Wang, 2002, Wyllie, 2010).

23

The extrinsic pathway is engaged when death receptors on the exterior plasma membrane (such as TNFR, death receptor 4 and 5 (DR4 and DR5) TRAIL and Fas receptors) are bounded to their cognate ligands TNFα, TRAIL and FasL (which can be decoy or soluble decoy receptors). This results in the oligomerisation of the adapter molecule Fas associated death domain (FADD) within the death-inducing signalling complex, the oligomerised FADD then binds to pro-caspases-8 and -10, causing their homodimerisation and activation thereby resulting in apoptosis (Gupta *et al.*, 2009, Parsons and Green, 2010, Igney and Krammer, 2002).

The intrinsic apoptotic pathway in which the mitochondria act as an intermediate gate keeper is activated by cellular stresses including radiation, chemotherapeutic drugs, oxidative and genotoxic stress. The mitochondria pathway is regulated by pro and anti-apoptotic proteins, when pro-apoptotic level increases, apoptogenic factors such as cytochrome *c* are released from the mitochondrial intermembrane space into the cytosol. It recruits pro-caspase-9 and Apaf-1 forming a multiprotein complex termed apoptosome, which cleaves and activates the executor caspase-3 and induces apoptosis (Fulda and Debatin, 2006, Riedl and Salvesen, 2007).
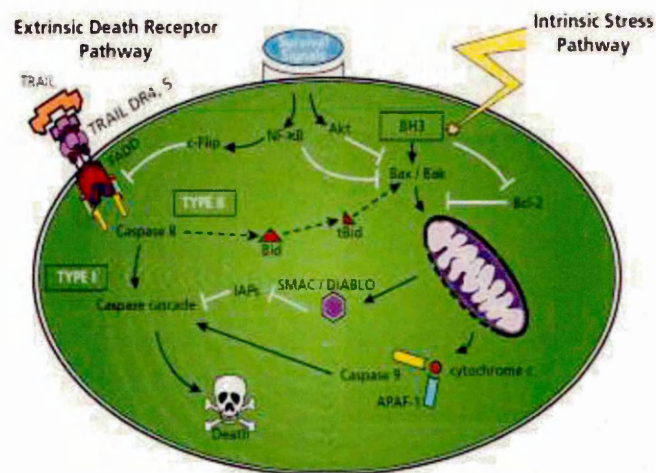
Figure 1.4 Apoptosis signalling pathways. The apoptosis pathway can be initiated through different entry sites; at the plasma membrane by death receptor ligation (extrinsic pathway) or at the mitochondria (intrinsic pathway). Diagram reprinted with permission from Sayers and Cross (Sayers and Cross, 2014).

The "apoptotic switch" is regulated by counterbalancing pro- and anti-apoptotic members of the Bcl-2 family of regulatory proteins; Bcl-2, Bcl-x_L, Bcl-w, Mcl-1 and A1 are anti-apoptotic proteins suppressing the two pro-apoptotic triggering proteins (Bax and Bak) (Adams and Cory, 2007, Kuwana and Newmeyer, 2003). Tumour cells evolve strategies to limit or avoid apoptosis; the loss of p53 tumour suppressor function is most common which removes this critical damage sensor from the apoptosis-inducing cycle. Alternatively, tumour cells down regulate pro-apoptotic factors (Bax, Bim and Puma) which enable them to escape the induction of cell death or by short-circuiting the extrinsic ligand-induced death pathway (Lowe and Lin, 2000, Fulda, 2009, Townson *et al.*, 2003).

1.2.5.5 Enabling Replicate Immortality

It has been established that normal cultured cells have a limited replicative potential meaning that when cells divide a finite number of times they stop growing (senescence) a phenomenon also known as the "Hayflick limit" (Shay and Wright, 2000). This restriction has been linked with senescence and crisis which involves cell death and are both distinct proliferation barriers, normally when cells undergo repeated cycles of cell division it leads to senescence, subsequently cells progressing pass this stage will reach a crisis phase where the majority of cells in the population dies. Cells that escape crisis will have acquired the capability to divide without limit, a transition termed immortalisation and is a widely accepted characteristic of cancer cells (Hayflick, 2000, Olaussen *et al.*, 2006). The ends of chromosomes are protected by specialised structures called telomeres; human telomeres consist of multiple tandem hexanucleotide repeats - TTAGGG. Evidence in the literature indicates that telomeres protecting chromosomal ends are centrally involved in enabling replicate immortality (Shay and Wright, 2006, Shay and Wright, 2002).

1.2.5.6 Inducing Angiogenesis

Oxygen and nutrients are essential for cells to survive and are thereby located within the diffusion limit of oxygen (100-200 μm) from blood vessels. Growing tumours must recruit new blood vessels by vasculogenesis and angiogenesis in order to sustain the growth (Carmeliet and Jain, 2000). In normal tissue once formed the angiogenesis process is carefully monitored; under certain

physiologic processes including wound healing and the female productive cycling, angiogenesis is transiently turned on while during tumour progression the "angiogenic switch" is usually on and active and thus enabling normal quiescent vasculature to continuously grow new blood vessels (Hanahan and Weinberg, 2011).

Angiogenic activators can be broadly classified into 6 groups: growth factors, cytokines, oncogenes, trace elements, endogenous modulators, proteases and protease inhibitors. Particularly the vascular endothelial growth factor (VEGF) family has been extensively studied and is one of the most well-known angiogenesis inducer (Nishida *et al.*, 2006).

VEGF expression is up-regulated by a number of factors including tumour necrosis factor, fibroblast growth factor, epidermal growth factor, transforming growth factor-β, interleukin-1 and hypoxia (Carmeliet, 2005, Kerbel, 2008). Angiogenesis is balanced by inducers and inhibitors; thrombospondin-1 (TSP-1) is a key inhibitor which counteracts the angiogenic switch by binding to CD36 on the endothelial cell membrane which mediates suppressive signals that can counterbalance proangiogenic stimuli. It has been shown in melanoma, bladder and colon cancer that a decrease in TSP-1 has been linked with p53 mutations (Lawler, 2002).

1.2.6 Emerging Hallmarks

A handful of other properties of cancer cells have been proposed to have important roles in the development of cancer and have been added to the core list of hallmarks by Weinberg and co-worker (Hanahan and Weinberg, 2011), these emerging hallmarks will be described individually below.

1.2.6.1 Deregulating Cellular Energetics

In order for cancer cells to fuel cell growth and division, they must adjust their energy metabolism. In the 1920s Otto Warburg made the ground breaking discovery that even in the presence of oxygen cancer cells reprogram their glucose metabolism to favour aerobic glycolysis, a phenomenon known as the "Warburg effect" (Hsu and Sabatini, 2008). This metabolic switch seems counterintuitive since cancer cells must overcome the lower efficiency offered

by glycolysis in relation to mitochondrial oxidative phosphorylation. This occurs by the up-regulation of glucose transporters, specifically GLUT1, which dramatically increases glucose import into the cytoplasm (DeBerardinis *et al.*, 2008, Jones and Thompson, 2009). It has been demonstrated that glycolytic fuelling is associated with mutant tumour suppressors such as P53 and activated oncogenes including RAS and c-Myc (Osthus *et al.*, 2000). This dependence on glycolysis can be emphasised under hypoxia conditions observed in almost all cancers; responses to hypoxia is mediated by the hypoxia-inducible factor 1 (HIF-1) transcription factor complex. Both RAS and hypoxia can increase levels of HIF1α and HIF2α and subsequently up-regulate glycolysis (Semenza, 2010, Gordan and Simon, 2007).

1.2.6.2 Avoiding Immune Destruction

Immune surveillance is necessary to prevent tumour formations in humans and thus immune escape is a vital pathway to malignancy; this field of research is still in its infancy with the interconnections between signalling pathways that control immune escape and those that control proliferation, senescence, apoptosis, angiogenesis, invasion and metastasis (Prendergast, 2008). Evidence in the literature indicated that the immune system can promote the emergence of primary tumours with reduced immunogenicity with the ability to escape immune recognition and destruction (Prendergast, 2008). This lead to the development of the cancer immunoediting hypothesis, which is now an emerging Hallmark of cancer and encompasses three phases: elimination, equilibrium and escape.

The first phase is elimination which involves eliminating cancer cells thereby inhibiting tumour development and/or growth, tumour cells not killed by the immune system in the elimination phase will advance forward to the second phase – equilibrium, where the remaining tumour persists in the immunocompetent host but is prevented from growing by immune pressure. Cancer cells that develop the ability to bypass immunological suppression of tumours enter the final stage of immunoediting – escape phase and will continue to divide and grow (Dunn *et al.*, 2006, Dunn *et al.*, 2004).

1.2.6.3 Genome Instability and Mutation

Almost all human cancers has the common trait of genomic instability; there are several forms of genomic instability including increased frequencies of base pair mutations, the expansion or contraction of the number of oligonucleotide repeats in microsatellite sequences also known as microsatellite instability and chromosomal instability. The latter is the most common, characterised by high alteration rates where chromosome number and structure changes over time (Negrini *et al.*, 2010). The high replication accuracy along with the remarkable ability of the genome maintenance mechanism to detect and repair defects in the DNA ensures mutation rates are kept to a minimum during cell cycle.

The majority of cancer cells have a higher mutation rate due to the accumulation of mutant genes required for tumorigenesis (Salk *et al.*, 2010). In hereditary cancers, genomic instability has been associated with mutations in DNA repair genes and thus driving cancer development. The most well-known example is hereditary nonpolyposis colon cancer also termed Lynch syndrome, where mutations in DNA mismatch repair genes result in microsatellite instability and a high mutation rate (Liu *et al.*, 1996, Lynch and Smyrk, 1996).

1.2.6.4 Tumour Promoting Inflammation

While the relationship between inflammation and cancer is not new and it dates back to the late 18th Century, it is only during the last decade where there has been an increase of evidence in the literature indicating that inflammation has pivotal roles throughout the different stages of tumour development, from initiation through to invasion and metastasis (Coussens and Werb, 2002, Grivennikov *et al.*, 2010).

Nowadays it is widely accepted that inflammation plays an important role in tumorigenesis with the majority of cancers (up to 95%) closely associated with chronic inflammation caused by environmental and lifestyle choices. Approximately 35% of all cancers can be attributed to dietary factors (up to 20% by obesity), 30% to tobacco smoke, 18% to infections and 7% to radiation and inhalation of environmental pollutants (Aggarwal *et al.*, 2009).

1.2.7 Cancer Therapeutics

To date the most common types of cancer treatment includes surgery, radiotherapy and chemotherapy. Surgery is most effective for the treatment of localised primary tumour and associated metastases in regional lymphatics, with advances in technology radical mastectomy has been replaced by partial mastectomy for breast cancer to minimise surgical trauma to tissues and organs and to retain as much of its function as possible (Urruticoechea *et al.*, 2010).

Radiotherapy utilises high energy radiation sources to cause damage to the DNA of cancer cells hence blocking their cell division cycle. Radiotherapy is an effective treatment; early cancers including prostate, lung, cervix, head and neck, lymphomas (Hodgkin's and low grade Non-Hodgkin's) and skin cancers (squamous and basal cell) are curable with radiation therapy alone. Furthermore radiotherapy is commonly used in conjunction with surgery and chemotherapy, around 50% of all patients will receive radiotherapy in due course of their illness contributing towards 40% of curative treatment of cancer. Even with high success rates, radiotherapy is highly cost effective and is only accountable for 5% of the total cancer care cost (Baskar *et al.*, 2012).

The first use of chemotherapy to treat cancer dates back to the early 20th Century with the first use of nitrogen mustards and antifolate drugs, since then cancer drugs have become one of the most researched areas and have evolved into a multi-billion dollar industry (Chabner and Roberts, 2005, DeVita and Chu, 2008). Chemotherapy involves the use of cytotoxic drugs that disrupt the cell cycle; alkylating agents such as cisplatin, cyclophosphamide forms adduct with DNA bases primarily at the guanine sites and interfere with DNA replication (Emadi *et al.*, 2009, Zamble and Lippard, 1995). Antimetabolites including methotrexate and 5-fluorouracil inhibit vital enzymes in metabolic processes thus halting cell growth (Kaye, 1998).

Conventional treatments possess several drawbacks; surgery is limited to large accessible tumours, radiation therapy is non-specific and kills both normal and abnormal cells in the radiated pathway, chemotherapeutic drugs have a narrow therapeutic index, it causes immuno-suppression and are highly expensive. Consequently, research has focused on the development of new, novel

therapies to decrease drug toxicity in healthy cells and increase efficacy, this has led to the development of targeted therapies (Arruebo *et al.*, 2011).

One approach is to use monoclonal antibodies to target receptors overexpressed on the surface of cancer cells, antibody-based therapy has become established over the past 15 years and is now often the preferred choice in the treatment of haematological malignancies and solid tumours (Scott *et al.*, 2012). Over the years several fully human monoclonal antibodies (e.g. Herceptin) have been approved by regulatory agencies and many more are at the clinical trial stages (Arruebo *et al.*, 2011). Alternative methods include targeting specific cellular signalling pathways with the use of tyrosine kinase inhibitors (e.g. Imatinib) (Arora and Scholar, 2005), triggering the extrinsic apoptotic pathway via the use of apoptosis-inducing ligand (e.g. TRAIL) (Mahmood and Shukla, 2010, Wang, 2010) and targeting the p53 gene therapy pathway to reactivate the p53 apoptosis pathway (Bykov and Wiman, 2003). Nanotechnology has arrived on the scene and the use of nanomaterials for novel applications in the field of oncology has emerged as hot topics, with plethora of publications in this area, selected reviews include Akhter *et al.*, 2012, Bilensoy 2010, Davis *et al.*, 2008, Dreaden *et al.*, 2011, Wang and Thanou 2010, Wesselinova 2011, Thanh and Green 2010, (Bertrand et al., 2014, Biswas and Torchilin, 2014, Sanna et al., 2014).

1.2.8 Cancer Nanotechnology

At present, there is a strong focus on the application of nanotechnology in cancer research; cancer nanotechnology is new field of interdisciplinary research cutting across chemistry, engineering, biology and medicine and is anticipated to revolutionised the detection, diagnosis and treatment of cancer (Llevot and Astruc, 2012, Portney and Ozkan, 2006, Srinivas *et al.*, 2002, Ferrari, 2005, Davis *et al.*, 2008).

Fluorescence techniques have many important biomedical applications including cell labelling, cell tracking, cellular and molecular imaging. Standard fluorescent labels such as organic dyes suffers from limitations particularly in multicolour experiments due to issues associated with signal intensity strength, narrow excitation ranges, broad emission spectra and relatively short lifetimes.

To overcome the limitations of organic dyes, new reporter species have been developed. Semiconductor nano-crystals also known as quantum dots (QDs) has been developed and they exhibit improved optical qualities that are desirable for biological applications and overcome the limitations of organic dyes (Walling et al., 2009).

The utilisation of nanomaterials for imaging applications has been widely investigated; cellular labelling using QDs has advanced the most and they are a promising new class of fluorescent probe for *in vivo* biomolecular and cellular imaging (Walling *et al.*, 2009, Gao *et al.*, 2004, Li *et al.*, 2009a, Bentolila *et al.*, 2009). Furthermore QDs have been used in cell tracking for the study of tumour metastasis (Voura *et al.*, 2004) and the binding of EGF to EGFR (Lidke *et al.*, 2004), magnetic nanoparticles have been exploited for magnetic resonance imaging and cell tracking (Arbab *et al.*, 2006, Pankhurst *et al.*, 2003, Singh, 2001, McCarthy and Weissleder, 2008).

The application of nanosize devices for drug delivery has blossomed over the years, with several nanomedicine products already available on the market (e.g. Doxil) and many more in the clinical trial stages (Wagner *et al.*, 2006, Kumar *et al.*, 2013a). A range of nanometric delivery vehicles have been showcased these include polymeric micelles, dendrimers, liposomes, QDs, carbon nanotubes and inorganic NPs (Rivera Gil *et al.*, 2010, Bawarski *et al.*, 2008, Elhissi *et al.*, 2012, Riggio *et al.*, 2011). Among the inorganic NPs, AuNPs have emerged as promising drug delivery carriers (Akhter *et al.*, 2012, Ahmad *et al.*, 2013, Han *et al.*, 2007).

1.2.8.1 Nanoparticles as Drug Delivery Carriers

As mentioned above, the majority of current anti-cancer agents are not specific and lack the ability to differentiate between normal and cancerous cells leading to systemic toxicity. Furthermore, because of the rapid elimination and wide spread distribution of agents into non-targeted organs and tissues, higher dosages are required which not economical and often result in adverse side effects due to non-specific toxicity (Nie *et al.*, 2007). The use of nanomaterials to delivery anti-cancer drugs to tumour sites is a promising platform, and can be achieved by either passive or active targeting.

1.2.8.1.1 Passive Targeting

Passive targeting refers to the accumulation of drug or drug delivery system at a desired site due to physico-chemical or pharmacological factors; the use of AuNPs takes advantage of its inherent size in the nature of the tumour microenvironment. Tumour vasculature differs dramatically compared to normal tissue; blood vessel walls in tumours are generally more porous and leaky owing to the formation of new blood vessel from existing ones, a process also known angiogenesis (Carmeliet and Jain, 2000, Nishida *et al.*, 2006). Angiogenic blood vessels in tumour tissues have gaps as large as 600-800 nm between adjacent endothelial cells.

Furthermore tumours have a dysfunctional lymphatic drainage resulting in AuNPs being retained longer at the tumour site. Together these effects induce a phenomenon called the enhanced permeability and retention (EPR) effect, enabling nanoparticles to extravasate through these large gaps into extravascular spaces and accumulate inside tumour tissues (Misra *et al.*, 2010, Ghosh *et al.*, 2008, Nie *et al.*, 2007).

A significant increase in tumour drug concentration can be achieved when the drug is delivered by a nanoparticle in comparison to the free drug form, however passive targeting does suffer from several limitations. It is not always feasible to target all cells within a tumour as some drugs cannot diffuse efficiently, in addition the random nature of passive targeting makes it difficult to control the process and could lead to multiple-drug resistance (Peer *et al.*, 2007). To complicate matters further the permeability of vessels may not be identical throughout the tumour and certain tumours do not exhibit the EPR effect, nanocarriers may potentially suffer from non-specific uptake and degradation in macrophages, therefore targeting is critical for achieving maximum drug efficacy with minimal size effects (Ghosh *et al.*, 2008).

1.2.8.1.2 Active Targeting

The development of nanocarriers with the capability of binding to specific cells/tumour sites of interest is an attractive proposition, this can be achieved by attaching targeting moieties of interest onto the nanoparticle scaffold to enable their selective uptake by specific interactions such as ligand-receptor, antibody-

antigen and lectin-carbohydrate (Allen, 2002). Lectin-carbohydrate binding is very specific, delivery based on this system have been developed to target organs as a whole (Yamazaki *et al.*, 2000, Kannagi *et al.*, 2004). The fact that receptors or antigens are usually over expressed in human cancer cells has been exploited, as receptor-ligand binding facilitates internalisation via receptor-mediated endocytosis. The strength of NP interactions with antigens or membrane receptors can be controlled by the property of the ligand (e.g. affinity) and by changing the ligand density (e.g. avidity) attached to the surface of the particle (Chou *et al.*, 2011).

Surface functionalisation of nanoparticles plays a major role in active targeting enabling scientists to engineer specific AuNPs with active targeting capabilities via specific surface modifications. These targeting groups can be broadly classified as proteins (antibodies and their fragments), nucleic acids or other receptor ligands (small molecules, peptides, vitamins and carbohydrates). Targeting agents developed to-date has been predominately for cancer applications (Chou *et al.*, 2011, Scheinberg *et al.*, 2010).

Folate receptors are overexpressed on the surfaces of many tumour cells and have been explored as a target; Dixit and co-workers (Dixit *et al.*, 2006) have shown that AuNPs (d = 10 nm) conjugated to folic acid were selectively taken up by folate receptor positive KB cells, with minimal uptake in cells that do not overexpress the folate receptor. Chen and colleagues (Chen *et al.*, 2007b) have demonstrated that AuNPs (d = 13 nm) (MTX-AuNPs) conjugated to methotrexate (a dihydrofolate reductase inhibitor that destroys folate metabolism) are rapidly taken-up and are more cytotoxic compared to methotrexate alone. Furthermore MTX-AuNPs have shown to suppress tumour growth in Lewis lung carcinoma cell line (LL2).

Transferrin (TF) interacts specifically with TF receptors which are actively expressed on the surface of a variety of tumour cells, as a result, the transferrin-receptor interaction has been investigated as a potential target for drug delivery. Yang and co-workers (Yang *et al.*, 2005) have shown that AuNPs (d = 20 nm) conjugated to transferrin were taken-up by human nasopharyngeal carcinoma cells (NPC, SUNE1). Tumour necrosis factor (TNF) is a potent cytokine with

anti-tumor properties, however the practical dosage is restricted due to its severe toxicity, this toxicity can be reduced by conjugation to AuNPs. PEG-AuNPs (d = 32 nm) conjugated TNF (PEG-cAu-TNF) have been injected in mice and the results illustrated that PEG-cAu-TNF were specifically accumulated in MC-38 colon carcinoma tumours and no accumulation were observed in the liver, spleens nor other healthy organs (Paciotti *et al.*, 2004).

Antibody based targeting is an alternative approach; in the 1950s the use of antibodies binded AuNPs for staining cellular components for electron microscopy was published, since then antibodies conjugated to AuNPs have been explored for cancer therapeutics (Huang *et al.*, 2008). Single chain antibody scFv has been conjugated to gold and iron oxide hybrid nanoparticles to target A33 antigens which is expressed in 95% of primary and metastatic human colorectal tumor cells for targeted phototherapy and cancer imaging (Kirui *et al.*, 2010). Several research groups have conjugated anti-human epidermal growth factor receptor 2 (anti-HER2) to a variety of AuNPs to take advantage of the overexpression of EGFR on the surface of breast cancer cells for imaging and therapeutic applications (Lee *et al.*, 2009, Loo *et al.*, 2005, Chen *et al.*, 2007a). El-Sayed's group have conjugated AuNPs (d = 35 nm) to monoclonal anti-epidermal growth factor receptor (anti-EGFR) antibodies to target overexpression EGFR on epithelial carcinoma cells for diagnosis and laser photothermal therapy (El-Sayed *et al.*, 2005, El-Sayed *et al.*, 2006).

There has been a growing interest in attaching chemotherapeutic drugs to AuNPs as an attempt to improve drug delivery to the tumour site; paclitaxel is a popular chemotherapeutic drug for the treatment of a variety of cancers however it suffers from lack of tumour specificity and low solubility in water, an approach to overcome these limitations is by conjugating paclitaxel to nanocarriers (Gibson *et al.*, 2007, Hwu *et al.*, 2009). AuNPs (d = 25 nm) conjugated to tamoxifen exhibited selective uptake by estrogen receptor positive breast cancer cells and an increase in drug potency of up to 2.7 fold was observed compared to the free drug (Dreaden *et al.*, 2009). Doxorubicin conjugated to AuNPs (d = 2.8 nm) are up to 5-fold more cytotoxic to B16 melanoma cells compared to the equivalent concentration of doxorubicin alone (Nadeau *et al.*, 2010).

34

The application of AuNPs for active targeting are not limited only for cell-specific targeting it can also be used for the localisation into desired organelles; a peptide sequence derived from the HIV-1 Tat peptide has been coupled to AuNPs for nucleus targeting (De La Fuente and Berry, 2005).

1.3 Mitochondria

The integrity of mitochondrial function is essential to cell life since many critical cellular parameters are controlled by mitochondria; these include energy production, modulation of redox status, generation of reactive oxygen species, maintenance of calcium homeostasis, involvement in a number of metabolic and biosynthetic pathways and the regulation of programmed cell death (apoptosis). Mitochondrial dysfunction contributes to a spectrum of human disorders such as neurodegenerative diseases (e.g. Parkinsons' and Alzheimers'), ischemia-reperfusion injury, diabetes and cancer (Gupta et al., 2009, Wallace, 2005, Weissig et al., 2004).

In the past few years mitochondrial research has become one of the fastest growing disciplines in biomedicine (Singh, 2001), current research activities includes targeting the mitochondrial apoptotic mechanism (D'Souza et al., 2011, Fulda, 2010, Fulda et al., 2010, Wallace, 2012, Wang, 2001), protecting mitochondria from oxidative stress (Kelso et al., 2002, James et al., 2004, Coulter et al., 2000, Sheu et al., 2006) and diseases caused by mutated mitochondrial DNA (mtDNA) (Pulkes and Hanna, 2001, Tuppen et al., 2010, D'Souza and Weissig, 2004).

1.3.1 Role of Mitochondria in Cell Death

At the centre of the intrinsic apoptotic pathway is the mitochondria (as mentioned briefly in chapter 1.2.5.4), it is the cell's reservoir of pro-apoptotic factors which reside in the mitochondrial intermembrane space (IMS). Following an apoptotic stimuli, pores are formed in the outer mitochondrial membrane (OMM) of the mitochondria in a process termed mitochondrial outer membrane permeabilisation (MOMP) this is a crucial event and is also referred to as the "point of no return" of cell death. Subsequently IMS proteins are released into the cytosol; while some of these proteins are considered to be "innocent bystanders" and do not cause any cellular response, cytochrome c and

Smac/DIABLO (Second mitochondria-derived activator of caspase/direct inhibitor of apoptosis-binding protein with low pI) promotes cell death via the activation of caspases (Parsons and Green, 2010, Gupta *et al.*, 2009).

Caspases are key players in the apoptotic response, to date 11 human caspase proteins have been identified, among them all only 7 of these are thought to have functions in apoptosis including the initiator caspases (caspase-2, -8, -9 and -10) and effector caspases (caspases-3, -6 and -7). In normal cells, caspases exist as zymogens (catalytically inactive) and must undergo proteolytic activity to become active. Following an apoptotic stimuli, initiator caspase (i.e. caspase-9) is auto-activated which activates the effector caspase (i.e. caspase-3) via the cleavage at specific aspartate residues between the small (~p10) and the large (~p20) subunits, the two subunits are closely associated with each other forming a caspase monomer (Riedl and Shi, 2004).

The activation of the caspase cascade is well regulated and requires the assembly of a multi-component complex; following the release of cytochrome *c* into the cyotosol, it forms a multimeric complex called an apoptosome (~1.4-MDa) with dATP, APAF1 (apoptotic–protease-activating factor-1) and the initiator caspase-9 which act as an activating platform for caspase-9 (Adams and Cory, 2002). Once activated, the effector caspases proteolytically cleaves regulatory and structural proteins within the cell and result in the physical and morphological characteristics of apoptosis including membrane blebbing, phosphatidylserine externalisation and chromatin condensation (Thornberry and Lazebnik, 1998).

The release of cytochrome *c* is a must for the formation of the apoptosome and the activation of caspase-9, hence without MOMP and the subsequent release of cytochrome *c* from the IMS, caspase-9 and the caspase cascade would not be activated. The integrity of MOMP is controlled by the B-cell lymphoma-2 (Bcl-2) family of proteins, which are further classified into one of three functional groups: anti-apoptotic proteins, pro-apoptotic effectors and BH3-only proteins. The Bcl-2 proteins share similar sequences of the Bcl-2 homology (BH) domains; anti-apoptotic proteins contain 4 BH domains, pro-apoptotic effectors

contains 3 BH domains and BH3-only proteins only contain the third BH domain (Wong and Puthalakath, 2008).

The anti-apoptotic family members (e.g. Bcl-2, Bcl-X_L, Bcl-w and Mcl-1) are potent anti-apoptotic molecules that inhibit MOMP and the subsequent release of cytochrome c and are found tethered to the OMM (Chipuk and Green, 2008). The pro-apoptotic family members (e.g. Bak and Bax) and BH3 only proteins (e.g. Bid, Bim, Bad, Bik and BIK) which are regarded as the essential initiators of the mitochondrial apoptotic pathway, all execute pro-death functions via different approaches. The majority of pro-apoptotic proteins are located in the cytosol with the exception of Bak which is located on the OMM (Wong and Puthalakath, 2008, Parsons and Green, 2010).

Beside the release of cytochrome c, other apoptogenic molecules including Smac/DIABLO, Htra2/Omi, apoptosis inducing factors (AIF) and endonuclease G (EndoG) are also released from the intermembrane and result in cell death via different ways. The release of cytochrome c triggers the caspase cascade and induces apoptosis, Smac/Diablo and Htra2/Omi inactivates the inhibitors of apoptosis, AIF and EndoG enter the nucleus and degrade nuclear DNA (Breckenridge and Xue, 2004, Wang, 2001).

1.3.2 Targeting Mitochondria for Cancer Therapy

Mitochondria have emerged as an attractive novel pharmacological target for cancer therapeutics (Gupta et al., 2009, Frantz and Wipf, 2010, Modica-Napolitano and Singh, 2002, Costantini et al., 2000, Weissig, 2003). Interestingly cancer cell mitochondria are structurally and functionally different in comparison to their normal counterparts (Gogvadze et al., 2008, Modica-Napolitano and Singh, 2004). These notable differences have been exploited as potential targets for anti-cancer therapy (Figure 1.5) by using agents that either interact directly at the site of mitochondria or target metabolic alterations caused by mitochondrial dysfunction.
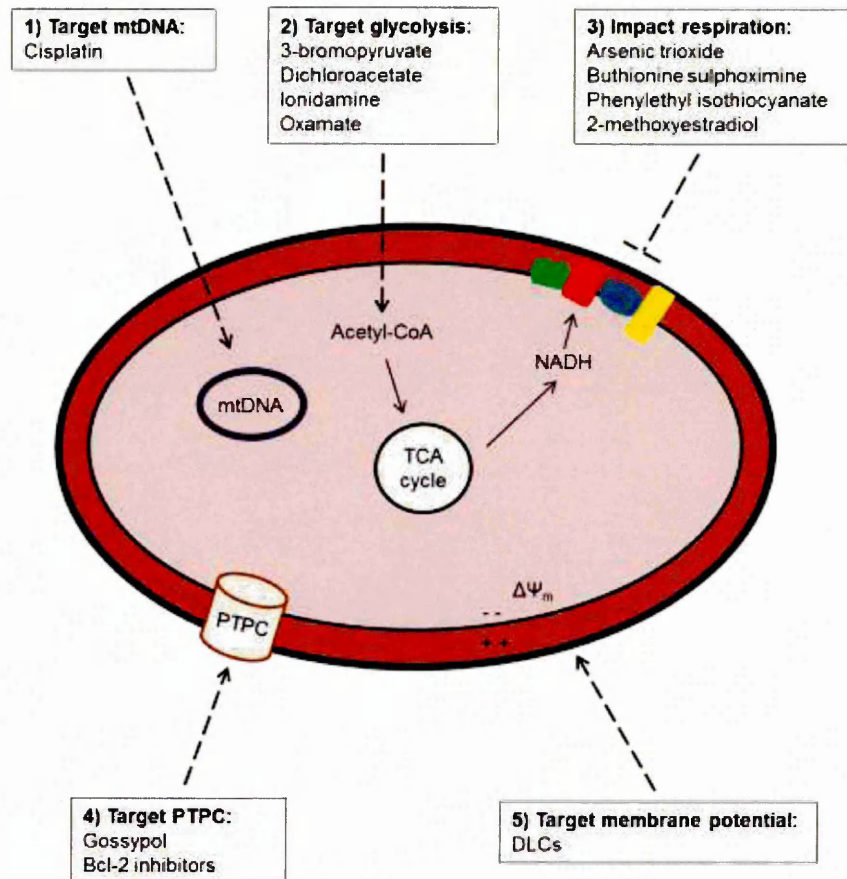
Figure 1.5 Summary of possible sites and functions of mitochondria as potential targets for anti-cancer therapyDiagram adapted from Wang *et al.* (2010).

The first approach is to target mtDNA, which encodes for 13 crucial proteins of the respiratory chain and are more vulnerable to damage than DNA due to the unique structure of lacking histone protection and having a weak repair capability (Carew *et al.*, 2003). Cisplatin is an alkylating agent and has been shown to preferentially bind to mtDNA 50 times more than DNA leading to the inhibition of NADH-ubiquinone reductase and the reduction in ATP generation (Murata *et al.*, 1990).

The second method is to target altered metabolisms associated with mitochondrial dysfunction; in cancer cells an important change is the increase in aerobic glycolysis also known as the "Warburg phenomenon" which is necessary for cancer cells to survive and proliferate. Altered expression and activities of enzymes involved in glycolysis and the tricarboxylic acid cycle have been observed in various cancer types (Kroemer and Pouyssegur, 2008). 3-

38

bromopyruvate, dichloroacetate, lonidamine and oxamate have all been shown to be effective in targeting cancer cells with high glycolytic profiles (Wang *et al.*, 2010).

The third tactic is to focus on the cancer mitochondrial respiration; evidence suggested that cancer cells have increased levels of reactive oxygen species (ROS) compared to their normal counterparts, the manipulation of ROS levels by redox modulation is a feasible approach to selectively kill cancer cells without causing significant toxicity to normal cells. ROS modulating agents include arsenic trioxide, buthionine sulphoximine, phenylethyl isothiocyanate and 2-methoxyestradiol (Trachootham *et al.*, 2009).

The fourth route is to target the mitochondrial membrane permeability; the permeability transition pore complex (PTPC) is a highly dynamic supra-molecular complex, its exact structural identity is not yet fully understood (Fulda *et al.*, 2010). In response to pro-apoptotic stimuli such as Ca^{2+} overload and ROS the PTPC enables the deregulated entry of small solutes into the mitochondrial matrix along their electrochemical gradient a process also known as the mitochondrial permeability transition pore (MPTP) which result in the immediate dissipation of the mitochondrial membrane potential and osmotic swelling of the mitochondrial matrix leading to MOMP (Kim *et al.*, 2003, Lemasters *et al.*, 1998, Fulda *et al.*, 2010).

Despite extensive research over the years, the exact mechanisms regulating mitochondrial permeability and the release of cytochrome *c* during apoptosis is not fully understood; the most accepted theory is that in response to an apoptotic stimulus pro-apoptotic proteins such as Bax and Bak undergo conformational changes, oligomerise and form pores on the outer mitochondrial membrane to facilitate the release of proteins into the cytosol (Antignani and Youle, 2006). Agents used to target the MPTP includes Bcl-2 inhibitors such as Gossypol which inhibits anti-apoptotic Bcl-2 proteins (e.g. Bcl-2, Bcl-XL and Mcl-1) (Kang and Reynolds, 2009) and ABT-737 that induces mitochondrial inner membrane permeabilisation and subsequently matrix swelling and rupturing of the outer mitochondrial membrane in leukemia and lymphoma cells (Vogler *et al.*, 2008).

The final approach is to target the mitochondrial transmembrane potential ($\Delta\Psi_m$); it is known that the $\Delta\Psi_m$ in cancer cells is significantly higher than in normal cells (Johnson *et al.*, 1980, Summerhayes *et al.*, 1982, Davis *et al.*, 1985, Modica-Napolitano and Aprille, 1987) and this biological difference has been exploited as a target. Delocalised lipophilic cations (DLCs) are able to selectively accumulate in the mitochondria of tumour cells due to the highly negatively-charged microenvironment inside the mitochondrial matrix and this specific accumulation has been demonstrated both *in vitro* (Sehy *et al.*, 1993, Rideout *et al.*, 1989, Steichen *et al.*, 1991, Manetta *et al.*, 1996, Patel *et al.*, 1994, Rideout *et al.*, 1994) and *in vivo* (Manetta *et al.*, 1996, Madar *et al.*, 2002, Li *et al.*, 2009b, Min *et al.*, 2004).

1.3.3 Strategies for Mitochondrial Pharmacology

With mitochondria emerging as a novel pharmacological target, there has been a growing interest in delivering biologically active molecules including proteins, enzyme and drugs to the site of mitochondria for therapeutic effects (Smith *et al.*, 2012, Malhi and Murthy, 2012).The main strategy employed in mitochondrial pharmacology for site specific delivery involves the conjugation of small molecules to a lipophilic cation which has been reviewed extensively elsewhere (Murphy, 1997, Murphy and Smith, 2007, Murphy and Smith, 2000, Ross *et al.*, 2005), other strategies include mitochondria targeted peptides (Yousif *et al.*, 2009a, Yousif *et al.*, 2009b, Jacotot *et al.*, 2006, Cai *et al.*, 2010) and making use of the high affinity mitochondria-specific binding sites (Smith *et al.*, 2011).

1.3.3.1 Conjugation to Lipophilic Cations

The term "lipophilic cations" refer to molecular cations in which the charge is "delocalised" by organic substituents, also referred to as delocalised lipophilic cations (DLCs) examples include rhodamine 123 (Rh 123) (a) dequalinium, Victoria Blue BO (b) choride (DECA) (c) MKT-077 (d) safranine O (e) and a family of compounds called lipophilic phosphonium compounds (LPCs) (Cooper *et al.*, 2001, Rideout *et al.*, 1989, Murphy, 2008, Pathania *et al.*, 2009), structures are shown in Figure 1.6.

Among all DLCs, LPCs have been extensively investigated for mitochondria specific targeting; whilst the ability of LPCs to permeate artificial phospholipids

bilayers has been known for some time, its first application in mitochondrial biology wasn't reported until the late 1960's when Skulachev and colleagues demonstrated that derivatives of triphenylphosphonium (Ph_3P^+R) (f) such as tetraphenylphosphonium (tetraPP) (g) and methytriphenylphosphonium (TPMP) (h) were able to cross the mitochondrial inner membrane without the facilitation from ionophores or carrier proteins and accumulate inside the mitochondria matrix due to the phenomenon of the mitochondrial transmembrane potential (Liberman *et al.*, 1969).

The mitochondrial transmembrane potential arises as a result of protons being pumped out of the mitochondrial matrix which creates a negative potential (Henry-Mowatt et al., 2004). The mitochondrial transmembrane potential within cells can be determine by the distribution of phosphonium cations, as the plasma membrane potential drives the uptake of phosphonium cations into the cytoplasm, which they are further accumulated in mitochondria by the mitochondrial transmembrane potential (Brand and Felber, 1984, Brand, 1995).

The finding that lipophilic cations were taken up by mitochondria made sense of the fact that several vital stains used since the 20th Century such as Janus Green and more recently Rh 123, JC-1 and Mitotracker have been widely used for visualising mitochondria in cells are in fact all lipophilic cations (Ross *et al.*, 2005). Since the ground breaking discovery of the accumulation of LPCs in the mitochondria by Skulachev's group (Liberman et al., 1969) , the TPP moiety has become the fundamental building blocks in the design of novel probes for investigating mitochondria function and treating mitochondria dysfunction.
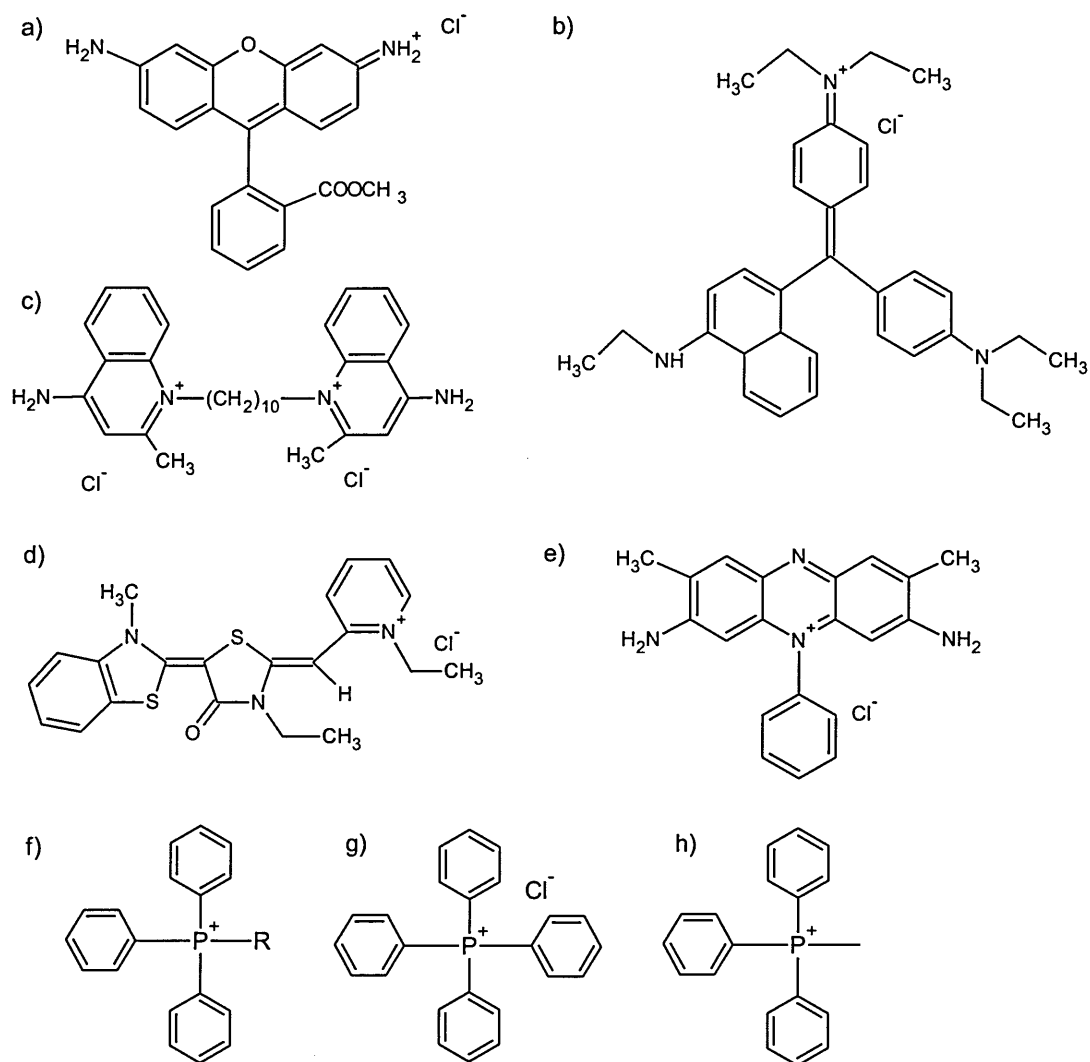
Figure 1.6 Chemical structures of DLCs: a) Rh 123, b) Victoria Blue BO, c) DECA, d) MKT-077, e) Safranin O, f) Ph3P+R, g) tetra PP and h) TPMP.

1.3.3.2 Mitochondrial Accumulation of Lipophilic Phosphonium Cations

LPCs such as tetra PP and TPMP are cationic in nature and are attracted to the negative energy potentials of the membrane bilayer, because their positive charge is delocalised over a large surface area the activation energy required to be taken-up by cells is lowered. Despite their net positive charge, LPCs have the unusual properties of being relatively lipid-soluble, enabling their passage through the lipid bilayers and accumulate specifically inside the mitochondria matrix, thereby making them ideal candidates for mitochondria-targeted diagnostics and therapeutics (Weissig, 2005, Yousif *et al.*, 2009b, Murphy, 1997, Porteous *et al.*, 2010, Ross *et al.*, 2008).

42

The uptake of LPCs into mitochondria is primarily governed by the large membrane potential across the mitochondrial inner membrane of up to 150-160 mV (negative inside) (Figure 1.7). The plasma membrane potential (usually 30-60 mV, negative inside) also drives the uptake of cations into the cell where they are further accumulated inside the mitochondria, with majority of the intracellular cation (90-95%) localising in the mitochondria (Burns and Murphy, 1997).
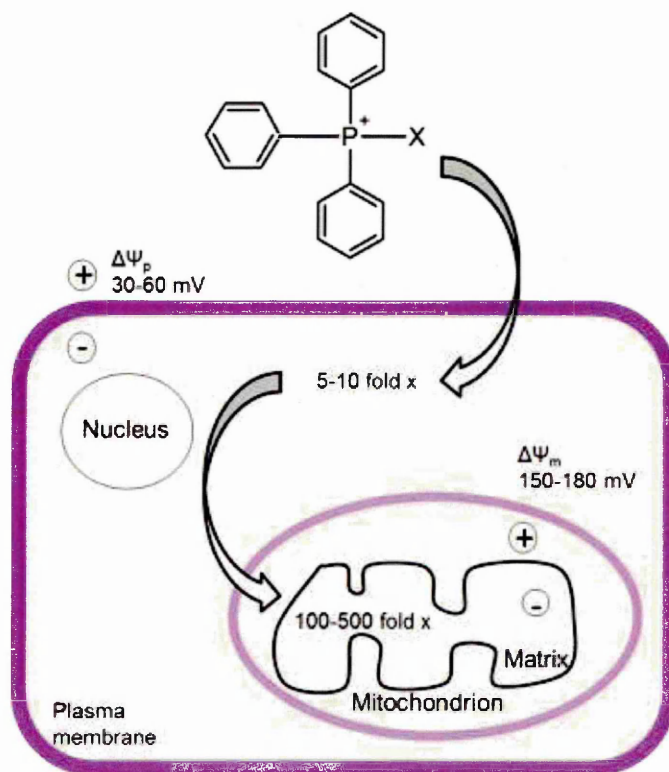
Figure 1.7 Uptake of LPCs by mitochondria within cells. This diagram shows a TPP moiety attached to a moiety (x) is taken-up 5-10 fold into the cytoplasm from the extracellular environment driven by the plasma transmembrane potential ($\Delta\Psi_p$). From the cytoplasm, the compound is further accumulated 100-500 fold into the mitochondria driven by the mitochondrial transmembrane potential ($\Delta\Psi_m$). (Diagram adapted from Ross *et al.* 2005).

The fact that lipophilic cations are taken-up by the mitochondria in cells, it was natural to consider linking molecules of interest to a lipophilic cation for targeted delivery to mitochondria *in vivo* (Murphy, 1997, Smith *et al.*, 2003, Weissig, 2005), this was first utilised by Chen who attached cisplatin to Rh 123 (Chen, 1988). In general alkyltriphenylphosphonium cations are better candidates for

targeted delivery to the site of mitochondria as they accumulate to a greater extent within the mitochondria.

Furthermore, the synthesis of alkyltriphenylphosphonium cations from the reaction of triphenylphosphine with an appropriate precursor (Smith *et al.*, 2004, Kelso *et al.*, 2001, Smith *et al.*, 1999) or by conjugation of a pre-formed alkyltriphenylphosphonium cation to a molecule is relatively simple (Murphy *et al.*, 2003, James *et al.*, 2003). This property has been exploited to direct a broad range of potential probe or therapeutic agents to the site of mitochondria and some are these are outlined below.

1.3.3.3 Mitochondria Targeted Anti-Cancer Agents

It has been demonstrated that the mitochondria transmembrane potential in cancerous cells is significantly higher compared to non-cancerous cells (-163 mV and -104 mV respectively) (Modica-Napolitano and Aprille, 1987) and this difference has a dramatic effect on the uptake of LPCs. The Nernst equation predicts a difference of 61.5 mV in trans-membrane potential at 37°C will result in a ten-fold increase in accumulation, therefore the concentration of LPCs in the mitochondrial matrix should then be several hundred- to a few thousand-fold greater in comparison to the extracellular environment (Ross *et al.*, 2005).

The Nernst equation describes the concentration of the free, unbound cations. In the presence of the mitochondrial transmembrane potential, the distribution of singly charged lipophilic cations such as TPMP (Figure 1.6 h) across the membrane will equilibrate with the mitochondrial transmembrane potential which will result in the extensive accumulation of the cation in the mitochondrial matrix to extent described by the Nernst equation (Ross *et al.*, 2005):

$$\Delta\Psi m = \frac{2.303RT}{F} log_{10} \left(\frac{cation_{in}}{cation_{out}}\right)$$

The idea of utilising LPCs as a delivery vector to take advantage of the elevated mitochondrial transmembrane potential observed in cancer cells has been investigated over the years; tetra PP has been administered at concentrations high enough to cause cell death in cancer cells due to non-specific disruption to mitochondrial function, but is non-toxic to control cells (Rideout *et al.*, 1989).

44

This approach has been extended to conjugate protein alkylating agents to the TPP moiety and thus increasing the concentration of these compounds within cancer cells to selectively promote cell death (Manetta *et al.*, 1996, Rideout *et al.*, 1989, Patel *et al.*, 1994).

1.3.3.4 Mitochondria Targeted Photodynamic Therapy

Photodynamic therapy (PDT) is novel treatment modality for several types of cancer; it involves photoreactions mediated by three key elements: photosensitisers, light and oxygen to generate ROS such as singlet oxygen, superoxide anion radical and hydroxyl radical. PDT benefit from the cytotoxic effects generated from the ROS to induce apoptosis or necrosis in cancerous cells (Lei *et al.*, 2010). The photosensitiser mesochlorine e_6 (Mce$_6$) has been conjugated to the TPP group (P-SS-TPP-lysince-Mce$_6$), while both unconjugated and conjugated photosensitiser displayed a time dependent cytotoxicity effect in ovarian carcinoma cells (SKOV-3) the conjugated, (Mce$_6$) exhibited greater cytotoxicity (Cuchelkar *et al.*, 2008).

Meso-tetraphenylporphyrin derivatives incorporating a TPP ion terminated alkoxy group at either *para-* or *meta-* position of one *meso*-phenyl group have shown to be phototoxic in human breast cancer (MCF-7) (Lei *et al.*, 2010). More recently, a core modified porphyrin-mono-triphenylphosphonium cation (CMP-tPP) has shown improvement in cellular uptake and photodynamic activity compared to the monohydroxy core modified porphyrin alone (Rajaputra *et al.*, 2013).

1.3.3.5 Mitochondria Targeted Radiotracers for Tumour Imaging

Conventional cationic radiotracers such as ^{99m}Tc-Tetrofosmin and ^{99m}Tc-Sestamibi have been used for the diagnosis of cancer by single-photon emission computed tomography (SPECT) and the monitor of the multidrug resistance transport function in tumours of different origin, however they suffer from low tumour selectivity and insufficient tumour localization and thus limiting their diagnostic and prognostic values in a clinical setting (Zhou and Liu, 2011).

Nearly 30 years ago, radiolabeled quaternary phosphonium cations were first investigated as perfusion radiotracers for myocardial perfusion imaging

(Srivastava *et al.*, 1985), since then several groups have proposed the use of radiolabeled triphenylphosphonium cations as PET radiotracers. These include ^{18}F labelled probes as mentioned previously in chapter 3.1 and ^{64}Cu labelled phosphonium cations including ^{64}Cu-labeled 2-(diphenylphosphoryl)-ethyldiphenylphosphonium cations (Yang *et al.*, 2008, Liu *et al.*, 2009, Yang *et al.*, 2007). ^{64}Cu-labeled phosphonium cations have emerged as a promising new class of PET radiotracers with high tumour selectivity and uptake (Wang *et al.*, 2007, Zhou and Liu, 2011).

1.3.3.6 Mitochondria Targeted Antioxidants

In contrast to sending drugs to the site of mitochondria to kill cells, therapeutic agents may also be used to protect the cell; the mitochondrial respiratory chain is a major source of ROS within the cell and the accumulation of these oxidative species contribute to a number of degenerative diseases (Raha and Robinson, 2000, Finkel and Holbrook, 2000). Protecting the mitochondria from oxidative damage is an attractive proposition, however the use of antioxidants to halt the progression of oxidative damage related disease has had limited success, one reason could be due to the non-specific targeting of the antioxidants which means that only a small fraction of the given dose is actually taken up by the mitochondria, consequently there has been considerable interest in developing mitochondria-specific antioxidants (Smith *et al.*, 1999, Sheu *et al.*, 2006, Murphy and Smith, 2007).

Researchers have taken advantage of the fact that LPCs are specifically accumulated in the mitochondria; the first mitochondria-targeted antioxidant MitoE$_2$, which consists of the α-tocopherol moiety of vitamin E conjugated to a TPP cation by a two-carbon chain was reported by Smith and colleagues (Smith *et al.*, 1999). To date, a number of mitochondria-targeted antioxidants have been published, these include mitochondria-targeted nitroxide (Mito-carboxy proxy) which consist of a carboxy proxy conjugated to TPP (Dhanasekaran *et al.*, 2005), MitoPeroxidase which contains an ebselen moiety covalently linked to a TPP cation (Filipovska *et al.*, 2005), MitoPBN a derivate of spin trap α-phenyl-*N*-*tert*-butylnitrone incorporating the TPP moiety (Murphy *et al.*, 2003) and MitoQ (ubiquinone conjugated to TPP) (Kelso *et al.*, 2001, James *et al.*, 2005, Cochemé *et al.*, 2007).

46

1.3.3.7 Mitochondria Targeted Peptides

Recently, peptides have been conjugated to the TPP cation to facilitate delivery to the site of mitochondria; Abu-Gosh and colleagues (Abu-Gosh *et al.*, 2009) have covalently linked a hydrophilic peptide Hemagglutinin A (HA) to a varied number of TPPs (0-3), data showed that increasing the number of TPP cations in the HA-TPP conjugates result in significant improvement in cellular uptake and mitochondrial localisation. Kolevzon and co-workers (Kolevzon *et al.*, 2011) have conjugated a pro-apoptotic peptide D-(KLAKLAK)$_2$ that induces mitochondria-dependent apoptosis but suffers from poor uptake in the cells to multiple TPPs (0-3), the biological activity of the peptide as a pro-apoptotic agent was dramatically increased with the attachment of three TPPs.

1.3.4 Mitochondria-Specific Nanocarriers

Several types of nanosystems have been developed for mitochondrial targeting: including DQAsomes (DeQuAlinium based liposome-like vesicles) (D'Souza *et al.*, 2003b), liposomes (nanolipid vesicles) (Boddapati *et al.*, 2005) and solid nanoparticles (Weissig and Torchilin, 2000) each system will be described in more detail below.

1.3.4.1 DQAsomes

DQAsomes were proposed as the first nanoscale mitochondria-specific drug-delivery system in the late 1990s; these drug carriers have been designed based on the basis that amphiphilic cations with a delocalised centre were able to accumulate inside the mitochondria of living cells in response to the mitochondrial transmembrane potential. (Weissig *et al.*, 1998). DQAsomes were the first delivery vector capable of selectively delivering plasmid DNA to mitochondria within living mammalian cells and thus opening doors to mitochondrial gene therapy (D'Souza *et al.*, 2007, D'Souza *et al.*, 2003a).

Weissig's group have also investigated the use of DQAsomes as mitochondria specific drug carriers for low-molecular-weight compounds; *in vitro* and *in vivo* data from on-going investigation in Weissig's lab strongly suggest that encapsulating paclitaxel into this delivery system increases the bioavailability of this drug in the mitochondria and subsequently improve the drugs' therapeutic efficiency (Cheng *et al.*, 2005).

1.3.4.2 Liposomes

The application of phospholipid vesicles (liposomes) as drug delivery vehicles were developed during the 1970s and 1980s and were available on the market from the mid 1990's. The first liposomal formulation Doxil® (doxorubicin stealth liposomes) was approved by the food and drug administration (FDA) in 1995, since then other liposomal formulations including Daunome® (daunorobicin), AmBiosome® (amphotericin) and DepoCyte® (cytarabine) have also entered the market (Durazo and Kompella, 2012).

With several products approved by the FDA, liposomes have become the most investigated class of nanovehicles for mitochondrial-targeted therapeutics. The advancement of liposomes in targeted mitochondrial research is essentially attributed to Professor Volkmar Weissig's research group (Boddapati et al., 2005, Boddapati et al., 2008, Boddapati et al., 2010, Patel et al., 2010, Weissig et al., 2006). On-going research in Weissig's group is exploring the feasibility of utilising mitochondria-specific liposomes for the targeted delivery of pro-apoptotic agents to enhance the drug's bioavailability and therapeutic efficiency (Weissig et al., 2007).

1.3.4.3 Solid Nanoparticles

In theory, membrane probes could enter mitochondria through a number of mechanisms including PT pores, mitochondrial apoptosis related channels, apoptosis-related ceramide pores, damage to the outer mitochondrial membrane, translocase of the outer membrane 40 (TOM40) and voltage-dependent anion channel (VDAC) (Mannella, 1998, Guo et al., 2004, Crompton, 1999, Siskind et al., 2006, Halestrap, 2005). However only the latter two are relevant to normal mitochondrial function, while the others are related to apoptosis or PT related mitochondrial swelling. The internal diameter of TOM has been determined to be between 2.0-2.6 nm using nanogold clusters conjugated to precursor proteins, this eliminated TOM40 as a possible entry route for nanoparticles ≥ 3 nm in size (Schwartz and Matouschek, 1999).

Salnikov and colleagues investigated the permeability of the OMM using calibrated AuNPs of different sizes (d = 3 and 6 nm) (Salnikov et al., 2007, Parfenov et al., 2006); the results showed that under control conditions the

OMM was impermeable to 6 nm AuNPs, in contrast 3 nm AuNPs could enter the mitochondrial intermembrane space in mitochondria of both permeabilised cells and isolated cardiac mitochondria.

The authors also established that the voltage-dependent anion channel (VDAC) was the port of entry for the 3 nm AuNPs; if the AuNPs were entering the mitochondria through the VDAC, inhibition of VDAC should therefore prevent their entry, because in the closed state the VDAC is only permeable to small cations (Rostovtseva *et al.*, 2005). Even in the presence of VDAC inhibitors 3 nm AuNPs were still able to enter the MIMS, therefore the AuNPs must have entered the MIMS through the VDAC. Based on the data obtained, the authors were able to assess the physical diameter of the VDAC pore is likely to be ≥ 3 nm and ≤ 6 nm.

A synthetic strategy for attaching mitochondria targeting moiety (Weissig, 2003) to the surface of AuNPs was introduced by Ju-Nam and co-workers (Ju-Nam *et al.*, 2006), it will be interesting to compare the mitochondrial accumulation inside living cells of plain 3 nm AuNPs reported by Parfenov and colleagues (Parfenov *et al.*, 2006) with AuNPs of the same size coated with mitochondria specific targeted ligands (Weissig *et al.*, 2007).

1.4 Hypothesis

Functionalised AuNPs are known to passively accumulate around tumours due to the phenomenon of the EPR effect (Wang and Thanou, 2010). AuNPs have the unique ability to absorb energy from an electromagnetic radiation source, causing them to become excited, generating local heating of tumour cells, a process known as PTT (Cherukuri *et al.*, 2010). This local heating can be enhanced by synthesising AuNPs that can be directed to target tumour cells, or to sub-cellular organelles such as mitochondria.

Mitochondria play a crucial role in controlling apoptosis and thus making them an attractive pharmacological target for cancer therapeutics (Smith *et al.*, 2012). LPCs are readily taken by cells and are preferentially accumulated in the mitochondria of tumour cells due to the elevated membrane potential observed in cancer cells (Ross *et al.*, 2005). By synthesising AuNPs with diameter in the

49

region of 3 nm functionalised with LPCs should result in their specific accumulation in the mitochondria, as it has been demonstrated that AuNPs with a diameter of 3 nm are able to permeate through both the outer and inner mitochondrial membrane (Salnikov et al., 2007). Therefore AuNPs functionalised with LPCs should lead to mitochondria specific accumulation inside tumour cells,when the cells are irradiated with a light source, the AuNPs will become excited, consequently rupturing the mitochondrial membrane, releasing cytochrome *c* into the cytosol and triggering the caspase cascade which ultimately induces apoptosis (Figure 1.8).
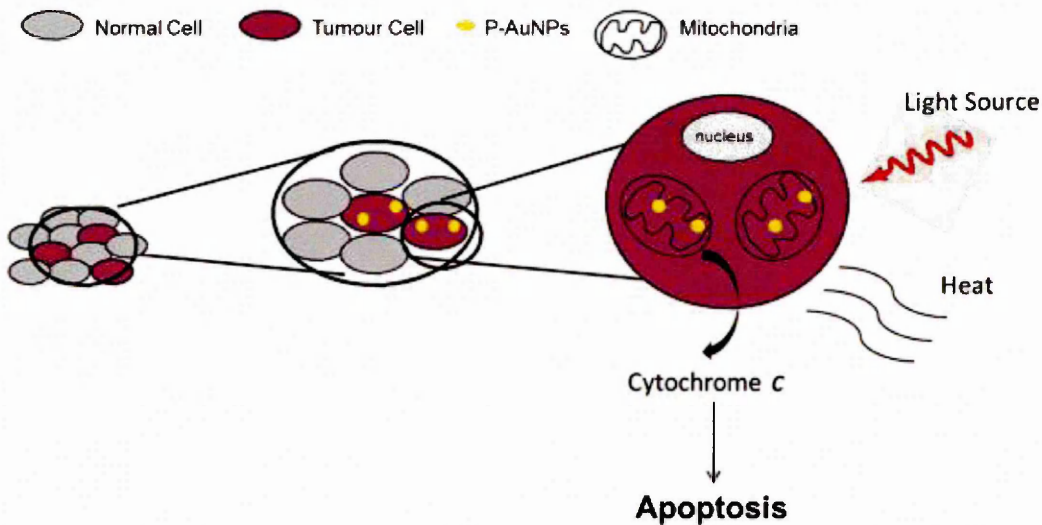
Figure 1.8 Diagram illustrating the hypothesis. TPP conjugated on the surface of AuNPs should lead to the specific delivery of AuNPs inside the mitochondria of cancer cells. When cells are irradiated with a light source the AuNPs should become excited, rupturing the membrane, causing the release of cytochrome *c* from the mitochondrial intermembrane space, triggering the caspase-3 activation and inducing apoptosis.

1.5 Scope of Thesis

The main aims of the work reported in this thesis include the synthesis and detailed characterisation of phosphonium ligands and phosphonium-functionalised AuNPs, the validation of use of these compounds inside cells, and to investigate their potential as PTT agents.

Chapter 3 describes the synthesis and the detailed characterisation of phosphonium compounds and phosphonium-functionalised AuNPs using a variety of techniques.

Chapter 4 presents the cytotoxicity studies of phosphonium ligands and the semi-quantification uptake studies of phosphonium compounds in cells using mass spectrometry.

Chapter 5 evaluates the possibility of using P-AuNPs as PTT agents, and their uptake in cells by electron microscopy.

Chapter 6 summaries the work reported in this thesis and makes some conclusions along with recommendations for future studies.

1.6 References

ABU-GOSH, S. E., KOLVAZON, N., TIROSH, B., RINGEL, I. & YAVIN, E. 2009. Multiple triphenylphosphonium cations shuttle a hydrophilic peptide into mitochondria. *Molecular Pharmaceutics,* 6, 1138-1144.

ADAMS, J. M. & CORY, S. 2002. Apoptosomes: engines for caspase activation. *Current Opinion in Cell Biology,* 14, 715-720.

ADAMS, J. M. & CORY, S. 2007. The Bcl-2 apoptotic switch in cancer development and therapy. *Oncogene,* 26, 1324-1337.

AGASTI, S. S., RANA, S., PARK, M. H., KIM, C. K., YOU, C. C. & ROTELLO, V. M. 2010. Nanoparticles for detection and diagnosis. *Advanced Drug Delivery Reviews,* 62, 316-328.

AGGARWAL, B. B., VIJAYALEKSHMI, R. V. & SUNG, B. 2009. Targeting inflammatory pathways for prevention and therapy of cancer: Short-term friend, long-term foe. *Clinical Cancer Research,* 15, 425-430.

AHMAD, M. Z., AKHTER, S., RAHMAN, Z., AKHTER, S., ANWAR, M., MALLIK, N. & AHMAD, F. J. 2013. Nanometric gold in cancer nanotechnology: current status and future prospect. *Journal of Pharmacy and Pharmacology,* 65, 634-651.

AKHTER, S., AHMAD, M. Z., AHMAD, F. J., STORM, G. & KOK, R. J. 2012. Gold nanoparticles in theranostic oncology: current state-of-the-art. *Expert Opinion on Drug Delivery,* 9, 1225-1243.

ALLEN, T. M. 2002. Ligand-targeted therapeutics in anticancer therapy. *Nature Reviews Cancer,* 2, 750-763.

ALRIC, C., TALEB, J., LE DUC, G., MANDON, C., BILLOTEY, C., LE MEUR-HERLAND, A., BROCHARD, T., VOCANSON, F., JANIER, M., PERRIAT, P., ROUX, S. & TILLEMENT, O. 2008. Gadolinium chelate coated gold nanoparticles as contrast agents for both X-ray computed tomography and magnetic resonance imaging. *Journal of the American Chemical Society,* 130, 5908-5915.

ANKER, J. N., HALL, W. P., LYANDRES, O., SHAH, N. C., ZHAO, J. & VAN DUYNE, R. P. 2008. Biosensing with plasmonic nanosensors. *Nature Materials,* 7, 442-453.

ANTIGNANI, A. & YOULE, R. J. 2006. How do Bax and Bak lead to permeabilization of the outer mitochondrial membrane? *Current Opinion in Cell Biology,* 18, 685-689.

ARBAB, A. S., LIU, W. & FRANK, J. A. 2006. Cellular magnetic resonance imaging: Current status and future prospects. *Expert Review of Medical Devices,* 3, 427-439.

ARNIDA, MALUGIN, A. & GHANDEHARI, H. 2010. Cellular uptake and toxicity of gold nanoparticles in prostate cancer cells: A comparative study of rods and spheres. *Journal of Applied Toxicology,* 30, 212-217.

ARORA, A. & SCHOLAR, E. M. 2005. Role of tyrosine kinase inhibitors in cancer therapy. *Journal of Pharmacology and Experimental Therapeutics,* 315, 971-979.

ARRUEBO, M., VILABOA, N., S EZ-GUTIERREZ, B., LAMBEA, J., TRES, A., VALLADARES, M. & GONZ LEZ-FERN NDEZ, A. 2011. Assessment of the evolution of cancer treatment therapies. *Cancers,* 3, 3279-3330.

ARVIZO, R. R., MIRANDA, O. R., THOMPSON, M. A., PABELICK, C. M., BHATTACHARYA, R., DAVID ROBERTSON, J., ROTELLO, V. M., PRAKASH, Y. S. & MUKHERJEE, P. 2010. Effect of nanoparticle surface charge at the plasma membrane and beyond. *Nano Letters,* 10, 2543-2548.

52

BAO, Q. & SHI, Y. 2007. Apoptosome: A platform for the activation of initiator caspases. *Cell Death and Differentiation,* 14, 56-65.

BARBOSA, S., AGRAWAL, A., RODR GUEZ-LORENZO, L., PASTORIZA-SANTOS, I., ALVAREZ-PUEBLA, R. A., KORNOWSKI, A., WELLER, H. & LIZ-MARZ N, L. M. 2010. Tuning size and sensing properties in colloidal gold nanostars. *Langmuir,* 26, 14943-14950.

BASKAR, R., LEE, K. A., YEO, R. & YEOH, K.-W. 2012. Cancer and Radiation Therapy: Current Advances and Future Directions. *International Journal of Medical Sciences,* 9, 193-199.

BAWARSKI, W. E., CHIDLOWSKY, E., BHARALI, D. J. & MOUSA, S. A. 2008. Emerging nanopharmaceuticals. *Nanomedicine: Nanotechnology, Biology, and Medicine,* 4, 273-282.

BENTOLILA, L. A., EBENSTEIN, Y. & WEISS, S. 2009. Quantum dots for in vivo small-animal imaging. *Journal of Nuclear Medicine,* 50, 493-496.

BERTRAND, N., WU, J., XU, X., KAMALY, N. & FAROKHZAD, O. C. 2014. Cancer nanotechnology: The impact of passive and active targeting in the era of modern cancer biology. *Advanced Drug Delivery Reviews,* 66, 2-25.

BERX, G. & VAN ROY, F. 2009. Involvement of Members of the Cadherin Superfamily in Cancer. *Cold Spring Harbor Perspectives in Biology,* 1.

BHOWMICK, N. A., NEILSON, E. G. & MOSES, H. L. 2004. Stromal fibroblasts in cancer initiation and progression. *Nature,* 432, 332-337.

BIELAS, J. H. & LOEB, L. A. 2005. Mutator phenotype in cancer: Timing and perspectives. *Environmental and Molecular Mutagenesis,* 45, 206-213.

BILENSOY, E. 2010. Cationic nanoparticles for cancer therapy. *Expert Opinion on Drug Delivery,* 7, 795-809.

BISWAS, S. & TORCHILIN, V. P. 2014. Nanopreparations for organelle-specific delivery in cancer. *Advanced Drug Delivery Reviews,* 66, 26-41.

BODDAPATI, S. V., D'SOUZA, G. G., ERDOGAN, S., TORCHILIN, V. P. & WEISSIG, V. 2008. Organelle-targeted nanocarriers: specific delivery of liposomal ceramide to mitochondria enhances its cytotoxicity in vitro and in vivo. *Nano Lett,* 8, 2559-63.

BODDAPATI, S. V., D'SOUZA, G. G. & WEISSIG, V. 2010. Liposomes for drug delivery to mitochondria. *Methods in molecular biology (Clifton, N.J.),* 605, 295-303.

BODDAPATI, S. V., TONGCHAROENSIRIKUL, P., HANSON, R. N., D'SOUZA, G. G., TORCHILIN, V. P. & WEISSIG, V. 2005. Mitochondriotropic liposomes. *J Liposome Res,* 15, 49-58.

BOGENRIEDER, T. & HERLYN, M. 2003. Axis of evil: molecular mechanisms of cancer metastasis. *Oncogene,* 22, 6524-6536.

BOISSELIER, E. & ASTRUC, D. 2009. Gold nanoparticles in nanomedicine: Preparations, imaging, diagnostics, therapies and toxicity. *Chemical Society Reviews,* 38, 1759-1782.

BRAND, M. D. 1995. Measurement of mitochondrial protonmotive force. *Bioenergetics - A Practical Approach,* 39-62.

BRAND, M. D. & FELBER, S. M. 1984. Membrane potential of mitochondria in intact lymphocytes during early mitogenic stimulation. *Biochemical Journal,* 217, 453-459.

BRECKENRIDGE, D. G. & XUE, D. 2004. Regulation of mitochondrial membrane permeabilization by BCL-2 family proteins and caspases. *Current Opinion in Cell Biology,* 16, 647-652.

BRENNER, D. J., DOLL, R., GOODHEAD, D. T., HALL, E. J., LAND, C. E., LITTLE, J. B., LUBIN, J. H., PRESTON, D. L., PRESTON, R. J., PUSKIN, J. S., RON, E., SACHS, R. K., SAMET, J. M., SETLOW, R. B. & ZAIDER, M. 2003. Cancer risks attributable to low doses of ionizing radiation: Assessing what we really know. *Proceedings of the National Academy of Sciences,* 100, 13761-13766.

BRUST, M., FINK, J., BETHELL, D., SCHIFFRIN, D. J. & KIELY, C. 1995. Synthesis and reactions of functionalised gold nanoparticles. *Journal of the Chemical Society, Chemical Communications,* 0, 1655-1656.

BRUST, M., WALKER, M., BETHELL, D., SCHIFFRIN, D. J. & WHYMAN, R. 1994. Synthesis of thiol-derivatised gold nanoparticles in a two-phase liquid-liquid system. *Journal of the Chemical Society, Chemical Communications,* 801-802.

BURKHART, D. L. & SAGE, J. 2008. Cellular mechanisms of tumour suppression by the retinoblastoma gene. *Nature Reviews Cancer,* 8, 671-682.

BURNS, R. J. & MURPHY, M. P. 1997. Labeling of mitochondrial proteins in living cells by the thiol probe thiobutyltriphenylphosphonium bromide. *Archives of Biochemistry and Biophysics,* 339, 33-39.

BYKOV, V. J. N. & WIMAN, K. G. 2003. Novel cancer therapy by reactivation of the p53 apoptosis pathway. *Annals of Medicine,* 35, 458-465.

CAI, H., YANG, H., XIANG, B., LI, S., LIU, S., WAN, L., ZHANG, J., LI, Y., CHENG, J. & LU, X. 2010. Selective apoptotic killing of solid and hematologic tumor cells by bombesin-targeted delivery of mitochondria-disrupting peptides. *Molecular Pharmaceutics,* 7, 586-596.

CANCER. *Cancer Researck UK* [Online]. Available: http://www.cancerresearchuk.org/home/?gclid=CJyBrp2v2LoCFfMctAodJ FOAVw.

CAO, Y. C., JIN, R. & MIRKIN, C. A. 2002. Nanoparticles with Raman spectroscopic fingerprints for DNA and RNA detection. *Science,* 297, 1536-1540.

CAREW, J. S., ZHOU, Y., ALBITAR, M., CAREW, J. F., KEATING, M. J. & HUANG, P. 2003. Mitochondrial DNA mutations in primary leukemia cells after chemotherapy: clinical significance and therapeutic implications. *Leukemia,* 17, 1437-1447.

CARMELIET, P. 2005. VEGF as a key mediator of angiogenesis in cancer. *Oncology,* 69, 4-10.

CARMELIET, P. & JAIN, R. K. 2000. Angiogenesis in cancer and other diseases. *Nature,* 407, 249-257.

CAVALLARO, U. & CHRISTOFORI, G. 2004. Cell adhesion and signalling by cadherins and Ig-CAMs in cancer. *Nature Reviews Cancer,* 4, 118-132.

CHABNER, B. A. & ROBERTS, T. G. 2005. Timeline - Chemotherapy and the war on cancer. *Nature Reviews Cancer,* 5, 65-72.

CHEN, H., KOU, X., YANG, Z., NI, W. & WANG, J. 2008. Shape- and size-dependent refractive index sensitivity of gold nanoparticles. *Langmuir,* 24, 5233-5237.

CHEN, J., SAEKI, F., WILEY, B. J., CANG, H., COBB, M. J., LI, Z. Y., AU, L., ZHANG, H., KIMMEY, M. B., LI, X. & XIA, Y. 2005. Gold nanocages: Bioconjugation and their potential use as optical imaging contrast agents. *Nano Letters,* 5, 473-477.

CHEN, J., WANG, D., XI, J., AU, L., SIEKKINEN, A., WARSEN, A., LI, Z. Y., ZHANG, H., XIA, Y. & LI, X. 2007a. Immuno gold nanocages with

tailored optical properties for targeted photothermal destruction of cancer cells. *Nano Letters,* 7, 1318-1322.

CHEN, L. B. 1988. Mitochondrial membrane potential in living cells. *Annual Review of Cell Biology,* 4, 155-181.

CHEN, M. & WANG, J. 2002. Initiator caspases in apoptosis signaling pathways. *Apoptosis,* 7, 313-319.

CHEN, Y. H., TSAI, C. Y., HUANG, P. Y., CHANG, M. Y., CHENG, P. C., CHOU, C. H., CHEN, D. H., WANG, C. R., SHIAU, A. L. & WU, C. L. 2007b. Methotrexate conjugated to gold nanoparticles inhibits tumor growth in a syngeneic lung tumor model. *Molecular Pharmaceutics,* 4, 713-722.

CHENG, N., CHYTIL, A., SHYR, Y., JOLY, A. & MOSES, H. L. 2008. Transforming growth factor-β signaling-deficient fibroblasts enhance hepatocyte growth factor signaling in mammary carcinoma cells to promote scattering and invasion. *Molecular Cancer Research,* 6, 1521-1533.

CHENG, S. M., PABBA, S., TORCHILIN, V. P., FOWLE, W., KIMPFLER, A., SCHUBERT, R. & WEISSIG, V. 2005. Towards mitochondria-specific delivery of apoptosis-inducing agents: DQAsomal incorporated paclitaxel. *Journal of Drug Delivery Science and Technology,* 15, 81-86.

CHERUKURI, P., GLAZER, E. S. & CURLEYA, S. A. 2010. Targeted hyperthermia using metal nanoparticles. *Advanced Drug Delivery Reviews,* 62, 339-345.

CHIPUK, J. E. & GREEN, D. R. 2008. How do BCL-2 proteins induce mitochondrial outer membrane permeabilization? *Trends in Cell Biology,* 18, 157-164.

CHITHRANI, B. D., GHAZANI, A. A. & CHAN, W. C. W. 2006. Determining the size and shape dependence of gold nanoparticle uptake into mammalian cells. *Nano Letters,* 6, 662-668.

CHO, E. C., XIE, J., WURM, P. A. & XIA, Y. 2009. Understanding the role of surface charges in cellular adsorption versus internalization by selectively removing gold nanoparticles on the cell surface with a I 2/KI etchant. *Nano Letters,* 9, 1080-1084.

CHOMPOOSOR, A., SAHA, K., GHOSH, P. S., MACARTHY, D. J., MIRANDA, O. R., ZHU, Z. J., ARCARO, K. F. & ROTELLO, V. M. 2010. The role of surface functionality on acute cytotoxicity, ROS generation and DNA damage by cationic gold nanoparticles. *Small,* 6, 2246-2249.

CHOU, L. Y. T., MING, K. & CHAN, W. C. W. 2011. Strategies for the intracellular delivery of nanoparticles. *Chemical Society Reviews,* 40, 233-245.

CLASSON, M. & HARLOW, E. 2002. The retinoblastoma tumour suppressor in development and cancer. *Nature Reviews Cancer,* 2, 910-917.

COBLEY, C. M., CHEN, J., CHO, E. C., WANG, L. V. & XIA, Y. 2011. Gold nanostructures: A class of multifunctional materials for biomedical applications. *Chemical Society Reviews,* 40, 44-56.

COCHEM , H. M., KELSO, G. F., JAMES, A. M., ROSS, M. F., TRNKA, J., MAHENDIRAN, T., ASIN-CAYUELA, J., BLAIKIE, F. H., MANAS, A. R. B., PORTEOUS, C. M., ADLAM, V. J., SMITH, R. A. J. & MURPHY, M. P. 2007. Mitochondrial targeting of quinones: Therapeutic implications. *Mitochondrion,* 7, S94-S102.

COHEN, S. M. & ARNOLD, L. L. 2011. Chemical carcinogenesis. *Toxicological Sciences,* 120, S76-S92.

COOPER, W. A., BARTIER, W. A., RIDEOUT, D. C. & DELIKATNY, E. J. 2001. H-1 NMR visible lipids are induced by phosphonium salts and 5-fluorouracil in human breast cancer cells. *Magnetic Resonance in Medicine,* 45, 1001-1010.

COSTANTINI, P., JACOTOT, E., DECAUDIN, D. & KROEMER, G. 2000. Mitochondrion as a novel target of anticancer chemotherapy. *Journal of the National Cancer Institute,* 92, 1042-1053.

COULTER, C. V., KELSO, G. F., LIN, T. K., SMITH, R. A. J. & MURPHY, M. P. 2000. Mitochondrially targeted antioxidants and thiol reagents. *Free Radical Biology and Medicine,* 28, 1547-1554.

COUSSENS, L. M. & WERB, Z. 2002. Inflammation and cancer. *Nature,* 420, 860-867.

CROCE, C. M. 2008. Molecular origins of cancer: Oncogenes and cancer. *New England Journal of Medicine,* 358, 502-511.

CROFTS, F. G., SUTTER, T. R. & STRICKLAND, P. T. 1998. Metabolism of 2-amino-1-methyl-6-phenylimidazo 4,5-b pyridine by human cytochrome P4501A1, P4501A2 and P4501B1. *Carcinogenesis,* 19, 1969-1973.

CROMPTON, M. 1999. The mitochondrial permeability transition pore and its role in cell death. *The Biochemical journal,* 341, Pt 2/.

CUCHELKAR, V., KOPEČKOV , P. & KOPEČEK, J. 2008. Novel HPMA copolymer-bound constructs for combined tumor and mitochondrial targeting. *Molecular Pharmaceutics,* 5, 776-786.

CWIKEL, J. G., GIDRON, Y. & QUASTEL, M. 2010. Low-dose environmental radiation, DNA damage, and cancer: The possible contribution of psychological factors. *Psychology Health & Medicine,* 15, 1-16.

D'SOUZA, G. G., RAMMOHAN, R., CHENG, S. M., TORCHILIN, V. P. & WEISSIG, V. 2003a. DQAsome-mediated delivery of plasmid DNA toward mitochondria in living cells. *J Control Release,* 92, 189-97.

D'SOUZA, G. G. M., BODDAPATI, S. V. & WEISSIG, V. 2007. Gene therapy of the other genome: The challenges of treating mitochondrial DNA defects. *Pharmaceutical Research,* 24, 228-238.

D'SOUZA, G. G. M., RAMMOHAN, R., CHENG, S. M., TORCHILIN, V. P. & WEISSIG, V. 2003b. DQAsome-mediated delivery of plasmid DNA toward mitochondria in living cells. *Journal of Controlled Release,* 92, 189-197.

D'SOUZA, G. G. M., WAGLE, M. A., SAXENA, V. & SHAH, A. 2011. Approaches for targeting mitochondria in cancer therapy. *Biochimica Et Biophysica Acta-Bioenergetics,* 1807, 689-696.

D'SOUZA, G. G. M. & WEISSIG, V. 2004. Approaches to mitochondrial gene therapy. *Current Gene Therapy,* 4, 317-328.

D'SOUZA, V. & SUMMERS, M. F. 2005. How retroviruses select their genomes. *Nature Reviews Microbiology,* 3, 643-655.

DANIEL, M. C. & ASTRUC, D. 2004. Gold nanoparticles: Assembly, supramolecular chemistry, quantum-size-related properties, and applications toward biology, catalysis, and nanotechnology. *Chemical Reviews,* 104, 293-346.

DAVIS, M. E., CHEN, Z. & SHIN, D. M. 2008. Nanoparticle therapeutics: An emerging treatment modality for cancer. *Nature Reviews Drug Discovery,* 7, 771-782.

DAVIS, S., WEISS, M. J., WONG, J. R., LAMPIDIS, T. J. & CHEN, L. B. 1985. Mitochondrial and plasma membrane potentials cause unusual accumulation and retention of rhodamine 123 by human breast

adenocarcinoma-derived MCF-7 cells. *Journal of Biological Chemistry,* 260, 13844-13850.

DE LA FUENTE, J. M. & BERRY, C. C. 2005. Tat peptide as an efficient molecule to translocate gold nanoparticles into the cell nucleus. *Bioconjugate Chemistry,* 16, 1176-1180.

DEBERARDINIS, R. J., LUM, J. J., HATZIVASSILIOU, G. & THOMPSON, C. B. 2008. The biology of cancer: metabolic reprogramming fuels cell growth and proliferation. *Cell Metabolism,* 7, 11-20.

DEVITA, V. T., JR. & CHU, E. 2008. A History of Cancer Chemotherapy. *Cancer Research,* 68, 8643-8653.

DHANASEKARAN, A., KOTAMRAJU, S., KARUNAKARAN, C., KALIVENDI, S. V., THOMAS, S., JOSEPH, J. & KALYANARAMAN, B. 2005. Mitochondria superoxide dismutase mimetic inhibits peroxide-induced oxidative damage and apoptosis: Role of mitochondrial superoxide. *Free Radical Biology and Medicine,* 39, 567-583.

DIXIT, V., VAN DEN BOSSCHE, J., SHERMAN, D. M., THOMPSON, D. H. & ANDRES, R. P. 2006. Synthesis and grafting of thioctic acid-PEG-folate conjugates onto Au nanoparticles for selective targeting of folate receptor-positive tumor cells. *Bioconjugate Chemistry,* 17, 603-609.

DREADEN, E. C., MACKEY, M. A., HUANG, X. H., KANG, B. & EL-SAYED, M. A. 2011. Beating cancer in multiple ways using nanogold. *Chemical Society Reviews,* 40, 3391-3404.

DREADEN, E. C., MWAKWARI, S. C., SODJI, Q. H., OYELERE, A. K. & EL-SAYED, M. A. 2009. Tamoxifen-Poly(ethylene glycol)-Thiol Gold Nanoparticle Conjugates: Enhanced Potency and Selective Delivery for Breast Cancer Treatment. *Bioconjugate Chemistry,* 20, 2247-2253.

DU, H., FUH, R. C. A., LI, J., CORKAN, L. A. & LINDSEY, J. S. 1998. PhotochemCAD++: A Computer-Aided Design and Research Tool in Photochemistry. *Photochemistry and Photobiology,* 68, 141-142.

DUBINA, M. & GOLDENBERG, G. 2009. Viral-associated nonmelanoma skin cancers: A Review. *American Journal of Dermatopathology,* 31, 561-573.

DUNN, G. P., KOEBEL, C. M. & SCHREIBER, R. D. 2006. Interferons, immunity and cancer immunoediting. *Nature Reviews Immunology,* 6, 836-848.

DUNN, G. P., OLD, L. J. & SCHREIBER, R. D. 2004. The immunobiology of cancer immunosurveillance and immunoediting. *Immunity,* 21, 137-148.

DURAZO, S. A. & KOMPELLA, U. B. 2012. Functionalized nanosystems for targeted mitochondrial delivery. *Mitochondrion,* 12, 190-201.

EGEBLAD, M. & WERB, Z. 2002. New functions for the matrix metalloproteinases in cancer progression. *Nature Reviews Cancer,* 2, 161-174.

EL-SAYED, I. H., HUANG, X. & EL-SAYED, M. A. 2005. Surface plasmon resonance scattering and absorption of anti-EGFR antibody conjugated gold nanoparticles in cancer diagnostics: Applications in oral cancer. *Nano Letters,* 5, 829-834.

EL-SAYED, I. H., HUANG, X. & EL-SAYED, M. A. 2006. Selective laser photo-thermal therapy of epithelial carcinoma using anti-EGFR antibody conjugated gold nanoparticles. *Cancer Letters,* 239, 129-135.

ELGHANIAN, R., STORHOFF, J. J., MUCIC, R. C., LETSINGER, R. L. & MIRKIN, C. A. 1997. Selective colorimetric detection of polynucleotides based on the distance-dependent optical properties of gold nanoparticles. *Science,* 277, 1078-1081.

ELHISSI, A., AHMED, W., DHANAK, V. R. & SUBRAMANI, K. 2012. *Carbon nanotubes in cancer therapy and drug delivery.*

EMADI, A., JONES, R. J. & BRODSKY, R. A. 2009. Cyclophosphamide and cancer: golden anniversary. *Nature Reviews Clinical Oncology,* 6, 638-647.

EUSTIS, S. & EL-SAYED, M. A. 2006. Why gold nanoparticles are more precious than pretty gold: Noble metal surface plasmon resonance and its enhancement of the radiative and nonradiative properties of nanocrystals of different shapes. *Chemical Society Reviews,* 35, 209-217.

FARADAY, M. 1857. The Bakerian Lecture: experimental relations of gold (and other metals) to light. *Philosophical Transactions of the Royal Society of London,* 147, 145-181.

FAULK, W. P. & TAYLOR, G. M. 1971. Communication to the editors. An immunocolloid method for the electron microscope. *Immunochemistry,* 8, 1081-1083.

FEARON, E. R. & VOGELSTEIN, B. 1990. A genetic model for colorectal tumorigenesis *Cell,* 61, 759-767.

FERRARI, M. 2005. Cancer nanotechnology: Opportunities and challenges. *Nature Reviews Cancer,* 5, 161-171.

FIDLER, I. J. 2003. Timeline - The pathogenesis of cancer metastasis: the 'seed and soil' hypothesis revisited. *Nature Reviews Cancer,* 3, 453-458.

FILIPOVSKA, A., KELSO, G. F., BROWN, S. E., BEER, S. M., SMITH, R. A. J. & MURPHY, M. P. 2005. Synthesis and characterization of a triphenylphosphonium-conjugated peroxidase mimetic: Insights into the interaction of ebselen with mitochondria. *Journal of Biological Chemistry,* 280, 24113-24126.

FINKEL, T. & HOLBROOK, N. J. 2000. Oxidants, oxidative stress and the biology of ageing. *Nature,* 408, 239-247.

FRANTZ, M. C. & WIPF, P. 2010. Mitochondria as a target in treatment. *Environmental and Molecular Mutagenesis,* 51, 462-475.

FRENS, G. 1973. Controlled nucleation for the regulation of the particle size in monodisperse gold suspensions. *Nature (London), Physical Science,* 241, 20-22.

FULDA, S. 2009. Tumor resistance to apoptosis. *International Journal of Cancer,* 124, 511-515.

FULDA, S. 2010. Exploiting mitochondrial apoptosis for the treatment of cancer. *Mitochondrion,* 10, 598-603.

FULDA, S. & DEBATIN, K. M. 2006. Extrinsic versus intrinsic apoptosis pathways in anticancer chemotherapy. *Oncogene,* 25, 4798-4811.

FULDA, S., GALLUZZI, L. & KROEMER, G. 2010. Targeting mitochondria for cancer therapy. *Nature Reviews Drug Discovery,* 9, 447-464.

GAO, X., CUI, Y., LEVENSON, R. M., CHUNG, L. W. K. & NIE, S. 2004. In vivo cancer targeting and imaging with semiconductor quantum dots. *Nature Biotechnology,* 22, 969-976.

GATENBY, R. A. & GILLIES, R. J. 2008. Hypoxia and metabolism - Opinion - A microenvironmental model of carcinogenesis. *Nature Reviews Cancer,* 8, 56-61.

GHOSH, P., HAN, G., DE, M., KIM, C. K. & ROTELLO, V. M. 2008. Gold nanoparticles in delivery applications. *Advanced Drug Delivery Reviews,* 60, 1307-1315.

58

GIBSON, J. D., KHANAL, B. P. & ZUBAREV, E. R. 2007. Paclitaxel-functionalized gold nanoparticles. *Journal of the American Chemical Society,* 129, 11653-11661.

GILBERT, E. S. 2009. Ionising radiation and cancer risks: What have we learned from epidemiology? *International Journal of Radiation Biology,* 85, 467-482.

GILJOHANN, D. A., SEFEROS, D. S., DANIEL, W. L., MASSICH, M. D., PATEL, P. C. & MIRKIN, C. A. 2010. Gold nanoparticles for biology and medicine. *Angewandte Chemie - International Edition,* 49, 3280-3294.

GILJOHANN, D. A., SEFEROS, D. S., PRIGODICH, A. E., PATEL, P. C. & MIRKIN, C. A. 2009. Gene regulation with polyvalent siRNA-nanoparticle conjugates. *Journal of the American Chemical Society,* 131, 2072-2073.

GL CKLER, J., KL TZKE, S., MEYER-ZAIKA, W., RELLER, A., GARC A-GARC A, F. J., STREHBLOW, H. H., KELLER, P., RENTSCHLER, E. & KL UI, W. 2007. With phosphinophosphonic acids to nanostructured, water-soluble, and catalytically active rhodium clusters. *Angewandte Chemie - International Edition,* 46, 1164-1167.

GOEL, G., MAKKAR, H. P. S., FRANCIS, G. & BECKER, K. 2007. Phorbol esters: Structure, biological activity, and toxicity in animals. *International Journal of Toxicology,* 26, 279-288.

GOGVADZE, V., ORRENIUS, S. & ZHIVOTOVSKY, B. 2008. Mitochondria in cancer cells: what is so special about them? *Trends in Cell Biology,* 18, 165-173.

GOODMAN, C. M., MCCUSKER, C. D., YILMAZ, T. & ROTELLO, V. M. 2004. Toxicity of gold nanoparticles functionalized with cationic and anionic side chains. *Bioconjugate Chemistry,* 15, 897-900.

GORDAN, J. D. & SIMON, M. C. 2007. Hypoxia-inducible factors: central regulators of the tumor phenotype. *Current Opinion in Genetics and Development,* 17, 71-77.

GREEN, M. & O'BRIEN, P. 2000. A simple one phase preparation of organically capped gold nanocrystals. *Chemical Communications,* 183-184.

GREEN, M., RAHMAN, P. & SMYTH-BOYLE, D. 2007. Ionic liquid passivated CdSe nanocrystals. *Chemical Communications,* 574-576.

GRIVENNIKOV, S. I., GRETEN, F. R. & KARIN, M. 2010. Immunity, Inflammation, and Cancer. *Cell,* 140, 883-899.

GUO, L., PIETKIEWICZ, D., PAVLOV, E. V., GRIGORIEV, S. M., KASIANOWICZ, J. J., DEJEAN, L. M., KORSMEYER, S. J., ANTONSSON, B. & KINNALLY, K. W. 2004. Effects of cytochrome c on the mitochondrial apoptosis-induced channel MAC. *American Journal of Physiology - Cell Physiology,* 286, C1109-C1117.

GUPTA, G. P. & MASSAGUE, J. 2006. Cancer metastasis: Building a framework. *Cell,* 127, 679-695.

GUPTA, S., KASS, G. E. N., SZEGEZDI, E. & JOSEPH, B. 2009. The mitochondrial death pathway: a promising therapeutic target in diseases. *Journal of Cellular and Molecular Medicine,* 13, 1004-1033.

HAINFELD, J. F., SLATKIN, D. N., FOCELLA, T. M. & SMILOWITZ, H. M. 2006. Gold nanoparticles: A new X-ray contrast agent. *British Journal of Radiology,* 79, 248-253.

HALESTRAP, A. 2005. Biochemistry: A pore way to die. *Nature,* 434, 578-579.

HAN, G., GHOSH, P. & ROTELLO, V. M. 2007. Functionalized gold nanoparticles for drug delivery. *Nanomedicine,* 2, 113-123.

59

HANAHAN, D. & WEINBERG, R. A. 2000. The hallmarks of cancer. *Cell,* 100, 57-70.

HANAHAN, D. & WEINBERG, R. A. 2011. Hallmarks of Cancer: The Next Generation. *Cell,* 144, 646-674.

HARNACK, O., FORD, W. E., YASUDA, A. & WESSELS, J. M. 2002. Tris(hydroxymethyl)phosphine-Capped Gold Particles Templated by DNA as Nanowire Precursors. *Nano Letters,* 2, 919-923.

HAYFLICK, L. 2000. The illusion of cell immortality. *British Journal of Cancer,* 83, 841-846.

HECHT, S. S. 1999. Tobacco smoke carcinogens and lung cancer. *Journal of the National Cancer Institute,* 91, 1194-1210.

HENRY-MOWATT, J., DIVE, C., MARTINOU, J. C. & JAMES, D. 2004. Role of mitochondrial membrane permeabilization in apoptosis and cancer. *Oncogene,* 23, 2850-2860.

HESKETH, R. 2013. *Introduction to Cancer Biology,* United States of America Cambridge University Press.

HIRSCH, L. R., STAFFORD, R. J., BANKSON, J. A., SERSHEN, S. R., RIVERA, B., PRICE, R. E., HAZLE, J. D., HALAS, N. J. & WEST, J. L. 2003. Nanoshell-mediated near-infrared thermal therapy of tumors under magnetic resonance guidance. *Proceedings of the National Academy of Sciences of the United States of America,* 100, 13549-13554.

HSU, P. P. & SABATINI, D. M. 2008. Cancer cell metabolism: Warburg and beyond. *Cell,* 134, 703-707.

HUANG, X., EL-SAYED, I. H., QIAN, W. & EL-SAYED, M. A. 2006. Cancer cell imaging and photothermal therapy in the near-infrared region by using gold nanorods. *Journal of the American Chemical Society,* 128, 2115-2120.

HUANG, X., JAIN, P. K., EL-SAYED, I. H. & EL-SAYED, M. A. 2008. Plasmonic photothermal therapy (PPTT) using gold nanoparticles. *Lasers in Medical Science,* 23, 217-228.

HUANG, X., NERETINA, S. & EL-SAYED, M. A. 2009. Gold nanorods: from synthesis and properties to biological and biomedical applications. *Advanced Materials,* 21, 4880-4910.

HUANG, X. H., JAIN, P. K., EL-SAYED, I. H. & EL-SAYED, M. A. 2007. Gold nanoparticles: interesting optical properties and recent applications in cancer diagnostic and therapy. *Nanomedicine,* 2, 681-693.

HWU, J. R., LIN, Y. S., JOSEPHRAJAN, T., HSU, M. H., CHENG, F. Y., YEH, C. S., SU, W. C. & SHIEH, D. B. 2009. Targeted paclitaxel by conjugation to iron oxide and gold nanoparticles. *Journal of the American Chemical Society,* 131, 66-68.

ICHIHASHI, M., UEDA, M., BUDIYANTO, A., BITO, T., OKA, M., FUKUNAGA, M., TSURU, K. & HORIKAWA, T. 2003. UV-induced skin damage. *Toxicology,* 189, 21-39.

IGNEY, F. H. & KRAMMER, P. H. 2002. Death and anti-death: Tumour resistance to apoptosis. *Nature Reviews Cancer,* 2, 277-288.

JACOTOT, E., DENIAUD, A., BORGNE-SANCHEZ, A., TOUAT, Z., BRIAND, J. P., LE BRAS, M. & BRENNER, C. 2006. Therapeutic peptides: Targeting the mitochondrion to modulate apoptosis. *Biochimica et Biophysica Acta - Bioenergetics,* 1757, 1312-1323.

JAIN, P. K., HUANG, X., EL-SAYED, I. H. & EL-SAYED, M. A. 2008. Noble metals on the nanoscale: optical and photothermal properties and some

applications in imaging, sensing, biology, and medicine. *Accounts of Chemical Research,* 41, 1578-1586.

JAIN, P. K., LEE, K. S., EL-SAYED, I. H. & EL-SAYED, M. A. 2006. Calculated absorption and scattering properties of gold nanoparticles of different size, shape, and composition: Applications in biological imaging and biomedicine. *Journal of Physical Chemistry B,* 110, 7238-7248.

JAMES, A. M., BLAIKIE, F. H., SMITH, R. A. J., LIGHTOWLERS, R. N., SMITH, P. M. & MURPHY, M. P. 2003. Specific targeting of a DNA-alkylating reagent to mitochondria: Synthesis and characterization of [4-((11aS)-7-methoxy-1,2,3,11a-tetrahydro-5H-pyrrolo[2,1-c][1,4] benzodiazepin-5-on-8-oxy)butyl]-triphenylphosphonium iodide. *European Journal of Biochemistry,* 270, 2827-2836.

JAMES, A. M., COCHEM , H. M., SMITH, R. A. J. & MURPHY, M. P. 2005. Interactions of mitochondria-targeted and untargeted ubiquinones with the mitochondrial respiratory chain and reactive oxygen species: Implications for the use of exogenous ubiquinones as therapies and experimental tools. *Journal of Biological Chemistry,* 280, 21295-21312.

JAMES, A. M., SMITH, R. A. J. & MURPHY, M. P. 2004. Antioxidant and prooxidant properties of mitochondrial Coenzyme Q. *Archives of Biochemistry and Biophysics,* 423, 47-56.

JEMAL, A., BRAY, F., CENTER, M. M., FERLAY, J., WARD, E. & FORMAN, D. 2011. Global Cancer Statistics. *Ca-a Cancer Journal for Clinicians,* 61, 69-90.

JOHNSON, L. V., WALSH, M. L. & CHEN, L. B. 1980. Localization of mitochondria in living cells with rhodamine 123. *Proceedings of the National Academy of Sciences of the United States of America,* 77, 990-994.

JONES, R. G. & THOMPSON, C. B. 2009. Tumor suppressors and cell metabolism: A recipe for cancer growth. *Genes and Development,* 23, 537-548.

JU-NAM, Y., ALLEN, D. W., GARDINER, P. H. E. & BRICKLEBANK, N. 2008. ω-Thioacetylalkylphosphonium salts: Precursors for the preparation of phosphonium-functionalised gold nanoparticles. *Journal of Organometallic Chemistry,* 693, 3504-3508.

JU-NAM, Y., BRICKLEBANK, N., ALLEN, D. W., GARDINER, P. H. E., LIGHT, M. E. & HURSTHOUSE, M. B. 2006. Phosphonioalkylthiosulfate zwitterions - new masked thiol ligands for the formation of cationic functionalised gold nanoparticles. *Organic & Biomolecular Chemistry,* 4, 4345-4351.

KALLURI, R. & WEINBERG, R. A. 2009. The basics of epithelial-mesenchymal transition. *Journal of Clinical Investigation,* 119, 1420-1428.

KANG, M. H. & REYNOLDS, C. P. 2009. Bcl-2 Inhibitors: Targeting mitochondrial apoptotic pathways in cancer therapy. *Clinical Cancer Research,* 15, 1126-1132.

KANNAGI, R., IZAWA, M., KOIKE, T., MIYAZAKI, K. & KIMURA, N. 2004. Carbohydrate-mediated cell adhesion in cancer metastasis and angiogenesis. *Cancer Science,* 95, 377-384.

KAYE, S. B. 1998. New antimetabolites in cancer chemotherapy and their clinical impact. *British Journal of Cancer,* 78, 1-7.

KELLY, K. L., CORONADO, E., ZHAO, L. L. & SCHATZ, G. C. 2003. The optical properties of metal nanoparticles: The influence of size, shape,

and dielectric environment. *Journal of Physical Chemistry B,* 107, 668-677.

KELSO, G. F., PORTEOUS, C. M., COULTER, C. V., HUGHES, G., PORTEOUS, W. K., LEDGERWOOD, E. C., SMITH, R. A. J. & MURPHY, M. P. 2001. Selective targeting of a redox-active ubiquinone to mitochondria within cells: Antioxidant and antiapoptotic properties. *Journal of Biological Chemistry,* 276, 4588-4596.

KELSO, G. F., PORTEOUS, C. M., HUGHES, G., LEDGERWOOD, E. C., GANE, A. M., SMITH, R. A. J. & MURPHY, M. P. 2002. Prevention of mitochondrial oxidative damage using targeted antioxidants. *In:* HARMAN, D. (ed.) *Increasing Healthy Life Span: Conventional Measures and Slowing the Innate Aging Process.*

KENNEDY, L. C., BICKFORD, L. R., LEWINSKI, N. A., COUGHLIN, A. J., HU, Y., DAY, E. S., WEST, J. L. & DREZEK, R. A. 2011. A New Era for Cancer Treatment: Gold-Nanoparticle-Mediated Thermal Therapies. *Small,* 7, 169-183.

KERBEL, R. S. 2008. Molecular origins of cancer: Tumor angiogenesis. *New England Journal of Medicine,* 358, 2039-2049.

KHLEBTSOV, N. G. & DYKMAN, L. A. 2010. Optical properties and biomedical applications of plasmonic nanoparticles. *Journal of Quantitative Spectroscopy and Radiative Transfer,* 111, 1-35.

KHOURY, C. G. & VO-DINH, T. 2008. Gold nanostars for surface-enhanced Raman scattering: synthesis, characterization and optimization. *Journal of Physical Chemistry C,* 112, 18849-18859.

KIM, C. K., GHOSH, P. & ROTELLO, V. M. 2009. Multimodal drug delivery using gold nanoparticles. *Nanoscale,* 1, 61-67.

KIM, J. H., STANSBURY, K. H., WALKER, N. J., TRUSH, M. A., STRICKLAND, P. T. & SUTTER, T. R. 1998. Metabolism of benzo a pyrene and benzo a pyrene-7,8-diol by human cytochrome P450 1B1. *Carcinogenesis,* 19, 1847-1853.

KIM, J. S., HE, L. & LEMASTERS, J. J. 2003. Mitochondrial permeability transition: A common pathway to necrosis and apoptosis. *Biochemical and Biophysical Research Communications,* 304, 463-470.

KIM, S. T., SAHA, K., KIM, C. & ROTELLO, V. M. 2013. The role of surface functionality in determining nanoparticle cytotoxicity. *Accounts of Chemical Research,* 46, 681-691.

KING, R. J. B. & ROBINS, M. W. 2006. *Cancer Biology.*

KIRUI, D. K., REY, D. A. & BATT, C. A. 2010. Gold hybrid nanoparticles for targeted phototherapy and cancer imaging. *Nanotechnology,* 21.

KNEIPP, J., KNEIPP, H., WITTIG, B. & KNEIPP, K. 2010. Novel optical nanosensors for probing and imaging live cells. *Nanomedicine: Nanotechnology, Biology, and Medicine,* 6, 214-226.

KNEIPP, K., HAKA, A. S., KNEIPP, H., BADIZADEGAN, K., YOSHIZAWA, N., BOONE, C., SHAFER-PELTIER, K. E., MOTZ, J. T., DASARI, R. R. & FELD, M. S. 2002. Surface-enhanced raman spectroscopy in single living cells using gold nanoparticles. *Applied Spectroscopy,* 56, 150-154.

KNUDSON, A. G. 2001. Two genetic hits (more or less) to cancer. *Nature Reviews Cancer,* 1, 157-162.

KOLEVZON, N., KUFLIK, U., SHMUEL, M., BENHAMRON, S., RINGEL, I. & YAVIN, E. 2011. Multiple triphenylphosphonium cations as a platform for the delivery of a pro-apoptotic peptide. *Pharmaceutical Research,* 28, 2780-2789.

KROEMER, G. & POUYSSEGUR, J. 2008. Tumor Cell Metabolism: Cancer's Achilles' Heel. *Cancer Cell,* 13, 472-482.

KUMAR, A., ZHANG, X. & LIANG, X. J. 2013a. Gold nanoparticles: Emerging paradigm for targeted drug delivery system. *Biotechnology Advances,* 31, 593-606.

KUMAR, D., SAINI, N., JAIN, N., SAREEN, R. & PANDIT, V. 2013b. Gold nanoparticles: an era in bionanotechnology. *Expert Opinion on Drug Delivery,* 10, 397-409.

KUWANA, T. & NEWMEYER, D. D. 2003. Bcl-2-family proteins and the role of mitochondria in apoptosis. *Current Opinion in Cell Biology,* 15, 691-699.

LARSON, T. A., JOSHI, P. P. & SOKOLOV, K. 2012. Preventing protein adsorption and macrophage uptake of gold nanoparticles via a hydrophobic shield. *ACS Nano,* 6, 9182-9190.

LAWLER, J. 2002. Thrombospondin-1 as an endogenous inhibitor of angiogenesis and tumor growth. *Journal of Cellular and Molecular Medicine,* 6, 1-12.

LAYTON, D. W., BOGEN, K. T., KNIZE, M. G., HATCH, F. T., JOHNSON, V. M. & FELTON, J. S. 1995. Cancer risk of heterocyclic amines in cooked food -an analysis and implications for research. *Carcinogenesis,* 16, 39-52.

LEE, S., CHON, H., LEE, M., CHOO, J., SHIN, S. Y., LEE, Y. H., RHYU, I. J., SON, S. W. & OH, C. H. 2009. Surface-enhanced Raman scattering imaging of HER2 cancer markers overexpressed in single MCF7 cells using antibody conjugated hollow gold nanospheres. *Biosensors and Bioelectronics,* 24, 2260-2263.

LEHMANN, A. R., MCGIBBON, D. & STEFANINI, M. 2011. Xeroderma pigmentosum. *Orphanet Journal of Rare Diseases,* 6.

LEI, W., XIE, J., HOU, Y., JIANG, G., ZHANG, H., WANG, P., WANG, X. & ZHANG, B. 2010. Mitochondria-targeting properties and photodynamic activities of porphyrin derivatives bearing cationic pendant. *Journal of Photochemistry and Photobiology B: Biology,* 98, 167-171.

LEMASTERS, J. J., NIEMINEN, A. L., QIAN, T., TROST, L. C., ELMORE, S. P., NISHIMURA, Y., CROWE, R. A., CASCIO, W. E., BRADHAM, C. A., BRENNER, D. A. & HERMAN, B. 1998. The mitochondrial permeability transition in cell death: A common mechanism in necrosis, apoptosis and autophagy. *Biochimica et Biophysica Acta - Bioenergetics,* 1366, 177-196.

LI, J.-L. & GU, M. 2010. Gold-Nanoparticle-Enhanced Cancer Photothermal Therapy. *Ieee Journal of Selected Topics in Quantum Electronics,* 16, 989-996.

LI, J. L., WANG, L., LIU, X. Y., ZHANG, Z. P., GUO, H. C., LIU, W. M. & TANG, S. H. 2009a. In vitro cancer cell imaging and therapy using transferrin-conjugated gold nanoparticles. *Cancer Letters,* 274, 319-326.

LI, Z., LOPEZ, M., HARDY, M., MCALLISTER, D. M., KALYANARAMAN, B. & ZHAO, M. 2009b. A 99mTc-Labeled Triphenylphosphonium Derivative for the Early Detection of Breast Tumors. *Cancer Biotherapy and Radiopharmaceuticals,* 24, 579-587.

LIAO, J. B. 2006. Viruses and human cancer. *The Yale journal of biology and medicine,* 79, 115-22.

LIBERMAN, E. A., TOPALY, V. P., TSOFINA, L. M., JASAITIS, A. A. & SKULACHEV, V. P. 1969. Mechanism of coupling of oxidative

phosphorylation and the membrane potential of mitochondria. *Nature,* 222, 1076-1078.

LIDKE, D. S., NAGY, P., HEINTZMANN, R., ARNDT-JOVIN, D. J., POST, J. N., GRECCO, H. E., JARES-ERIJMAN, E. A. & JOVIN, T. M. 2004. Quantum dot ligands provide new insights into erbB/HER receptor-mediated signal transduction. *Nature Biotechnology,* 22, 198-203.

LINK, S. & EL-SAYED, M. A. 1999. Size and temperature dependence of the plasmon absorption of colloidal gold nanoparticles. *Journal of Physical Chemistry B,* 103, 4212-4217.

LIU, B., PARSONS, R., PAPADOPOULOS, N., NICOLAIDES, N. C., LYNCH, H. T., WATSON, P., JASS, J. R., DUNLOP, M., WYLLIE, A., PELTOM KI, P., DE LA CHAPELLE, A., HAMILTON, S. R., VOGELSTEIN, B. & KINZLER, K. W. 1996. Analysis of mismatch repair genes in hereditary non-polyposis colorectal cancer patients. *Nature Medicine,* 2, 169-174.

LIU, S., KIM, Y. S., ZHAI, S., SHI, J. & HOU, G. 2009. Evaluation of 64Cu(DO3A-xy-TPEP) as a potential PET radiotracer for monitoring tumor multidrug resistance. *Bioconjugate Chemistry,* 20, 790-798.

LIZ-MARZ N, L. M. 2004. Nanometals: Formation and color. *Materials Today,* 7, 26-31.

LLEVOT, A. & ASTRUC, D. 2012. Applications of vectorized gold nanoparticles to the diagnosis and therapy of cancer. *Chemical Society Reviews,* 41, 242-257.

LOO, C., LOWERY, A., HALAS, N., WEST, J. & DREZEK, R. 2005. Immunotargeted nanoshells for integrated cancer imaging and therapy. *Nano Letters,* 5, 709-711.

LOVE, J. C., ESTROFF, L. A., KRIEBEL, J. K., NUZZO, R. G. & WHITESIDES, G. M. 2005. Self-assembled monolayers of thiolates on metals as a form of nanotechnology. *Chemical Reviews,* 105, 1103-1169.

LOWE, S. W. & LIN, A. W. 2000. Apoptosis in cancer. *Carcinogenesis,* 21, 485-495.

LYNCH, H. T. & SMYRK, T. 1996. Hereditary nonpolyposis colorectal cancer (Lynch syndrome): An updated review. *Cancer,* 78, 1149-1167.

MADAR, I., WEISS, L. & IZBICKI, G. 2002. Preferential accumulation of 3H-tetraphenylphosphonium in non-small cell lung carcinoma in mice: Comparison with 99mTc-MIBI. *Journal of Nuclear Medicine,* 43, 234-238.

MAHMOOD, Z. & SHUKLA, Y. 2010. Death receptors: Targets for cancer therapy. *Experimental Cell Research,* 316, 887-899.

MALHI, S. S. & MURTHY, R. S. 2012. Delivery to mitochondria: a narrower approach for broader therapeutics. *Expert Opin Drug Deliv,* 9, 909-35.

MANETTA, A., GAMBOA, G., NASSERI, A., PODNOS, Y. D., EMMA, D., DORION, G., RAWLINGS, L., CARPENTER, P. M., BUSTAMANTE, A., PATEL, J. & RIDEOUT, D. 1996. Novel phosphonium salts display in vitro and in vivo cytotoxic activity against human ovarian cancer cell lines. *Gynecologic Oncology,* 60, 203-212.

MANNELLA, C. A. 1998. Conformational changes in the mitochondrial channel protein, VDAC, and their functional implications. *Journal of Structural Biology,* 121, 207-218.

MATSUMURA, Y. & ANANTHASWAMY, H. N. 2004. Toxic effects of ultraviolet radiation on the skin. *Toxicology and Applied Pharmacology,* 195, 298-308.

MCCARTHY, J. R. & WEISSLEDER, R. 2008. Multifunctional magnetic nanoparticles for targeted imaging and therapy. *Advanced Drug Delivery Reviews,* 60, 1241-1251.

MICALIZZI, D. S., FARABAUGH, S. M. & FORD, H. L. 2010. Epithelial-mesenchymal transition in cancer: parallels between normal development and tumor progression. *Journal of Mammary Gland Biology and Neoplasia,* 15, 117-134.

MIN, J. J., BISWAL, S., DEROOSE, C. & GAMBHIR, S. S. 2004. Tetraphenylphosphonium as a novel molecular probe for imaging tumors. *Journal of Nuclear Medicine,* 45, 636-643.

MIRKIN, C. A., LETSINGER, R. L., MUCIC, R. C. & STORHOFF, J. J. 1996. A DNA-based method for rationally assembling nanoparticles into macroscopic materials. *Nature,* 382, 607-609.

MISRA, R., ACHARYA, S. & SAHOO, S. K. 2010. Cancer nanotechnology: Application of nanotechnology in cancer therapy. *Drug Discovery Today,* 15, 842-850.

MODICA-NAPOLITANO, J. S. & APRILLE, J. R. 1987. Basis for the selective cytotoxicity of rhodamine 123. *Cancer Research,* 47, 4361-4365.

MODICA-NAPOLITANO, J. S. & SINGH, K. K. 2002. Mitochondria as targets for detection and treatment of cancer. *Expert reviews in molecular medicine,* 4, 1-19.

MODICA-NAPOLITANO, J. S. & SINGH, K. K. 2004. Mitochondrial dysfunction in cancer. *Mitochondrion,* 4, 755-762.

MOMAND, J., WU, H. H. & DASGUPTA, G. 2000. MDM2 - master regulator of the p53 tumor suppressor protein. *Gene,* 242, 15-29.

MOORES, A. & GOETTMANN, F. 2006. The plasmon band in noble metal nanoparticles: An introduction to theory and applications. *New Journal of Chemistry,* 30, 1121-1132.

MOSEROVA, M., KOTRBOVA, V., AIMOVA, D., SULC, M., FREI, E. & STIBOROVA, M. 2009. Analysis of benzo a pyrene metabolites formed by rat hepatic microsomes using high pressure liquid chromatography: optimization of the method. *Interdisciplinary toxicology,* 2, 239-44.

MURATA, T., HIBASAMI, H., MAEKAWA, S., TAGAWA, T. & NAKASHIMA, K. 1990. Preferential binding of cisplatin to mitochondrial DNA and suppression of ATP generation in human malignant melanoma cells. *Biochemistry International,* 20, 949-955.

MURPHY, M. P. 1997. Selective targeting of bioactive compounds to mitochondria. *Trends in Biotechnology,* 15, 326-330.

MURPHY, M. P. 2008. Targeting lipophilic cations to mitochondria. *Biochimica et Biophysica Acta - Bioenergetics,* 1777, 1028-1031.

MURPHY, M. P., ECHTAY, K. S., BLAIKIE, F. H., ASIN-CAYUELAT, J., COCHEM , H. M., GREEN, K., BUCKINGHAM, J. A., TAYLORT, E. R., HURRELLT, F., HUGHES, G., MIWA, S., COOPER, C. E., SVISTUNENKO, D. A., SMITH, R. A. J. & BRAND, M. D. 2003. Superoxide activates uncoupling proteins by generating carbon-centered radicals and initiating lipid peroxidation: Studies using a mitochondria-targeted spin trap derived from α-phenyl-N-tert-butylnitrone. *Journal of Biological Chemistry,* 278, 48534-48545.

MURPHY, M. P. & SMITH, R. A. J. 2000. Drug delivery to mitochondria: The key to mitochondrial medicine. *Advanced Drug Delivery Reviews,* 41, 235-250.

MURPHY, M. P. & SMITH, R. A. J. 2007. Targeting antioxidants to mitochondria by conjugation to lipophilic cations.

NADEAU, J., ZHANG, E. & CHIBLI, H. Enhanced cytotoxicity of doxorubicin conjugated to ultrasmall Au nanoparticles. 2010. 316-319.

NARAYANAN, D. L., SALADI, R. N. & FOX, J. L. 2010. Ultraviolet radiation and skin cancer. *International Journal of Dermatology,* 49, 978-986.

NARISAWA-SAITO, M. & KIYONO, T. 2007. Basic mechanisms of high-risk human papillomavirus-induced carcinogenesis: Roles of E6 and E7 proteins. *Cancer Science,* 98, 1505-1511.

NEGRINI, S., GORGOULIS, V. G. & HALAZONETIS, T. D. 2010. Genomic instability an evolving hallmark of cancer. *Nature Reviews Molecular Cell Biology,* 11, 220-228.

NEVINS, J. R. 2001. The Rb/E2F pathway and cancer. *Human Molecular Genetics,* 10, 699-703.

NIE, S. M., XING, Y., KIM, G. J. & SIMONS, J. W. 2007. Nanotechnology applications in cancer. *Annual Review of Biomedical Engineering.*

NISHIDA, N., YANO, H., NISHIDA, T., KAMURA, T. & KOJIRO, M. 2006. Angiogenesis in cancer. *Vascular health and risk management,* 2, 213-9.

NORMANNO, N., DE LUCA, A., BIANCO, C., STRIZZI, L., MANCINO, M., MAIELLO, M. R., CAROTENUTO, A., DE FEO, G., CAPONIGRO, F. & SALOMON, D. S. 2006. Epidermal growth factor receptor (EGFR) signaling in cancer. *Gene,* 366, 2-16.

OLAUSSEN, K. A., DUBRANA, K., DOMONT, J., SPANO, J. P., SABATIER, L. & SORIA, J. C. 2006. Telomeres and telomerase as targets for anticancer drug development. *Critical Reviews in Oncology/Hematology,* 57, 191-214.

OSTHUS, R. C., SHIM, H., KIM, S., LI, Q., REDDY, R., MUKHERJEE, M., XU, Y., WONSEY, D., LEE, L. A. & DANG, C. V. 2000. Deregulation of glucose transporter 1 and glycolytic gene expression by c-Myc. *Journal of Biological Chemistry,* 275, 21797-21800.

PACIOTTI, G. F., MYER, L., WEINREICH, D., GOIA, D., PAVEL, N., MCLAUGHLIN, R. E. & TAMARKIN, L. 2004. Colloidal gold: a novel nanoparticle vector for tumor directed drug delivery. *Drug Delivery: Journal of Delivery and Targeting of Therapeutic Agents,* 11, 169-183.

PANKHURST, Q. A., CONNOLLY, J., JONES, S. K. & DOBSON, J. 2003. Applications of magnetic nanoparticles in biomedicine. *Journal of Physics D: Applied Physics,* 36, R167-R181.

PAPAVRAMIDOU, N., PAPAVRAMIDIS, T. & DEMETRIOU, T. 2010. Ancient Greek and Greco-Roman Methods in Modern Surgical Treatment of Cancer. *Annals of Surgical Oncology,* 17, 665-667.

PARFENOV, A. S., SALNIKOV, V., LEDERER, W. J. & LUKY NENKO, V. 2006. Aqueous diffusion pathways as a part of the ventricular cell ultrastructure. *Biophysical Journal,* 90, 1107-1119.

PARSONS, M. J. & GREEN, D. R. 2010. Mitochondria in cell death. *Essays in Biochemistry,* 47, 99-114.

PATEL, J., RIDEOUT, D., MCCARTHY, M. R., CALOGEROPOULOU, T., WADWA, K. S. & OSEROFF, A. R. 1994. Antineoplastic activity, synergism, and antagonism of triarylalkylphosphonium salts and their combinations. *Anticancer Research,* 14, 21-28.

PATEL, N. R., HATZIANTONIOU, S., GEORGOPOULOS, A., DEMETZOS, C., TORCHILIN, V. P., WEISSIG, V. & D'SOUZA, G. G. M. 2010.

Mitochondria-targeted liposomes improve the apoptotic and cytotoxic action of sclareol. *Journal of Liposome Research,* 20, 244-249.

PATHANIA, D., MILLARD, M. & NEAMATI, N. 2009. Opportunities in discovery and delivery of anticancer drugs targeting mitochondria and cancer cell metabolism. *Advanced Drug Delivery Reviews,* 61, 1250-1275.

PEER, D., KARP, J. M., HONG, S., FAROKHZAD, O. C., MARGALIT, R. & LANGER, R. 2007. Nanocarriers as an emerging platform for cancer therapy. *Nature Nanotechnology,* 2, 751-760.

PERONA, R. 2006. Cell signalling: Growth factors and tyrosine kinase receptors. *Clinical and Translational Oncology,* 8, 77-82.

PETO, R., DARBY, S., DEO, H., SILCOCKS, P., WHITLEY, E. & DOLL, R. 2000. Smoking, smoking cessation, and lung cancer in the UK since 1950: combination of national statistics with two case-control studies. *British Medical Journal,* 321, 323-329.

PFEIFER, G. P., DENISSENKO, M. F., OLIVIER, M., TRETYAKOVA, N., HECHT, S. S. & HAINAUT, P. 2002. Tobacco smoke carcinogens, DNA damage and p53 mutations in smoking-associated cancers. *Oncogene,* 21, 7435-7451.

PISSUWAN, D., NIIDOME, T. & CORTIE, M. B. 2011. The forthcoming applications of gold nanoparticles in drug and gene delivery systems. *Journal of Controlled Release,* 149, 65-71.

PITSILLIDES, C. M., JOE, E. K., WEI, X. B., ANDERSON, R. R. & LIN, C. P. 2003. Selective cell targeting with light-absorbing microparticles and nanoparticles. *Biophysical Journal,* 84, 4023-4032.

PORTEOUS, C. M., LOGAN, A., EVANS, C., LEDGERWOOD, E. C., MENON, D. K., AIGBIRHIO, F., SMITH, R. A. J. & MURPHY, M. P. 2010. Rapid uptake of lipophilic triphenylphosphonium cations by mitochondria in vivo following intravenous injection: Implications for mitochondria-specific therapies and probes. *Biochimica et Biophysica Acta - General Subjects,* 1800, 1009-1017.

PORTNEY, N. G. & OZKAN, M. 2006. Nano-oncology: Drug delivery, imaging, and sensing. *Analytical and Bioanalytical Chemistry,* 384, 620-630.

PRENDERGAST, G. C. 2008. Immune escape as a fundamental trait of cancer: Focus on IDO. *Oncogene,* 27, 3889-3900.

PULKES, T. & HANNA, M. G. 2001. Human mitochondrial DNA diseases. *Advanced Drug Delivery Reviews,* 49, 27-43.

RAHA, S. & ROBINSON, B. H. 2000. Mitochondria, oxygen free radicals, disease and ageing. *Trends in Biochemical Sciences,* 25, 502-508.

RAJAPUTRA, P., NKEPANG, G., WATLEY, R. & YOU, Y. 2013. Synthesis and in vitro biological evaluation of lipophilic cation conjugated photosensitizers for targeting mitochondria. *Bioorganic and Medicinal Chemistry,* 21, 379-387.

RANA, S., BAJAJ, A., MOUT, R. & ROTELLO, V. M. 2012. Monolayer coated gold nanoparticles for delivery applications. *Advanced Drug Delivery Reviews,* 64, 200-216.

RASCHKE, G., KOWARIK, S., FRANZL, T., S NNICHSEN, C., KLAR, T. A., FELDMANN, J., NICHTL, A. & K RZINGER, K. 2003. Biomolecular recognition based on single gold nanoparticle light scattering. *Nano Letters,* 3, 935-938.

RICHTER, M., KARSCHIN, A., SPINGLER, B., KUNZ, P. C., MEYER-ZAIKA, W. & KL UI, W. 2012. Stabilisation of water-soluble platinum nanoparticles by phosphonic acid derivatives. *Dalton Transactions,* 41, 3407-3413.

RIDEOUT, D., BUSTAMANTE, A. & PATEL, J. 1994. Mechanism of inhibition of FaDu hypopharyngeal carcinoma cell growth by tetraphenylphosphonium chloride. *International Journal of Cancer,* 57, 247-253.

RIDEOUT, D. C., CALOGEROPOULOU, T., JAWORSKI, J. S., DAGNINO R, R. J. & MCCARTHY, M. R. 1989. Phosphonium salts exhibiting selective anti-carcinoma activity in vitro. *Anti-Cancer Drug Design,* 4, 265-280.

RIEDL, S. J. & SALVESEN, G. S. 2007. The apoptosome: Signalling platform of cell death. *Nature Reviews Molecular Cell Biology,* 8, 405-413.

RIEDL, S. J. & SHI, Y. G. 2004. Molecular mechanisms of caspase regulation during apoptosis. *Nature Reviews Molecular Cell Biology,* 5, 897-907.

RIGGIO, C., PAGNI, E., RAFFA, V. & CUSCHIERI, A. 2011. Nano-oncology: Clinical application for cancer therapy and future perspectives. *Journal of Nanomaterials,* 2011.

RIVERA GIL, P., H HN, D., DEL MERCATO, L. L., SASSE, D. & PARAK, W. J. 2010. Nanopharmacy: Inorganic nanoscale devices as vectors and active compounds. *Pharmacological Research,* 62, 115-125.

ROJANATHANES, R., SEREEMASPUN, A., PIMPHA, N., BUASORN, V., EKAWONG, P. & WIWANITKIT, V. 2008. Gold nanoparticle as an alternative tool for a urine pregnancy test. *Taiwanese Journal of Obstetrics and Gynecology,* 47, 296-299.

ROSI, N. L. & MIRKIN, C. A. 2005. Nanostructures in biodiagnostics. *Chemical Reviews,* 105, 1547-1562.

ROSS, M. F., KELSO, G. F., BLAIKIE, F. H., JAMES, A. M., COCHEM , H. M., FILIPOVSKA, A., DA ROS, T., HURD, T. R., SMITH, R. A. J. & MURPHY, M. P. 2005. Lipophilic triphenylphosphonium cations as tools in mitochondrial bioenergetics and free radical biology. *Biochemistry (Moscow),* 70, 222-230.

ROSS, M. F., PRIME, T. A., ABAKUMOVA, I., JAMES, A. M., PORTEOUS, C. M., SMITH, R. A. J. & MURPHY, M. P. 2008. Rapid and extensive uptake and activation of hydrophobic triphenylphosphonium cations within cells. *Biochemical Journal,* 411, 633-645.

ROSTOVTSEVA, T. K., TAN, W. & COLOMBINI, M. 2005. On the role of VDAC in apoptosis: Fact and fiction. *Journal of Bioenergetics and Biomembranes,* 37, 129-142.

ROUHANA, L. L., JABER, J. A. & SCHLENOFF, J. B. 2007. Aggregation-resistant water-soluble gold nanoparticles. *Langmuir,* 23, 12799-12801.

SALK, J. J., FOX, E. J. & LOEB, L. A. 2010. Mutational Heterogeneity in Human Cancers: Origin and Consequences.

SALNIKOV, V., LUKY NENKO, Y. O., FREDERICK, C. A., LEDERER, W. J. & LUKY NENKO, V. 2007. Probing the outer mitochondrial membrane in cardiac mitochondria with nanoparticles. *Biophysical Journal,* 92, 1058-1071.

SAMALI, A., ZHIVOTOVSKY, B., JONES, D., NAGATA, S. & ORRENIUS, S. 1999. Apoptosis: Cell death defined by caspase activation [1]. *Cell Death and Differentiation,* 6, 495-496.

SANNA, V., PALA, N. & SECHI, M. 2014. Targeted therapy using nanotechnology: Focus on cancer. *International Journal of Nanomedicine,* 9, 467-483.

SAYERS, T. J. & CROSS, N. A. 2014. Triggering death receptors as a means of inducing tumoricidal activity *In:* REES, R. C. (ed.) *Tumor Immunology and Immunotherapy.* Oxford: Oxford University Press.

SCHEINBERG, D. A., VILLA, C. H., ESCORCIA, F. E. & MCDEVITT, M. R. 2010. Conscripts of the infinite armada: systemic cancer therapy using nanomaterials. *Nature Reviews Clinical Oncology, 7*, 266-276.

SCHUT, H. A. J. & SNYDERWINE, E. G. 1999. DNA adducts of heterocyclic amine food mutagens: implications for mutagenesis and carcinogenesis. *Carcinogenesis, 20*, 353-368.

SCHWARTZ, M. P. & MATOUSCHEK, A. 1999. The dimensions of the protein import channels in the outer and inner mitochondrial membranes. *Proceedings of the National Academy of Sciences of the United States of America, 96*, 13086-13090.

SCHWARZ, D., KISSELEV, P., CASCORBI, I., SCHUNCK, W. H. & ROOTS, I. 2001. Differential metabolism of benzo a pyrene and benzo a pyrene-7,8-dihydrodiol by human CYP1A1 variants. *Carcinogenesis, 22*, 453-459.

SCOTT, A. M., WOLCHOK, J. D. & OLD, L. J. 2012. Antibody therapy of cancer. *Nature Reviews Cancer, 12*, 278-287.

SEHY, D. W., SHAO, L. E., RIDEOUT, D. & YU, J. 1993. Sensitivity of committed hematopoietic progenitor cells in vitro (BFU-E, CFU-E, CFU-GM) and two human carcinoma cell lines toward rhodamine-123 and phosphonium salt II-41. *Leukemia Research, 17*, 247-253.

SEMENZA, G. L. 2010. Defining the role of hypoxia-inducible factor 1 in cancer biology and therapeutics. *Oncogene, 29*, 625-634.

SHAN, J. & TENHU, H. 2007. Recent advances in polymer protected gold nanoparticles: Synthesis, properties and applications. *Chemical Communications*, 4580-4598.

SHANKAR, S. S., RAI, A., ANKAMWAR, B., SINGH, A., AHMAD, A. & SASTRY, M. 2004. Biological synthesis of triangular gold nanoprisms. *Nature Materials, 3*, 482-488.

SHAY, J. W. & WRIGHT, W. E. 2000. Hayflick, his limit, and cellular ageing. *Nature Reviews Molecular Cell Biology, 1*, 72-76.

SHAY, J. W. & WRIGHT, W. E. 2002. Telomerase: A target for cancer therapeutics. *Cancer Cell, 2*, 257-265.

SHAY, J. W. & WRIGHT, W. E. 2006. Telomerase therapeutics for cancer: Challenges and new directions. *Nature Reviews Drug Discovery, 5*, 577-584.

SHEM, P. M., SARDAR, R. & SHUMAKER-PARRY, J. S. 2009. One-step synthesis of phosphine-stabilized gold nanoparticles using the mild reducing agent 9-BBN. *Langmuir, 25*, 13279-13283.

SHERR, C. J. & MCCORMICK, F. 2002. The RB and p53 pathways in cancer. *Cancer Cell, 2*, 103-112.

SHEU, S. S., NAUDURI, D. & ANDERS, M. W. 2006. Targeting antioxidants to mitochondria: A new therapeutic direction. *Biochimica et Biophysica Acta - Molecular Basis of Disease, 1762*, 256-265.

SINGH, K. K. 2001. Mitochondrial me and the Mitochondrion journal. *Mitochondrion, 1*, 1-2.

SISKIND, L. J., KOLESNICK, R. N. & COLOMBINI, M. 2006. Ceramide forms channels in mitochondrial outer membranes at physiologically relevant concentrations. *Mitochondrion, 6*, 118-125.

SKRABALAK, S. E., CHEN, J., SUN, Y., LU, X., AU, L., COBLEY, C. M. & XIA, Y. 2008. Gold nanocages: Synthesis, properties, and applications. *Accounts of Chemical Research, 41*, 1587-1595.

SMITH, R. A. J., HARTLEY, R. C., COCHEM , H. M. & MURPHY, M. P. 2012. Mitochondrial pharmacology. *Trends in Pharmacological Sciences,* 33, 341-352.

SMITH, R. A. J., HARTLEY, R. C. & MURPHY, M. P. 2011. Mitochondria-targeted small molecule therapeutics and probes. *Antioxidants and Redox Signaling,* 15, 3021-3038.

SMITH, R. A. J., KELSO, G. F., JAMES, A. M. & MURPHY, M. P. 2004. Targeting Coenzyme Q Derivatives to Mitochondria.

SMITH, R. A. J., PORTEOUS, C. M., COULTER, C. V. & MURPHY, M. P. 1999. Selective targeting of an antioxidant to mitochondria. *European Journal of Biochemistry,* 263, 709-716.

SMITH, R. A. J., PORTEOUS, C. M., GANE, A. M. & MURPHY, M. P. 2003. Delivery of bioactive molecules to mitochondria in vivo. *Proceedings of the National Academy of Sciences of the United States of America,* 100, 5407-5412.

SOKOLOV, K., AARON, J., HSU, B., NIDA, D., GILLENWATER, A., FOLLEN, M., MACAULAY, C., ADLER-STORTHZ, K., KORGEL, B., DESCOUR, M., PASQUALINI, R., ARAP, W., LAM, W. & RICHARDS-KORTUM, R. 2003a. Optical Systems for In Vivo Molecular Imaging of Cancer. *Technology in Cancer Research and Treatment,* 2, 491-504.

SOKOLOV, K., FOLLEN, M., AARON, J., PAVLOVA, I., MALPICA, A., LOTAN, R. & RICHARDS-KORTUM, R. 2003b. Real-time vital optical imaging of precancer using anti-epidermal growth factor receptor antibodies conjugated to gold nanoparticles. *Cancer Research,* 63, 1999-2004.

SPERLING, R. A., RIVERA GIL, P., ZHANG, F., ZANELLA, M. & PARAK, W. J. 2008. Biological applications of gold nanoparticles. *Chemical Society Reviews,* 37, 1896-1908.

SRINIVAS, P. R., BARKER, P. & SRIVASTAVA, S. 2002. Nanotechnology in early detection of cancer. *Laboratory Investigation,* 82, 657-662.

SRIVASTAVA, P. C., HAY, H. G. & KNAPP JR, F. F. 1985. Effects of alkyl and aryl substitution on the myocardial specificity of radioiodinated phosphonium, arsonium, and ammonium cations. *Journal of Medicinal Chemistry,* 28, 901-904.

STEICHEN, J. D., WEISS, M. J., ELMALEH, D. R. & MARTUZA, R. L. 1991. Enhanced in vitro uptake and retention of 3H-tetraphenylphosphonium by nervous system tumor cells. *Journal of Neurosurgery,* 74, 116-122.

SUGIMURA, T., WAKABAYASHI, K., NAKAGAMA, H. & NAGAO, M. 2004. Heterocyclic amines: Mutagens/carcinogens produced during cooking of meat and fish. *Cancer Science,* 95, 290-299.

SUMMERHAYES, I. C., LAMPIDIS, T. J., BERNAL, S. D., NADAKAVUKAREN, J. J., NADAKAVUKAREN, K. K., SHEPHERD, E. L. & CHEN, L. B. 1982. Unusual retention of rhodamine 123 by mitochondria in muscle and carcinoma cells. *Proceedings of the National Academy of Sciences of the United States of America,* 79, 5292-5296.

TALMADGE, J. E. & FIDLER, I. J. 2010. AACR Centennial Series: The Biology of Cancer Metastasis: Historical Perspective. *Cancer Research,* 70, 5649-5669.

TEMPLETON, A. C., WUELFING, W. P. & MURRAY, R. W. 2000. Monolayer-protected cluster molecules. *Accounts of Chemical Research,* 33, 27-36.

THORNBERRY, N. A. & LAZEBNIK, Y. 1998. Caspases: Enemies within. *Science,* 281, 1312-1316.

TLSTY, T. D. & COUSSENS, L. M. 2006. Tumor stroma and regulation of cancer development. *Annual Review of Pathology-Mechanisms of Disease.*

TOWNSON, J. L., NAUMOV, G. N. & CHAMBERS, A. F. 2003. The role of apoptosis in tumor progression and metastasis. *Current Molecular Medicine,* 3, 631-642.

TRACHOOTHAM, D., ALEXANDRE, J. & HUANG, P. 2009. Targeting cancer cells by ROS-mediated mechanisms: A radical therapeutic approach? *Nature Reviews Drug Discovery,* 8, 579-591.

TUPPEN, H. A. L., BLAKELY, E. L., TURNBULL, D. M. & TAYLOR, R. W. 2010. Mitochondrial DNA mutations and human disease. *Biochimica Et Biophysica Acta-Bioenergetics,* 1797, 113-128.

TURESKY, R. J., LANG, N. P., BUTLER, M. A., TEITEL, C. H. & KADLUBAR, F. F. 1991. Metabolic-activation of carcinogenic heterocylic aromstic-amines by human liver and colon. *Carcinogenesis,* 12, 1839-1845.

TURKEVICH, J., STEVENSON, P. C. & HILLIER, J. 1953. The formation of colloidal gold. *Journal of Physical Chemistry,* 57, 670-673.

UNDERWOOD, C. E. & CROSS, S. S. 2009. *General and systematic pathology,* Endinburgh, Churchill Livingstone.

UREN, A. G., KOOL, J., BERNS, A. & VAN LOHUIZEN, M. 2005. Retroviral insertional mutagenesis: past, present and future. *Oncogene,* 24, 7656-7672.

URRUTICOECHEA, A., ALEMANY, R., BALART, J., VILLANUEVA, A., VINALS, F. & CAPELLA, G. 2010. Recent Advances in Cancer Therapy: An Overview. *Current Pharmaceutical Design,* 16, 3-10.

VALASTYAN, S. & WEINBERG, R. A. 2011. Tumor Metastasis: Molecular Insights and Evolving Paradigms. *Cell,* 147, 275-292.

VAUTHIER, C., TSAPIS, N. & COUVREUR, P. 2011. Nanoparticles: Heating tumors to death? *Nanomedicine,* 6, 99-109.

VERMA, A. & STELLACCI, F. 2010. Effect of surface properties on nanoparticle-cell interactions. *Small,* 6, 12-21.

VIGDERMAN, L., KHANAL, B. P. & ZUBAREV, E. R. 2012. Functional gold nanorods: synthesis, self-assembly, and sensing applications. *Advanced Materials,* 24, 4811-4841.

VOGELSTEIN, B. & KINZLER, K. W. 1993. The multistep nature of cancer. *Trends in Genetics,* 9, 138-141.

VOGELSTEIN, B. & KINZLER, K. W. 2004. Cancer genes and the pathways they control. *Nature Medicine,* 10, 789-799.

VOGLER, M., DINSDALE, D., SUN, X. M., YOUNG, K. W., BUTTERWORTH, M., NICOTERA, P., DYER, M. J. S. & COHEN, G. M. 2008. A novel paradigm for rapid ABT-737-induced apoptosis involving outer mitochondrial membrane rupture in primary leukemia and lymphoma cells. *Cell Death and Differentiation,* 15, 820-830.

VOURA, E. B., JAISWAL, J. K., MATTOUSSI, H. & SIMON, S. M. 2004. Tracking metastatic tumor cell extravasation with quantum dot nanocrystals and fluorescence emission-scanning microscopy. *Nature Medicine,* 10, 993-998.

WAGNER, V., DULLAART, A., BOCK, A. K. & ZWECK, A. 2006. The emerging nanomedicine landscape. *Nature Biotechnology,* 24, 1211-1217.

WAKEFORD, R. 2004. The cancer epidemiology of radiation. *Oncogene,* 23, 6404-6428.

WALKEY, C. D., OLSEN, J. B., GUO, H., EMILI, A. & CHAN, W. C. W. 2012. Nanoparticle size and surface chemistry determine serum protein adsorption and macrophage uptake. *Journal of the American Chemical Society,* 134, 2139-2147.

WALLACE, D. C. 2005. A mitochondrial paradigm of metabolic and degenerative diseases, aging, and cancer: A dawn for evolutionary medicine.

WALLACE, D. C. 2012. Mitochondria and cancer. *Nature Reviews Cancer,* 12, 685-698.

WALLING, M. A., NOVAK, J. A. & SHEPARD, J. R. E. 2009. Quantum dots for live cell and in vivo imaging. *International Journal of Molecular Sciences,* 10, 441-491.

WANG, A. Z., LANGER, R. & FAROKHZAD, O. C. 2012. Nanoparticle delivery of cancer drugs.

WANG, F., OGASAWARA, M. A. & HUANG, P. 2010. Small mitochondria-targeting molecules as anti-cancer agents. *Molecular Aspects of Medicine,* 31, 75-92.

WANG, J. & LENARDO, M. J. 2000. Roles of caspases in apoptosis, development, and cytokine maturation revealed by homozygous gene deficiencies. *Journal of Cell Science,* 113, 753-757.

WANG, J., YANG, C. T., KIM, Y. S., SREERAMA, S. G., CAO, Q., LI, Z. B., HE, Z., CHEN, X. & LIU, S. 2007. 64Cu-labeled triphenylphosphonium and triphenylarsonium cations as highly tumor-selective imaging agents. *Journal of Medicinal Chemistry,* 50, 5057-5069.

WANG, M. & THANOU, M. 2010. Targeting nanoparticles to cancer. *Pharmacological Research,* 62, 90-99.

WANG, S. 2010. Trail: A sword for killing tumors. *Current Medicinal Chemistry,* 17, 3309-3317.

WANG, X. 2001. The expanding role of mitochondria in apoptosis. *Genes and Development,* 15, 2922-2933.

WANG, Z. & MA, L. 2009. Gold nanoparticle probes. *Coordination Chemistry Reviews,* 253, 1607-1618.

WEINBERG, R. A. 1995. The retinoblastoma protein and cell cycle control. *Cell,* 81, 323-330.

WEINBERG, R. A. 2013. *The Biology of Cancer,* New York, Garland Science.

WEISSIG, V. 2003. Mitochondrial-targeted drug and DNA delivery. *Critical Reviews in Therapeutic Drug Carrier Systems,* 20, 1-62.

WEISSIG, V. 2005. Targeted drug delivery to mammalian mitochondria in living cells. *Expert Opinion on Drug Delivery,* 2, 89-102.

WEISSIG, V., BODDAPATI, S., JABR, L. & D'SOUZA, G. G. 2007. Mitochondria-specific nanotechnology. *Nanomedicine,* 2, 275-285.

WEISSIG, V., BODDAPATI, S. V., CHENG, S. M. & D'SOUZA, G. G. M. 2006. Liposomes and liposome-like vesicles for drug and DNA delivery to mitochondria. *Journal of Liposome Research,* 16, 249-264.

WEISSIG, V., CHENG, S. M. & D'SOUZA, G. G. M. 2004. Mitochondrial pharmaceutics. *Mitochondrion,* 3, 229-244.

WEISSIG, V., LASCH, J., ERDOS, G., MEYER, H. W., ROWE, T. C. & HUGHES, J. 1998. DQAsomes: A novel potential drug and gene delivery system made from dequalinium(TM). *Pharmaceutical Research,* 15, 334-337.

WEISSIG, V. & TORCHILIN, V. P. 2000. Mitochondriotropic cationic vesicles: a strategy towards mitochondrial gene therapy. *Curr Pharm Biotechnol*, 1, 325-46.

WHIBLEY, C., PHAROAH, P. D. P. & HOLLSTEIN, M. 2009. p53 polymorphisms: cancer implications. *Nature Reviews Cancer*, 9, 95-107.

WILSON, R. 2008. The use of gold nanoparticles in diagnostics and detection. *Chemical Society Reviews*, 37, 2028-2045.

WITSCH, E., SELA, M. & YARDEN, Y. 2010. Roles for Growth Factors in Cancer Progression. *Physiology*, 25, 85-101.

WIWANITKIT, V., SEREEMASPUN, A. & ROJANATHANES, R. 2007. Gold nanoparticle as an alternative tool for urine microalbumin test: The first world report. *Renal Failure*, 29, 1047-1048.

WOGAN, G. N., HECHT, S. S., FELTON, J. S., CONNEY, A. H. & LOEB, L. A. 2004. Environmental and chemical carcinogenesis. *Seminars in Cancer Biology*, 14, 473-486.

WONG, W. W. L. & PUTHALAKATH, H. 2008. Bcl-2 family proteins: The sentinels of the mitochondrial apoptosis pathway. *IUBMB Life*, 60, 390-397.

WYLLIE, A. H. 2010. "where, o death, is thy sting?" A brief review of apoptosis biology. *Molecular Neurobiology*, 42, 4-9.

WYLLIE, A. H., KERR, J. F. & CURRIE, A. R. 1980. Cell death: the significance of apoptosis. *Int Rev Cytol*, 68, 251-306.

YAMAZAKI, N., KOJIMA, S., BOVIN, N. V., ANDRE, S., GABIUS, S. & GABIUS, H. J. 2000. Endogenous lectins as targets for drug delivery. *Advanced Drug Delivery Reviews*, 43, 225-244.

YANG, C. T., KIM, Y. S., WANG, J., WANG, L., SHI, J., LI, Z. B., CHEN, X., FAN, M., LI, J. J. & LIU, S. 2008. 64Cu-labeled 2-(diphenylphosphoryl)ethyldiphenylphosphonium cations as highly selective tumor imaging agents: Effects of linkers and chelates on radiotracer biodistribution characteristics. *Bioconjugate Chemistry*, 19, 2008-2022.

YANG, C. T., LI, Y. & LIU, S. 2007. Synthesis and structural characterization of complexes of a DO3A-conjugated triphenylphosphonium cation with diagnostically important metal ions. *Inorganic Chemistry*, 46, 8988-8997.

YANG, P. H., SUN, X., CHIU, J. F., SUN, H. & HE, Q. Y. 2005. Transferrin-mediated gold nanoparticle cellular uptakeP. *Bioconjugate Chemistry*, 16, 494-496.

YOKOTA, J. 2000. Tumor progression and metastasis. *Carcinogenesis*, 21, 497-503.

YOKOTA, J. & SUGIMURA, T. 1993. Multiple steps in carcinogenesis involving alterations of multiple tumor suppressor genes. *Faseb Journal*, 7, 920-925.

YOUSIF, L. F., STEWART, K. M., HORTON, K. L. & KELLEY, S. O. 2009a. Mitochondria-penetrating peptides: Sequence effects and model cargo transport. *ChemBioChem*, 10, 2081-2088.

YOUSIF, L. F., STEWART, K. M. & KELLEY, S. O. 2009b. Targeting mitochondria with organelle-specific compounds: Strategies and applications. *ChemBioChem*, 10, 1939-1950.

ZAGOROVSKY, K. & CHAN, W. C. W. 2013. A plasmonic DNAzyme strategy for point-of-care genetic detection of infectious pathogens. *Angewandte Chemie - International Edition*, 52, 3168-3171.

ZAMBLE, D. B. & LIPPARD, S. J. 1995. CISPLATIN AND DNA-REPAIR IN CANCER-CHEMOTHERAPY. *Trends in Biochemical Sciences,* 20, 435-439.

ZENG, D., LUO, W., LI, J., LIU, H., MA, H., HUANG, Q. & FAN, C. 2012. Gold nanoparticles-based nanoconjugates for enhanced enzyme cascade and glucose sensing. *Analyst,* 137, 4435-4439.

ZHOU, Y. & LIU, S. 2011. 64Cu-labeled phosphonium cations as PET radiotracers for tumor imaging. *Bioconjugate Chemistry,* 22, 1459-1472.

ZHU, Z. J., GHOSH, P. S., MIRANDA, O. R., VACHET, R. W. & ROTELLO, V. M. 2008. Multiplexed screening of cellular uptake of gold nanoparticles using laser desorption/ionization mass spectrometry. *Journal of the American Chemical Society,* 130, 14139-14143.

ZUR HAUSEN, H. 2002. Papillomaviruses and cancer: From basic studies to clinical application. *Nature Reviews Cancer,* 2, 342-350.

Chapter 2.

Experimental methods

2.1 Solvents

General solvents including acetonitrile (MeCN), methanol (MeOH), ethanol (EtOH), dichloromethane (DCM), diethyl ether were all laboratory grade reagents acquired from Fisher Scientific (Loughborough, Leicestershire, UK). Deionised water (DIH$_2$O) was purified in house by ELGA PURELAB Maxima system (18.2 MΩ).

2.2 Thin Layer Chromatography

Analytical thin layer chromatography (TLC) was performed on Alugram, SIL G/UV$_{254}$ plates using 80:20 DCM:MeOH as the mobile phase. All samples analysed were dissolved in DCM.

2.3 Nuclear Magnetic Resonance

^{1}H and ^{31}P nuclear magnetic resonance (NMR) spectra were obtained in deuterated chloroform (CDCl$_3$) or deuterated DCM (CD$_2$Cl$_2$) on a Brucker AVANCE III (400 MHz) NMR spectrometer (Brucker, Coventry, West Midlands, UK). NMR proton and ^{31}P spectra were interpreted by using NMR interpretation tables (Sørensen, 2006, Duus, 2002).

2.4 Fourier Transform Infrared Spectroscopy

Fourier transform infrared (FTIR) spectra were recorded on a PerkinElmer spectrum 100 FTIR spectrometer (PerkinElmer, Waltham, Massachusetts, USA). FTIR spectra were interpreted using interpretation tables (Günzler and Gremlich, 2002, Larkin, 2011).

2.5 Elemental Analysis

All samples submitted for elemental analysis were dried in an oven at 60°C. Carbon and Hydrogen analysis were carried out by MEDAC Ltd (Chobham, Surrey, UK). Values obtained are compared to the calculated therotically value.

2.6 X-Ray Crystallography

The compounds dissolved in DCM, were placed in a sealed container containing diethyl ether which was left to slowly diffuse into the DCM solution. Samples were than submitted for analysis by the UK National Crystallography

Service at the University of Southampton (School of Chemistry, Highfield, Southampton, UK).

2.7 Ultraviolet-Visible Spectroscopy

Ultraviolet-visible (UV-vis) absorption spectra of aqueous colloidal solutions were recorded at room temperature on a Jenway 6715 UV/Vis spectrophotometer (Bibby Scientific Limited, Stone, Staffordshire, UK) with UV-quartz cuvettes (1 mm optical path). Spectra obtained were compared to spectra reported in the literature for gold nanoparticles of similar size (Daniel and Astruc, 2004).

2.8 Electrospray Ionization Mass Spectrometry

Samples were dissolved in EtOH: DIH_2O (50:50) to a concentration of approximately 1 mg/mL for molecular ion determination. Electrospray mass spectra were recorded using a Thermo Finnigan MAT LCQ classic electrospray ionisation mass spectrometer (ESI-MS) (Thermo Scientific, Sanjose, California, USA) in positive ion mode. Samples were introduced by direct infusion using the syringe pump on the instrument at a flow rate of 5 μL/min with an acquisition time of one minute. Spectra obtained are compared to the expected value of the compounds and calculating the possibility of cleaved peak, to confirm the correct compound has been synthesised.

2.9 Matrix-Assisted Laser Desorption/Ionization Mass Spectrometry

Matrix-assisted laser desorption ionisation mass spectrometry (MALDI-MS)) and laser desorption ionisation mass spectrometry (LDI-MS) experiments were performed in positive ion mode on an applied Biosystems/MDS Sciex hybrid quadrupole time-of-flight mass spectrometer (Q-Star Pulsar-*i)* with an orthogonal MALDI ion source (Applied Biosystems, Foster City, California, USA) and a high repetition Neodymium-doped yttrium vandate (Nd: YVO_4 laser (5 KHz)) (Elforlight Ltd, Daventry, Northamptonshire, UK). Spectrum were collected with an acquisition time of one minute.

In MALDI experiments, the compound analysed was dissolved in a solution of small organic molecules in a solvent called the matrix. Prior to analysis, this

mixture is dried so the solvent is removed, and result in a "solid solution" deposit of analyte-doped matrix crystals. A matrix is incorporated into the sample preparation stage to provide efficient desorption and soft ionisation, hence the name matrix assisted laser desorption ionisation. CHCA is the most common matrix used for the analysis of small molecules and is also known as the universal matrix (Hoffmann and Stroobant, 2007). MALDI matrices were made to a concentration of 10 mg/mL in 70:30 MeCN: water with 0.1% TFA.

MALDI analysis of AuNPs were conducted using an Applied Biosystems MALDI TOF Voyager De-STR mass spectrometer (Applied Biosystems, Foster City, California, USA) equipped with a 355 nm Nd-YAG solid state laser operating at a repetition rate of 60 Hz. 100 shots were accumulated per spectrum, the accelerating voltage was set at 93% and the delay time was 150 ns.

For analysis, the peak area of the analyte was divided by the peak area of the internal standard to give an analyte to internal standard ratio. The standard curve for PPTA and FPPTA are plotted by plotting the concentration of the compound with the respective analyte to internal standard ratio.

2.10 Inductively Coupled Plasma Optical Emission Spectrometry

Inductively coupled plasma optical emission spectrometry (ICP-OES) analyses were performed on a HORIBA Jobin Yvon ACTIVA (HORIBA Scientific, Stanmore, Middlesex, UK). Calibration curves were generated from ICP-standard solutions purchased from Sigma Aldrich (Gillingham, Dorset, UK).

2.11 Thermogravimetric Analysis

Thermogravimetric analyses (TGA) were carried out on a Mettler Toledo (Beaumont Leys, Leicester, UK) TGA/DSC (Materials and Engineering Research Institute, Sheffield Hallam University, Sheffield, UK). 5mg of AuNPs were initially held at 35°C for 15 minutes and then heated to 800°C at 20°C/min with a gas flow rate of 40 mL/min under nitrogen atmosphere.

2.12 X-Ray Photoelectron Spectroscopy

Freeze-dried P-AuNPs were sent to the Experimental Techniques Centre (ETC) at Brunel University for analysis. X-ray photoelectron spectroscopy (XPS) measurements were made on a VG Escalab 210 Photoelectron Spectrometer (ETC, Brunel University, Middlesex, UK). The X-ray source was a non-monochromated Al Kα source (1486.6 eV), operated with an X-ray emission current of 20 mA and an anode high tension (acceleration voltage) of 12 kV. Freeze-dried sample was placed on a standard sample stud using double sided adhesive tape with a take-off angle fixed at 90° relative to the sample plane. The area of each acquisition was 0.79 mm².

Each analysis consisted of a wide survey scan (pass energy 50 eV, 1.0 eV step size) and high-resolution scans (pass energy 50 eV, 0.05 eV step size) for component speciation. The binding energy scale of the instrument was calibrated using the Au $4f_{5/2}$ (83.9 eV), Cu $2p_{3/2}$ (932.7 eV) and Ag $3d_{5/2}$ (368.27 eV) lines of cleaned gold, copper and silver standards obtained from the National Physical Laboratory, UK. CasaXPS 2.3.15 software was used to fit the XPS spectra peaks, and the binding energies obtained in the XPS spectra were corrected for specimen charging by referencing the C 1s to 284.6 eV.

2.13 Secondary Ion Mass Spectrometry

Freeze-dried P-AuNPs were sent to the Experimental Techniques Centre (ETC) at Brunel University for analysis. Secondary ion mapping studies were performed with a Kore Technology Ltd. time-of-flight secondary ion mass spectrometry (TOF-SIMS) instrument (ETC, Brunel University, Middlesex, UK). Using a 25 keV Indium primary ion source 9FEI Liquid Metal Ion Gun operating at 1 µA current. Secondary ions were analysed in a reflectron mass spectrometry and detected with a dual microchannel plate assembly. Flight times were recorded with a 0.5 ns time-to-digital converter. Spectra were taken from an area of approximately 250 x 250 µm. Freeze-dried AuNPs was placed on a standard sample stud using double-sided adhesive tape. Calibration of the mass spectra was established by defining a common series of CxHy peaks with a known mass using the mass calibration function in the instrument's software.

2.14 Transmission Electron Microscopy

For particle size distribution analysis, freeze-dried P-AuNPs were sent to the Experimental Techniques Centre (ETC) at Brunel University for analysis. Freeze-dried P-AuNP samples were re-suspended in ethanol, and placed on a Holey coated copper grid, and the grids were left to dry in air at room temperature. The grid was then examined using a Jeol 2000 FX transmission electron microscope (TEM) (ETC, Brunel University, Middlesex, UK), set at 200 KV. A few images were acquired under bright field mode and particle size distribution was obtained over 1000 AuNPs using Abel imaging software.

PC3 cells treated with P-AuNPs were fixed in 2% aqueous osmium tetroxide and embedded in epoxy resin. The samples were taken to ETC at Brunel University for sectioning using a PowerTome XL Ultramicrotome (Boeckeler, Tuscon, Arizona, USA). The sections 100nm in thickness were placed on a Holey coated copper grid, the grid was then examined using a Joel JEM-2100F TEM, set at 100 KV.

2.15 Cell Culture

Human prostate cancer cells (PC3) obtained from ATTC were maintained in complete media (cDMEM) which contains Dulbecco's modified Eagle medium with GlutaMAX, 4.5 g/L D-Glucose and sodium puruvate (Invitrogen Life Technologies, Paisley, Renfrewshire, UK) containing 10% heat-inactivated fetal bovine serum (Biosera, East Sussex, Sussex, UK) and 1% penicillin-streptomycin (Invitrogen Life Technologies, Paisley, Renfrewshire, UK) at 37°C in 5% CO_2 and 95% air. Cells were sub-cultured every 3 days and routinely screened for mycoplasma.

2.16 Cytotoxicity Assay

Cytotoxicity was assessed using CellTiter-Glo luminescent cell viability assay kit (Promega Corporation, Southampton, Hampshire, UK). Cell viability was measured according to the manufacturer's instructions. In brief plates were equilibrated at room temperature for 30 minutes, 100 µL of assay reagent was added to each well, placed on an orbital shaker for 2 minutes, left to stand at room temperature for 10 minutes and read on a Wallac Victor2 1420 multilabel

80

counter (PerkinElmer, Cambridge, Cambridgeshire, UK). For detailed experimental procedure refer to chapter 4.2.2.

Data obtained are expressed as a percentage of live cells normalised to control. The average, standard deviation and IC_{50} values were plotted and calculated using GraphPad Prism (GraphPad software, La Jolla, California, USA). Staistical analyses were then conducted using the method described below in chapter 2.16.

2.17 Statistical Analysis

Cell viability and microscopy data obtained in this project were found to be non-parametric in distribution, thereby the Kruskall-Wallis with Conver Inman *post hoc* analysis test was used to identify sinficant differences between treatments ($P \leq 0.05$). All statistical analyses were performed on StatsDirect statistics software (StatsDirect Ltd, Cheshire, UK).

2.18 References

DANIEL, M. C. & ASTRUC, D. 2004. Gold nanoparticles: Assembly, supramolecular chemistry, quantum-size-related properties, and applications toward biology, catalysis, and nanotechnology. *Chemical Reviews,* 104, 293-346.

DUUS, J. 2002. Roger S. Macomber. A complete introduction to modern NMR spectroscopy. Wiley, Chichester, 1998, xvii+ 383 pp. Price £45. ISBN 0 471 15736 8. *Magnetic Resonance in Chemistry,* 40, 430-430.

GÜNZLER, H. & GREMLICH, H.-U. 2002. *IR spectroscopy: an introduction,* Weinheim, Wiley-VCH.

HOFFMANN, D., E & STROOBANT, V. 2007. *Mass spectrometry: principles and applications* England, John Wiley & Sons Ltd

LARKIN, P. 2011. *Infrared and Raman spectroscopy: principles and spectral interpretation,* Boston; Amsterdam, Elsevier.

S RENSEN, O. W. 2006. James Keeler. Understanding NMR Spectroscopy. *Magnetic Resonance in Chemistry,* 44, 820-820.

Chapter 3.

The synthesis and characterisation of phosphonium ligands and phosphonium-functionalised gold nanoparticles

3.1 Introduction

Functionalised or tagged AuNPs are readily taken-up by cells making them an attractive delivery platform for transporting drugs, biomolecules and other therapeutic agents into the cells (Giljohann *et al.*, 2010, Thanh and Green, 2010). The surface of AuNPs can be coated with a diverse range of ligands; the most widely used ligands for protecting AuNPs are organic thiolates derived from thiols (Ulman, 1996, Shon et al., 2000) or disulfides (Heister et al., 1999, Biebuyck and Whitesides, 1993).

Thiolate-protected AuNPs offer great stability, can easily be isolated, re-suspended in a range of solvents, and most importantly they can be manipulated and functionalised further with a diverse range of organic and biological compounds to enhance selectivity, sensitivity and practicality for specific applications (Daniel and Astruc, 2004). Other ligands commonly used include citrate (Turkevich *et al.*, 1951, Frens, 1973) and tertiary phosphines (Shem *et al.*, 2009).

Incorporating ionic ligands to the surface of AuNPs is an attractive proposition for improving the aqueous solubility of the AuNPs thereby facilitating cellular uptake and biomolecular recognition through non-covalent interactions (Verma and Stellacci, 2010). Thiolate derivatives of carboxylic acids have been used to produce anionic charged AuNPs (Cho *et al.*, 2009, Song *et al.*, 2003), thiolates incorporating ammonium groups (McIntosh *et al.*, 2001, Sandhu *et al.*, 2002) including tetraoctylammonium thiosulfate (Isaacs *et al.*, 2005) and cetyl trimethylammonium bromide (Vigderman *et al.*, 2012) or other cationic nitrogen systems such as ethidium (Wang *et al.*, 2002) have been used to synthesise cationic charged AuNPs. Zwitterionic ligands for example a thiolate incorporating an ammonium alkyl sulfonate head group (Rouhana *et al.*, 2007) and phosphorylcholine thiolate (Jin *et al.*, 2008), have been employed to generate neutral AuNPs.

While there have been many reports on the use of organophosphorous ligands, particularly phosphines (Shem *et al.*, 2009) and phosphine oxides (Green and O'Brien, 2000) to produce functionalised AuNPs, there have been fewer studies

on the use of organophosphorus ligands to impart functionality. Examples include tris(hydroxymethyl)phosphine which has been used to synthesise AuNPs that form conjugates with DNA (Harnack *et al.*, 2002) and cadmium selenide nanoparticles have been prepared using phosphonium ionic liquid trihexyl(tetradecyl)phosphonium bis(2,4,4-trimethylpentylphosphinate) to enhance surface passivation (Green *et al.*, 2007).

Organic phosphonium salts are an important class of lipophilic cations that are readily taken-up by cells and are preferentially accumulated in the mitochondria; this has resulted in the use of phosphonium compounds as agents for tumour imaging, cancer therapeutics and as intra-cellular transport vectors (Ross *et al.*, 2005). With this in mind Bricklebank and co-workers have previously published the synthesis of a series of phosphonioalkylthiosulfate zwitterions (Ju-Nam *et al.*, 2006) and ω-thioacetylalkylphosphonium salts (Ju-Nam *et al.*, 2008) that behave as "masked thiolate" ligands, in which the thiolate group is protected as a thiosulfate or thioacetate. Under reducing conditions or in contact with the surface of Au, the sulfur-sulfur or sulfur-carbon bond cleaves respectively to yield cationic-functionalised AuNPs.

It has been demonstrated that the rate and extent of uptake of phosphonium compounds *in vitro* are affected by the hydrophobicity of the compound (Ross *et al.*, 2008). The addition of fluorine has been routinely applied in medicinal chemistry to modify the physiochemical properties of drugs; fluorine has been incorporated into compounds to improve metabolic stability, lipophilicity and binding affinity with an overall target to increase the bioavailability of the product (Böhm *et al.*, 2004, Filler and Saha, 2009). Fluorinated drugs have been used to treat a range of human disorders including the central nervous system, cardiovascular diseases, obesity (Kirk, 2006) and cancer (Isanbor and O'Hagan, 2006).

Furthermore phosphonium compounds labelled with radioactive ^{18}F have been developed as a new class of lipophilic positron emission tomography (PET) radiotracers. There is an increasing demand in a clinical setting for PET myocardial perfusion imaging, however conventional single photon emission

tomography (SPECT) suffers from technical limitations including low spatial resolution and tracer inhomogeneities. Although PET overcomes the downfalls of SPECT, PET tracers currently used for myocardial imaging including [13N]-ammonia, 82Rb and [15O]H₂O, all of which have short half-lives and require an on-site cyclotron or generator thus limiting clinical applications of PET (Kim *et al.*, 2012).

Analogues of TPMP labelled with [18F] have been exploited as PET tracers since phosphonium cations exhibit similar properties to popular SPECT tracers such as [99mTc]-sestamibi and [99mTc] tetrofosmin in terms of increasing accumulation in cardiomyocytes compared to normal cells (Madar *et al.*, 2007). A number of [18F] labelled phosphonium radiotracers have been synthesised, these include (4-[18F]fluorophenyl)triphenylphosphonium (a) (Cheng *et al.*, 2005) 3-[18F]fluoropropyltriphenylphosphonium (b) (Ravert *et al.*, 2004), [18F](2-(2-fluoroethoxy)ethyltris(4-methoxyphenyl)phosphonium (d) (Kim *et al.*, 2012) and [18F]-fluorobenzyltriphenylphosphonium (c) (Madar *et al.*, 2006). The latter has also been investigated for quantifying time-dependent apoptotic action both *in vitro* and *in vivo* (Madar *et al.*, 2009).
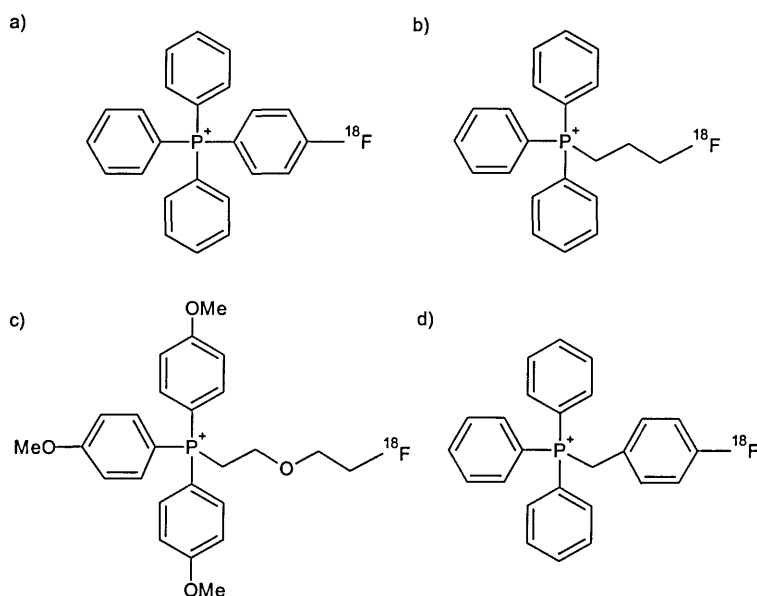
Figure 3.1 Chemical structures of phosphonium PET radiotracers; a) (4-[18F] fluorophenyl)triphenylphosphonium, b)3[18F]fluoropropyltriphenylphosphonium, c) 18F-fluorobenzyltriphenylphosphonium and d) [18F](2-(2-fluoroethyoxy)ethyltris(4-methyoxphenyl)phosphonium.

Recently it has been demonstrated the incorporation of phosphonium groups into the lipid bilayer of liposomes or onto the surface of dendrimers or core-shell nanoparticles can facilitate their preferential uptake by mitochondria (Weissig, 2011, Biswas *et al.*, 2012, Weissig *et al.*, 2008, Weissig *et al.*, 2009, Wang *et al.*, 2013). Thereby the attachment of phosphonium compounds to the surface of nanoparticles has emerged as an attractive proposition for mitochondria-targeted pharmaceutical nanotechnology.

The work presented in this chapter includes the synthesis of phosphonium ligands incorporating fluorine which are used as protecting ligands to produce cationic functionalised AuNPs. In addition the detailed characterisation of water-soluble phosphonioalkylthiolate-capped AuNPs will also be reported.

3.2 Materials and Methods

3.2.1 Chemicals

All chemicals were used as received: 3(bromopropyl)triphenylphosphonium bromide, tris(4-fluorophenyl)phosphine, sodium thiosulfate ($Na_2S_2O_3$), potassium thioacetate ($KSCOCH_3$), gold(III) chloride trihydrate ($HAuCl_4$), hydrobromic acid (HBr), potassium bromide (KBr), magnesium sulfate ($MgSO_4$) were obtained from Sigma-Aldrich (Gillingham, Dorset, UK). Deuterated chloroform and dichloromethane NMR solvents and an ICP Au standard were purchased from Sigma-Aldrich (Gillingham, Dorset, UK).

3.2.2 Synthesis of Phosphonium Compounds

3-triphenylphosphoniopropylthiosulfate (PPTS) (2) and (3-thioacetylpropyl)triphenylphosphonim bromide salt (PPTA) (3) were synthesised using methods described by Ju-Nam and colleagues (Ju-Nam *et al.*, 2006, Ju-Nam *et al.*, 2008). In brief, both compounds were prepared by either refluxing (3-bromopropyl)triphenylphosphonium bromide (1) (1.0 g, 2.15 x 10^{-3} mol) with $Na_2S_2O_3$ (0.8 g, 3.23 x 10^{-3} mol) in aqueous EtOH or stirred overnight under nitrogen with $KSCOCH_3$ (0.37 g, 3.23 x 10^{-3} mol) to obtained products (2) and (3) respectively. The progress of the reaction was monitored by TLC, using 80:20 DCM:MeOH as the mobile phase; upon completion KBr (20mL, 10% w/w) was added prior to isolating the bromide salt (3). Both compounds were obtained by

solvent extraction with DCM (3 x 10 mL) and purified by triturating with diethyl ether and characterised by FTIR, ESI-MS and NMR.
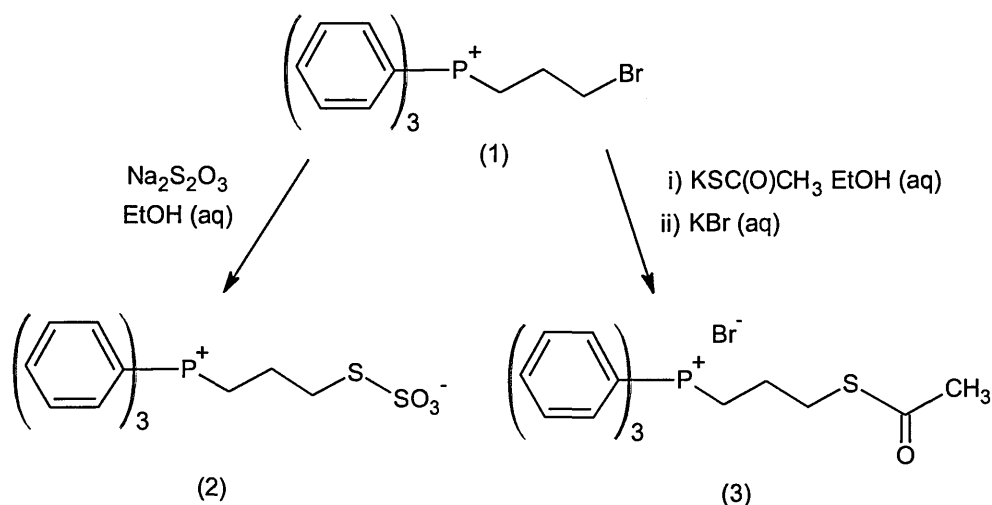
Figure 3.2 Synthesis scheme for 3-triphenylphosphoniopropylthiosulfate (PPTS) (2) and (3-thioacetylpropyl)triphenylphosphonim bromide salt (PPTA) (3).

3.2.3 Synthesis of Tri(p-fluorophenyl)phosphonium Compounds

Tri(p-fluorophenyl)phosphoniopropyl thiosulfate zwitterion (FPPTS) (7) and ω-thioacetylpropyl(tri-p-fluorophenyl)phsophonium bromide (FPPTA) (8) were synthesised following protocols reported by Ju-Nam and co-workers (Ju-Nam *et al.*, 2006, Ju-Nam *et al.*, 2008). Both compounds were generated by refluxing tris(4-fluorophenyl)phosphine (4) (1.0 g, 3.16 x 10^{-3} mol) with 3-bromo-1-propanol (1.1 mL, 1.25 x 10^{-2} mol) in MeCN (20 mL) overnight to obtain tris(4-fluorophenyl)hydroxypropylphosponium salt (5). The salt (5) was then treated with HBr (48%, 10 mL) and refluxed overnight to yield the (3-bromopropyl)tris(4-fluorophenyl)phosphonium salt (6). The salt (6) (0.250 g, 5.70 x 10^{-4} mol) was refluxed overnight with $Na_2S_2O_3$ (0.212 g, 8.56 x 10^{-4} mol) in aqueous EtOH or stirred overnight under nitrogen with $KSC(O)CH_3$ (0.098 g, 8.56 x 10^{-4} mol) in aqueous EtOH to obtained the zwitterion (7) and the bromide salt (8) respectively. The progress of the reaction was monitored by TLC, prior to isolating the intermediate salt (5) 10 mL of DIH_2O was added; all compounds were obtained by DCM extraction (3 X 10 mL) and purified by triturating with diethyl ether. All intermediates and end products were confirmed by conducting ESI-MS, FTIR and NMR analysis.
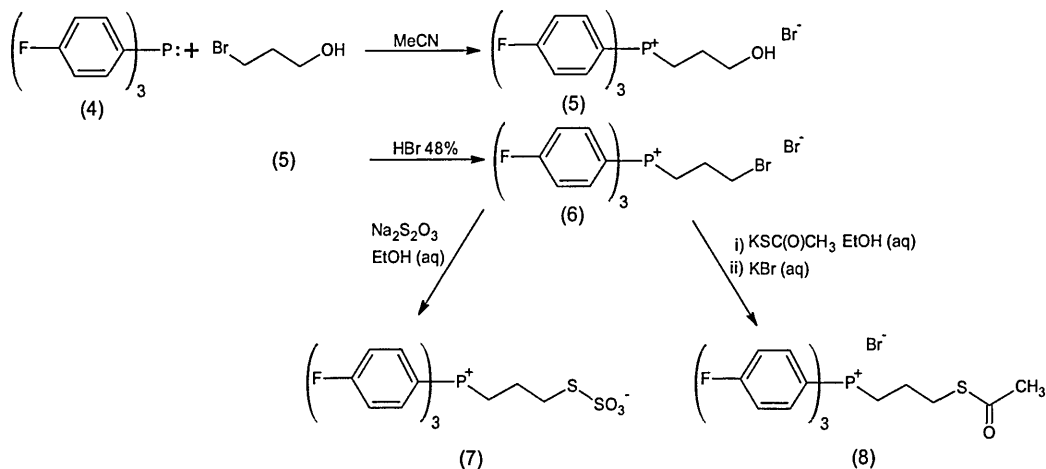
Figure 3.3 Synthesis scheme for Tri(*p*-fluorophenyl)phosphoniopropyl thiosulfate zwitterion (FPPTS) (7) and ω-thioacetylpropyl(tri-*p*-fluorophenyl)phsophonium bromide (FPPTA) (8).

3.2.4 Synthesis of Phosphonium-Functionalised Gold Nanoparticles

Phosphonium-functionalised AuNPs were synthesised based on methods described previously (Ju-Nam *et al.*, 2006, Ju-Nam *et al.*, 2008); in brief a solution of the phosphonium compound corresponded to the protecting ligand (0.25 mmol) was prepared in $HAuCl_4$ (0.12 mmol) and DCM (15 mL). The solution was stirred vigorously under nitrogen for 6 hours, subsequently $NaBH_4$ (3 mL, 400 mmol L^{-1}) was added drop wise followed by the addition of DIH_2O (15 mL) and stirred under nitrogen overnight. After 24 hours the colloidal solution was purified by DCM extraction (3 x 10 mL), freeze dried, flushed with nitrogen and retained for further analysis.

3.2.5 Characterisation of Phosphonium Ligands

All phosphonium ligands were characterised using a range of techniques including ^1H and ^{31}P NMR, ESI-MS, FT-IR. FPPTS and FPPTA were further characterised by elemental analysis, x-ray crystallography and accurate mass analysis by MALDI. Mass spectra from Analyst software were exported in the form of text files and imported into mMass, an open source mass spectrometry software used for mass spectral processing (Strohalm *et al.*, 2010).

3.2.6 Characterisation of Phosphonium-Functionalised Gold Nanoparticles

Phosphonium-functionalised gold nanoparticles were characterised by ^{31}P NMR, UV-Vis, MALDI-MS, ICP, TGA, XPS and TEM as outlined in chapter 2. MALDI matrices were made to a concentration of 10 mg/mL in 70:30 MeCN:H$_2$O, for positive ion mode analysis an additional 0.1% TFA was added to the matrix solution.

3.3 Results and Discussion

3.3.1 Synthesis of Phosphonium Ligands

3.3.1.1 3-Triphenylphosphoniopropylthiosulfate (PPTS)

Colourless crystals, δ ^{31}P NMR (CDCl$_2$) = 23.3 ppm, δ ^{31}P NMR (CDCl$_2$) = 2.2 (2H, m), 3.3 (2H, m), 3.6 (2H, m), 7.6-8.0 ppm (15H, m). ESMS 417.1 [M+H]$^+$, 439.1 [M+Na]$^+$. All results obtained supported the successful synthesis of PPTS.

3.3.1.2 (3-Thioacetylpropyl)triphenylphosphonium Bromide Salt (PPTA)

Isolated as a pale yellow powder, δ ^{31}P NMR (CDCl$_3$) = 24.3 ppm, δ ^{31}P NMR (CDCl$_3$) = 1.7 (3H, m), 2.0 (2H, m), 3.0 (2H, m), 4.1 (2H, m), 7.5-8.0 ppm (15H, m). ESMS 379.2 [M]$^+$, 380.2 [M+H]$^+$. FT-IR = 1680 cm^{-1} ν(C=O). All results obtained supported the successful synthesis of PPTA.

3.3.1.3 Tri(p-fluoropheny)phosphoniopropyl thiosulfate zwitterion (FPPTS)

The chemical structure of FPPTS is shown in Figure 3.4. This compound was isolated as colourless crystals and is soluble in polar organic solvents including DCM, MeOH and MeCN. All analytical and spectroscopy data support the formulation of this compound.
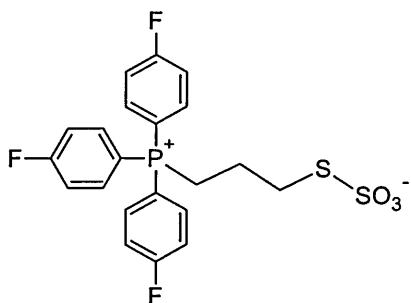
Figure 3.4 Chemical structure of FPPTS.

Formula: $C_{21}H_{18}F_3O_3PS_2$

ESI-MS: 471 [M+H$^+$], 493 [M+Na$^+$].

NMR: δ ^{31}P NMR (CDCl$_2$) = 23.4 ppm; δ ^{1}H NMR (CDCl$_2$) = 2.2 (2H, m), 3.2 (2H, m), 3.6 (2H, m), 7.3-7.9 (12H, m) ppm.

Elemental analysis: found: C, 53.89; H, 3.93; $C_{21}H_{18}F_3O_3PS_2$ requires: C, 53.61; H, 3.86.

Accurate mass analysis: found 471.0474 [M]$^+$; cation $C_{21}H_{18}F_3O_3PS_2$ requires 433.471.0465 [M]$^+$.

X-ray crystallography: The structure of FPPTS was confirmed by x-ray crystallography. Single crystals of FPPTS were grown by slow diffusion of a diethyl ether into a DCM solution of FPPTS which gave colourless needles. The crystals were sent for full structure analysis at the EPSRC X-ray Crystallography Service at the University of Southampton. The molecular structure is shown in Figure 3.5, selected bond lengths and bond angles are listed in Table 3.1. Crystal data and structure refinement details are presented in appendix 1.
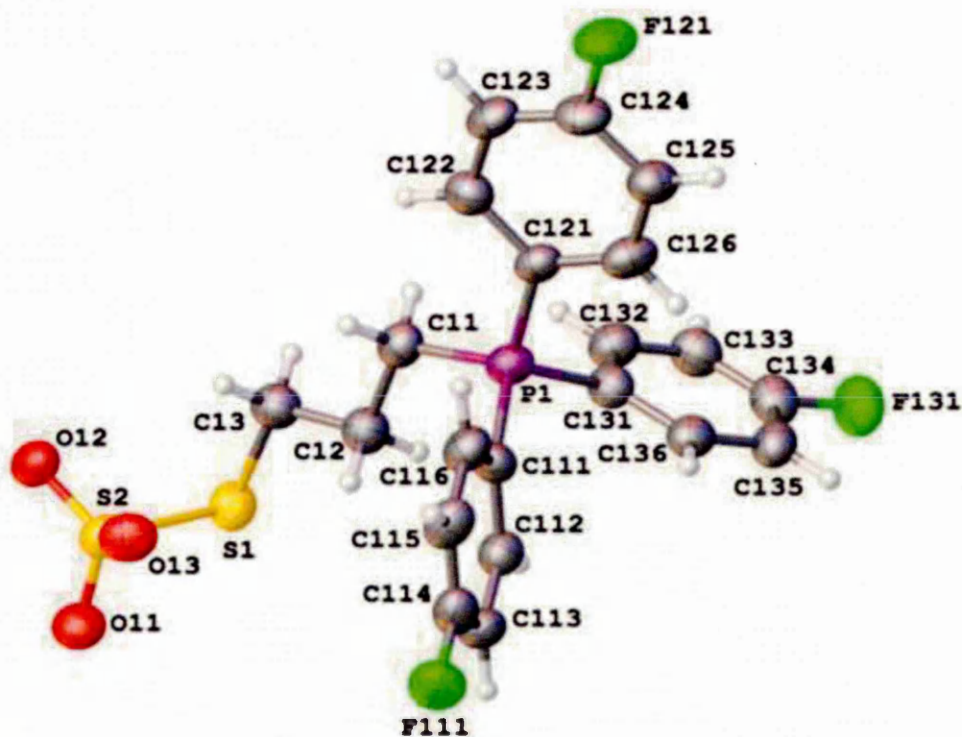
Figure 3.5 An Ortep representation of the molecular structure of FPPTS. Thermal ellipsoids are drawn at 50% probability level.

P1–C11	1.792(5)	S1–S2	2.0930(18)
P1–C111	1.784(5)	S2–O11	1.442(3)
P1–C121	1.791(5)	S2–O12	1.444(3)
P1–C131	1.788(5)	S2–O13	1.447(3)
S1–C13	1.824(5)		
C121–P1–C11	109.9(2)	O11–S2–O12	113.9(2)
C131–P1–C121	108.3(2)	O11–S2–O13	114.9(2)
C131–P1–C11	110.4(2)	O12–S2–O13	112.2(2)
C111–P1–C121	109.5(2)	O11–S2–S1	101.24(15)
C111–P1–C11	109.8(2)	O12–S2–S1	106.94(15)
C111–P1–C131	108.9(2)	O13–S2–S1	106.58(17)
C13–S1–S2	100.27(17)		
C116–C13–P1	120.1(4)		
C12–C13–S1	111.5(3)		

Table 3.1 Selected bond lengths [Å] and angles [°] in FPPTS.

Perhaps surprisingly, the structures of few other organic thiosulfate zwitterions have been described in the literature. The crystal structures of the triphenyl (Figure 3.6a) and tributyl (Figure 3.6b) phosphonium zwitterions have been reported previously (Ju-Nam *et al.*, 2006) and the only other example being an ammonium zwitterion, S-[4-(trimethylammonio)phenyl]thiosulfate (Figure 3.6c) (Chen *et al.*, 2004).
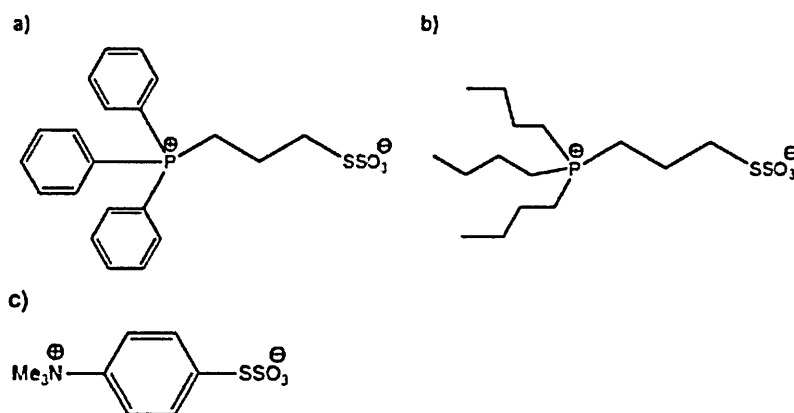
Figure 3.6 Chemical structures of thiosulfate zwitterions; a) 3-triphenylphosphoniopropylthiosulfate, b) 3-tributylphosphoniopropylthiosulfate (Ju-Nam *et al.*, 2006) and c) S-[4-(trimethylammonio)phenyl]thiosulfate (Chen *et al.*, 2004).

Zwitterion PPTS (Figure 3.6a) exhibits the expected tetrahedral geometry around the phosphorus atoms with a mean C-P-C bond angle of 109.47(2)°. The corresponding values for the triphenyl (FPPTS, Figure 3.4) and tributyl (Figure 3.6b) analogues are 109.47(11)° and 109.47(17)° respectively. The bond lengths and angles in the aryl rings are unremarkable and the C-F bonds [mean length 1.359(6) Å] are similar to those in the parent phosphine $(p\text{-}FC_6H_4)_3P$ [mean length 1.366(6) Å] (Shawkataly *et al.*, 1996).

The S-O bonds in the thiosulfate group of compound FPPTS are all similar, with a mean length of 1.4478(19) Å [*c.f.* 1.4478(19)Å and 1.440(3) Å in then phenyl analogue and 1.440(3) Å in the butyl compound], indicative of multiple bond character. The mean S-S bond length [2.1081 (18) Å] is slightly shorter than that in the phenyl derivative [2.1117(9) Å], and longer than that in the butyl compound [2.1030(14) Å], but are all longer than the established length of a single S-S bond [2.05 Å].

The ammonium thiosulfate zwitterion (Figure 3.6c) ha an S-S bond length of 2.1137(7) Å, similar to those in FPPTS and related phosphonium zwitterions, but are all appreciably shorter than the S-S bond in the monoanion of thiosulfuric acid, $HSSO_3^-$ [2.155 Å] (Miaskiewicz and Steudel, 1992). The lengthening of the S-O bond and S-S bonds in the zwitterions is consistent with the delocalisation of the negative charge across the entire thiosulfate group. Furthermore, the longer and weaker S-S bond of the phosphonium zwitterions expedites the dissociation of the thiosulfate group with the concomitant formation of the corresponding thiolate ion which is a key step in the application of these compounds in the synthesis of metal nanoparticles.
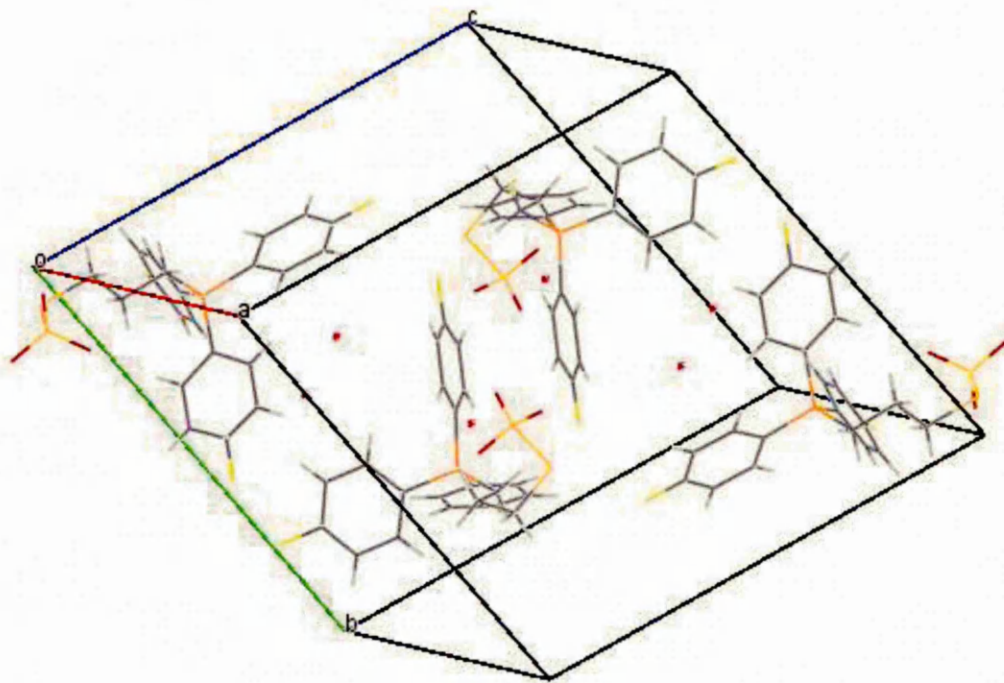
Figure 3.7 Molecular packing in FPPTS.

The zwitterions are packed fairly loosely within the crystal lattice (Figure 3.7), held together in a head-to-tail manner, by hydrogen-bonding interactions between the sulfate oxygen's and the phenyl hydrogen's. Analysis of the supramolecular structure reveals interactions between phenyl groups on adjacent molecules (Figure 3.8) (Hunter and Sanders, 1990). The centroid-centroid distance between these two rings is 3.65 Å which fits well with the interplaner spacing observed in stacked arenes which lie in the range between 3.6 – 3.8 Å (Cozzi et al., 2008).

The molecules also display intramolecular C-F....H hydrogen bonding interactions between adjacent aryl rings. The F...H distance (2.409 Å). The nature of C-F...H interactions is the subject of debate (Dunitz and Taylor, 1997, Reichenbacher et al., 2005). Nonetheless, the distances are shorter than the sum of the van der Waals radii for hydrogen and fluorine (2.67 Å) and are similar in length to those found in other fluorine-containing organic molecules (Reichenbacher et al., 2005).
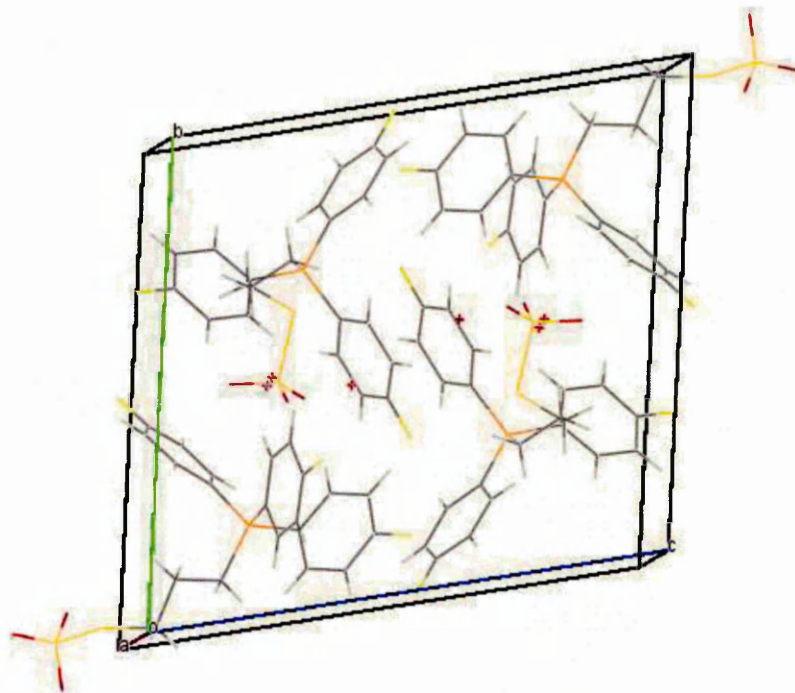
Figure 3.8 Molecular packing in FPPTS with the interaction between adjacent phenyl rings highlighted. The distance between the centres of the phenyl rings is 3.65 Å.

3.3.1.4 ω-thioacetylpropyl(tri-*p*-fluorophenyl)phosphonium Bromide (FPPTA)

The chemical structure of FPPTA is shown in Figure 3.9. This compound was isolated as a pale cream powder and is soluble in organic solvents such as DCM, EtOH and MeOH. All analytical and spectroscopy data supported the formulation of this compound; x-ray crystallography data show the presence of a water molecule which is further supported by elemental analysis.
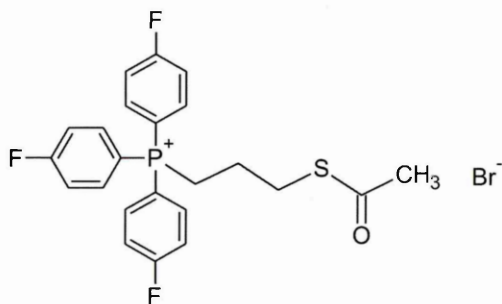
Figure 3.9 Molecular structure of FPPTA.

Formula: $C_{23}H_{21}F_3SOPBr$

ESI-MS: 433 [M$^+$], 434 [M+H$^+$].

NMR: δ ^{31}P NMR (CDCl$_3$) = 23.9 ppm; δ ^{1}H NMR (CDCl$_3$) = 1.9 (5H, m), 3.2 (2H, m), 4.3 (2H, m), 7.3-8.1 (12H, m) ppm.

FT-IR: 1680 cm^{-1} ν(C=O).

Elemental analysis: found: C, 52.47%; H, 4.09%; $C_{23}H_{21}F_3SOPBr$ + H_2O requires: C, 51.97%; H, 4.33%.

Accurate mass analysis: found 433.0976 [M]$^+$; cation $C_{23}H_{21}F_3SOPBr$ requires 433.1003 [M]$^+$.

X-ray crystallography: The structure of FPPTA was confirmed by x-ray crystallography. Single crystals of FPPTS were grown by slow diffusion of a diethyl ether into a DCM solution of FPPTS which yield colourless needless. The crystals were sent for full structure analysis at the EPSRC X-ray Crystallography Service at the University of Southampton. The molecular structure is shown in Figure 3.10, selected bond lengths and bond angles are listed in Table 3.2. Crystal data and structure refinement details are presented in appendix 2. This compound is the first example of a phosphoniumalkylthioacetate salt to be characterised crystallographically.
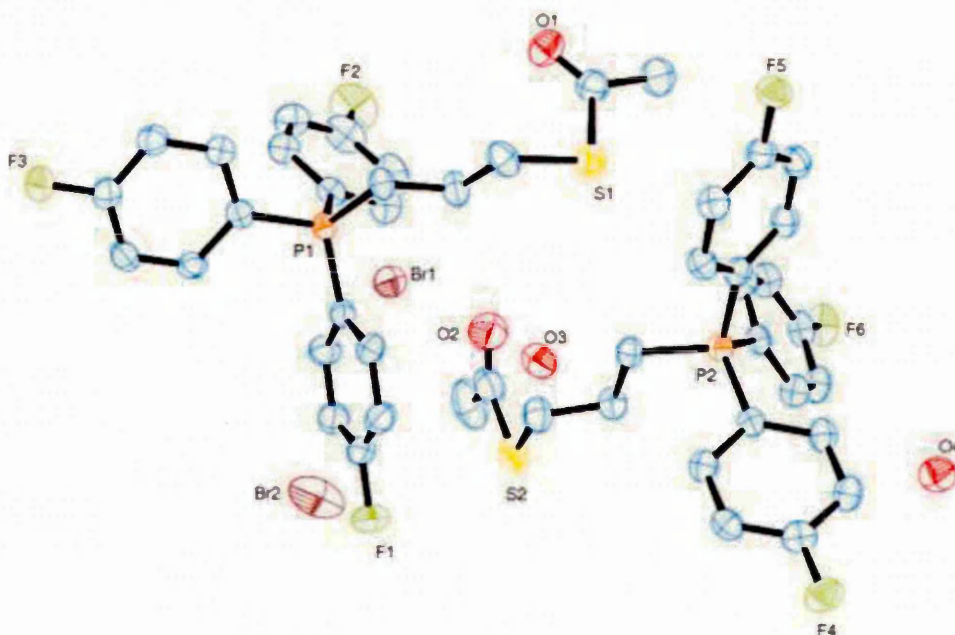
Figure 3.10 An Ortep representation of the asymmetric unit of FPPTA. Thermal ellipsoids are drawn at 50% probability level. Hydrogen atoms are omitted for the sake of clarity.

C1-P1	1.783(6)	C21-S1	1.783(7)
C7-P1	1.790(6)	C22-S1	1.770(7)
C18-P1	1.789(6)	C22-C23	1.506(10)
C19-P1	1.810(6)	C22-O1	1.191(8)
C21-S1	1.783(7)	C4-F1	1.363(8)
		C10-F2	1.354(8)
		C15-F3	1.355(7)
C20-C19-P1	113.8(4)	C22-S1-C21	100.4(3)
C20-C21-S1	112.2(5)	O1-C22-C23	124.6(7)
C7-P1-C19	111.0(3)	C23-C22-S1	112.6(5)
C18-P1-C7	109.3(3)	O1-C22-S1	122.7(6)
C18-P1-C19	107.7(3)	F1-C4-C5	118.9(7)
C1-P1-C7	109.6(3)	F1-C4-C3	117.7(7)
C1-P1-C19	109.9(3)	F2-C10-C9	117.0(8)
C1-P1-C18	109.3(3)	F2-C10-C11	119.2(8)
		F3-C15-C14	118.6(6)
		F3-C15-C16	118.4(6)

Table 3.2 Selected bond lengths [Å] and angles [°] in FPPTA.

The asymmetric unit contains two crystallographically independent phosphonium cations, two bromide anions and two water molecules of crystallisation. The compound exhibits the expected tetrahedral geometry around the phosphorus atom with a mean bond angle of 109.47(3)° identical to the zwitterion (FPPTS). The C-F bonds in the phenyl rings lie in the range 1.354(8)-1.369(2), similar to the zwitterion (FPPTS) and the parent phosphine which have an average length of 1.366(6) Å (Ju-Nam et al., 2006).

The C-S [1.783(7) Å and 1.770(7) Å and C-O[1.191(8) Å] bond lengths of the thioacetate group in FPPTA are similar to the expected distances for C-S single and C=O bonds, c.a.1.8 Å and 1.2 Å respectively (Huheey, 1972) and are close to the values reported in dimethylmonothiocarbonate, $CH_3OC(S)CH_3$, which has C-S bond lengths of 1.791(2) Å, 1.759(1) Å and a C=O bond length of 1.195(2) Å (Erben et al., 2006). The FPPTA molecules display the expected angular geometry around the sulfur atom with bond angles of 100.4(3)° and 101.2(4)° for the two cations in the unit cell.

The molecular packing displays some interesting features (Figure 3.11); the unit cell contained eight cations together with eight bromide anions and the water molecules are associated with the bromide ions, held together through a complex network of hydrogen bonds and intermolecular interactions between the different species. The structural parameters for these hydrogen bond interactions are presented in Table 3.3. The molecules also display intramolecular C-F....H interactions which lie in the range 2.639 - 2.670 Å. These distances are slightly longer than those observed in the FPPTA zwitterion and are close to the sum of the van der Waals radii of fluorine and hydrogen (2.67 Å) but are comparable with the distances observed in other organofluorine compounds (Reichenbacher et al., 2005).
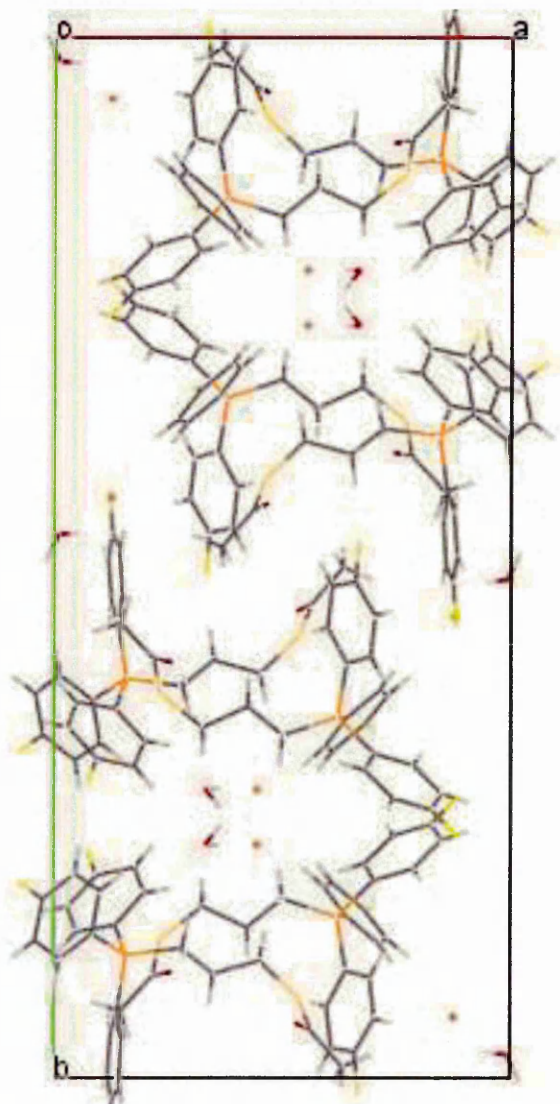
Figure 3.11 Unit cell of the FPPTA salt parallel to c axis.

D–H···A	d(H···A)	d(D–H)	d(D···A)	∠(DHA)
O3–H3A···Br1	0.937(18)	2.44(3)	3.347(5)	163(7)
O3–H3B···Br1[i]	0.84(2)	2.51(2)	3.350(5)	175(7)
O4–H4A···Br2[ii]	0.963(18)	2.35(3)	3.296(6)	165(7)
O4–H4B···Br2[iii]	0.86(2)	2.36(5)	3.141(6)	152(9)

Table 3.3 Hydrogen bonds in FPPTA [Å and °]. Symmetry transformations used to generate equivalent atoms: (i) x,–y+1/2,z–1/2 (ii) x+1,y,z (iii) –x+1,–y+1,–z.

3.3.2 Synthesis of Phosphonium-Functionalised Gold Nanoparticles

The first indication that AuNPs had been successfully prepared was the visually observation of the colour change of the solutions during the synthesis; when HAuCl$_4$ was added to the solution of the corresponding protecting ligand PPTS, PPTA, FPPTS and FPPTA in DCM the stirring organic solution turned yellow. The addition of NaBH$_4$ induced a colour change from yellow to a characteristic deep red wine colour which indicated the reduction had taken place (Daniel and Astruc, 2004). When the reaction was stopped after 24 hours, the DCM layer was colourless and the aqueous phase was a dark red-purple colour for protecting ligands: PPTS, PPTA and FPPTS, with no evidence of aggregation indicating that functionalised AuNPs were present in the aqueous phase. The interface between the organic and aqueous phase for FPPTA, dark blue/black particles of aggregated colloidal gold were observed, showing no affinity with either the DCM or water layer. Since the use of either FPPTS or FPPTA will produce the same functionalised AuNPs (Figure 3.12) it was decided that FPPTS would be used for the synthesis of functionalised AuNPs for future experiments.
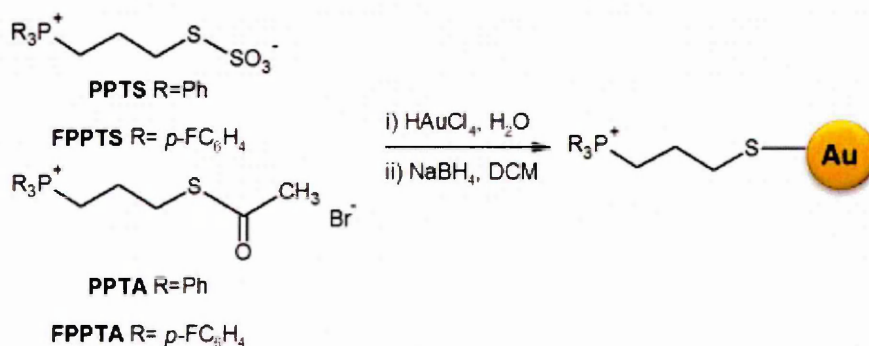
Figure 3.12 Synthesis scheme of phoshonium-functionalised AuNPs using different phosphonium capping ligands.

98

3.3.3 8Characterisation of Phosphonium-Functionalised Gold Nanoparticles

Characterisation of AuNPs is challenging but essential for their application; chemists rely on a number of techniques to determine the structure and purity of NPs synthesised these include NMR, TGA, DLS, MS and TEM (Kim *et al.*, 2013). Samples of AuNPs functionalised with phosphonioalkyl-thiosulfate and – thioacetate ligands were analysed using UV-visible spectroscopy, NMR, TGA, LDI, ICP, XPS and TEM.

3.3.3.1 UV-Visible (UV-vis) Spectroscopy

UV-Vis absorption spectroscopy has been widely used to characterise the optical properties of nanoparticles, as the absorption bands is governed by a number of factors predominantly the size and shape of metal nanoparticles. Evidence for the successful formation of AuNPs was supported by UV-vis spectroscopy; a broad absorption band in the visible region ~520 nm was observed for AuNPs prepared from PPTA, PPTS and FPPTA (Figure 3.13). This demonstrated that all P-AuNPs synthesised were all similar in size, a peak absorption band ~520 nm indicated that particle synthesised are between 2-10 nm in diameter (Daniel and Astruc, 2004)However they are slight differences between the P-AuNPs.

The peaks for the thiosulfate species (PPTS and FPPTS) are very similar, which suggested that these two particles synthesised are similar in size, this observation is in agreement with TEM data reported in section 3.3.3.2. PPTS and FPPTS has a mean particle size of 3.0 nm and 2.7 nm respectively. A difference of 0.3 nm in size can be observed in the slight difference in the peak in their visible spectra shown in Figure 3.13,

Interestingly the peak for PPTS and FPPTS are different compared to the peak for PPTA, thereby suggesting that the particle size for PPTA are different to PPTS and FPPTS. This observation is in agreement with TEM data reported in section 3.3.3.2, PPTA has a mean particle size of 4.9 nm, which is ~ 2 nm larger than PPTS and FPPTS, this difference in size was also observed in the UV-vis results (Figure 3.13).

99
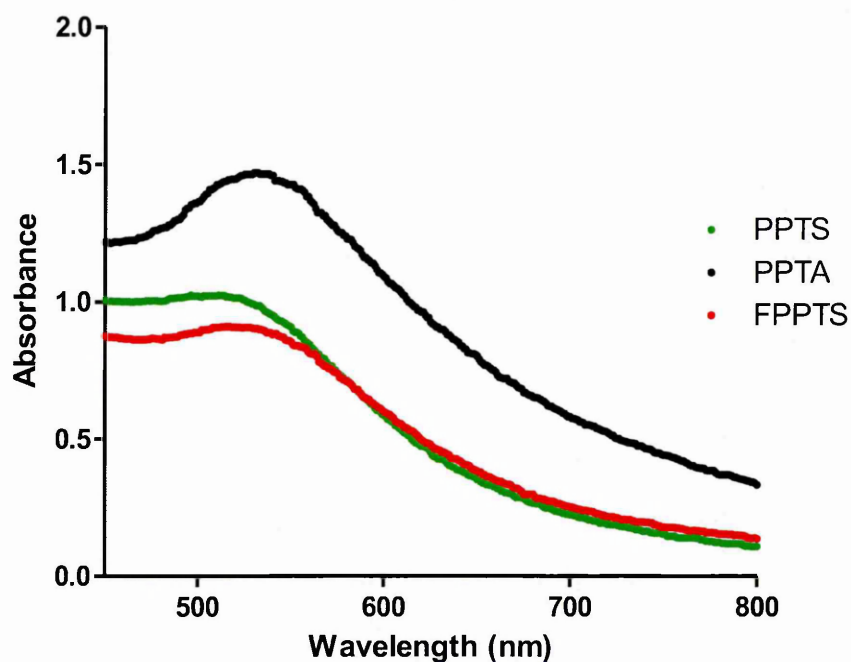
Figure 3.13 Visible spectra of phosphonium-functionalised AuNPs prepared from PPTS, PPTA and FPPTS.

All solutions of phosphonium-functionalised AuNPs were freeze-dried to remove water to keep them stable for longer periods; previous studies have shown that phosphonioalkylthioacetate functionalised AuNPs are stable for 6 months (Ju-Nam *et al.*, 2008). UV-Vis spectra (Figure 3.14) showed no changes in the SPR band for the freeze-dried AuNPs re-suspended in water compared to the freshly prepared colloidal solution, this demonstrated that P-AuNPs can be stored in the freeze-dried form and be re-suspended in solvents at a later date for further analyses and experiments.
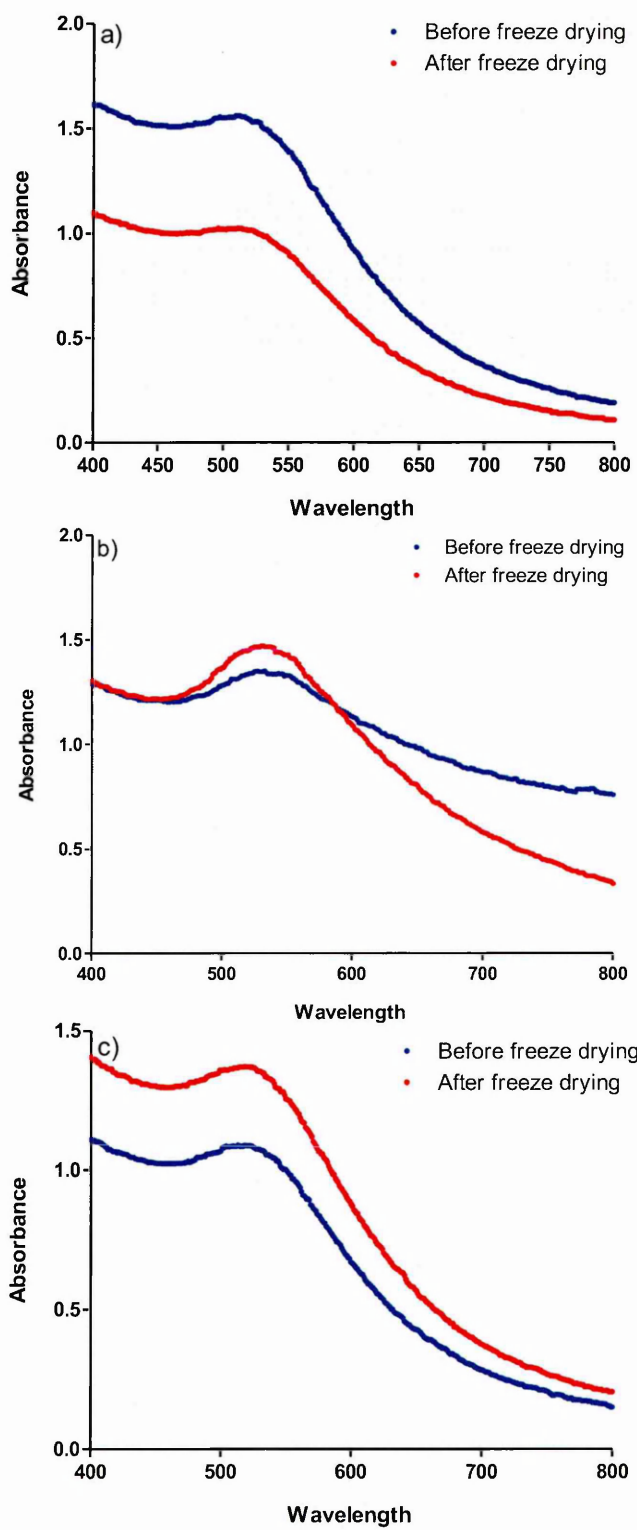
Figure 3.14 UV-vis spectra of the fresh solution of AuNPs capped with a) PPTS, b) PPTA and C) FPPTS re-suspended in water after freeze-drying.

3.3.3.2 Transmission Electron Microscopy (TEM)

TEM is routinely used for the characterisation of nanoparticles, which provides a photograph of the gold core and size information (Daniel and Astruc, 2004). The size and morphology of AuNPs functionalised with different phosphonium ligands were investigated by TEM.
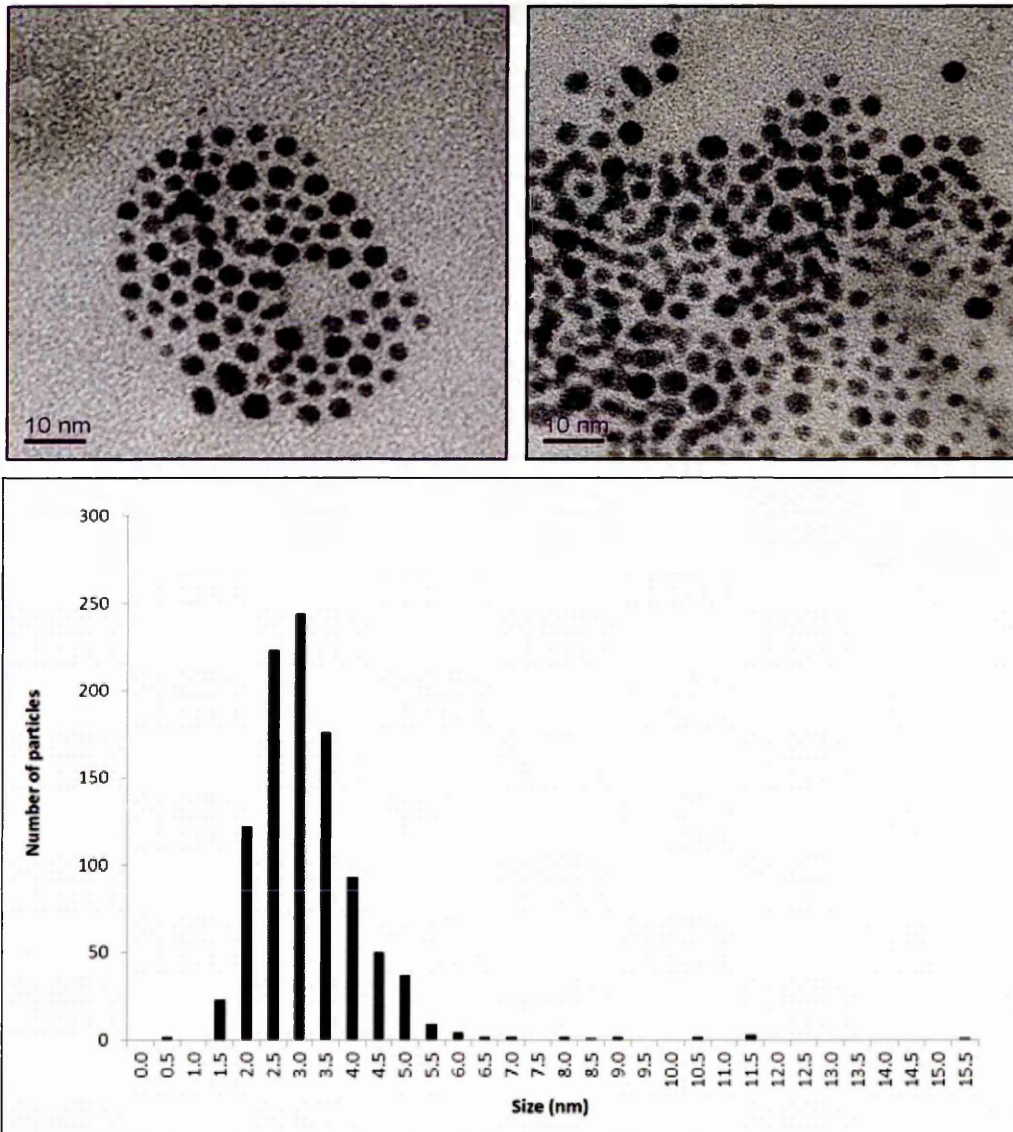
Figure 3.15 Typical TEM micrographs and particle size histograms of phosphonium-functionalised AuNPs with precursor PPTS ligand. Mean particle size 3.0 ± 1.2., in each histogram 1,000 nanoparticles were counted.
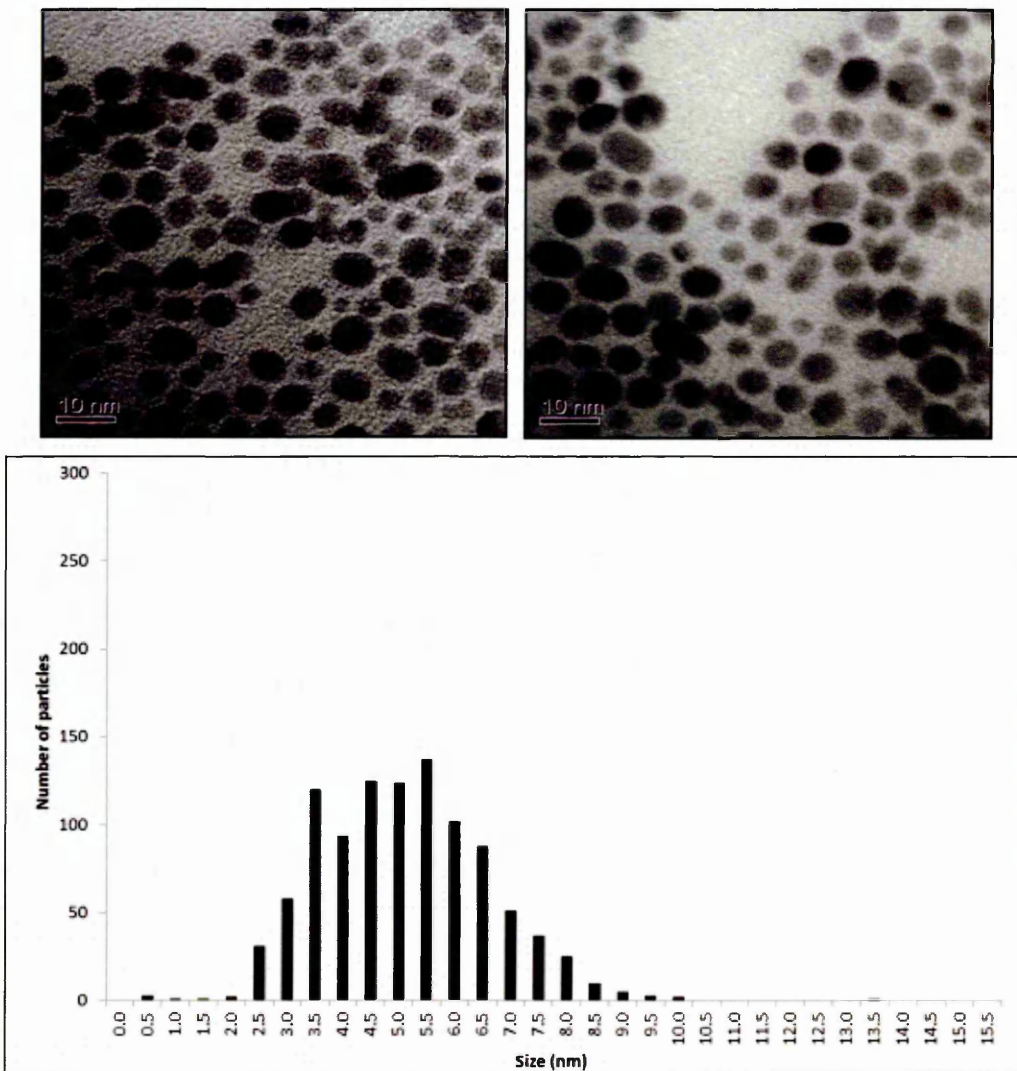
Figure 3.16 Typical TEM micrographs and particle size histograms of phosphonium-functionalised AuNPs with precursor PPTA ligand. Mean particle size 4.9 ± 1.5, in each histogram 1,000 nanoparticles were counted.
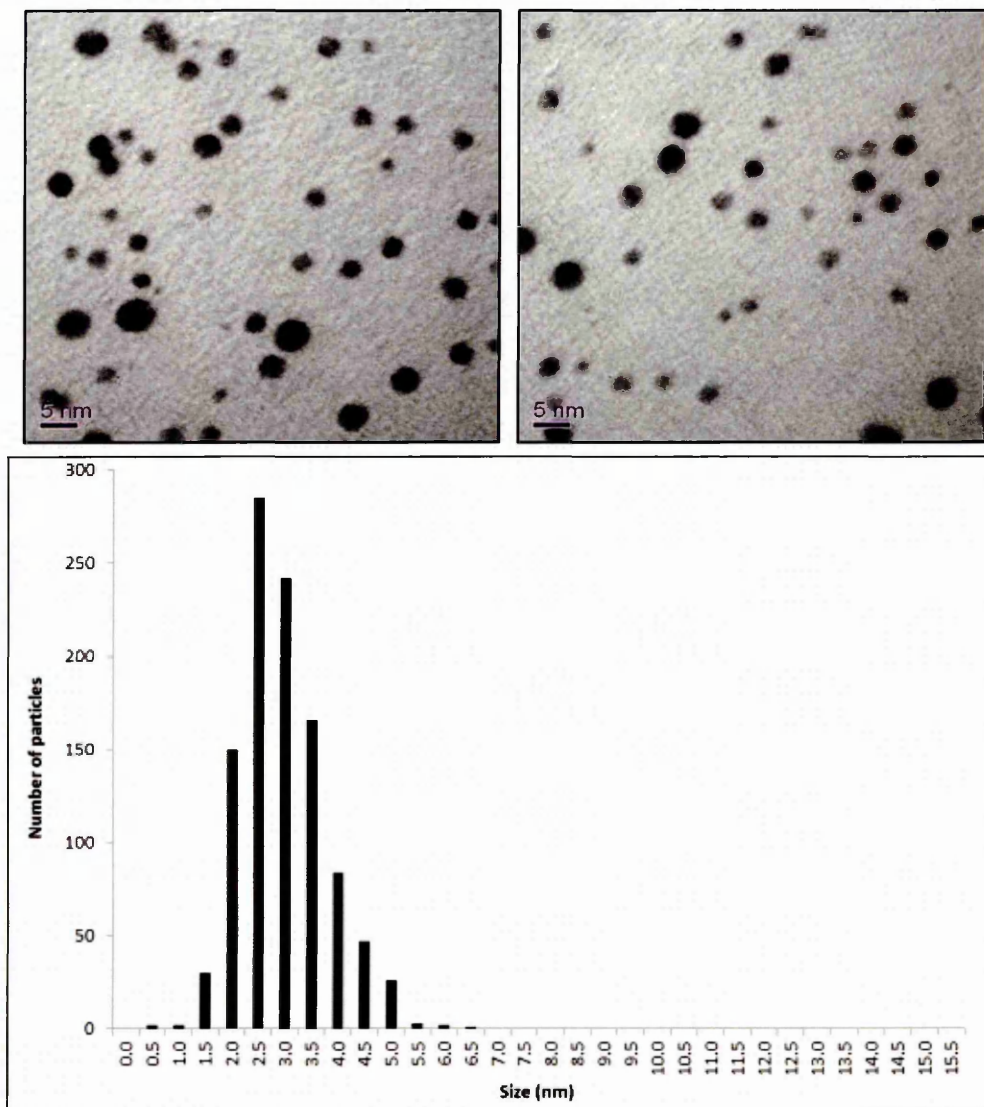
Figure 3.17 Typical TEM micrographs and particle size histograms of phosphonium-functionalised AuNPs with precursor FPPTS ligand. Mean particle size 2.7 ± 0.8, in each histogram 1,000 nanoparticles were counted.

TEM studies showed that all the samples are spherical in shape (Figure 3.15-3.17), the particle size count revealed that AuNPs prepared from thiosulfate species (PPTS and FPPTS) produces particles of similar size and distribution. In contrast AuNPs prepared using thioacetate precursor ligand (PPTA) produces larger particle sizes and with a broader particle size distribution (Table 3.4).

Precursor Phosphonium Ligand	Mean Particle Size (nm)
PPTS	3.0 ± 1.2
PPTA	4.9 ± 1.5
FPPTS	2.7 ± 0.8

Table 3.4 Average particle size of phosphonium-functionalised AuNPs prepared from different phosphonium ligands. Mean particle size was calculated from 1000 nanoparticles.

The differences in size between AuNPs derived from the PPTS zwitterion and PPTA salt can be explained on the basis of the differing passivation kinetics of the two types of ligand (Lohse *et al.*, 2010, Singh *et al.*, 2010, Zhang *et al.*, 2009). The first stage of the synthesis should be adsorption of the ligand on the surface of the growing particles and the thioacetate might be expected to be a more weakly binding ligand than the thiosulfate. The next stage involves the transformation of the thiosulfate or thioacetate to the thiolate.

The exact mechanism of this step in this system is unclear at present, the mechanisms of the formation of self-assembled monolayers on gold using alkyl thiosulfates (Bunte Salts) as the precursor ligands has been the subject of recent studies (Lohse et al., 2010, Fealy et al., 2011). Recent studies into the formation of monolayers on gold surfaces from alkylthiosulfates show hydrolysis by the presence of trace amounts of water in the solvent (Fealy *et al.*, 2011, Pillai and Freund, 2011).

Phosphonium-functionalised AuNPs reported in this chapter were prepared in a two-phase water/DCM system, the possibility of the growing AuNPs and/or the reducing agent cannot be excluded being involved in the cleavage of the thiosulfate sulfur-sulfur bond (S-S) or thioacetate sulfur-carbon (S-C) bonds. The cleavage step for thioacetate bond appears to be slower than the sulfate bond and thus result in slower monolayer formation.

3.3.3.3 Nuclear Magnetic Resonance Spectroscopy (NMR)

NMR is a useful technique in determining the structure of organic materials, because the NMR shifts changes depending on the magnetic field at the nucleus which is very sensitive to the surrounding electrons. NMR is also commonly used to characterise capping ligands on the surface of nanoparticles (Liu *et al.*, 2012).

In this chapter, ^{31}P NMR has been used for the initial characterisation of the protecting ligands surrounding the surface of AuNPs. Data are summarised in Table 3.5.

	Free Ligand	Phosphonium-AuNPs
PPTS	23.3 ppm	23.5 ppm
PPTA	24.3 ppm	23.3 ppm
FPPTS	23.4 ppm	23.0 ppm

Table 3.5 Summary of ^{31}P NMR chemical shift for phosphonium precursor ligands and the corresponding phosphonium-AuNPs.

Overall no significant changes were observed in the ^{31}P NMR spectra for all free ligands (PPTS, PPTA and FPPTS) and the corresponding phosphonium-AuNPs (Table 3.5). All free ligands have a ^{31}P chemical shift of approximately 23 ppm and the functionalised AuNPs have a ^{31}P chemical shift around 23 ppm. The similarity between the ^{31}P chemical shift of the free ligand and its corresponding functionalised AuNP, provided evidence that the chemical structure of the ligand stabilising the Au core is the same structure of the ligand itself and that the phosphonium head group remains unchanged.
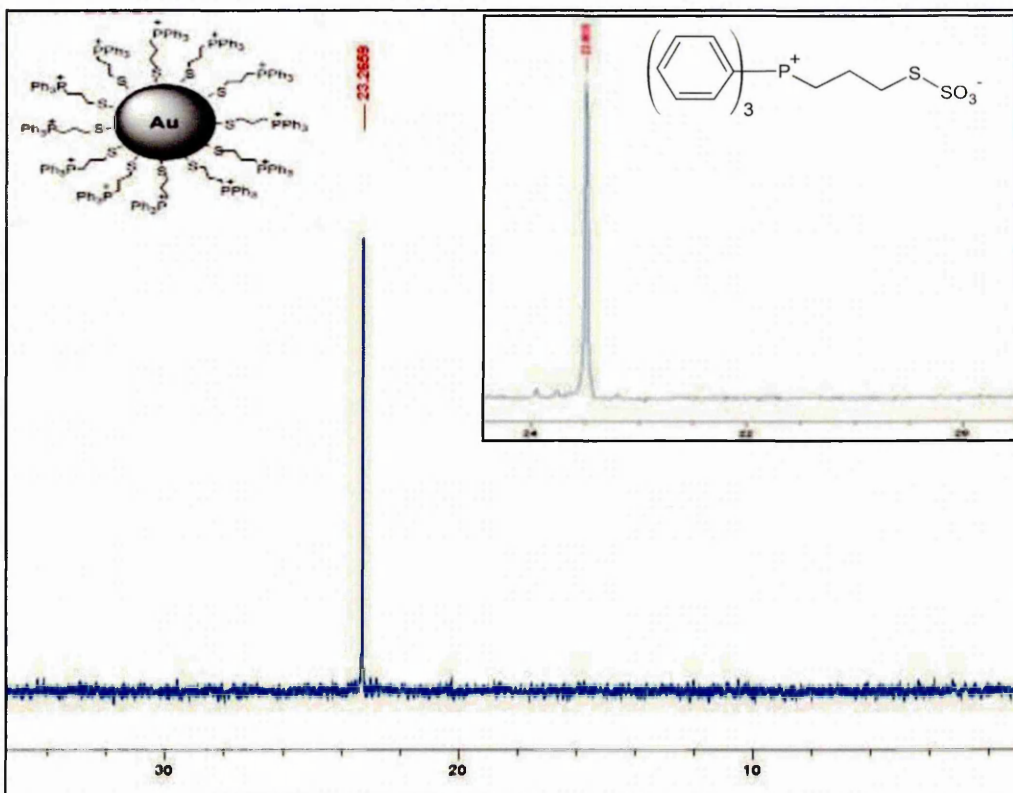
Figure 3.18 The ^{31}P NMR spectra (CD$_2$Cl$_2$) of PPTS (insert) and PPTS functionalised AuNP: with ^{31}P peak at 23.49 ppm and 23.27 ppm respectively. This shows that the phosphorous head group for both the free ligand and the functionalised AuNPs form are in similar chemical environments.

The ^{31}P NMR spectra of the free ligand (PPTS) and the corresponding AuNPs are shown above in Figure 3.18. The free ligand (PPTS) has a ^{31}P value of 23.5 ppm and the capped AuNPs has a ^{31}P value of 23.3 ppm, both values are very similar with a slight difference of 0.2 ppm. This indicated that the phosphonium head group are in a similar chemical environment in both cases, thereby confirming that the chemical structure of the ligand stabilising the Au core is the same structure of the ligand itself and that the phosphonium head group remains unchanged.

3.3.3.4 X-Ray Photoelectron Spectroscopy (XPS)

XPS has become a useful surface analysis tool for understanding the nature of different types of surfaces, particularly nanomaterials as it can provide valuable information regarding the atomic composition of the surface ligands as well as the chemical state of surfaces and interfaces (5-10 nm depth) which have strong influence on the properties of the nanomaterials (Baer and Engelhard, 2010). XPS has been widely used to study numerous monolayer-protected metal cluster and self-assembled monolayer systems (Shon *et al.*, 2000, Love *et al.*, 2005).

XPS has been employed in this project to determine the elemental composition of the phosphonium-AuNPs and the nature of the Au-S linkage, that data are summarised in Table 3.6.

Precursor Ligand	Au		S
	$4f_{7/2}$	$4f_{5/2}$	$2p_{3/2}$
PPTS	84.0	87.5	162.9
PPTA	84.1	87.8	162.1
FPPTS	83.8	87.5	162.5

Table 3.6 Summary of gold and sulfur XPS binding energies (eV) for phosphonium-AuNPs.

Binding energy values reported for S ($2p_{3/2}$) in Table 3.6 are consistent with a system in which the sulfur species is bound to the surface of gold as a thiolate, which usually occur in the range between 162.0 to 162.9 eV (Bourg *et al.*, 2000, Bain *et al.*, 1989).

Wide scan spectra of AuNPs prepared from thiosulfate precursor ligands (PPTS and FPPTS) (Figure 3.17) were very similar, showing signals due to Au, P and S. In addition, the XPS spectrum of the AuNP capped with the FPPTS compound contained a F(1s) peak (Figure 3.20), with a binding energy of 687.4 eV this is consistent with the presence of fluorine in this sample.
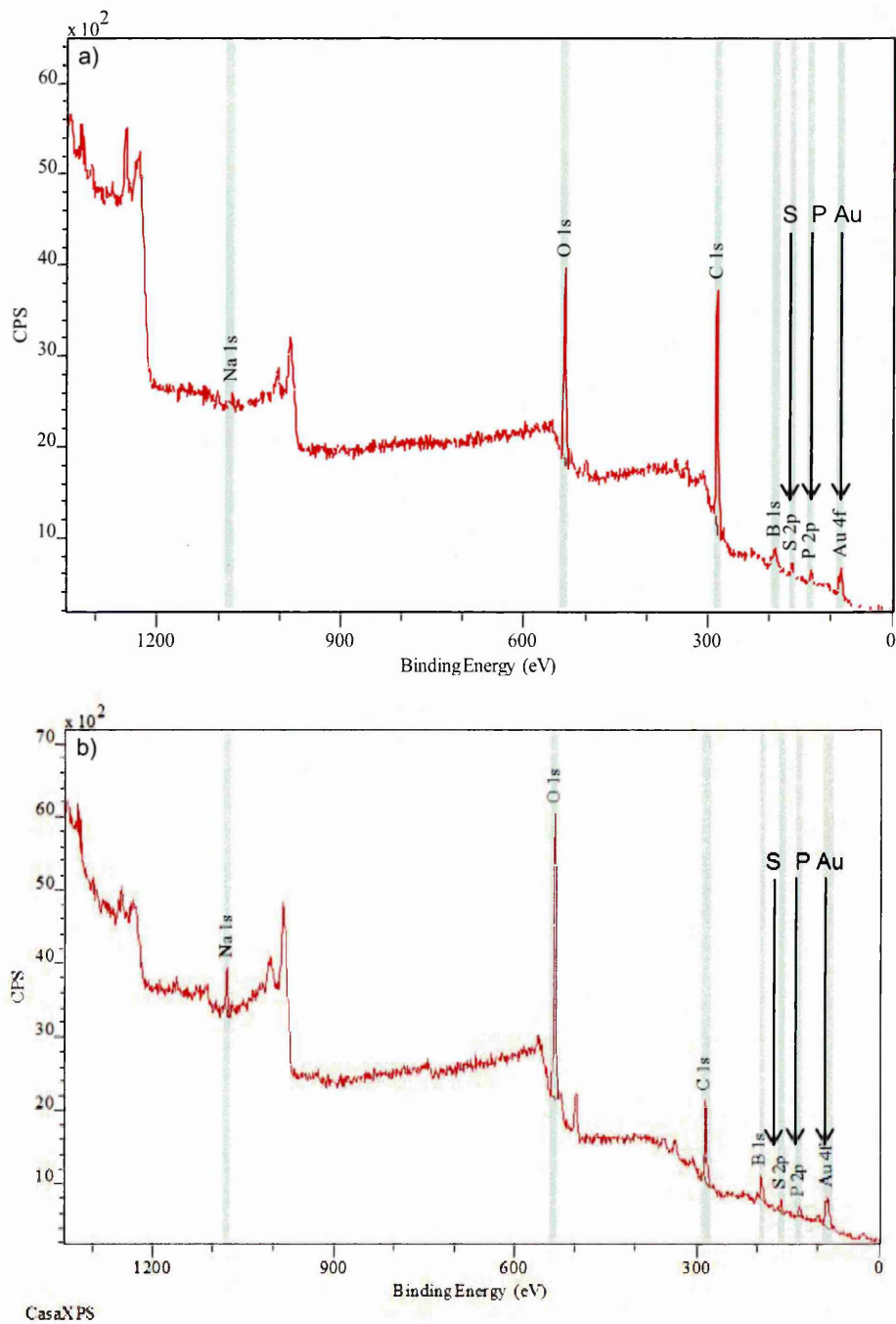
Figure 3.19 XPS wide scan spectrum corresponding to the freeze-dried sample of AuNPs functionalised with a) PPTS and b) PPTA and. Spectrum showing the bonding energies for sulfur (S 2p), phosphorous (P 2p) and gold (Au 4f) peaks at 170, 133 and 84 eV respectively for both samples.
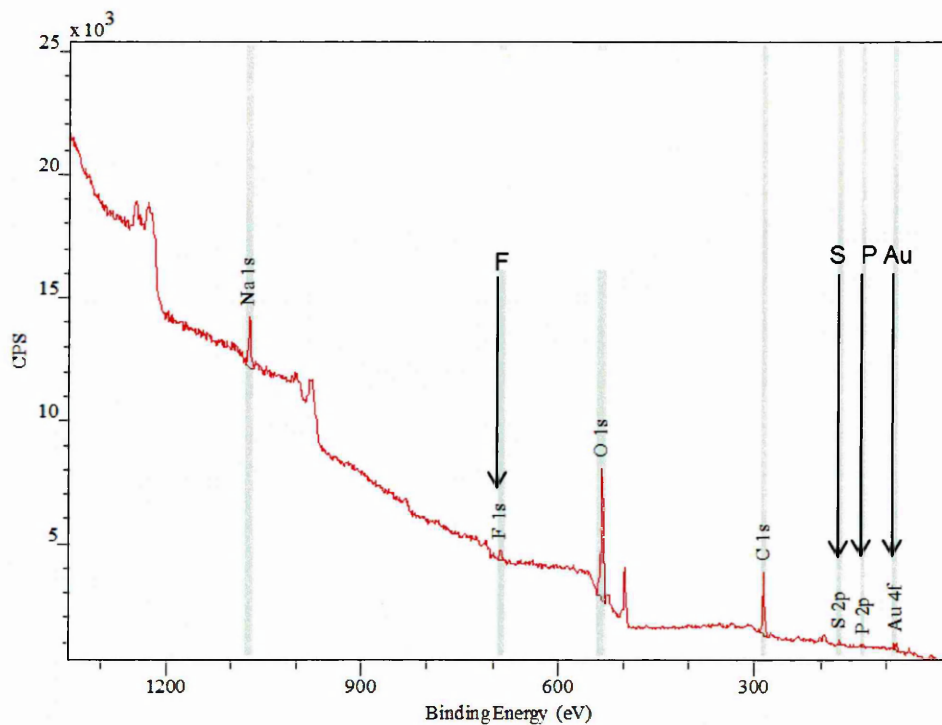
Figure 3.20 XPS wide scan spectrum corresponding to the freeze-dried sample of AuNPs functionalised with FPPTS. Spectrum showing the binding energies for sulfur (S 2p), phosphorous (P 2p), gold (Au 4f) and fluorine (F 1s) at 170, 133, 84 and 688 eV respectively. The fluorine peak confirmed the presence of fluorine in the sample.
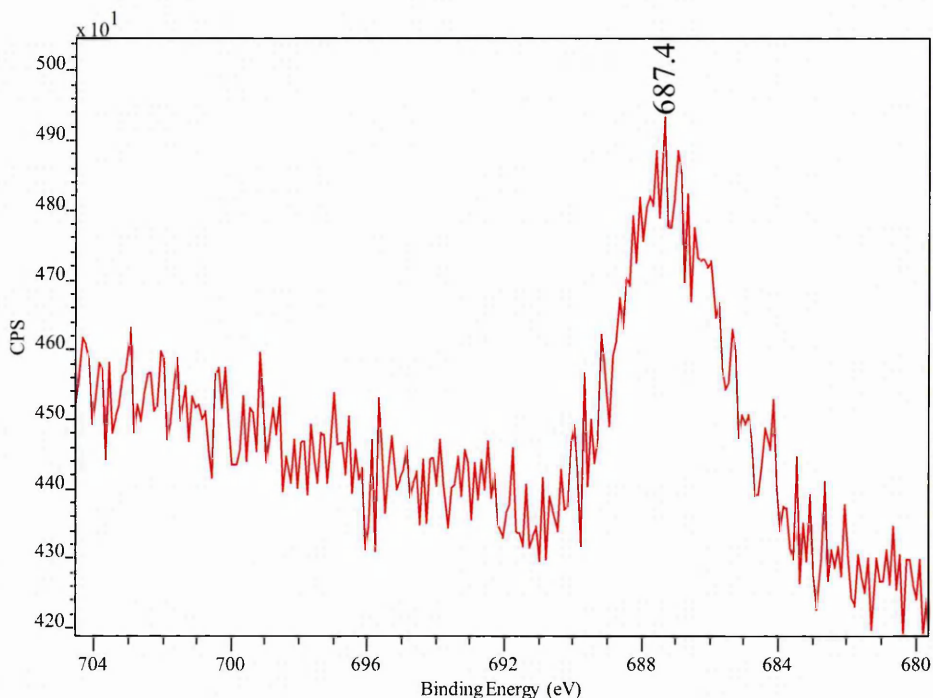
Figure 3.21 High resolution F(1s) XPS spectra of phosphonium-AuNP capped with FPPTS compound showing F 1s peak with a binding energy at 687.4 eV, confirming the present of fluorine in the sample.

The high resolution Au (4f) spectra for both samples contain a doublet for Au $(4f_{7/2})$ and Au $(4f_{5/2})$ with binding energies *c.a.* 83.8 and 87.5 eV, respectively (Figure 3.22). These values are similar to those reported by Brust (83.8 eV and 87.5 eV) (Brust *et al.*, 1994) and Yee and colleagues (84.2 eV and 87.85 eV) (Yee *et al.*, 2003) for AuNPs capped with dodecanethiol.

The binding energy of Au(I) in a gold thiolate is 86 eV and AuNPs that are reported to contain a fraction of their surface atoms in the Au(I) oxidation state show a Au $4f_{7/2}$ peak with a binding energy of 84.9 eV (McNeillie *et al.*, 1980). The Au $(4f_{7/2})$ observed at 84.0 eV in the phosphonium-AuNPs (Figure 3.22) suggested that the bulk of the gold atoms are in the Au(0) oxidation state.

111
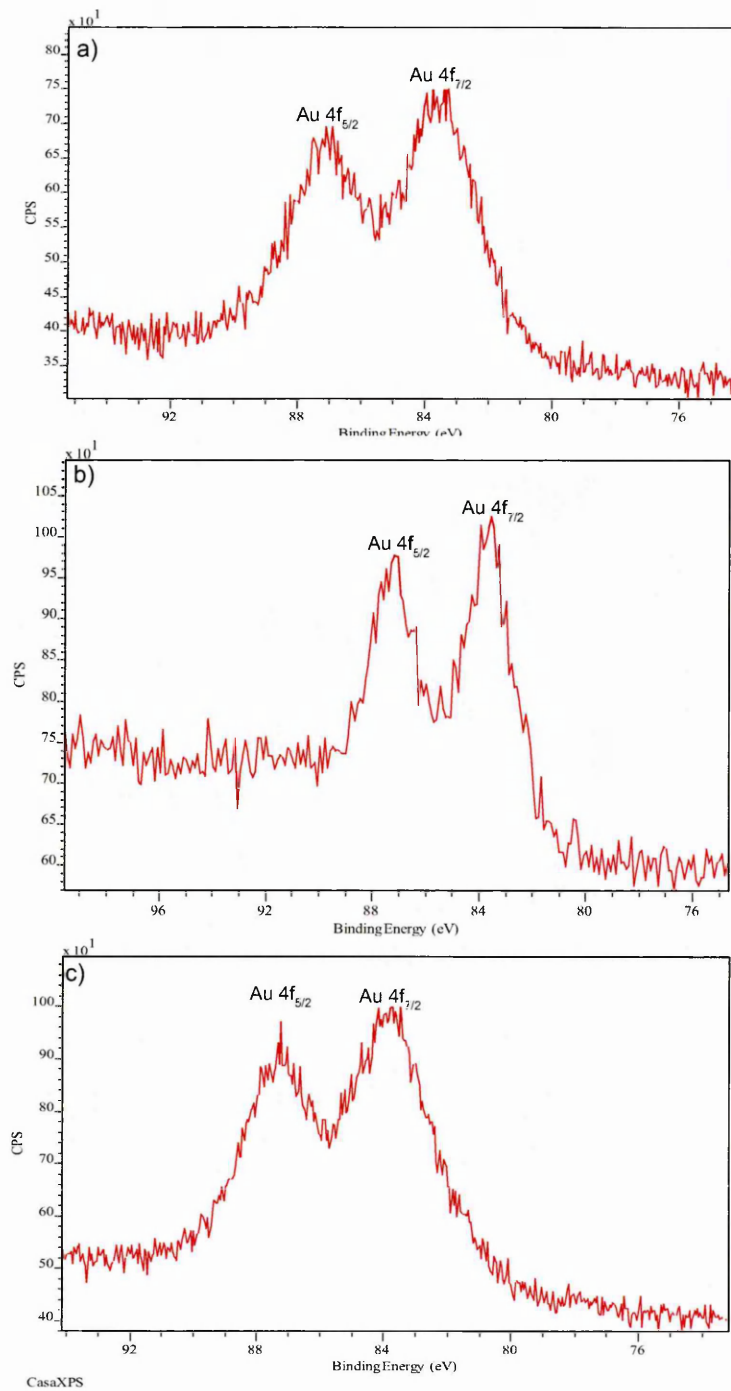
Figure 3.22 High resolution Au (4f) XPS spectrum of freeze-dried phosphonium-AuNPs derived from a) PPTS, b) PPTA and c) FPPTS. All spectrum show samples containing a doublet for Au at Au $4f_{7/2}$ and Au $4f_{5/2}$ with binding energies 84.0 and 87.5 eV for PPTS, 84.1 and 87.8 eV for PPTA, 83.8 and 87.5 eV for FPPTS.

112

High resolution S (2p) XPS spectra (Figure 3.23) displayed a peak with a binding energy of 162.9 eV corresponding to S ($2p_{3/2}$) (Bourg et al., 2000), providing strong evidence for the cleavage of the sulfur-sulfur bond in the phosphoniopropylthiosulfate zwitterions during the synthesis with the concomitant expulsion of SO_3^{2-} (or some other sulfur species derived from it) at the ligand/Au interface. There was no evidence for oxidised sulfur which appears at ~167 eV on gold clusters (Lee *et al.*, 1998, Schoenfisch and Pemberton, 1998).
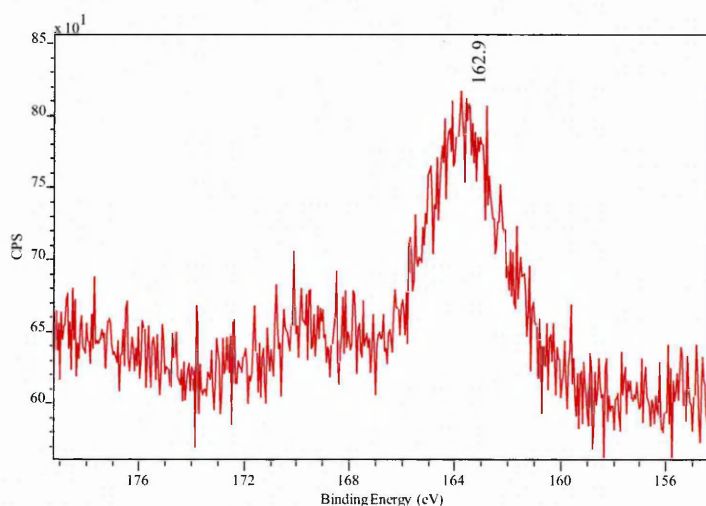
Figure 3.23 High resolution S (2p) XPS spectrum of freeze-dried phosphonium-AuNP derived from PPTS zwitterion. Showing S (2p) has a binding energy of 162.9 eV confirming the sulfur species is bound to the surface of gold as a thiolate.

Overall XPS data have provided valuable information regarding the ligands coating the surface of AuNPs. A wide scan spectrum confirmed the presence of sulfur, phosphorous and gold in all the samples, in addition fluorine was present in FPPTS, which was expected and agrees with the chemical structure. The high resolution of Au (4f) spectrum showed a doublet for Au at Au ($4f_{7/2}$) and Au ($4f_{5/2}$) for all samples in the region of 84 and 88 eV respectively, which are similar to the values of gold thiolates reported in the literature (Brust *et al.*, 1994, Yee *et al.*, 2003). Furthermore the presence of the peak for Au ($4f_{7/2}$) shows that the bulk of the gold atom are in the Au(0) oxidation state, confirming the successful synthesis of gold nanoparticles.

113

3.3.3.5 Secondary Ion Mass Spectrometry (SIMS)

The surface chemical analysis is an important part of the characterisation of both natural and synthetic nanoparticles; SIMS is a useful surface technique for the characterisation of the surfaces of nanoparticles and is predominantly used to extract molecular information. Furthermore, SIMS has also shown to be a useful tool in determining the basic composition of nanoparticles (Baer *et al.*, 2010).

In SIMS analysis, a high energy primary beam is directed onto a sample surface which penetrates the surface region and induces a collision cascade, and releases secondary ions in the form of neutral and charged secondary species. Static mode is used to extract surface molecular details, which involved the use of low density and low primary ion dose which reduces the interactions of the primary ions to the top monolayers of the sample and thus resulting in minimal surface damage (Baer *et al.*, 2010, Senoner and Unger, 2012).

The surface sensitivity of SIMS is considerably higher than XPS; SIMS was used in this chapter as an attempt to obtain additional data regarding the basic composition and the surface coatings on the nanoparticles. Zoomed-in SIMS spectra in positive ion mode of P-AuNPs derived from PPTS, PPTS and FPPTS (Figure 3.24 and 3.25) shows a peak at 197 Daltons, this corresponded to the molecular weight of gold. Along with UV-vis (chapter 3.3.3.1), TEM (chapter 3.3.3.2) and XPS (chapter 3.3.3.4) results reported previously in this thesis, all data supports each other and confirmed the successful synthesis of Au nanoparticles.

In the case of the AuNPs prepared from phosphonium ligand containing fluorine (FPPTS), a peak at 19 dalton corresponding to fluorine was observed (Figure 3.22b) this results confirmed the presence of fluorine in the sample, and SIMS data are agrees with data obtained previously by x-ray crystallography (chapter 3.3.1.3) and XPS (chapter 3.3.3.4).
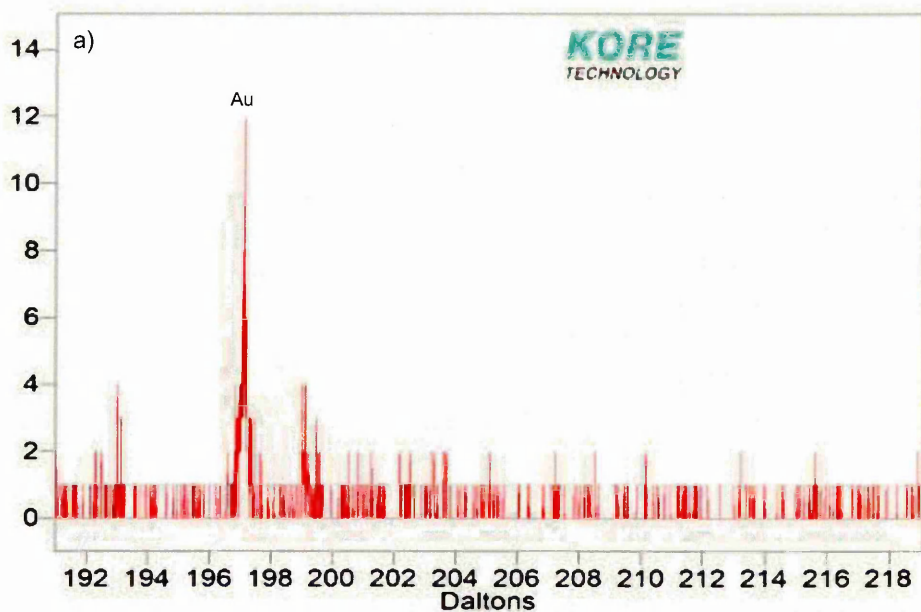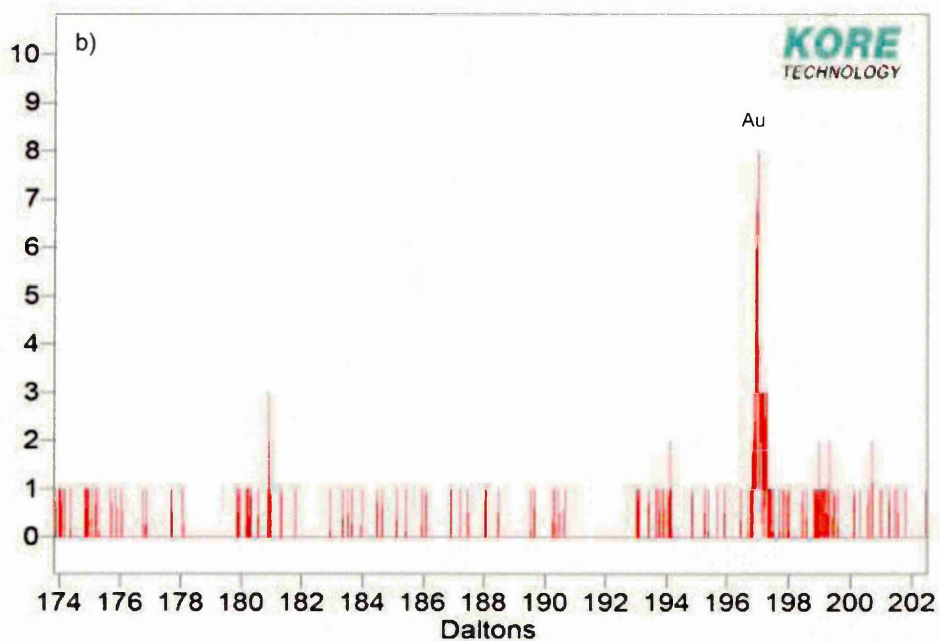
Figure 3.24 Zoomed-in SIMS spectrum in positive ion mode of P-AuNPs derived from a) PPTS and b) PPTA. Spectrum shows a peak for Au corresponding to its molecular weight at 197 and this confirms the present of Au.
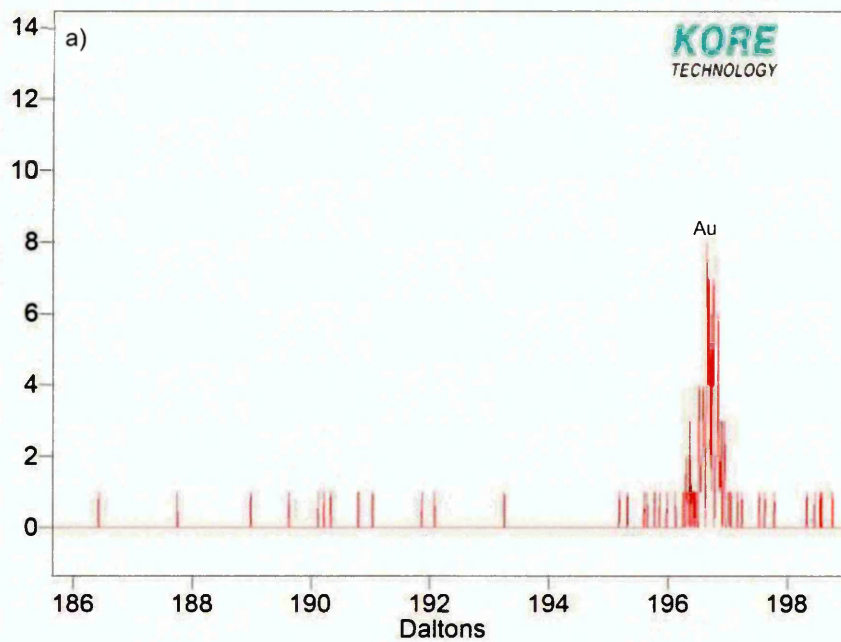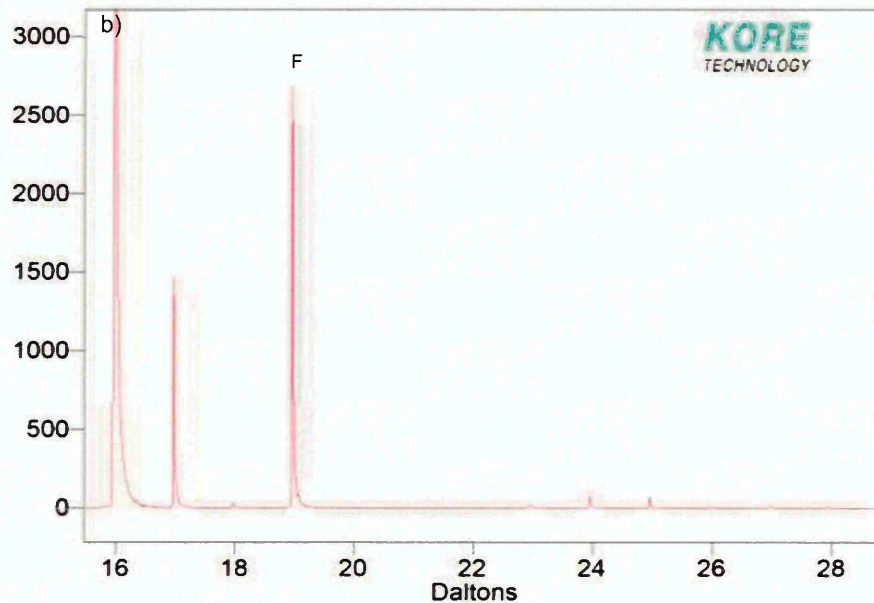
Figure 3.25 Zoomed in SIMS spectrum in positive ion mode of P-AuNPs derived from FPPTS. Figure 3.22a shows a peak for Au corresponding to its molecular weight at 197 and this confirms the present of Au. Figure 3.22b shows a peak corresponding to F, which confirms the presence of fluorine in the sample.

116

3.3.3.6 Matrix Assisted Laser Desorption/Ionization Mass Spectrometry (MALDI-MS)

Since it's invention in the late 1980s, MALDI-MS has become an important analytical tool for the analysis of a wide variety of biomolecules including proteins and peptides (Karas and Hillenkamp, 1988, Hoffmann and Stroobant, 2007). MALDI is a soft ionization technique that involves the use of a matrix (hence the name matrix assisted) of small, laser absorbing organic molecules to minimize damage to the analyte sample from laser irradiation (Chiang et al., 2011).

MALDI-MS has been successfully used in the quantitative analysis of AuNP clusters (Helfrich and Bettmer, 2011, Harkness et al., 2010). The earliest work for characterising thiolate-protected AuNPs by mass spectrometry dates back to the late 1990s, since then several papers have reported the characterisation of Au clusters using a number of different matrices including α-cyano-4-hydroxycinnamic acid (CHCA), 2-(4'-Hydroxybenzeneazo)benzoic acid (HABA) and sinapinic acid (Pena-Mendez et al., 2008, Schaaff, 2004, Arnold and Reilly, 1998, Dass et al., 2008a). While the use of common weak organic acid MALDI matrices enables the analysis of the core of ligand-protected AuNPs, these matrices do not prevent extensive ligand fragmentation (Harkness et al., 2010).

In 2008 Dass and co-workers published the first MALDI spectra of intact ligand-protected AuNPs with the use of an alternative matrix – trans-2-[3-(4-tert-butylphenyl)-2-methyl-2-propenylidene] malononitrile (DCTB). The success was due to ionisation assisted by electron transfer rather than proton transfer from weak organic acid matrices (Dass et al., 2008b). Recently Kouchi and colleagues (Kouchi et al., 2012) have successfully demonstrated that a new matrix – α, β-diphenylfumaronitrile (DPF) can be used to detect intact thiolate-protected gold clusters with stronger ion peak intensities compared to DCTB.

While MALDI-TOF-MS can be an invaluable tool in determining the number of gold atoms/ligand molecules in thiolated Au clusters, the elucidation of the exact formula is not straightforward and remains technically challenging (Kouchi et al.,

2012). To date, MALDI-MS has been successfully used to identify and quantify AuNPs with diameter 2 nm or smaller (Yu and Andriola, 2010).

In this chapter different matrices have been investigated as an attempt to determine the exact formula of AuNPs synthesised; due to the nature of looking for peaks with m/z greater than 1000, a MALDI-TOF Voyager De-STR mass spectrometer was used for the analysis, for instrument details refer to chapter 2.9. PPTS capped AuNPs were analysed by MALDI-TOF-MS both in positive and negative ion modes with CHCA, DCTB and DPF, with m/z up to 10,000 as well as varying laser intensity.

When PPTS capped AuNPs were analysed using CHCA as the matrix, peaks corresponding to the matrix and the PPTS ligand were detected (Figure 3.26). Peaks for CHCA were observed at m/z 191 $[M+H]^+$ and 380 $[2M+H]^+$, peaks for the PPTS ligand were observed at m/z 304 $[M-S]^+$ and 338 $[M-SCH_2]^+$. All peaks detected were 1 dalton higher than expected; CHCA matrix peak were expected at m/z 190 $[M+H]^+$ and 379 $[2M+H]^+$, PPTS ligand peaks were expected to be at m/z 303 $[M-S]^+$ and 337 $[M-SCH_2]^+$. This could be due to instrument being calibrated using cytochrome c which was a suitable standard to calibrate the instrument to higher mass ranges in the region of m/z 10,000. The De-STR is suitable for the analysis of high molecular weight samples such as proteins, in contrast the QSTAR (MALDI-QTOF-MS) has greater sensitivity for the analysis of samples with smaller molecular weights below m/z 1000. The use of the QSTAR for the analysis of PPTS capped AuNPs is reported in the next section (chapter 3.3.3.7).
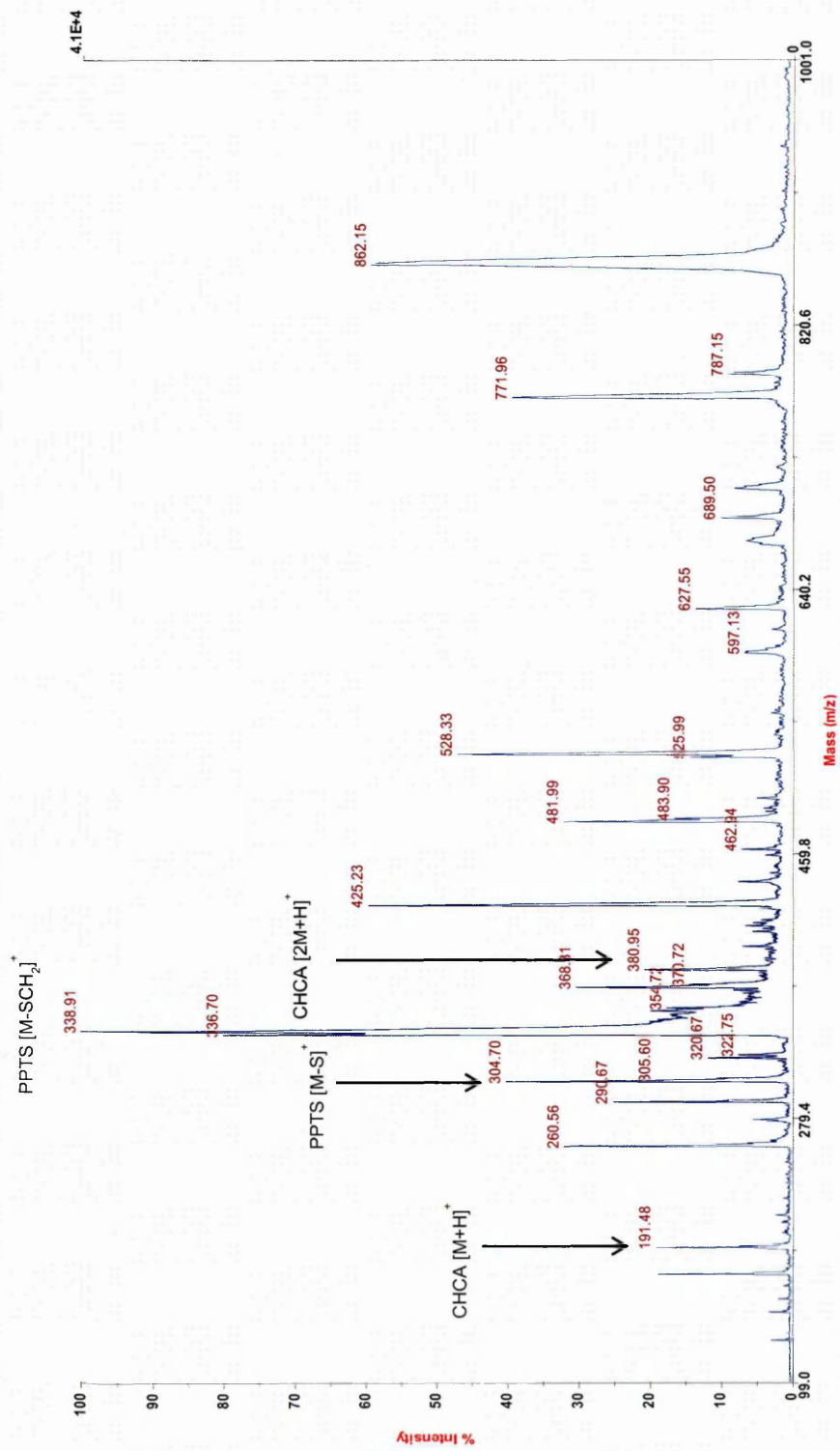
Figure 3.26 Typical MALDI spectrum of PPTS capped AuNPs with CHCA matrix analysed in positive ion mode. Peaks corresponding to CHCA at *m/z* 191 [M+H]$^+$, 380 [2M+H]$^+$, PPTS ligand at *m/z* 304 [M-S]$^+$ and 338 [M-SCH$_2$]$^+$.

119
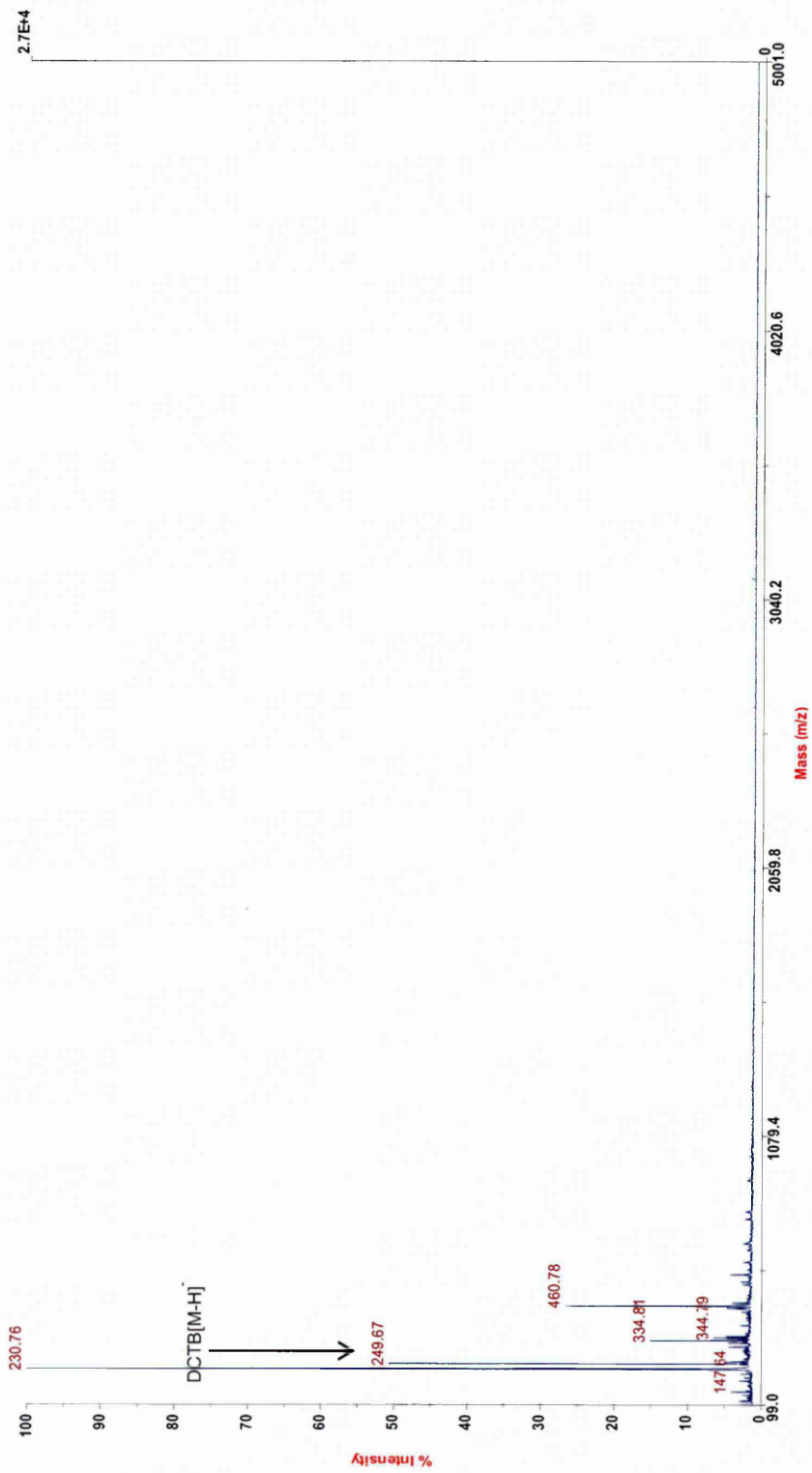
Figure 3.27 Typical MALDI spectrum of PPTS capped AuNPs with DCTB matrix analysed in negative ion mode. Peak corresponding to the matrix at *m/z* 249.67 [M-H]⁻.
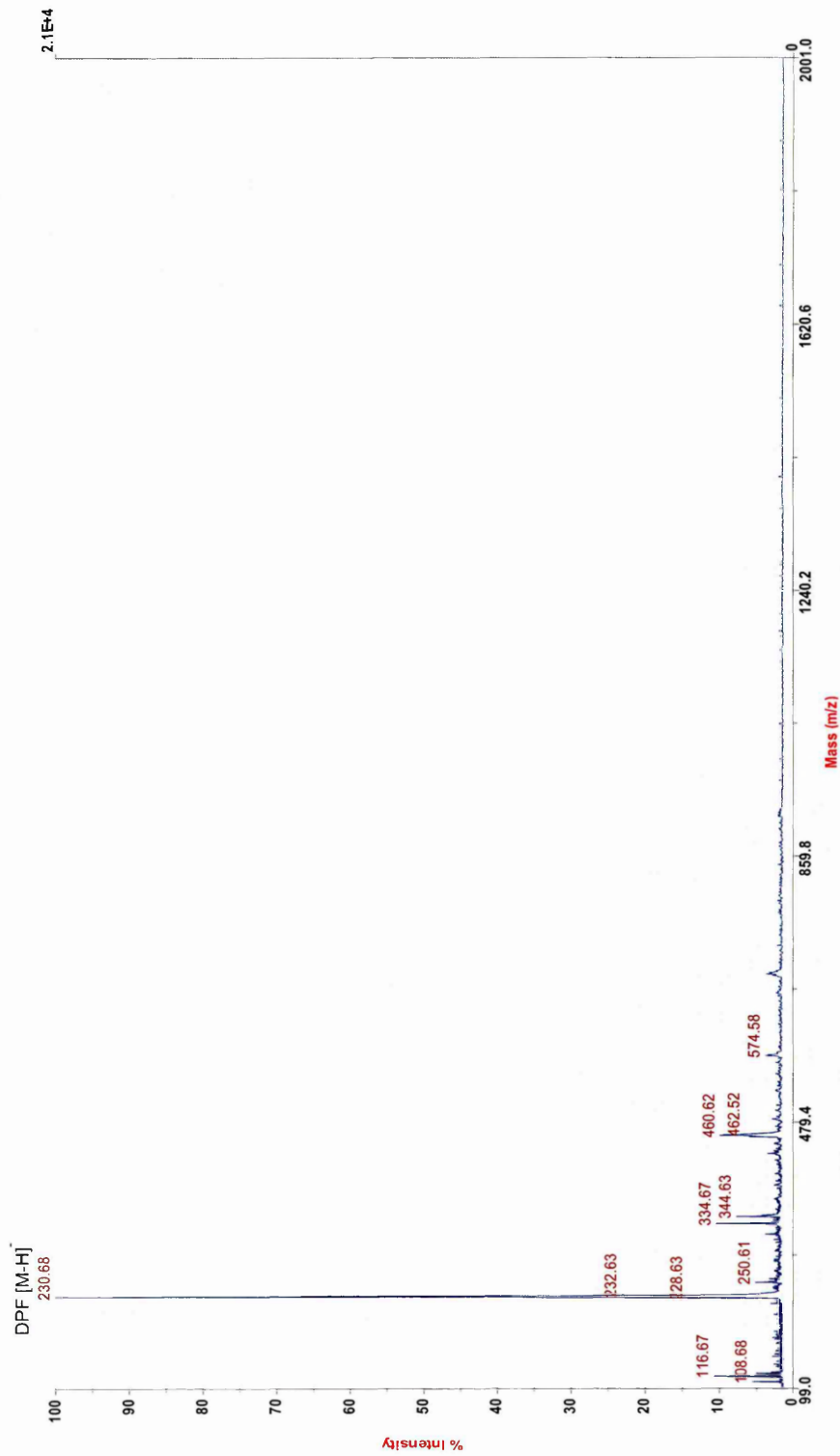
Figure 3.28 Typical MALDI spectrum of PPTS capped AuNPs with DPF matrix analysed in negative ion mode. Peak corresponding to the matrix at m/z 230.68 [M-H]⁻.

121

Although peaks below m/z of 500 were observed with all the matrices investigated, the matrix peaks has been identified, however the expected peaks for the sample analysed in negative ion modes (Figure 3.27 and 3.28) were not observed. Peaks for PPTA ligand are expected to at m/z 261 $[M-S(CH_2)_3]^-$, 274 $[M-S(CH_2)_2]^-$, 288 $[M-S(CH_2)]^-$ and 302 $[M-S]^-$, No major peaks corresponding to the intact AuNPs were observed above m/z 500 (Figure 3.26 and 3.28).

In general the use of CHCA produces noiser spectra compared to DPF and DCTB, this observation is in agreement with the literature; Dass *et al.* (2008b) and Kouchi et al (2012) have both successfully used alternative matrices (DCTB and DPF respectively) which assist ionisation by electron transfer to overcome the extensive ligand fragmentation observed when using the universal matrix – CHCA which assist ionisation by proton transfer. The use of MALDI-MS to characterise P-AuNPs synthesised in this project has been investigated; different matrices (CHCA, DPF and DCTB) have been employed in this section with varying different laser intensities and different mass ranges. Despite exploring different matrices and instrumentation settings, intact peak of the AuNPs was not observed during the experiments, and due to time restrictions the analysis of P-AuNPs by MALDI-MS was not continued.

MALDI-MS analysis of PPTS capped AuNPs with the use of CHCA showed that the reaction has gone to completion, with no free ligand of PPTS present, due to the absence of the PPTS $[M]^+$ peak at m/z 379. This result is in agreement with LDI-MS data obtained in the section 3.3.3.7. This observation is also in agreement with the TEM data reported previously in section 3.3.3.2; AuNPs prepared from the PPTS precursor produces particles with narrower particle size distribution, as the cleavage step for the thiosulfate sulfur-sulfur bond (S-S) is faster which result in complete reaction thus produces AuNPs with narrower particle size distributions.

For future work, it might be worth investigating further into the unidentified peaks in Figure 3.26 and try to identify them, a feasible approach is to analyse the peaks of interest by tandem MS-MS to gain more information about a specific peak

MALDI-MS analysis is limited to small AuNPs due to common detectors used decreases sensitivity with increase mass, and since the mass of AuNPs increases exponentially with diamater size, therefore larger AuNP clusters will become unobservable (Harkness *et al.*, 2010). To the best of the authors knowledge MS characterisation has only been successfully conducted on AuNP's with diameter size of up to 2 nm (Chaki *et al.*, 2008, Yu and Andriola, 2010). AuNPs synthesised in this project are larger than 2 nm in diameter, which may explain why initial experiments using MALDI-MS for the analysis of P-AuNPs did not yield positive results, nevertheless the use of MALDI-MS for the characterisation of AuNPs is an active area of research being pursued by other research groups and further experiments are required in order to obtain useful information to aid in the determination of the exact formula.

3.3.3.7 Laser Desorption/Ionization Mass Spectrometry (LDI-MS)

MALDI has become a powerful technique in the analysis of biomolecules. Several groups have demonstrated the use of an organic chemical matrix in MALDI MS, and the technique is capable of detecting a range of biomolecules (peptides, proteins and nucleic aicds) (Wu *et al.*, 2009, Chiang *et al.*, 2011).

AuNPs have been studied as potential inorganic matrices, compared with organic chemical matrices, nanomaterial matrices offer the advantages of eliminating matrix ion interference and improving the sample homogeneity (McLean *et al.*, 2005, Wu *et al.*, 2009). As a result LDI-TOF-MS has become a powerful analytical tool for the analysis of functionalised AuNPs since the surface ligands can be efficiently ionised due to the ability of the gold particles to absorb at wavelengths commonly used by mass spectrometers (Spencer *et al.*, 2008, Su and Tseng, 2007).

In this section LDI-TOF-MS has been employed as an additional technique to characterise the surface ligands coated on the surface of AuNPs.

Figure 3.29 LDI-MS spectrum of PPTS capped AuNPs analysed in positive ion mode. The spectrum shows the cleaved peaks for PPTS [M-SO₃+H]⁺ at *m/z* 337.0667, [M-SSO₃]⁺ at *m/z* 303.0571, [M-(CH₂)SSO₃]⁺ at *m/z* 289.0468, [M-(CH₂)₂SSO₃]⁺ at *m/z* 275.0392 and [M-(CH₂)₃SSO₃]⁺ at *m/z* 262.0338. All peaks identified supported the correct structure for PPTS.
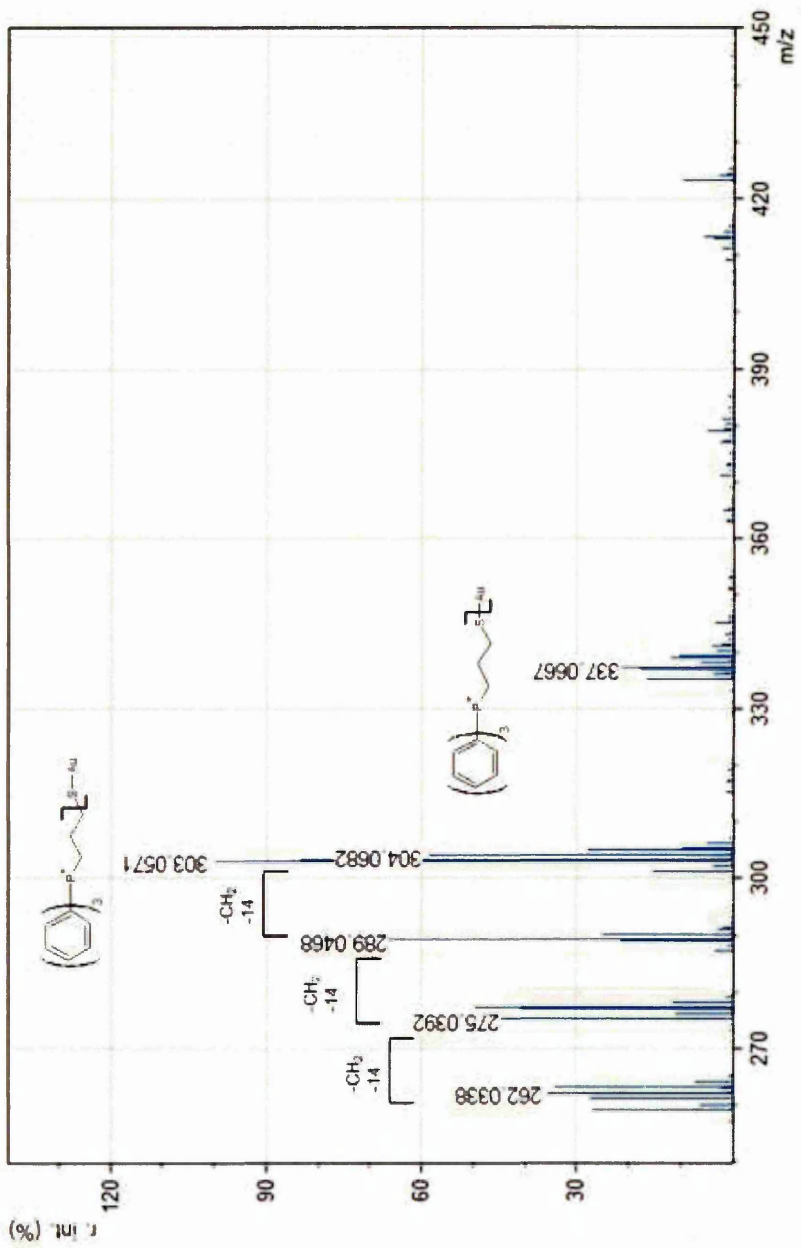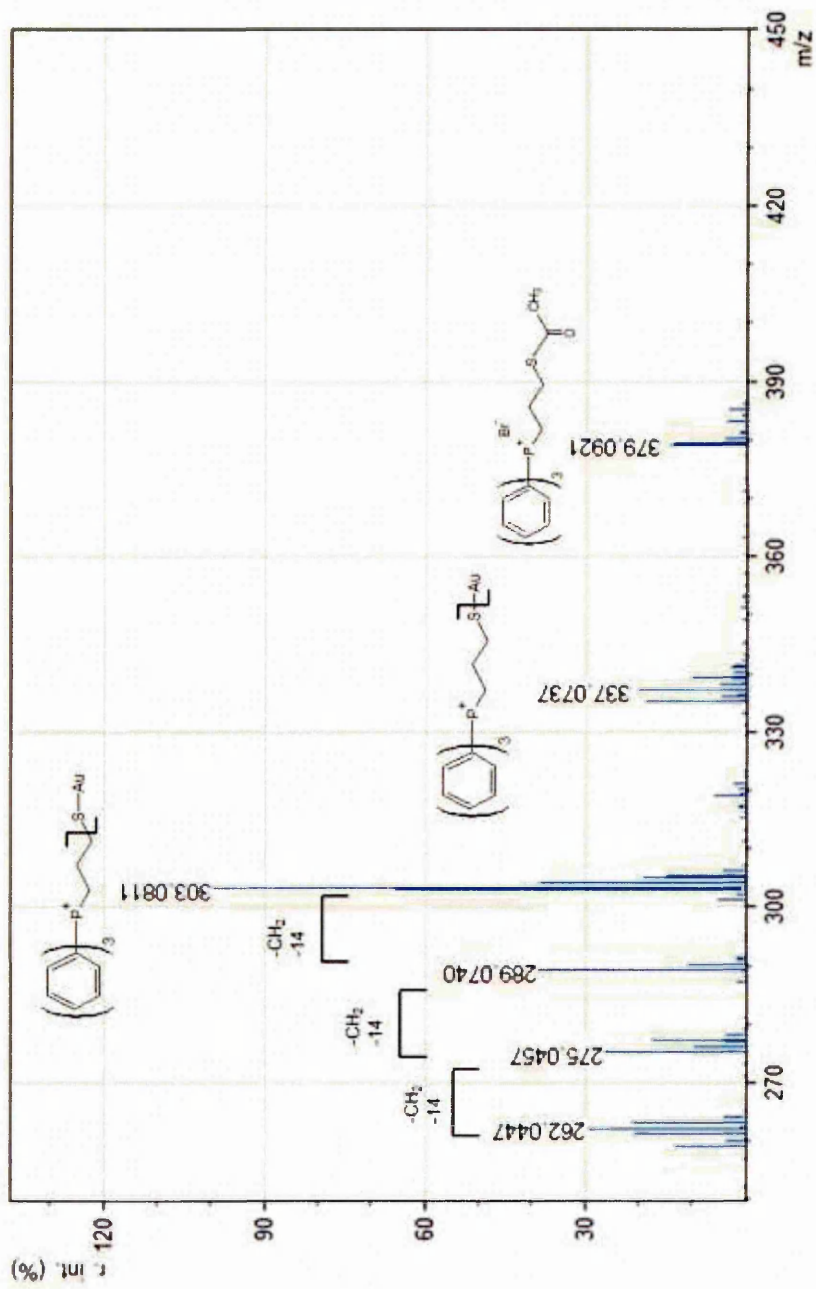
Figure 3.30 LDI-MS spectrum of PPTA capped AuNPs analysed in positive ion mode. The spectrum shows the presence of the PPTA ligand [M]⁺ at *m/z* 379.0921 and the cleaved peaks for PPTA [M-SOCH₃+H]⁺ at *m/z* 337.0737, [M-SSOCH₃]⁺ at *m/z* 303.0811, [M-(CH₂)SSOCH₃]⁺ at 289.0740, [M-(CH₂)₂ SSOCH₃]⁺ at *m/z* 275.0457 and [M-(CH₂)₃SSOCH₃]⁺ at *m/z* 262.0447. All peaks identified supported the correct structure for PPTA.

125
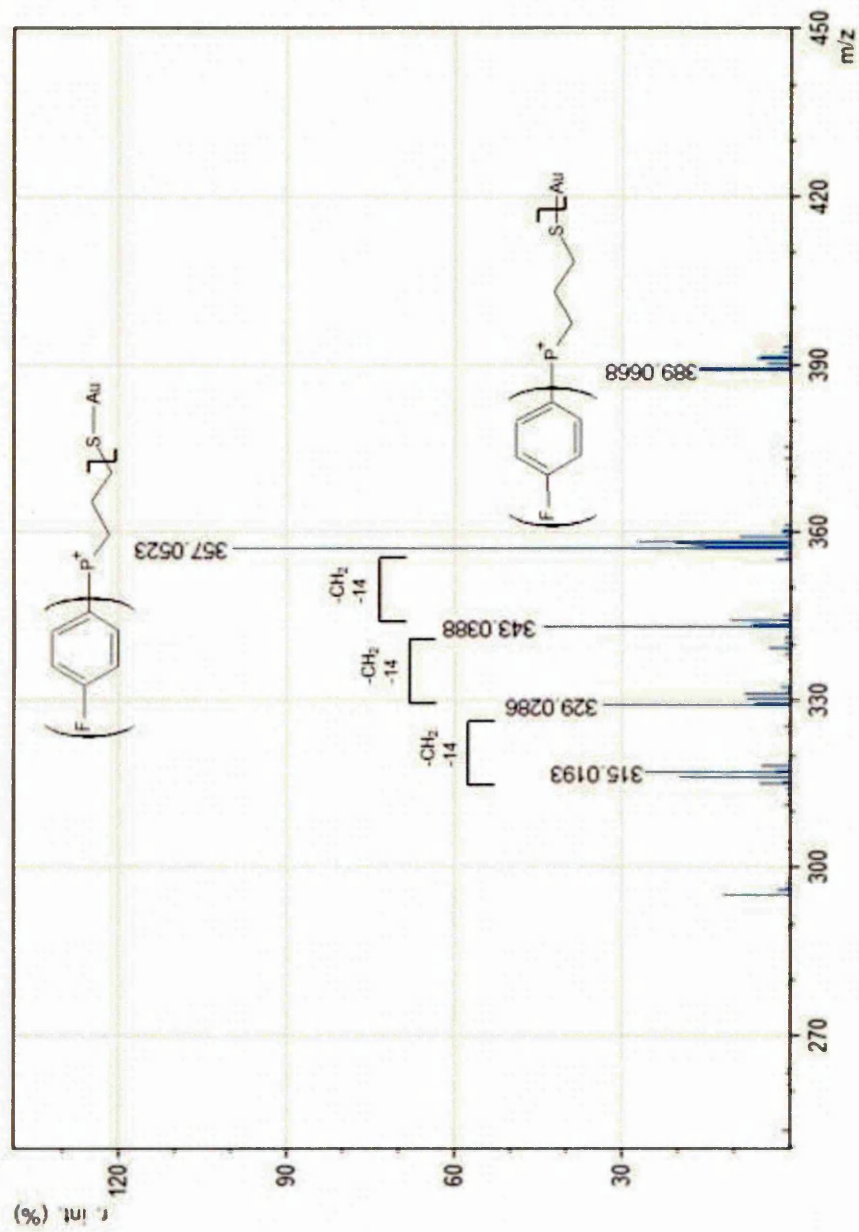
Figure 3.31 LDI-MS spectrum of FPPTS capped AuNPs analysed in positive ion mode. The spectrum shows the cleaved peaks for FPPTA $[M-SO_3]^+$ at m/z 389.0668, $[M-SSO_3]^+$ at m/z 357.0523, $[M-(CH_2)SSO_3]^+$ at 343.0388, $[M-(CH_2)_2 SSO_3]^+$ at m/z 329.0286 and $[M-(CH_2)_3SSO_3]^+$ at m/z 315.0193. All peaks identified supported the correct structure for FPPTS.

126

All LDI-MS spectra obtained from AuNPs capped with PPTS, PPTA and FPPTS (Figure 3.29-3.31) exhibited cleaved peaks; both PPTS and PPTA showed the cleaved phosphoniopropylthiolate ion $[Ph_3P^+(CH_2)_3S]^+$ at m/z 377, and FPPTS showed the cleaved peak $[p\text{-}FC_6H_4P^+(CH_2)_3S]^+$ at m/z 389.

The molecular ions for the parent PPTS and FPPTS species were absent in their LDI-MS spectrum (Figure 3.29 and 3.30), this confirmed the successful synthesis of functionalised AuNPs, as all ligands were cleaved at the thiosfulate S-S bond and formed strong Au-S bonds to the surface of the nanoparticles. In contrast, AuNPs capped with PPTA displayed the molecular ion peak corresponding to the parent molecular ion at m/z 379. This observation of the molecular ion for the PPTA salt is in accord with the TEM analysis (chapter 3.3.3.2) of this sample with larger diameter than those prepared from the corresponding PPTS zwitterion which is consistent with slower, or incomplete, reaction.

Furthermore all spectra showed in-source fragmentation peaks with 14 m/z which corresponded to the consecutive loss a CH_2 group, in total the loss of 3 CH_2 groups were observed in the LDI-MS spectra (Figure 3.29-3.31) which further supported the structure of the ligands present on the surface of AuNPs.

Overall LDI-MS analyses have provided valuable information regarding the chemical composition of the surface ligands; the spectrum showed that the S-S bond of the thiolate $(S\text{-}SO_3)$ (PPTS and FPPTS) and thioacetate $(S\text{-}SOCH3_3)$ (PPTA) have successfully been cleaved forming strong Au-S bonds, particularly the thiolate species (PPTS and FPPTS) had very clean cleavage which was confirmed from LDI-MS with the absence of the molecular ion peak. This observation is in agreement with TEM data obtained previously in chapter 3.3.3.2 with smaller particle size and distribution produced in comparison to AuNPs prepared from the thioacetate precursor ion. Along with the loss of three CH_2 groups which could clearly be identified from the spectrum, LDI-MS data provided strong evidence that the surface ligands coated on the surface of the AuNPs were as expected.

3.3.3.8 Thermogravimetric Analysis (TGA)

TGA is a relatively simple technique that requires no special sample preparation. During the analysis samples are heated to elevated temperatures and the mass of the sample is recorded giving a decomposition curve. The decomposition curve provides information on the temperature at which the bulk of the material decomposes and the residual mass of the sample (Mansfield et al., 2014). TGA has been used in evaluating the purity of nanomaterials (Mansfield et al., 2010) and the determination of the organic weight fraction of Au thiolate-MPCs; MPCs decompose thermally leaving elemental gold residue therefore the thiol/Au ratio can be determined and thus the average number of sulfur ligands can be calculated (Hostetler et al., 1998). In this project, TGA analysis has been conducted to obtain additional information on the P-AuNPs synthesised, and attempt to deduce the number of sulphur ligands in relation to number of Au atoms.

TGA thermograms (Figure 3.32) showed two main thermal events; the first weight loss around 50-150°C (~7%) is due to the loss of solvents with the majority of solvents lost in this region. The second weight loss starts from 250°C until 500°C (~33%), then plateaus and decreases again until 750°C (~0.9%), this major weight loss is due to the loss of the organic capping agent. Visual inspection of the sample holder showed that the material remaining after thermolysis is most likely to be pure Au due to the gold colour of the sample, and no other element in the sample other than gold has a decomposition value above 750°C.

The loss of organic capping ligands on the gold surface starts around at 250°C, this will not have an effect of the end application of utilising these P-AuNPs in photothermal therapy applications, which involve increasing the temperature of cells between 41-46°C to induce apoptotic cell death (Cherukuri et al., 2010). If the loss of organic ligands at low temperatures around 40-50°C this would have been an issue, as when the cells get heated up to above this temperature, the ligands will begin to detach from the surface of the AuNPs, this will no doubt change the functionality of the AuNPs this can induce a change in the properties of the AuNPs thus effecting its end application.

The TGA results showed that there is a large organic fraction ~ 40% which suggest the ratio between thiol/Au is nearly 1:1, suggesting that AuNPs synthesised are small MPCs, since smaller MPCs have a larger organic weight fraction as they have a larger surface area per unit of Au mass. AuNPs (3.7 nm) prepared with S-dodecylthiosulfate has shown to have 18.5% of organic coverage, while AuNPs (2.2 nm) prepared with dodecanethiol were shown to have a higher organic coverage of 41.6% (Shon *et al.*, 2000). Based on the data reported in the literature, TGA data suggested that the size of P-AuNPs synthesised are between 2.2 and 3.7 nm in size, this size range is in agreement with TEM data reported previously in section 3.3.3.2, with a mean particle size of 3.0 nm.

TGA data provides the general picture of the sample indicated the presence of a large organic fraction, in contrast TEM is capable of providing size data on a particle by particle basis, the size distribution showed that not all particles synthesised are the same size, which suggest that there is variation between the organic fractions on each gold nanoparticle. As the different in the ratio between the thiol and Au will result in the formation of AuNPs with different sizes (Frenkel et al., 2005)

To further support data obtained from TGA and TEM, future work will be to conduct DLS analysis to provide data on the hydrodynamic radius of the P-AuNPs. It would be interesting to compare the results obtained DLS with TEM, the results obtained can help to calculate the thickness of the capping ligands coating the surface of the gold nanoparticles, from this an estimate of the ratio of the organic ligand compared to the Au core can be calculated (Jans et al., 2009).
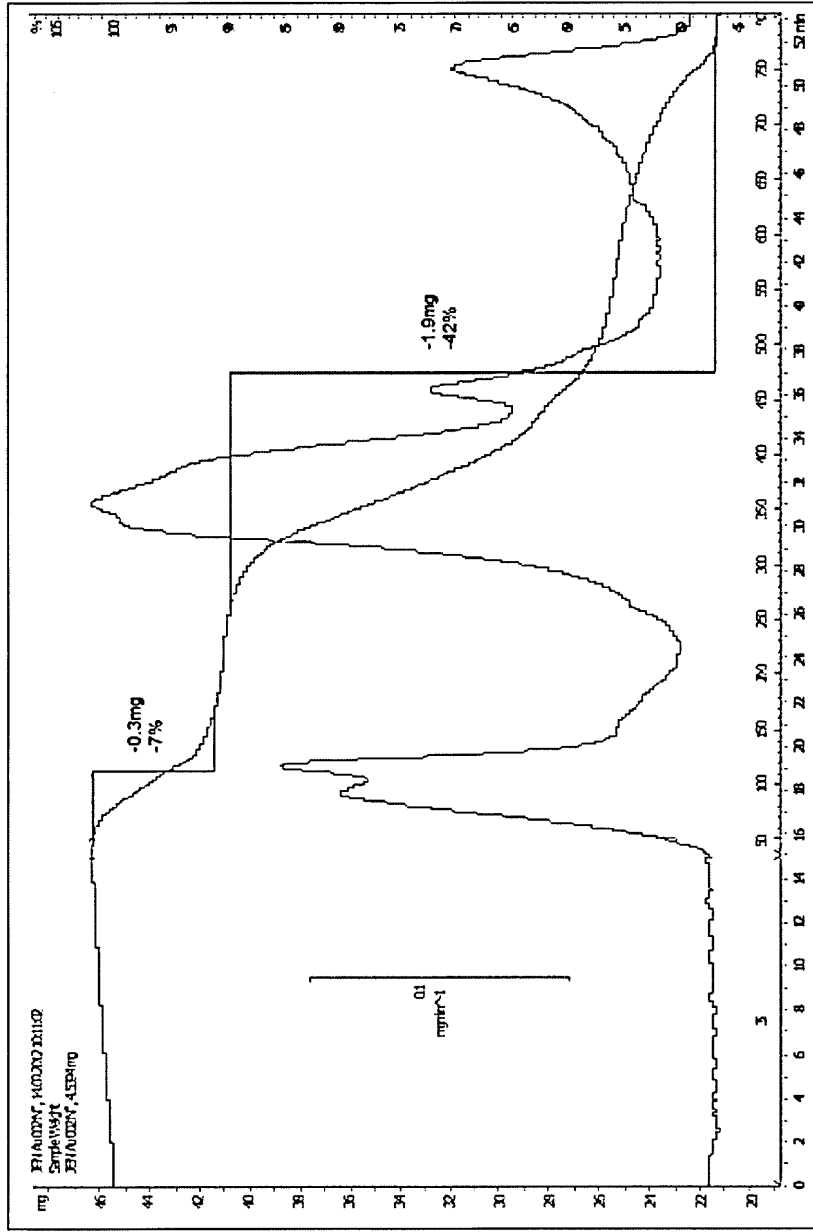
Figure 3.32 TGA curve for PPTS capped AuNPs describing the weight loss over temperature; first weight loss step between 50-150°C contribute to ~7% of total weight loss, the second weight loss step between 250-750°C contribute to ~42% of total weight loss. This suggests that the ratio between thiol/Au is approximately 1:1.

130

3.3.3.9 Inductively Coupled Plasma Mass Spectrometry (ICP-MS)

ICP coupled plasma mass spectrometry (ICP-MS) has emerged as an important and useful technique for the analysis of AuNPs; both ICP-OES (Elzey *et al.*, 2012) and ICP-MS (Scheffer *et al.*, 2008) have been used for the characterisation of AuNPs. ICP-MS has a limit of detection of Au ~1 pg/mL (1 part per trillion) and is more sensitive than ICP-OES by around 3 orders of magnitude. ICP-MS is the method of choice when maximum sensitivity is required. Overall ICP offers a fast and reliable method for quantifying AuNPs in solution (Scheffer *et al.*, 2008).

ICP has been commonly used to determine the concentration of elemental Au in colloidal solutions. It has been demonstrated that AuNP dispersions can be analysed directly without previous digestion, excellent spike recovery >90% was observed using 1% (v/v) HCl (Allabashi *et al.*, 2009). Recent studies have extended the application of ICP for the characterisation of AuNPs to quantify the ligand packing density on AuNPs (Elzey *et al.*, 2012, Hinterwirth *et al.*, 2013). In this chapter, the use of ICP to determine the Au concentration has been investigated.

ICP-MS results indicated that PPTS capped AuNPs have a lower Au concentration of 7.54 mg/L when dissolved in DIH$_2$O compared to 9.59 mg/L when dissolved in 1% (v/v) HCl. This decrease in Au concentration is consistent with the results of Allabashi and colleagues (Allabashi *et al.*, 2009) who reported a reduction in Au concentration when AuNP dispersion was diluted by DIH$_2$O compared to 1% (v/v) HCl. In addition to analysing gold, phosphorous and sulfur have also been quantified using ICP-OES to obtain additional information regarding the surface ligands. To confirm the results obtained, samples were sent to MEDAC (Chobham, Surrey, UK) for analysis. Both sets of results were very similar, data are shown in Table 3.7.

Element	Concentration (mg/mL)	
	In house	MEDAC
Au	95.9	102.7
P	26.4	28.7
S	75.4	77.2

Table 3.7 Elemental analysis of Au, P and S of PPTS capped AuNPs using ICP-MS; ICP-MS data obtained in house and externally (MEDAC) are reported.

Preliminary results suggest that the ratio Au:S is approximately 5:4, this value is very similar to TGA data obtained previously (chapter 3.3.3.8) Au and organic fraction of 49% and 42% respectively.

The average number of gold atoms per nanoparticle ($N_{Au/GNP}$) can be calculated theoretically. Assuming a spherical shape and a uniform structure, the average number of gold atoms (N) can be calculated using Equation1, where p is the density for gold (19.3 g/cm^3) (Zhang et al., 2004, Cui et al., 2002) and M stands for atomic weight of gold (197 g/mol).

With an increase in diameter, the average number of gold atoms per gold nanoparticle ($N_{Au/GNP}$) will increase with cube (Liu et al., 2007). Based on TEM results reported previously in chapter 3.3.3.2 and substituting in Equation 1, the average number of gold atoms calculated to be 1.39×10^{-21}.

$$N_{Au/GNP} = \frac{\pi p D^3}{6M} \text{ (Equation 1)}$$

The ligand coverage *via* the gold-to-sulfur ratio can be calculated based on the fact that the gold atoms constitute the particle core with each ligand on the nanoparticle surface carrying a single surfur atom only, The number of sulfur atoms per gold nanoparticle ($N_{S/GNP}$) will increase to the square of the AuNP diameter and is proportional to the maximal coverage factor k_{max} and can be calculated using Equation 2.

$$N_{S/GNP} = \kappa \pi D^2 \text{ (Equation 2).}$$

Combining the two equations (Equation 3), it assumes that spherical nanoparticles monodispersed with complete saturation with a monolayer of thiol ligands on the particle surface.

$$\frac{N_{Au/GNP}}{N_{s/GNP}}=\frac{\frac{\pi\rho D^3}{6M}}{K_{max}\pi D^2}=k_{max}^{-1} \times 9.83 \times D \text{ (Equation 3).}$$

Using equation 3, the calculated theoretical maximum number of PPTA ligands on the surface of gold nanoparticles is 8.39×10^{-19}. Therefore based on ICP-MS (Chapter 3.3.3.9) and TGA (3.3.3.8) data obtained that the ratio of Au:S was approximately 5:4, based on this ratio and the calculated values for Au and S are 4.66×10^{-19} and 3.73×10^{-19} respectively.

3.4 Conclusion

Results in this chapter, showed that triarylphosphoniopropylthiosulfate zwitterions and ω-thioacetylpropyl(triphenyl)phosphonium salts can be used to prepared cationic AuNPs with average core sizes between 2.7-5.0 nm. A variety of techniques incorporating both qualitative and quantitative analysis have been employed throughout this section to characterise phosphonium-AuNPs synthesised.

Spectroscopy results (^{31}P NMR, ^{1}H NMR, ESMS, FTIR) all supported the successful synthesis of phosphonium ligands (PPTS, PPTA, FPPTS and FPPTA). X-ray crystallography further confirmed the expected structure for FPPTS and FPPTA.

The first indication for the successful synthesis of P-AuNPs was the visual observation of the colour change to the characteristic deep red wine colour of colloidal gold. UV-vis results showed SPR band ~520 nm for all AuNPs prepared, this result is in agreement with AuNPs in the region of 5 nm (Daniel and Astruc, 2004). ^{31}P NMR provided evidence that the chemical structure of the ligand stabilising the gold core is the same structure of the ligand itself and that the phosphonium head group remained intact.

XPS data provided valuable information about the ligands coating the surface of AuNPs, wide scan spectrum confirmed the presence of phosphorous, sulfur and gold in all the samples. Furthermore, AuNPs prepared from FPPTS, a fluorine peak was observed, which agrees with the chemical structure. High resolution of Au (4f) spectrum showed a double for Au at Au ($4f_{7/2}$) and Au ($4f_{5/2}$) for all samples analysed in the region of 84 and 88 eV respectively, which are similar to the values of gold thiolates reported in the literature (Brust *et al.*, 1994, Yee *et al.*, 2003). The presence of the peak for Au ($4f_{7/2}$) shows that the bulk of the gold atom are in the Au(0) oxidation state, confirming the successful synthesis of AuNPs.

LDI-MS data also provided useful information regarding the chemical composition of the surface ligands on the AuNPs. LDI-MS spectrum showed that the S-S bond of the thiolate (S-SO_3) (PPTS and FPPTS) and thioacetate (S-$SOCH3_3$) (PPTA) have successfully been cleaved forming strong Au-S bonds, particularly the thiolate species (PPTS and FPPTS) had very clean cleavage which was confirmed from LDI-MS with the absence of the molecular ion peak.

Preliminary TGA data suggest there is a high thiol/Au ratio, which is in accord with ICP-OES data. ICP-OES and MALDI-TOF-MS are two powerful techniques for the quantitative analysis of AuNPs, initial results are certainly of interest, however further investigation is required in order to gain useful quantification information on the ligand density.

TEM results showed all nanoparticles synthesised have a uniform spherical shape, although phosphonium-AuNPs produced from the PPTS zwitterion or PPTA salt all yield the same Au-S ligation, the PPTA salt produces slightly larger AuNPs in comparison to the corresponding PPTS zwitterion which is consistent with slower or incomplete reaction, this is supported by molecular ion observed for the PPTA salt in LDI-TOF-MS spectra. PPTS capped AuNPs were taken forward to investigate their cytotoxicity and uptake in cells (chapter 4).

3.5 References

ALLABASHI, R., STACH, W., DE LA ESCOSURA-MU IZ, A., LISTE-CALLEJA, L. & MERKO I, A. 2009. ICP-MS: A powerful technique for quantitative determination of gold nanoparticles without previous dissolving. *Journal of Nanoparticle Research,* 11, 2003-2011.

ARNOLD, R. J. & REILLY, J. P. 1998. High-resolution time-of-flight mass spectra of alkanethiolate-coated gold nanocrystals. *Journal of the American Chemical Society,* 120, 1528-1532.

B HM, H. J., BANNER, D., BENDELS, S., KANSY, M., KUHN, B., M LLER, K., OBST-SANDER, U. & STAHL, M. 2004. Fluorine in medicinal chemistry. *ChemBioChem,* 5, 637-643.

BAER, D. R. & ENGELHARD, M. H. 2010. XPS analysis of nanostructured materials and biological surfaces. *Journal of Electron Spectroscopy and Related Phenomena,* 178-179, 415-432.

BAER, D. R., GASPAR, D. J., NACHIMUTHU, P., TECHANE, S. D. & CASTNER, D. G. 2010. Application of surface chemical analysis tools for characterization of nanoparticles. *Analytical and Bioanalytical Chemistry,* 396, 983-1002.

BAIN, C. D., BIEBUYCK, H. A. & WHITESIDES, G. M. 1989. Comparison of self-assembled monolayers on gold: Coadsorption of thiols and disulfides. *Langmuir,* 5, 723-727.

BIEBUYCK, H. A. & WHITESIDES, G. M. 1993. Interchange between monolayers on gold formed from unsymmetrical disulfides and solutions of thiols: evidence for sulfur-sulfur bond cleavage by gold metal. *Langmuir,* 9, 1766-1770.

BISWAS, S., DODWADKAR, N. S., DESHPANDE, P. P. & TORCHILIN, V. P. 2012. Liposomes loaded with paclitaxel and modified with novel triphenylphosphonium-PEG-PE conjugate possess low toxicity, target mitochondria and demonstrate enhanced antitumor effects in vitro and in vivo. *J Control Release,* 159, 393-402.

BOURG, M. C., BADIA, A. & BRUCE LENNOX, R. 2000. Gold-sulfur bonding in 2D and 3D self-assembled monolayers: XPS characterization. *Journal of Physical Chemistry B,* 104, 6562-6567.

BRUST, M., WALKER, M., BETHELL, D., SCHIFFRIN, D. J. & WHYMAN, R. 1994. Synthesis of thiol-derivatised gold nanoparticles in a two-phase liquid-liquid system. *Journal of the Chemical Society, Chemical Communications,* 801-802.

CHAKI, N. K., NEGISHI, Y., TSUNOYAMA, H., SHICHIBU, Y. & TSUKUDA, T. 2008. Ubiquitous 8 and 29 kDa gold:alkanethiolate cluster compounds: Mass-spectrometric determination of molecular formulas and structural implications. *Journal of the American Chemical Society,* 130, 8608-8610.

CHEN, J. X., XU, Q. F., ZHANG, Y., ZAIN, S. M., NG, S. W. & LANG, J. P. 2004. S-[4-(Trimethylammonio)phenyl] thiosulfate, an aromatic organic thiosulfate. *Acta Crystallographica Section C: Crystal Structure Communications,* 60, o572-o574.

CHENG, Z., SUBBARAYAN, M., CHEN, X. & GAMBHIR, S. S. 2005. Synthesis of (4-[18F]fluorophenyl)triphenylphosphonium as a potential imaging agent for mitochondrial dysfunction. *Journal of Labelled Compounds and Radiopharmaceuticals,* 48, 131-137.

135

CHERUKURI, P., GLAZER, E. S. & CURLEYA, S. A. 2010. Targeted hyperthermia using metal nanoparticles. *Advanced Drug Delivery Reviews,* 62, 339-345.

CHIANG, C. K., CHEN, W. T. & CHANG, H. T. 2011. Nanoparticle-based mass spectrometry for the analysis of biomolecules. *Chemical Society Reviews,* 40, 1269-1281.

CHO, E. C., XIE, J., WURM, P. A. & XIA, Y. 2009. Understanding the role of surface charges in cellular adsorption versus internalization by selectively removing gold nanoparticles on the cell surface with a I 2/KI etchant. *Nano Letters,* 9, 1080-1084.

COZZI, F., ANNUNZIATA, R., BENAGLIA, M., BALDRIDGE, K. K., AGUIRRE, G., ESTRADA, J., SRITANA-ANANT, Y. & SIEGEL, J. S. 2008. Through-space interactions between parallel-offset arenes at the van der Waals distance: 1,8-diarylbiphenylene syntheses, structure and QM computations. *Physical Chemistry Chemical Physics,* 10, 2686-2694.

CUI, X. D., PRIMAK, A., ZARATE, X., TOMFOHR, J., SANKEY, O. F., MOORE, A. L., MOORE, T. A., GUST, D., NAGAHARA, L. A. & LINDSAY, S. M. 2002. Changes in the electronic properties of a molecule when it is wired into a circuit. *Journal of Physical Chemistry B,* 106, 8609-8614.

DANIEL, M. C. & ASTRUC, D. 2004. Gold nanoparticles: Assembly, supramolecular chemistry, quantum-size-related properties, and applications toward biology, catalysis, and nanotechnology. *Chemical Reviews,* 104, 293-346.

DASS, A., GUO, R., TRACY, J. B., BALASUBRAMANIAN, R., DOUGLAS, A. D. & MURRAY, R. W. 2008a. Gold nanoparticles with perfluorothiolate ligands. *Langmuir,* 24, 310-315.

DASS, A., STEVENSON, A., DUBAY, G. R., TRACY, J. B. & MURRAY, R. W. 2008b. Nanoparticle MALDI-TOF mass spectrometry without fragmentation: Au 25(SCH2CH2Ph)18 and mixed monolayer Au25(SCH2CH2Ph)18-x(L)x. *Journal of the American Chemical Society,* 130, 5940-5946.

DUNITZ, J. D. & TAYLOR, R. 1997. Organic Fluorine Hardly Ever Accepts Hydrogen Bonds. *Chemistry – A European Journal,* 3, 89-98.

ELZEY, S., TSAI, D. H., RABB, S. A., YU, L. L., WINCHESTER, M. R. & HACKLEY, V. A. 2012. Quantification of ligand packing density on gold nanoparticles using ICP-OES. *Analytical and Bioanalytical Chemistry,* 403, 145-149.

ERBEN, M. F., BOESE, R., DELLA V DOVA, C. O., OBERHAMMER, H. & WILLNER, H. 2006. Toward an intimate understanding of the structural properties and conformational preference of oxoesters and thioesters: Gas and crystal structure and conformational analysis of dimethyl monothiocarbonate, CH 3OC(O)SCH3. *Journal of Organic Chemistry,* 71, 616-622.

FEALY, R. J., ACKERMAN, S. R. & FERGUSON, G. S. 2011. Mechanism of spontaneous formation of monolayers on gold from alkyl thiosulfates. *Langmuir,* 27, 5371-5376.

FILLER, R. & SAHA, R. 2009. Fluorine in medicinal chemistry: A century of progress and a 60-year retrospective of selected highlights. *Future Medicinal Chemistry,* 1, 777-791.

FRENKEL, A. I., NEMZER, S., PISTER, I., SOUSSAN, L., HARRIS, T., SUN, Y. & RAFAILOVICH, M. H. 2005. Size-controlled synthesis and

characterization of thiol-stabilized gold nanoparticles. *Journal of Chemical Physics,* 123.

FRENS, G. 1973. Controlled Nucleation for the Regulation of the Particle Size in Monodisperse Gold Suspensions. *Nature Physical Science,* 241, 20-22.

GILJOHANN, D. A., SEFEROS, D. S., DANIEL, W. L., MASSICH, M. D., PATEL, P. C. & MIRKIN, C. A. 2010. Gold nanoparticles for biology and medicine. *Angewandte Chemie - International Edition,* 49, 3280-3294.

GREEN, M. & O'BRIEN, P. 2000. A simple one phase preparation of organically capped gold nanocrystals. *Chemical Communications,* 183-184.

GREEN, M., RAHMAN, P. & SMYTH-BOYLE, D. 2007. Ionic liquid passivated CdSe nanocrystals. *Chemical Communications,* 574-576.

HARKNESS, K. M., CLIFFEL, D. E. & MCLEAN, J. A. 2010. Characterization of thiolate-protected gold nanoparticles by mass spectrometry. *Analyst,* 135, 868-874.

HARNACK, O., FORD, W. E., YASUDA, A. & WESSELS, J. M. 2002. Tris(hydroxymethyl)phosphine-Capped Gold Particles Templated by DNA as Nanowire Precursors. *Nano Letters,* 2, 919-923.

HEISTER, K., ALLARA, D. L., BAHNCK, K., FREY, S., ZHARNIKOV, M. & GRUNZE, M. 1999. Deviations from 1:1 compositions in self-assembled monolayers formed from adsorption of asymmetric dialkyl disulfides on gold. *Langmuir,* 15, 5440-5443.

HELFRICH, A. & BETTMER, J. 2011. Analysis of gold nanoparticles using ICP-MS-based hyphenated and complementary ESI-MS techniques. *International Journal of Mass Spectrometry,* 307, 92-98.

HINTERWIRTH, H., KAPPEL, S., WAITZ, T., PROHASKA, T., LINDNER, W. & L MMERHOFER, M. 2013. Quantifying thiol ligand density of self-assembled monolayers on gold nanoparticles by inductively coupled plasma-mass spectrometry. *ACS Nano,* 7, 1129-1136.

HOFFMANN, D., E & STROOBANT, V. 2007. *Mass spectrometry: principles and applications* England, John Wiley & Sons Ltd

HOSTETLER, M. J., WINGATE, J. E., ZHONG, C. J., HARRIS, J. E., VACHET, R. W., CLARK, M. R., LONDONO, J. D., GREEN, S. J., STOKES, J. J., WIGNALL, G. D., GLISH, G. L., PORTER, M. D., EVANS, N. D. & MURRAY, R. W. 1998. Alkanethiolate gold cluster molecules with core diameters from 1.5 to 5.2 nm: Core and monolayer properties as a function of core size. *Langmuir,* 14, 17-30.

HUHEEY, J. E. 1972. Inorganic chemistry : principles of structure and reactivity. New York, NY :: Joanna Cotler Books.

HUNTER, C. A. & SANDERS, J. K. M. 1990. The nature of .pi.-.pi. interactions. *Journal of the American Chemical Society,* 112, 5525-5534.

ISAACS, S. R., CUTLER, E. C., PARK, J. S., LEE, T. R. & SHON, Y. S. 2005. Synthesis of tetraoctylammonium-protected gold nanoparticles with improved stability. *Langmuir,* 21, 5689-5692.

ISANBOR, C. & O'HAGAN, D. 2006. Fluorine in medicinal chemistry: A review of anti-cancer agents. *Journal of Fluorine Chemistry,* 127, 303-319.

JANS, H., LIU, X., AUSTIN, L., MAES, G. & HUO, Q. 2009. Dynamic light scattering as a powerful tool for gold nanoparticle bioconjugation and biomolecular binding studies. *Analytical Chemistry,* 81, 9425-9432.

137

JIN, Q., XU, J. P., JI, J. & SHEN, J. C. 2008. Zwitterionic phosphorylcholine as a better ligand for stabilizing large biocompatible gold nanoparticles. *Chemical Communications*, 3058-3060.

JU-NAM, Y., ALLEN, D. W., GARDINER, P. H. E. & BRICKLEBANK, N. 2008. ω-Thioacetylalkylphosphonium salts: Precursors for the preparation of phosphonium-functionalised gold nanoparticles. *Journal of Organometallic Chemistry*, 693, 3504-3508.

JU-NAM, Y., BRICKLEBANK, N., ALLEN, D. W., GARDINER, P. H. E., LIGHT, M. E. & HURSTHOUSE, M. B. 2006. Phosphonioalkylthiosulfate zwitterions - new masked thiol ligands for the formation of cationic functionalised gold nanoparticles. *Organic & Biomolecular Chemistry*, 4, 4345-4351.

KARAS, M. & HILLENKAMP, F. 1988. Laser desorption ionization of proteins with molecular masses exceeding 10 000 daltons [1]. *Analytical Chemistry*, 60, 2299-2301.

KIM, D. Y., KIM, H. J., YU, K. H. & MIN, J. J. 2012. Synthesis of [18F]-labeled (2-(2-fluoroethoxy)ethyl)tris(4-methoxyphenyl)phosphonium cation as a potential agent for positron emission tomography myocardial imaging. *Nuclear Medicine and Biology*, 39, 1093-1098.

KIM, S. T., SAHA, K., KIM, C. & ROTELLO, V. M. 2013. The role of surface functionality in determining nanoparticle cytotoxicity. *Accounts of Chemical Research*, 46, 681-691.

KIRK, K. L. 2006. Fluorine in medicinal chemistry: Recent therapeutic applications of fluorinated small molecules. *Journal of Fluorine Chemistry*, 127, 1013-1029.

KOUCHI, H., KAWASAKI, H. & ARAKAWA, R. 2012. A new matrix of MALDI-TOF MS for the analysis of thiolate-protected gold clusters. *Analytical Methods*, 4, 3600-3603.

LEE, M. T., HSUEH, C. C., FREUND, M. S. & FERGUSON, G. S. 1998. Air oxidation of self-assembled monolayers on polycrystalline gold: The role of the gold substrate. *Langmuir*, 14, 6419-6423.

LIU, X., ATWATER, M., WANG, J. & HUO, Q. 2007. Extinction coefficient of gold nanoparticles with different sizes and different capping ligands. *Colloids and Surfaces B: Biointerfaces*, 58, 3-7.

LIU, X., YU, M., KIM, H., MAMELI, M. & STELLACCI, F. 2012. Determination of monolayer-protected gold nanoparticle ligand-shell morphology using NMR. *Nature Communications*, 3.

LOHSE, S. E., DAHL, J. A. & HUTCHISON, J. E. 2010. Direct synthesis of large water-soluble functionalized gold nanoparticles using bunte salts as ligand precursors. *Langmuir*, 26, 7504-7511.

LOVE, J. C., ESTROFF, L. A., KRIEBEL, J. K., NUZZO, R. G. & WHITESIDES, G. M. 2005. Self-assembled monolayers of thiolates on metals as a form of nanotechnology. *Chemical Reviews*, 105, 1103-1169.

MADAR, I., HUANG, Y., RAVERT, H., DALRYMPLE, S. L., DAVIDSON, N. E., ISAACS, J. T., DANNALS, R. F. & FROST, J. J. 2009. Detection and quantification of the evolution dynamics of apoptosis using the PET voltage sensor18F-fluorobenzyl triphenyl phosphonium. *Journal of Nuclear Medicine*, 50, 774-780.

MADAR, I., RAVERT, H., DIPAULA, A., DU, Y., DANNALS, R. F. & BECKER, L. 2007. Assessment of severity of coronary artery stenosis in a canine model using the PET agent 18F-fluorobenzyl triphenyl phosphonium:

Comparison with 99mTc-tetrofosmin. *Journal of Nuclear Medicine,* 48, 1021-1030.

MADAR, I., RAVERT, H. T., DU, Y., HILTON, J., VOLOKH, L., DANNALS, R. F., FROST, J. J. & HARE, J. M. 2006. Characterization of uptake of the new PET imaging compound 18F-fluorobenzyl triphenyl phosphonium in dog myocardium. *Journal of Nuclear Medicine,* 47, 1359-1366.

MANSFIELD, E., KAR, A. & HOOKER, S. A. 2010. Applications of TGA in quality control of SWCNTs. *Analytical and Bioanalytical Chemistry,* 396, 1071-1077.

MANSFIELD, E., TYNER, K. M., POLING, C. M. & BLACKLOCK, J. L. 2014. Determination of nanoparticle surface coatings and nanoparticle purity using microscale thermogravimetric analysis. *Analytical Chemistry,* 86, 1478-1484.

MCINTOSH, C. M., ESPOSITO III, E. A., BOAL, A. K., SIMARD, J. M., MARTIN, C. T. & ROTELLO, V. M. 2001. Inhibition of DNA transcription using cationic mixed monolayer protected gold clusters. *Journal of the American Chemical Society,* 123, 7626-7629.

MCLEAN, J. A., STUMPO, K. A. & RUSSEL, D. H. 2005. Size-selected (2-10 nm) gold nanoparticles for matrix assisted laser desorption ionization of peptides. *Journal of the American Chemical Society,* 127, 5304-5305.

MCNEILLIE, A., BROWN, D. H., SMITH, W. E., GIBSON, M. & WATSON, L. 1980. X-ray photoelectron spectra of some gold compounds. *Journal of the Chemical Society, Dalton Transactions,* 767-770.

MIASKIEWICZ, K. & STEUDEL, R. 1992. The structures of thiosulfuric acid H2S2O3 and its monoanion HS2O- 3. *Angewandte Chemie (International Edition in English),* 31, 58-59.

PENA-MENDEZ, E. M., HERNANDEZ-FERNAUD, J. R., NAGENDER, R., HOUSKA, J. & HAVEL, J. 2008. The chemistry of gold clusters in plasma generated with MALDI, laser desorption ionisation and laser ablation from various precursors. *Chemicke Listy,* 102, S1394-S1398.

PILLAI, R. G. & FREUND, M. S. 2011. Self-assembly of alkylthiosulfates on gold: Role of electrolyte and trace water in the solvent. *Langmuir,* 27, 9028-9033.

RAVERT, H. T., MADAR, I. & DANNALS, R. F. 2004. Radiosynthesis of 3-[18F]fluoropropyl and 4-[18F]fluorobenzyl triarylphosphonium ions. *Journal of Labelled Compounds and Radiopharmaceuticals,* 47, 469-476.

REICHENBACHER, K., SUSS, H. I. & HULLIGER, J. 2005. Fluorine in crystal engineering-"the little atom that could". *Chemical Society Reviews,* 34, 22-30.

ROSS, M. F., KELSO, G. F., BLAIKIE, F. H., JAMES, A. M., COCHEM , H. M., FILIPOVSKA, A., DA ROS, T., HURD, T. R., SMITH, R. A. J. & MURPHY, M. P. 2005. Lipophilic triphenylphosphonium cations as tools in mitochondrial bioenergetics and free radical biology. *Biochemistry (Moscow),* 70, 222-230.

ROSS, M. F., PRIME, T. A., ABAKUMOVA, I., JAMES, A. M., PORTEOUS, C. M., SMITH, R. A. J. & MURPHY, M. P. 2008. Rapid and extensive uptake and activation of hydrophobic triphenylphosphonium cations within cells. *Biochemical Journal,* 411, 633-645.

ROUHANA, L. L., JABER, J. A. & SCHLENOFF, J. B. 2007. Aggregation-resistant water-soluble gold nanoparticles. *Langmuir,* 23, 12799-12801.

SANDHU, K. K., MCINTOSH, C. M., SIMARD, J. M., SMITH, S. W. & ROTELLO, V. M. 2002. Gold nanoparticle-mediated transfection of mammalian cells. *Bioconjugate Chemistry,* 13, 3-6.

SCHAAFF, T. G. 2004. Laser desorption and matrix-assisted laser desorption/ionization mass spectrometry of 29-kDa Au:SR cluster compounds. *Analytical Chemistry,* 76, 6187-6196.

SCHEFFER, A., ENGELHARD, C., SPERLING, M. & BUSCHER, W. 2008. ICP-MS as a new tool for the determination of gold nanoparticles in bioanalytical applications. *Analytical and Bioanalytical Chemistry,* 390, 249-252.

SCHOENFISCH, M. H. & PEMBERTON, J. E. 1998. Air stability of alkanethiol self-assembled monolayers on silver and gold surfaces. *Journal of the American Chemical Society,* 120, 4502-5413.

SENONER, M. & UNGER, W. E. S. 2012. SIMS imaging of the nanoworld: Applications in science and technology. *Journal of Analytical Atomic Spectrometry,* 27, 1050-1068.

SHAWKATALY, O. B., SINGH, J., SIVAKUMAR, K. & FUN, H. K. 1996. Tris(4-chlorophenyl)phosphine and tris(4-fluorophenyl)phosphine. *Acta Crystallographica Section C: Crystal Structure Communications,* 52, 2243-2245.

SHEM, P. M., SARDAR, R. & SHUMAKER-PARRY, J. S. 2009. One-step synthesis of phosphine-stabilized gold nanoparticles using the mild reducing agent 9-BBN. *Langmuir,* 25, 13279-13283.

SHON, Y. S., GROSS, S. M., DAWSON, B., PORTER, M. & MURRAY, R. W. 2000. Alkanethiolate-protected gold clusters generated from sodium S-dodecylthiosulfate (bunte salts). *Langmuir,* 16, 6555-6561.

SINGH, A., DAHANAYAKA, D. H., BISWAS, A., BUMM, L. A. & HALTERMAN, R. L. 2010. Molecularly ordered decanethiolate self-assembled monolayers on Au(111) from in situ cleaved decanethioacetate: An NMR and STM study of the efficacy of reagents for thioacetate cleavage. *Langmuir,* 26, 13221-13226.

SONG, Y., HUANG, T. & MURRAY, R. W. 2003. Heterophase ligand exchange and metal transfer between monolayer protected clusters. *Journal of the American Chemical Society,* 125, 11694-11701.

SPENCER, M. T., FURUTANI, H., OLDENBURG, S. J., DARLINGTON, T. K. & PRATHER, K. A. 2008. Gold nanoparticles as a matrix for visible-wavelength single-particle matrix-assisted laser desorption/ionization mass spectrometry of small biomolecules. *Journal of Physical Chemistry C,* 112, 4083-4090.

STROHALM, M., KAVAN, D., NOV K, P., VOLN , M. & HAVL ČEK, V. 2010. MMass 3: A cross-platform software environment for precise analysis of mass spectrometric data. *Analytical Chemistry,* 82, 4648-4651.

SU, C. L. & TSENG, W. L. 2007. Gold nanoparticles as assisted matrix for determining neutral small carbohydrates through laser desorption/ionization time-of-flight mass spectrometry. *Analytical Chemistry,* 79, 1626-1633.

THANH, N. T. K. & GREEN, L. A. W. 2010. Functionalisation of nanoparticles for biomedical applications. *Nano Today,* 5, 213-230.

TURKEVICH, J., STEVENSON, P. C. & HILLIER, J. 1951. A study of the nucleation and growth processes in the synthesis of colloidal gold. *Discussions of the Faraday Society,* 11, 55-75.

140

ULMAN, A. 1996. Formation and structure of self-assembled monolayers. *Chemical Reviews,* 96, 1533-1554.

VERMA, A. & STELLACCI, F. 2010. Effect of surface properties on nanoparticle-cell interactions. *Small,* 6, 12-21.

VIGDERMAN, L., MANNA, P. & ZUBAREV, E. R. 2012. Quantitative replacement of cetyl trimethylammonium bromide by cationic thiol ligands on the surface of gold nanorods and their extremely large uptake by cancer cells. *Angewandte Chemie - International Edition,* 51, 636-641.

WANG, G., ZHANG, J. & MURRAY, R. W. 2002. DNA binding of an ethidium intercalator attached to a monolayer-protected gold cluster. *Analytical Chemistry,* 74, 4320-4327.

WANG, X. H., PENG, H. S., YANG, L., YOU, F. T., TENG, F., TANG, A. W., ZHANG, F. J. & LI, X. H. 2013. Poly-l-lysine assisted synthesis of core-shell nanoparticles and conjugation with triphenylphosphonium to target mitochondria. *Journal of Materials Chemistry B,* 1, 5143-5152.

WEISSIG, V. 2011. From serendipity to mitochondria-targeted nanocarriers. *Pharmaceutical Research,* 28, 2657-2668.

WEISSIG, V., BODDAPATI, S., D'SOUZA, G. & HOROBIN, R. W. 2008. *Funtionalization of pharmaceutical nanocarriers for mitochondria-targeted drug and DNA delivery.*

WEISSIG, V., D'SOUZA, G. M., CHENG, S.-M. & BODDAPATI, S. 2009. Mitochondrial Nanotechnology for Cancer Therapy. *Mitochondria and Cancer.* Springer New York.

WU, H. P., YU, C. J., LIN, C. Y., LIN, Y. H. & TSENG, W. L. 2009. Gold Nanoparticles as Assisted Matrices for the Detection of Biomolecules in a High-Salt Solution through Laser Desorption/Ionization Mass Spectrometry. *Journal of the American Society for Mass Spectrometry,* 20, 875-882.

YEE, C. K., ULMAN, A., RUIZ, J. D., PARIKH, A., WHITE, H. & RAFAILOVICH, M. 2003. Alkyl Selenide- and Alkyl Thiolate-Functionalized Gold Nanoparticles: Chain Packing and Bond Nature. *Langmuir,* 19, 9450-9458.

YU, L. & ANDRIOLA, A. 2010. Quantitative gold nanoparticle analysis methods: A review. *Talanta,* 82, 869-875.

ZHANG, H., HUSSAIN, I., BRUST, M. & COOPER, A. I. 2004. Emulsion-Templated Gold Beads Using Gold Nanopartides as Building Blocks. *Advanced Materials,* 16, 27-30.

ZHANG, S., LEEM, G. & RANDALL LEE, T. 2009. Monolayer-protected gold nanoparticles prepared using long-chain alkanethioacetates. *Langmuir,* 25, 13855-13860.

Chapter 4.

Investigation of the cytotoxicity and cellular uptake of phosphonium ligands in cells

4.1 Introduction

Organic phosphonium compounds are an important class of compounds with applications in chemistry and biology; triphenylphosphine has been widely used as a Wittig reagent in the synthesis of phosphorus ylides (Wittig, 1980). As biological reagents, phosphonium compounds of the type of Ph_3P^+R (in which four aryl and/or alkyl groups are appended to a central phosphorus atom) belong to the group of lipophilic phosphonium cations (LPCs) which are of interest for mitochondria targeted therapeutics because they are preferentially taken up by mitochondria (Ross *et al.*, 2005, Weissig, 2005, Weissig, 2011, Smith *et al.*, 2011).

Mitochondria have emerged as an important pharmacological target in many areas of biomedical science; beside their well-recognised roles in oxidative phosphorylation and in mitochondrial biogenesis, it has become evident that mitochondrial play a crucial role in cell death, calcium metabolism, the innate immune system, neoplasia, oxygen and hypoxia sensing. Since mitochondrial dysfunction contributes to a range of human diseases, there has been an increase in effort made towards the development of pharmacological strategies to address mitochondrial dysfunction (Gupta *et al.*, 2009, Smith *et al.*, 2012, Weissig *et al.*, 2004). A common approach has been to conjugate therapeutic molecules to a triphenylphosphonium moiety, which have been shown to preferentially accumulate inside the mitochondria due to the phenomenon of the mitochondrial membrane potential, thereby making them ideal candidates for applications in mitochondrial biology including measuring the membrane potential, visualising and controlling drug delivery to the mitochondria (Ross *et al.*, 2005).

The TPP moiety has been widely used due to their simplicity and ease of synthesis and derivatisation. To date, a number of different species have been successfully attached to the TPP moiety for mitochondrial biology applications including fluorescent reactive oxygen species probes (Dickinson and Chang, 2008, Shioji *et al.*, 2010), thiol probes (Burns *et al.*, 1995, Coulter *et al.*, 2000), spin traps (Murphy *et al.*, 2003), antioxidants (Smith *et al.*, 1999, Murphy and Smith, 2007) and anti-cancer agents (Patel *et al.*, 1994, Manetta *et al.*, 1996).

As anti-cancer agents, phosphonium cations offer promising potential as they are preferentially accumulated in cancerous cells due to elevated membrane potential observed in cancer cells compared to their normal cell counterparts. This specific accumulation of LPCs has been demonstrated both *in vitro* and *in vivo* (Patel *et al.*, 1994, Rideout *et al.*, 1989, Manetta *et al.*, 1996), furthermore phosphonium compounds also exhibit anti-neoplastic properties (Patel *et al.*, 1994, Millard *et al.*, 2010).

MALDI-MS is a widely used analytical tool due to its high-speed analysis, simplicity and excellent sensitivity; MALDI is a soft-ionisation technique introduced in 1987 primarily for the analysis of proteins (Karas and Hillenkamp, 1988, Tanaka *et al.*, 1988). Since then MALDI-MS has gained a prominent role in the qualitative analysis of various non-volatile and fragile biopolymers including proteins, oligosaccharides and oligonucleotides (Aebersold and Mann, 2003, Burnum *et al.*, 2008, Mechref *et al.*, 2003, Stühler and Meyer, 2004, Pieles *et al.*, 1993).

While MALDI-MS has transformed the analysis of large biomolecules, its application to small molecules with molar masses typically below 1,000 Da has lagged behind. With escalating demand for high-throughput methods in drug discovery and biotechnology this has driven the utilisation of MALDI-MS in small molecule analysis (Cohen and Gusev, 2002). A range of biological and organic small molecules have been successfully analysed by MALDI-MS, these include small peptides (Zhu *et al.*, 1995), carbohydrates (Harvey, 2011), lipids (Fuchs *et al.*, 2010), synthetic polymers (Choi *et al.*, 2007), retinoids (Wingerath *et al.*, 1999), amino acids (Gogichaeva and Alterman, 2012) and pharmaceutical compounds such as prazosine and its synthetic analogues (Andal *et al.*, 2001).

Although MALDI-MS has always been regarded as a qualitative technique, researchers have been pushing the boundaries for quantitative analysis using MALDI-MS (Szájli *et al.*, 2008); to date quantification applications of MALDI-MS ranging from small to large molecules including amino acids, drugs, oligonucleotides, lipids, peptides and proteins have been published (Duncan *et al.*, 2008). While the quantification of small molecules is difficult due to the

strong interferences from MALDI matrix ions (m/z < 500) (Krutchinsky and Chait, 2002, Gobey *et al.*, 2005), papers published in this area of research all suggest that MALDI-MS can be a powerful tool in the quantitative analysis of small compounds.

Various small molecules have been quantified using MALDI-MS, including amine biomolecules (Lee *et al.*, 2004), quaternary ammonium salts (Lou *et al.*, 2009), pharmaceutical drugs (e.g. Quinidine, Nadolol and Danofloxacin) (Sleno and Volmer, 2005), antibiotics (e.g. Ampicillin, Imipenem and Meropenem) (Sparbier *et al.*, 2012) and anti-viral drug (e.g. tenofovir) (Meesters *et al.*, 2011). What is of particular interest is that MALDI-MS has been applied to the quantification of tetraphenylphosphonium (TPP) in human hypopharyngeal carcinoma cells (Rideout *et al.*, 1993) and more recently MALDI-MS has been used to study the ability of phosphonium cations to accumulate in a C6 rat glioma cell line (Cheng *et al.*, 2005).

The main experimental work reported in this chapter is the study of the use of MALDI-MS for quantifying the uptake and cytotoxicity of phosphonium ligands synthesised previously (in chapter 3) in a prostate cancer cell line.

4.2 Materials and Experimental Methods

4.2.1 Chemicals

Alpha-cyano-4-hydroxycinnamic acid (CHCA), 2,5-dihydroxybenzoic acid (DHB), sinapinic acid, trifluoroacetic acid (TFA), tetraphenylphosphonium bromide, sodium chloride (NaCl), calcium chloride (CaCl$_2$), MgSO$_4$, 4-(2-hydroxyethyl)piperazine-1-ethanesulfonic acid (HEPES), dextrose, sodium hydroxide pellets, dimethyl sulfoxide (DMSO), toluene, acetone, tetrahydrofuran (THF) and β-cyclodextrin were obtained from Sigma (Gillingham, Dorset, UK).

4.2.2 Cell Culture

Human prostate cancer cells (PC3) were obtained from ATTC. PC3 were maintained in complete media (cDMEM) which contains Dulbecco's modified Eagle medium with GlutaMAX, 4.5 g/L D-Glucose and sodium puruvate (Invitrogen Life Technologies, Paisley, Renfrewshire, UK) containing 10% heat-

145

inactivated fetal bovine serum (Biosera, East Sussex, Sussex, UK) and 1% penicillin-streptomycin (Invitrogen Life Technologies, Paisley, Renfrewshire, UK) at 37°C in 5% CO_2 and 95% air. Cells were sub-cultured every 3 days and routinely screened for mycoplasma.

PC3 cell line was selected because P-AuNPs synthesised previously in chapter 3 were gold nanospheres, gold nanospheres has a SPR band that lies in the visible region at 520 nm. The strong plasmon absorption and photothermal conversion of AuNPs has been widely exploited for cancer therapeutics through the selective localization of photothermal heating of cancer cells.

Gold nanorods and nanoshells have SPR band in the near-infrared region (650-900nm) and are suited for *in vivo* therapy of tumours under skin and deeply within tissue such as ovarian cancer (Fourkal et al., 2009) and colon cancer (Goodrich et al., 2010, Huang et al., 2006). NIR light is required because of its deep penetration due to minimal absorption of the hemoglobin and water molecules between 650 and 900 nm (Jain et al., 2008). In contrast, gold nanospheres has a plamon absorption in the visible region and thus is more suitable for localised cancers such as breast (Shao et al., 2013, Li et al., 2009) and oral cancer (El-Sayed et al., 2005).

To the best of the author knowledge there has been no publication on the use gold nanospheres for the photothermal therapy on prostate cancers, reports available includes the use of gold nanorods (Wang et al., 2013, Manuchehrabadi et al., 2012), gold coated silica nanoshells (Gobin et al., 2008) gold nanoshells (Stern et al., 2008) gold nanocages (Cobley et al., 2010) gold nano popcorn(Lu et al., 2010) and magnetic nanoparticles (Kawai et al., 2005), thereby in this project, PC3 was selected as a model of prostate cancer cells.

4.2.3 Methods
4.2.3.1 Cytotoxicity Assay
Cytotoxicity was assessed using CellTiter-Glo luminescent cell viability assay kit (Promega Corporation, Southampton, Hampshire, UK). CellTiter glo is a homogeneous assay based on the direct determination of the intracellular ATP

level in cells, a high level of ATP in cells indicates the presence of metabolically active cells. This method involves mixing the CellTiter-Glo substrate with the CellTitre-Glo buffer which is then added directly to cultured cells. Subseuqently this induces cell lysis and generates a luminescent signal which is proportional to the amount of ATP present in the cells, the luminescent signal is recorded on a microplate reader (Promega).

PC3 cells were seeded in opaque-walled 96-well plates at a density of 10,000 cells/well and allowed to adhere overnight. Cells were subsequently treated with the corresponding phosphonium ligand (0-1000 µM) for 24, 48 and 72 hours. After each incubation period cell viability was measured according to the manufacturer's instructions. In brief plates were equilibrated at room temperature for 30 minutes, 100 µL of assay reagent was added to each well, placed on an orbital shaker for 2 minutes, left to stand at room temperature for 10 minutes and read on a Wallac Victor2 1420 multilabel counter (PerkinElmer, Cambridge, Cambridgeshire, UK).

All plates contain control wells and all measurements were performed in quadruplicates, 3 independent experiments were conducted (n = 12). All plates contained the following control wells; control 1 - cells plus CDMEM only, control 2 - cells plus CDMEM with 0.1 % DMSO, control 3 – cells plus CDMEM with 0.01 % DMSO and control 4 - cells plus CDMEM with 0.001 % DMSO. Data are expressed as a percentage of live cells normalised to control, the average, standard deviation and IC_{50} values were plotted and calculated using GraphPad Prism (GraphPad software, La Jolla, California, USA).

4.2.3.2 Cellular Uptake Studies of Phosphonium Compounds by MALDI-MS

Uptake studies of phosphonium compounds by MALDI were conducted using the method reported previously by Cheng and colleagues (Cheng *et al.*, 2005), this method has been adapted and optimised with own phosphonium compounds and instrumentation.

4.2.3.2.1 Calibration Curve of Phosphonium Ligands for Semi-Quantification Analysis by MALDI-MS

PC3 cells were cultured in T75 flasks, after trypsinsation the cells were washed twice with PBS (Invitrogen Life Technologies, Paisley, Renfrewshire, UK), re-suspended to lyse the cells and aliquoted at a density of 3.5 x 10^6 cells/mL (labelled as cell lysate). Phosphonium compounds and internal standards were dissolved in methanol and diluted with PC3 cell lysate to make various concentrations and stored at 4°C. 10 µL of phosphonium compound and 10 µL of internal standard were mixed thoroughly, sequentially 10 µL of this solution was mixed with 10 µL of matrix and 0.5 µL of sample was deposited on the target MALDI plate.

MALDI matrices were made to a concentration of 10 mg/mL in 70:30 MeCN: water with 0.1% TFA. Triplicate standards were prepared and analysed, standards collected from 3 independent cell lysates were prepared for each study.

4.2.3.2.2 Sample Preparation of Phosphonium Ligands for Semi-Quantification Analysis by MALDI-MS

PC3 cells were cultured in T75 flasks, after trypsinsation the cells were washed with PBS twice, re-suspended in low K^+ HEPES buffer (NaCl, 135 mM, KCl 5 mM, CaCl$_2$ 1.8 mM, MgSO$_4$ mM, HEPES 50 mM, dextrose 5.5 mM, pH 7.4) and aliquoted at a density of 10 x 10^6 cells/mL.

For cellular uptake studies, PC3 cells (0.5 x 10^6 cells/50 µL) were incubated with 10 µL of 100 µM stock solution of corresponding phosphonium salt (final concentration, 5 µM) and 140 µL of low K^+ HEPES buffer and incubated between 0-120 minutes at 37°C. Subsequent to each incubation period, cells were centrifuged (500 x g, 4 minutes) and washed twice in cold PBS. Cell pellets were then lysed with 150 µL of cold DIH$_2$O and placed on dry ice (labelled as sample cell lysate).

Prior to MALDI analysis, samples were thawed and centrifuged (12,000 x g, 5 minutes). The sample cell lysate (90 µL) and 10 µM (10 µL) of the internal

standard were mixed together, subsequently 10 µL of this solution was mixed with 10 µL of matrix and 0.5 µL of sample was deposited on the target MALDI plate. Triplicate samples were prepared and analysed, samples collected from 3 independent cell lysates were prepared for each study.

4.2.3.3 Investigating the Cellular Uptake of Phosphonium Ligands in the Mitochondrial Fraction by MALDI-MS

Mitochondria/cytosol fractionation kit was purchased from Abcam (Cambridge, Cambridgeshire, UK) and conducted according to the manufacturer's instructions. PC3 cells were plated out in a 6-well plate at a density of 5×10^6 cells/mL and allowed to adhere overnight. The following day, cells were treated with phosphonium ligand for different length of time (0-120 minutes), cells were then centrifuged (600 x g, 5 minutes, 4°C), washed in ice-cold PBS, re-suspended in 1 mL of 1 x cytosol extraction buffer (CEB) mixture and incubated on ice for 10 minutes.

Cells were homogenised in an ice-cold Dounce tissue grinder (Sigma, Gillingham, Dorset, UK); 10 passes using the large pestle for initial sample reduction followed by 30-50 passes using a smaller pestle, the efficiency of homogenisation was checked under a light microscope.

The homogenate was transferred to a microcentrifgue tube and centrifuged (700 x g, 10 minutes, 4°C), the supernatant was collected and transferred to a new microcentrifuge tube and centrifuged (12,000 x g, 30 minutes, 4°C). The supernatant (labelled as cytosolic fraction (CF)) was stored at -80°C. The pellet (intact mitochondria) was re-suspened in 100 µL mitochondrial extraction buffer (MEB) and vortexed for 10 seconds to obtain mitochondrial protein lysate (labelled as mitohcondria fraction (MF)) and stored at -80°C.

Prior to MALDI analysis CF and MF were thawed and 10 µL of sample were mixed with 10 µL of internal standard, 10 µL of this solution was then mixed with 10 µL of matrix and 0.5 µL of sample was deposited on the target MALDI plate.

4.3 Results and Discussion

4.3.1 Solubility Studies of Phosphonium Compounds

Phosphonium compounds PPTS, PPTA and FPTTS are all readily dissolved in DCM however when added to aqueous media two distinct layers were observed and it is not a suitable solvent for dissolving phosphonium compounds for cell biology studies. Thioacetate salts (PPTA and FPPTA) are soluble in DMSO and methanol and thus can be further diluted in biological media for biological experiments. In contrast the zwitterions (PPTS and FPPTS) are insoluble in DMSO and methanol.

A number of different solvents including toluene, THF, methanol, acetone and PBS, cell culture media, and β-cyclodextrin, which is widely used in the pharmaceutical industry to enhance drug solubility (Loftsson and Brewster, 1996), have all been investigated. None of these solvents were suitable for dissolving the zwitterions for cell biology experiments. The poor solubility of the zwitterions in solutions could possibly be due to the molecules being held together in the lattice via strong electrostatic interactions. Overall the thioacetates are readily soluble compared to the corresponding zwitterions, therefore the thioacetates (PPTA and FPPTA) were taken forward for cell biology studies.

4.3.2 Cytotoxicity of Phosphonium Ligands

Phosphonium compounds are known to selectively accumulate in the mitochondria of cancer cells and their anti-cancer activity have been of interest and has been investigated by several groups (Millard *et al.*, 2010, Rideout *et al.*, 1989, Sehy *et al.*, 1993, Manetta *et al.*, 1996, Bergeron *et al.*, 2009). Cell viability results presented below (table 4.1 and Figure 4.1) illustrated that the thioacetates described in chapter 3 are toxic towards PC3 cells at high concentrations and at prolonged treatment periods.
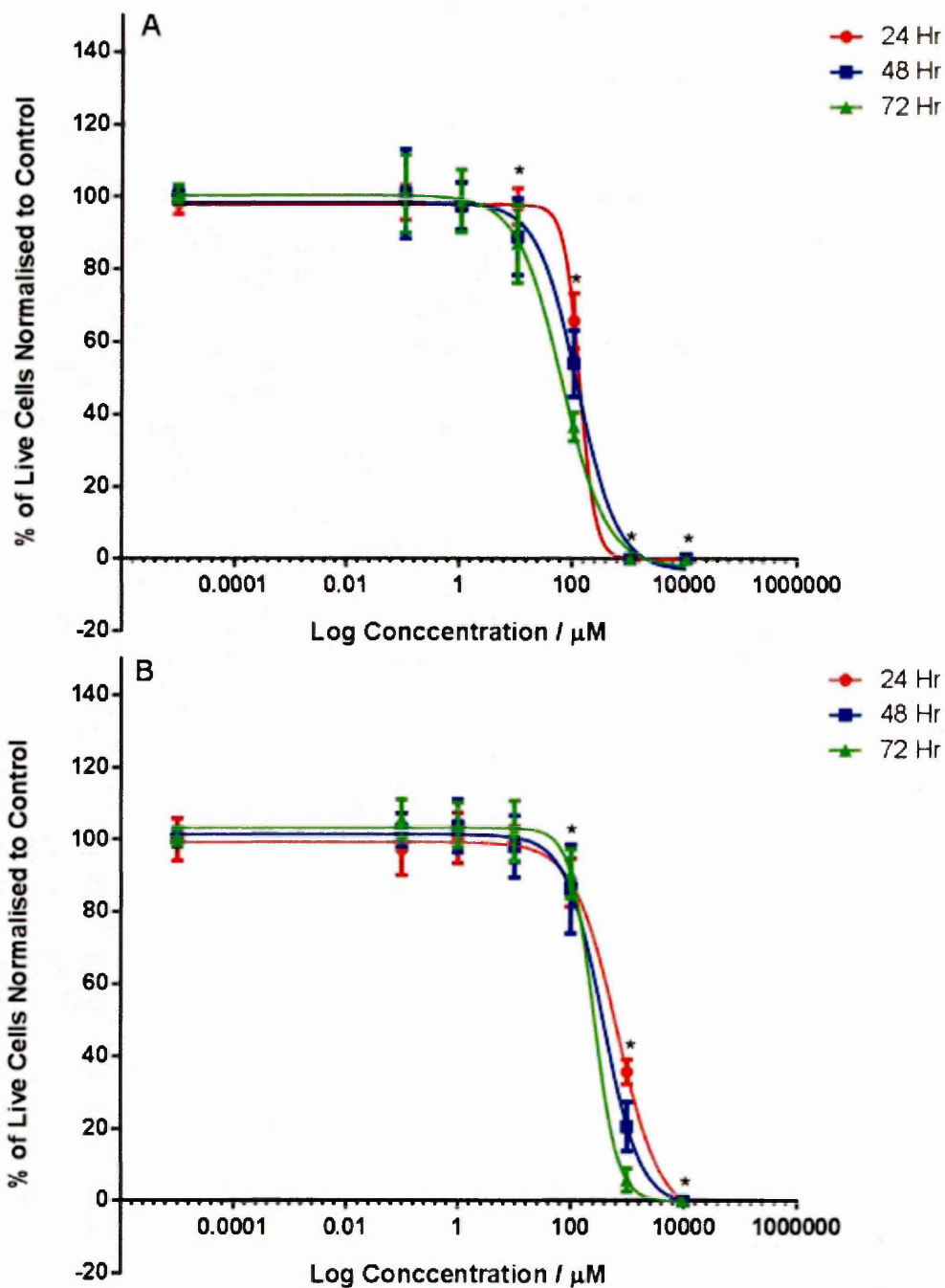
Figure 4.1 PC3 cells treated with thioacetate compound A) PPTA and B) FPPTA for 24, 48 and 72 hours. Cell proliferation was determined by the CellTiter-Glo luminescent cell viability assay kit. Data are expressed as a percentage of live cells normalised to control, mean ± SD (n = 12). *Statisitcal significance between the levels of viable cells, $P \leq 0.05$.

151

Staisitical analysis showed that the treatment of PC3 with PPTA (Figure 4.1a) was significantly increased compared to untreated cells: at 24 hrs at 109 µm P = <0.0001, 1090 µm P = <0.0001 and 10900 µm P = <0.0001, At 48 hrs 10.9 µm P = 0.00292, 109 µm P = <0.0001, 1090 µm P = <0.0001 and 10900 µm P = <0.0001. At 72 hrs 10.9 µm P = 0.0031, 109 µm P = <0.0001, 1090 µm P = <0.0001 and 10900 µm P = <0.0001.

Staisitical analysis showed that the treatment of PC3 with FPPTA (Figure 4.1b) was significantly increased compared to untreated cells: at 24 hrs at 98 µm P = 0.0001, 980 µm P = <0.0001 and 9080 µm P = <0.0001. At 48 hrs at 98 µm P = 0.0008, 980 µm P = <0.0001 and 9080 µm P = <0.0001. At 72 hrs at 98 µm P = 0.0004, 980 µm P = <0.0001 and 9080 µm P = <0.0001.

	IC$_{50}$ values (µM)		
	24 Hr	48 Hr	72 Hr
PPTA	137.9	127.0	67.1
FPPTA	654.7	367.7	252.6

Table 4.1 IC$_{50}$ values for thioacetate compounds, IC$_{50}$ values calculated using non-linear regression analysis on GraphPad Prism software.

The IC$_{50}$ values reported here are considerably higher than those of other TPP-containing molecules. Millards and co-workers have determined the cytotoxicity of 33 phosphonium compounds (all containing the TPP moiety with different side chains) in five different cell lines (Millard et al., 2010). The compounds investigated had IC$_{50}$ values between 0.4 -8.0 µM at 72 hours in PC3 cell lines.

To make the comparison for the IC$_{50}$ values of TPP analogues reported by Millard et al., 2010 with phosphonium ligands synthesised in chapter 3 easier, the values are shown below in Table 4.2, for comparison reasons only the 3 most and least toxic compounds are reported, for the full list of IC$_{50}$ values of TPP analogues please refer to their publication (Millard et al. 2010).

Compound	IC$_{50}$ values (μM)
TPP 731	0.40
TPP 824	0.42
TPP 726	0.50
TPP 764	8.00
TPP 752, 781, 825	5.00
PPTA	67.10
FPPTA	252.60

Table 4.2 IC$_{50}$ values of different TPP analogues at 72 hours in PC3 cells reported by Millard *et al.*, 2010 and IC$_{50}$ values of phosphonium ligands PPTA and FPPTA at 72 hours in PC3 cells.

Millard and co-workers (2010) showed that their most toxic compound (TPP 731) (Figure 4.2) was ~160 fold more toxic that PPTA while their least toxic compound (TPP 764) (Figure 4.2) which was still ~8 fold more toxic than PPTA, this demonstrated that the phosphonium compounds synthesised in this study are comparatively non-toxic towards cells and can therefore be used as a transport vector to deliver AuNPs specifically to the cells.
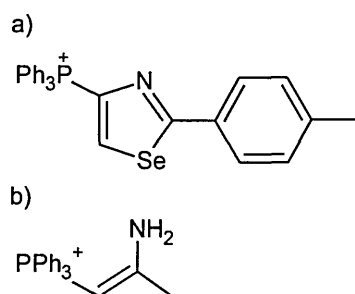
Figure 4.2 Chemical structures of a) TPP 731 and b) TPP 764 (Millard *et al.*, 2010).

A further interesting feature is that the two phosphonium compounds exhibit different IC$_{50}$ values PPTA has a lower IC$_{50}$ value than FPPTA, the difference between the two thioacetate compounds is the replacement of hydrogen in the

para position with fluorine. This slight modification has a dramatic effect on the cytotoxicity of these compounds in cells and a decrease in cytotoxicity by approximately 4 fold was observed.

This suggested that the toxicity of these compounds is primarily determined by the TPP cation itself rather than the side chain (as the side chains are identical), and this observation is in agreement with the work reported by Smith and co-workers (Smith *et al.*, 2003). They showed that the maximum tolerated acute dosage for TPMP, MitoVit E and MitoQ (structures shown in Figure 4.3) in mice were generally similar (97 ± 13 µmol, 105 ± 9.2 µmol and 154 ± 4 µmol/kg/day respectively), despite their differences in their side chains and hydrophobicities. The side chains have shown to have an effect on the rate and extent of uptake; *in vitro* and *in vivo* experiments have demonstrated that the uptake of LPCs into the mitochondria is influenced by the length of the alkyl chain which contributes to the increase in hydrophobicity (Porteous *et al.*, 2010, Ross *et al.*, 2008).
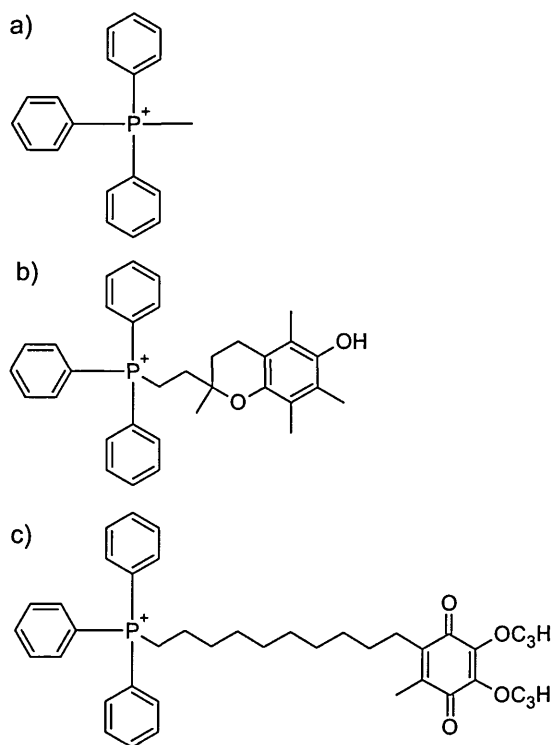
Figure 4.3 Chemical structures of lipophilic phosphonium cations; a) TPMP (Porteous *et al.*, 2010), b) MitoVit E (Ross *et al.*, 2008) and c) MitoQ (Porteous *et al.*, 2010).

The PPTS and FPPTS free ligand themselves are relatively non-toxic to PC3 cells, when these precursor ligands are used to synthesised P-AuNPs the S-C bond cleaves to form S-Au bonds. This slight modification in the side chain, may affect the rate and the extent of uptake of these P-AuNPs into cells. It has been shown that the uptake of LPCs into the mitochondria is influenced by the length of the alkyl chain (Porteous *et al.*, 2010, Ross *et al.*, 2008). However the functionalised AuNPs containing the TPP moiety maybe cytotoxic to cells, as the toxicity of LPCs is primarily determined by the TPP cation itself rather than the side chain (Smith et al., 2003).

4.3.1 Semi-Quantification Studies of Phosphonium Ligands in Cells using MALDI-MS

4.3.1.1 Matrix optimisation for the Study of Phosphonium Ligands in Cells using MALDI-MS

CHCA was unsuitable for the analysis of PPTA as the molecular ion peak for this compound $[M]^+$ is at *m/z* 379 which also correspond to the CHCA dimer peak $[2M+H]^+$ at *m/z* 379 (Figure 4.4). This would be a problem for quantification work, as the peak area would be either under or overestimated which will dramatically affect the interpretation and the results will also be inaccurate and unreliable. The other common matrix used for the analysis of small organic molecules is DHB (Cohen and Gusev, 2002), going forward for MALDI-MS experiments, DHB would be the matrix of choice for the analysis of PPTA to overcome the problem of the overlapping peaks observed for the analyte (PPTA) and the matrix (CHCA).
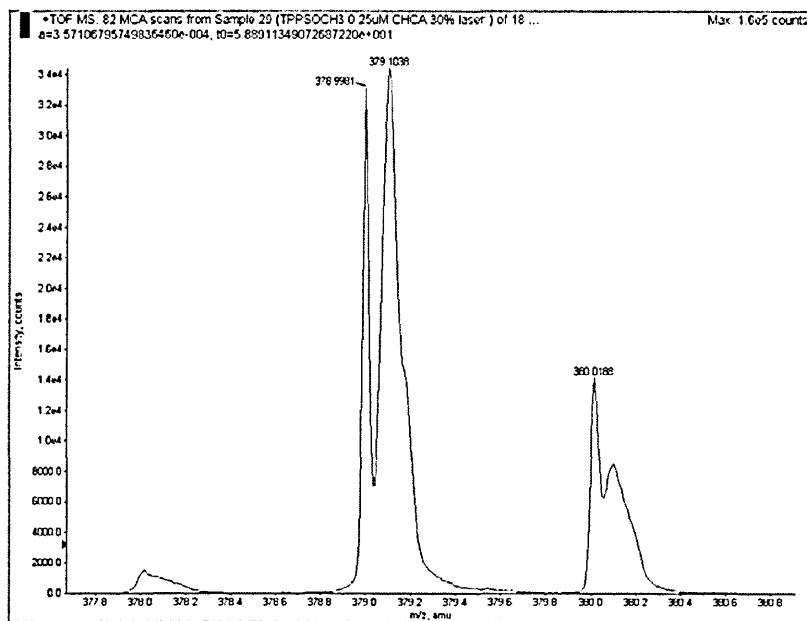
Figure 4.4 MALDI-MS spectrum of PPTA, zoomed in at *m/z* 379 peak. The spectrum shows two non-fully resolved peaks around *m/z 379*. *m/z* 378.9981 and 379.1038 corresponding to the molecular ion peak for PPTA and CHCA dimer peak respectively. The peaks at around *m/z* 380 correspond to the protonated peaks of 379 ([CHCA+H]⁺ and [PPTA+H]⁺).

4.3.1.2 Internal Standard Optimisation for the Study of Phosphonium Ligands in Cells using MALDI-MS

Due to the fact that MALDI suffers from low "shot-to-shot" reproducibility, for quantitation experiments an internal standard (IS) can be employed to compensate for signal deviations. The use of an IS has shown to minimise deviations of analyte to IS signal ratio therefore improving experimental reproducibility. It is also important to take into consideration that peak heights for equimolar loadings of different analytes may vary significantly (Cohen and Gusev, 2002, Duncan *et al.*, 1993, Duncan *et al.*, 2008, Sleno and Volmer, 2006).

In this project tetraphenylphosphonium bromide was used as the IS; the PPTA signal was significantly greater compared to FPPTA (Figure 4.5), therefore the IS to analyte ratio was optimised individually for each thioacetate compound before any more experiments were conducted. Ideally, the concentration of the

IS should be roughly at a 1:1 ratio to the concentration of the highest standard. If the intensity of the IS is too high in relation to the analyte signal it will suppress the sample signal dramatically, and it would be hard to distinguish if the signal was actually a peak or background noise (Hoffmann and Stroobant, 2007).
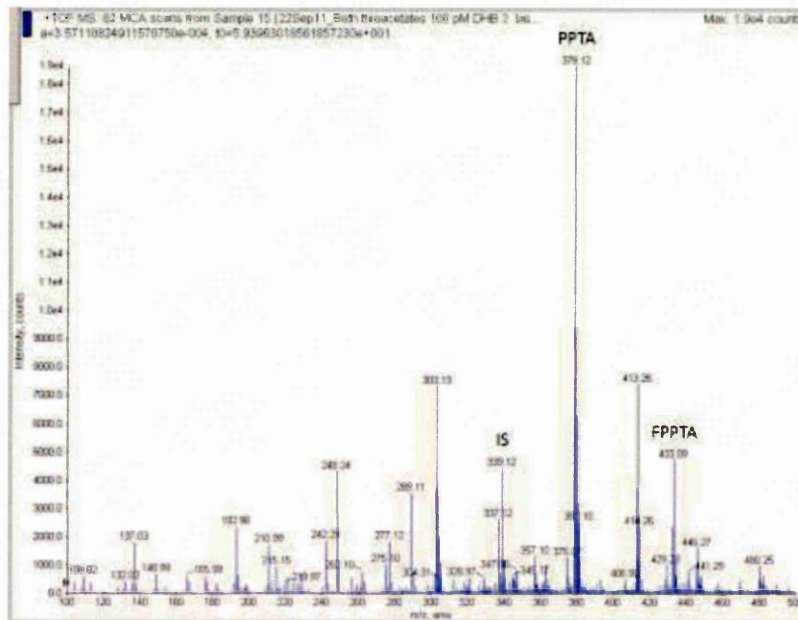
Figure 4.5 MALDI-MS spectrum of IS, PPTA and FPPTA at the same concentration of 100 µM. Peaks corresponding to IS at m/z 339.12, PPTA $[M]^+$ at m/z 379.12 and FPPTA $[M]^+$ at m/z 433.09.

MALDI-MS spectrum of varying the ratio of the analyte (PPTA) to the IS ratio indicated that using a ratio of 1:10 (Figure 4.6a) was unsuitable because the signal of the IS was too high and thereby suppressing the sample signal. Using a ratio of 1:1 (Figure 4.6b) was a possibility, considering that both the PPTA and IS peaks have similar intensity counts.

However the IS was still greater than the PPTA peak. As mentioned previously, the ideal ratio between the peaks should ideally be 1:1 at the highest concentration of the standard. Using a ratio of 1:0.1 (Figure 4.6c), the PPTA peak was greater compared to the IS peak, therefore a ratio between 1:1 and 1:0.1 should result in a ratio roughly in the region of 1:1 therefore the optimised ratio for PPTA was found to be 1:0.5.
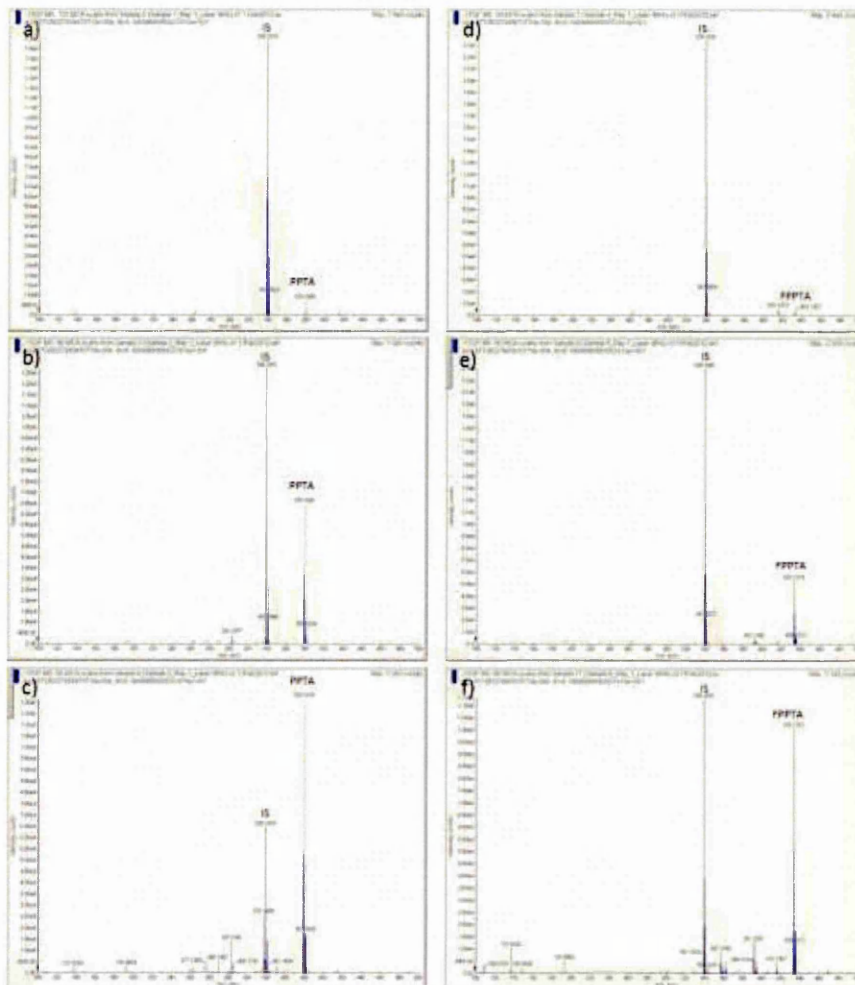
Figure 4.6 MALDI-MS spectrum of analyte to IS with varying different ratios; a) PPTA:IS 1:10, b) PPTA:IS 1:1, c) PPTA:IS 1:0.1, d) FPPTA:IS 1:10, e) FPPTA:IS 1:1, f) FPPTA:IS 1:0.1.Peaks corresponding to IS at m/z 339.14, PPTA [M]$^+$ at m/z 379.15 and FPPTA [M]$^+$ at m/z 433.12.

MALDI-MS spectrum of varying the ratio of the analyte (FPPTA) to the IS ratio indicated that using a ratio of 1:10 (Figure 4.6d) was unsuitable because the signal of the IS was too high, and thereby suppressing the sample signal significantly. Using a ratio of 1:1 (Figure 4.6e) was also unsuitable as the IS peak was still considerably high in comparison to the sample peak. Using a ratio of 1:0.1 was ideal, since both the IS and FPPTA peaks give a roughly 1:1 ratio (Figure 4.6f). As mentioned previously the ideal ratio between the analyte and IS is around 1:1 and thus the optimised ratio for FPPTA and IS was found to be 1:0.1.

4.3.1.3 Calibration Curve of Phosphonium Ligands for Semi-Quantification Analysis by MALDI-MS

The graphs displayed in Figure 4.12 show the ion intensity ratio of the product ion *m/z* 379 and *m/z* 433 for PPTA and FPPTA respectively against the IS at *m/z* 339. The calibration curves demonstrate that the ion intensity ratio increases with concentration of PPTA and PPTS.
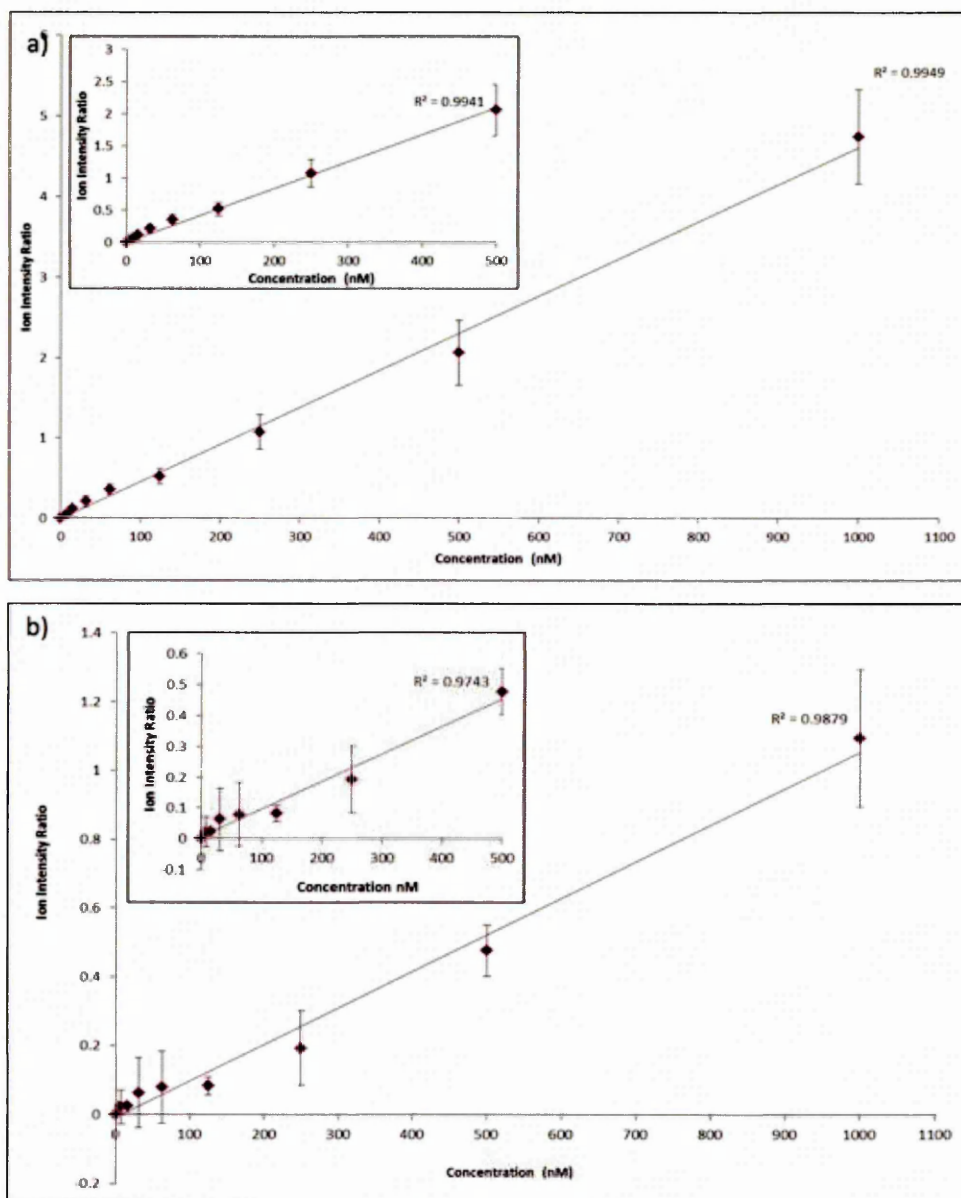
Figure 4.7 Standard curve for a) PPTA and b) FPPTA. The graph showed that between 0-1,000 nM, PPTA and FPPTA has a linear response of R^2 = 0.9949 and 0.9879 respectively. The insert in each graph shows the expanded region between 0-500 nM for each compound.

159

4.3.1.4 Semi-Quantification Studies on the Cellular Uptake of Phosphonium Compounds in PC3 Cells by MALDI-MS

MALDI-MS spectrum shown below in Figure 4.13 shows a typical MALDI-MS spectra for a control and a treated sample.
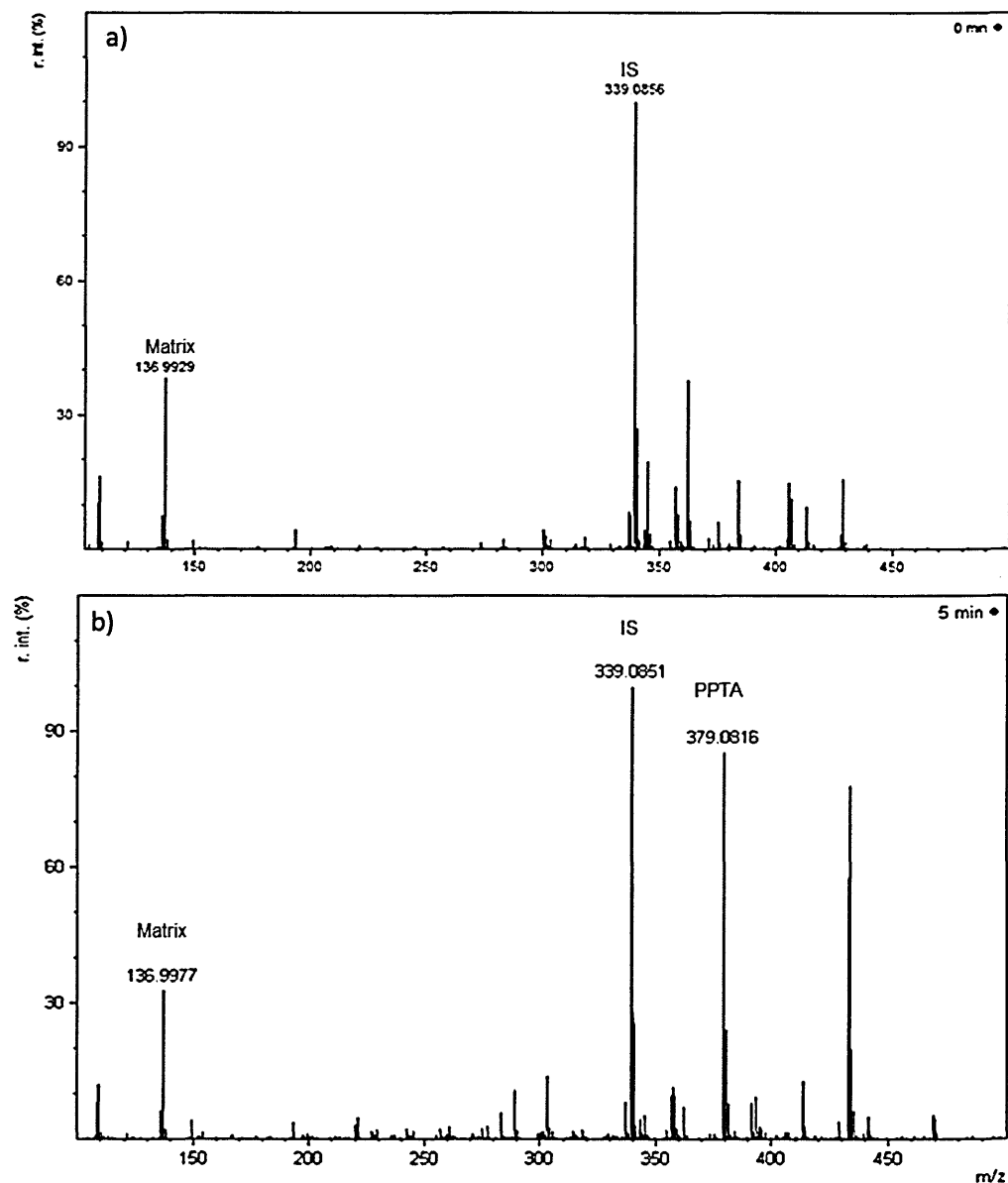
Figure 4.8 Typical MALDI-MS spectrum of the uptake of PPTA in PC3 cells for a) the control sample and b) PC3 cells treated with PPTA. Peaks corresponding to matrix CHCA at m/z 136.99 and IS at m/z 339.01 were observed. No analyte peak for PPTA was observed at m/z 379 (Figure 4.13a) confirming the absence of PPTA in the untreated sample. PPTA peak observed at m/z 379.08 (Figure 4.13b) confirmed the presence of PPTA in PC3 cells.

All data obtained showed the presence of PPTA peak at *m/z* 379 across all incubation periods (5-90 minutes). This demonstrated that PPTA is taken-up by cells. The data obtained from the instrument were converted to ion intensity ratios and plotted in Excel for a visual representation of the uptake of the phosphonium compounds in cells. The diagram displayed below in Figure 4.9 shows the concentration of phosphonium compounds against time.
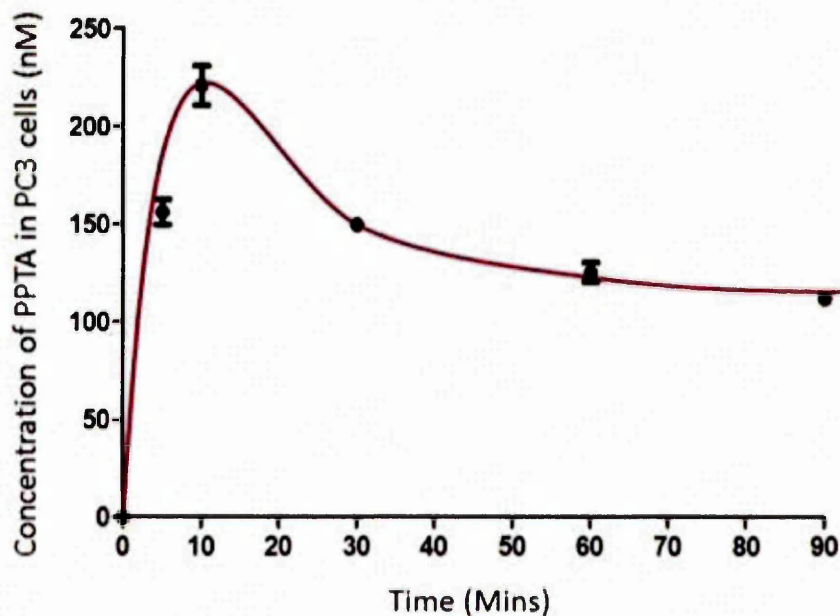
Figure 4.9 The uptake of PPTA by PC3 cells; PC3 cells were treated with 5 µM PPTA and incubated between 0-90 minutes. Concentrations were determined from the calibration curve, each sample was analysed in triplicate from 3 independent experiments. Graph showed that PPTA is rapidly taken-up within 10 minutes and plateaus >30 minutes. Using the Kruskal-Wallis test, the p value is < 0.0001.
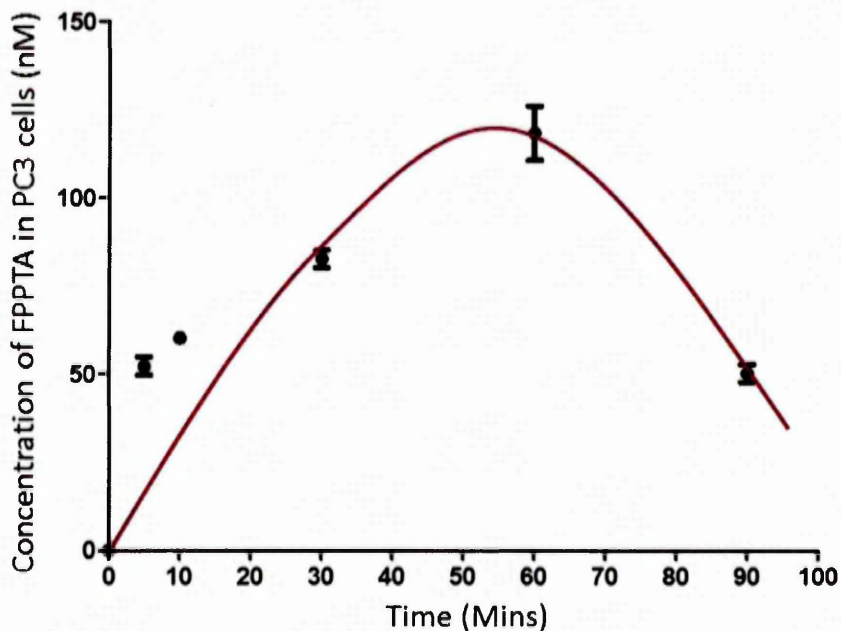
Figure 4.10 The uptake of FPPTA by PC3 cells; PC3 cells were treated with 5 µM FPPTA and incubated between 0-90 minutes. Concentrations were determined from the calibration curve, each sample was analysed in triplicate from 3 independent experiments. Graph showed that FPPTA is rapidly taken-up within 10 minutes and drops after 60 minutes. Using the Kruskal-Wallis test the p value is < 0.0001.

Figures 4.9 and 4.10 showed that both PPTA and FPPTA are taken-up by PC3 cells however the compounds exhibit different uptake profiles; PPTA is rapidly taken-up by the cells reaching a maximum uptake of 10 minutes, then drops slightly and finally plateau off after 30 minutes. This rapid increase in concentration of PPTA between 0 and 10 minutes was observed visually from the PPTA peak at *m/z* 379 (Figure 11a), between 30-90 minutes where the uptake plateaus off this could also be seen visually by overlaying the peaks at these specific time points (Figure 4.11b).
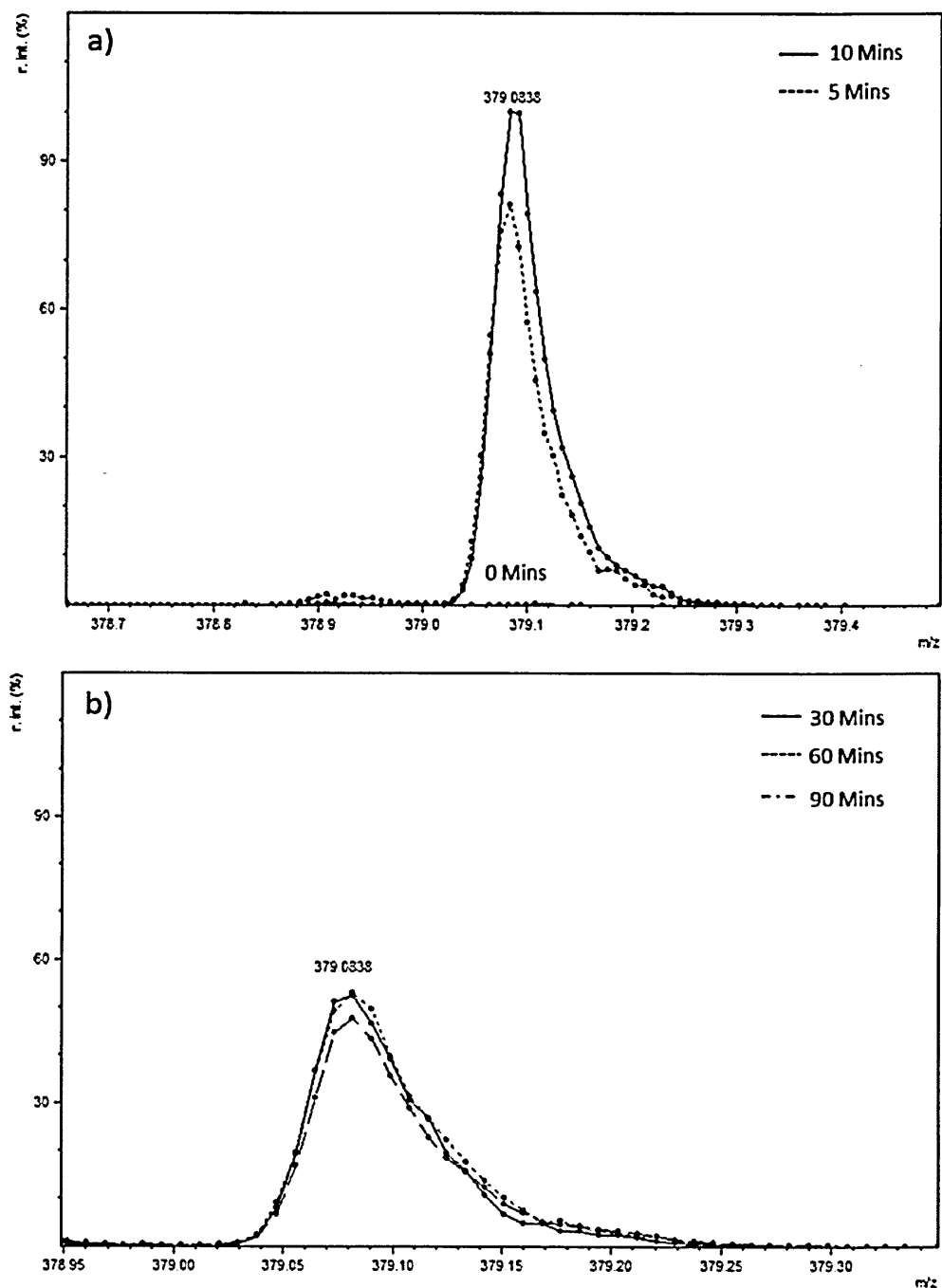
Figure 4.11 Overlay of MALDI-MS spectra of the PPTA product ion at *m/z* 379 at different time points; a) shows the overlay between 0 and 10 minutes and b) shows the overlay between 30-90 minutes. Figure (a) shows the dramatic increase of PPTA following the 5 minute treatment. Figure (b) shows that the uptake between 30-90 minutes were very similar.

In contrast, FPPTA reaches a maximum uptake 3 times slower than PPTA and drops and potentially reaching a plateau after 90 minutes, further experiments would be required to confirm this. Overall PPTA are taken-up to a greater extent in comparison to FPPTA with concentrations in the region of 100-200 nM for PPTA and 50-120 nM for FPPTA.
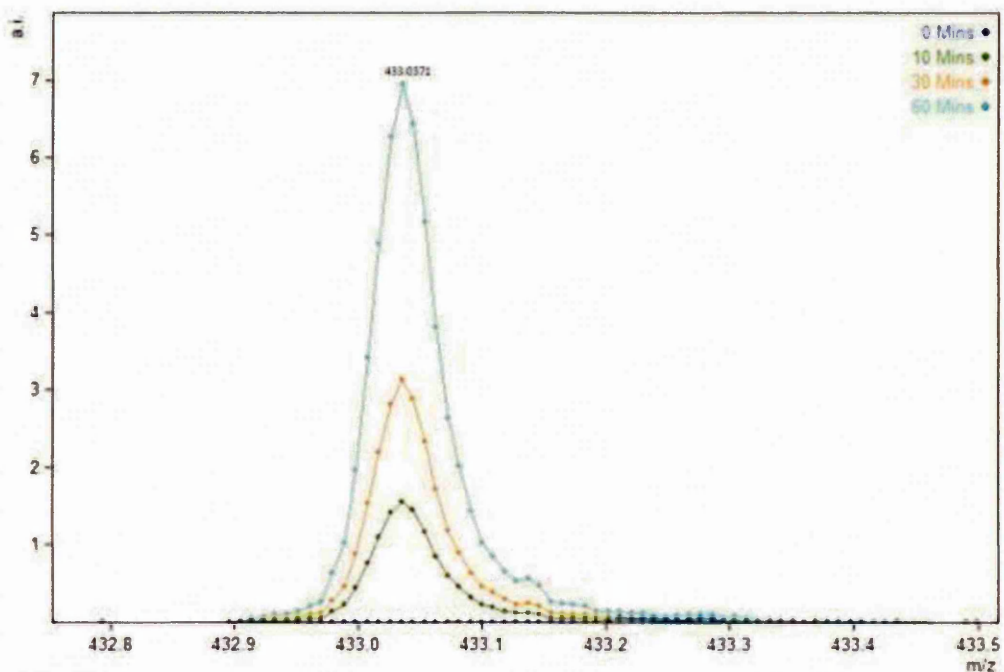
Figure 4.12 Overlay of MALDI-MS spectra of the FPPTA product ion at *m/z* 433 at varies different time points between 0-60 minutes.

Phosphonium compounds analysed in this chapter by MALDI-MS have shown to be taken-up by PC3 in the nanomolar region which is significantly higher compared to those reported in the literature. To the best of the authors knowledge to date there are only two reports available on the use of MALDI-MS for quantifying the uptake of phosphonium compounds in cells. Rideout and colleagues (Rideout *et al.*, 1993) were the first to report the quantitative analysis of phosphonium cations by MALDI-MS, they have shown that tetraphenylphosphonium were taken up in sub-femtomole amounts in carcinoma cell lines. Cheng and co-workers (Cheng *et al.*, 2005) reported the uptake of various phosphonium cations in the sub-femtomole region by C6 cells using MALDI-MS. Different phosphonium compounds (incorporating the TPP moiety with different side chains) exhibit different cellular uptake profiles, which

indicates that the side chains have an effect on their cellular uptake, this observation is consistent with Ross *et al.* (2006) who have shown that the hydrophobicity of the side chains has an effect on the rate and extent of uptake of phosphonium compounds *in vitro*.

4.3.1.5 Investigating the Cellular Uptake of Phosphonium Compounds in the Mitochondrial Fraction

Once it had been confirmed that these phosphonium compounds are taken-up by cells, the next stage was to determine if these phosphonium compounds are taken up by the mitochondria and if so to compare their uptake in the mitochondrial fraction versus the cytosolic fraction. A mitochondrial fractionation kit was used for this part of the experiment (details of kit refer to chapter 4.2.2.3).

For both the mitochondrial and cytosolic fraction, the intensity counts were extremely low, below 100 counts (Figure 4.12). Even when the buffer was spiked with PPTA and the internal standard, the intensity signal was still extremely low (Figure 4.13). This illustrated that the buffer was not suitable to be analysed by MALDI-MS, it appeared that the buffer suppresses the signal, as on average the matrix gives an intensity count in the region of $1 - 2 \times 10^5$, and an intensity count in the region of 100 is extremely poor and thus any results obtained would be unreliable.

Despite the low intensity signals given, what was interesting was that in the cytosolic fraction (Figure 4.12a) the molecular ion peak for PPTA at *m/z* 379.17 was observed, and the corresponding cleaved peak for the sample was observed at *m/z* 289.13, 275.10 and 262.10. These cleave peak observed are in agreement with the LDI-MS spectra for PPTA capped AuNPs reported in chapter 3(Figure 3.26). This confirmed that the PPTA is present in the cytosolic fraction of the cell.

The IS at *m/z* 339.14, and the cleaved PPTA peak at *m/z* 303.16 is observed in the mitochondrial fraction (Figure 4.12b), there is a small peak at *m/z* 379 which suggested it is the sample peak, along with the present of the cleaved peak for PPTA at *m/z* 303.16 this shows that PPTA is present in the mitochondrial

fraction of the cell thus demonstrating that PPTA is taken-up in the cell and specifically by the mitochondria. This observation is confirmed by TEM analysis which is reported in next chapter (chapter 5).
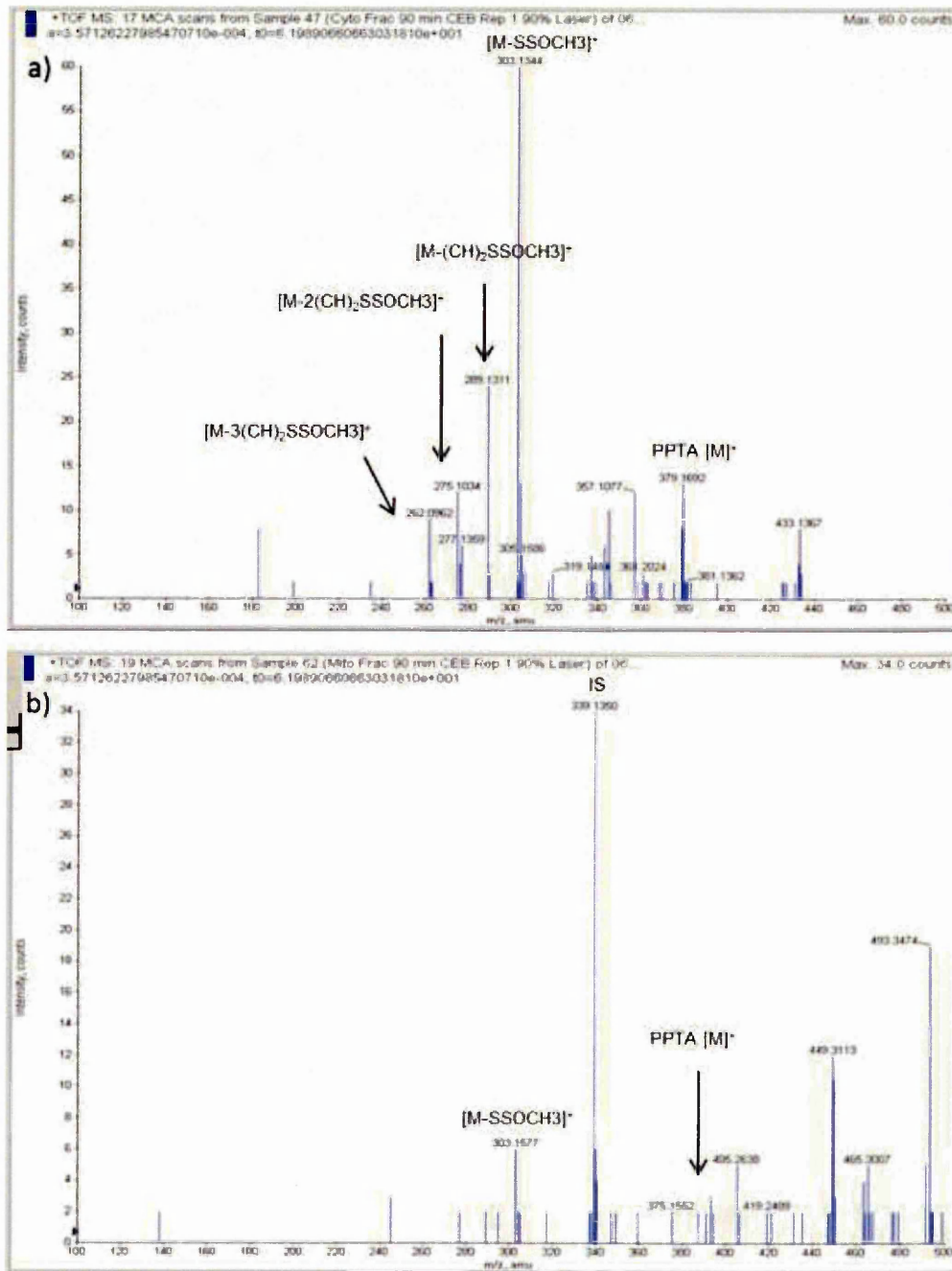
Figure 4.13 Typical MALDI-MS spectrum of the uptake of TPPA in a) the cytosolic fraction and b) mitochondrial fraction. Both spectra exhibited extremely low intensity counts below 100 counts, thereby illustrating that the buffer suppresses the signal and is not suitable to be analysed by MALDI-MS.
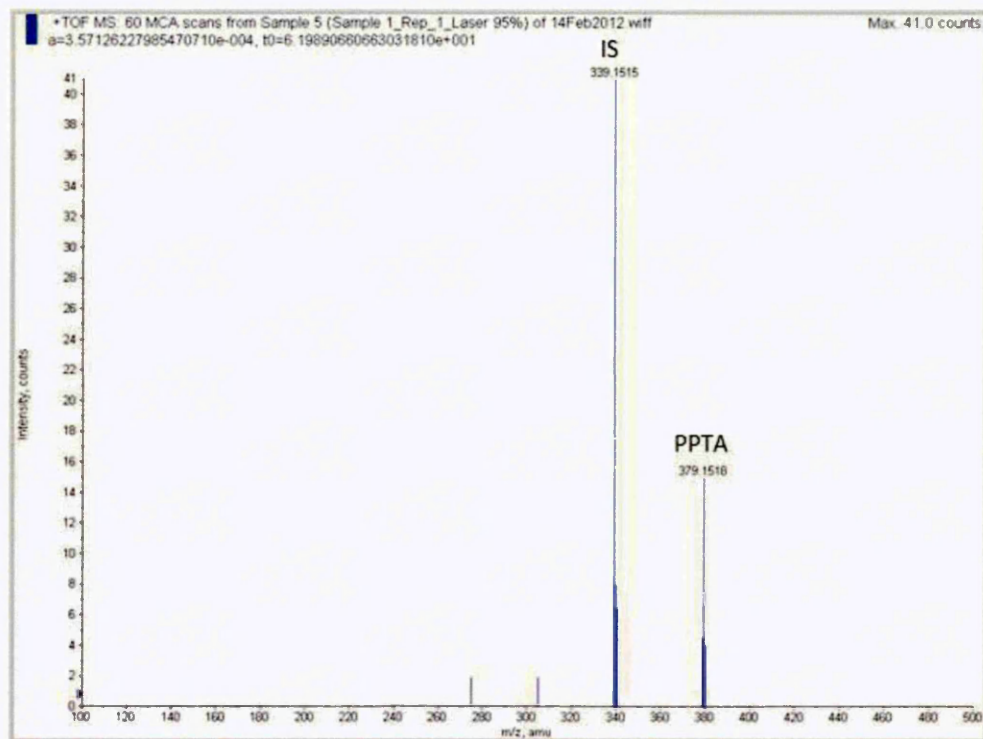
Figure 4.14 Typical MALDI-MS spectrum of extraction buffer spiked with PPTA and IS, even when buffer was spiked, the intensity counts were still below 100, thereby confirming that the buffer results in supression when analysed by MALDI-MS.

4.4 Conclusion

The first aim of this chapter was to evaluate the cytotoxicity of PPTA and FPPTA in PC3 cells; the results showed that both compounds were cytotoxic towards cells at very high concentrations and at long incubation times of 72 hours. Rather than synthesising compounds containing the TPP moiety that are cytotoxic towards cells for therapeutic effects like many other research groups (Millard *et al.*, 2010, Rideout *et al.*, 1989, Patel *et al.*, 1994, Manetta *et al.*, 1996) the aim of this project was to exploit relatively non-cytotoxic phosphonium compound as described previously in chapter 3 to act as transport vector to delivery AuNPs into the cells for photothermal therapy applications.

The IC_{50} value for PPTA at 72 hours is approximately 16 times lower than the least cytotoxic phosphonium salt reported by Millard *et al.* (2010), this demonstrates that these compounds are relatively non-toxic to the cells and it

167

would be feasible to these compounds to the surface of nanoparticles to produce functionalised AuNPs for targeted drug delivery to the site of mitochondria for other therapeutic effects such as PTT (this will be investigated in the next chapter).

The second aim of the work reported in this chapter is the semi-quantification studies of phosphonium compounds in cells by MALDI-TOF-MS; cellular uptake studies provided evidence that both thioacetate compounds are rapidly taken up by cells in the nanomolar region. The use of MALDI-MS for quantitative applications is very complicated and challenging due to the irreproducible analyte signal arises from non-homogenous co-crystallisation of the sample with the matrix. CHCA is routinely used in the analysis of small molecules as it produces uniform crystallisation (Sleno and Volmer, 2006). DHB was employed in this study to compensate for the isobaric interference with the CHCA dimer peak ([2M+H]$^+$) at m/z 379, an IS was also used to improve overall experimental reproducibility.

The uptake of phosphonium compounds in the mitochondrial fractions have been attempted, however the buffers in the mitochondrial isolation kit appeared to suppress sample signals and gave extremely low intensity counts (< 100). In future, in order to obtain useful information on the uptake of phosphonium compounds in the mitochondria fraction, it is critical to find alternative approaches to isolate the mitochondria fraction and use buffers that do not suppress the intensity count in the MS.

4.5 References

AEBERSOLD, R. & MANN, M. 2003. Mass spectrometry-based proteomics. *Nature,* 422, 198-207.

ANDAL, C., BOCCHINI, P., POZZI, R. & GALLETTI, G. C. 2001. Accurate mass measurement of synthetic analogues of prazosine by matrix-assisted laser desorption/ionisation time-of-flight mass spectrometry. *Rapid Communications in Mass Spectrometry,* 15, 665-669.

BERGERON, K. L., MURPHY, E. L., MAJOFODUN, O., MU OZ, L. D., WILLIAMS JR, J. C. & ALMEIDA, K. H. 2009. Arylphosphonium salts interact with DNA to modulate cytotoxicity. *Mutation Research - Genetic Toxicology and Environmental Mutagenesis,* 673, 141-148.

BURNS, R. J., SMITH, R. A. J. & MURPHY, M. P. 1995. Synthesis and characterization of thiobutyltriphenylphosphonium bromide, a novel thiol reagent targeted to the mitochondrial matrix. *Archives of Biochemistry and Biophysics,* 322, 60-68.

BURNUM, K. E., FRAPPIER, S. L. & CAPRIOLI, R. M. 2008. Matrix-assisted laser desorption/ionization imaging mass spectrometry for the investigation of proteins and peptides.

CHENG, Z., WINANT, R. C. & GAMBHIR, S. S. 2005. A new strategy to screen molecular imaging probe uptake in cell culture without radiolabeling using matrix-assisted laser desorption/ionization time-of-flight mass spectrometry. *Journal of Nuclear Medicine,* 46, 878-886.

CHOI, H., EUN, K. C., EUN, K. Y., JANG, S. & CHAN, R. P. 2007. Characterization of synthetic polyamides by MALDI-TOF mass spectrometry. *Bulletin of the Korean Chemical Society,* 28, 2354-2358.

COBLEY, C. M., AU, L., CHEN, J. & XIA, Y. 2010. Targeting gold nanocages to cancer cells for photothermal destruction and drug delivery. *Expert Opinion on Drug Delivery,* 7, 577-587.

COHEN, L. H. & GUSEV, A. I. 2002. Small molecule analysis by MALDI mass spectrometry. *Analytical and Bioanalytical Chemistry,* 373, 571-586.

COULTER, C. V., KELSO, G. F., LIN, T. K., SMITH, R. A. J. & MURPHY, M. P. 2000. Mitochondrially targeted antioxidants and thiol reagents. *Free Radical Biology and Medicine,* 28, 1547-1554.

DICKINSON, B. C. & CHANG, C. J. 2008. A targetable fluorescent probe for imaging hydrogen peroxide in the mitochondria of living cells. *Journal of the American Chemical Society,* 130, 9638-9639.

DUNCAN, M. W., MATANOVIC, G. & CERPA-POLJAK, A. 1993. Quantitative analysis of low molecular weight compounds of biological interest by matrix-assisted laser desorption ionization. *Rapid communications in mass spectrometry : RCM,* 7, 1090-1094.

DUNCAN, M. W., RODER, H. & HUNSUCKER, S. W. 2008. Quantitative matrix-assisted laser desorption/ionization mass spectrometry. *Briefings in Functional Genomics & Proteomics,* 7, 355-370.

EL-SAYED, I. H., HUANG, X. & EL-SAYED, M. A. 2005. Surface plasmon resonance scattering and absorption of anti-EGFR antibody conjugated gold nanoparticles in cancer diagnostics: Applications in oral cancer. *Nano Letters,* 5, 829-834.

FOURKAL, E., VELCHEV, I., TAFFO, A., MA, C., KHAZAK, V. & SKOBELEVA, N. 2009. Photo-Thermal Cancer Therapy Using Gold Nanorods. *In:* D SSEL, O. & SCHLEGEL, W. (eds.) *World Congress on Medical Physics*

169

and Biomedical Engineering, September 7 - 12, 2009, Munich, Germany. Springer Berlin Heidelberg.

FUCHS, B., SUSS, R. & SCHILLER, J. 2010. An update of MALDI-TOF mass spectrometry in lipid research. *Progress in Lipid Research,* 49, 450-475.

GOBEY, J., COLE, M., JANISZEWSKI, J., COVEY, T., CHAU, T., KOVARIK, P. & CORR, J. 2005. Characterization and performance of MALDI on a triple quadrupole mass spectrometer for analysis and quantification of small molecules. *Analytical Chemistry,* 77, 5643-5654.

GOBIN, A. M., MOON, J. J. & WEST, J. L. 2008. Ephrin A1-targeted nanoshells for photothermal ablation of prostate cancer cells. *International Journal of Nanomedicine,* 3, 351-358.

GOGICHAEVA, N. V. & ALTERMAN, M. A. 2012. Amino acid analysis by means of MALDI TOF mass spectrometry or MALDI TOF/TOF tandem mass spectrometry. *Methods Mol Biol,* 828, 121-35.

GOODRICH, G. P., BAO, L., GILL-SHARP, K., SANG, K. L., WANG, J. & PAYNE, J. D. 2010. Photothermal therapy in a murine colon cancer model using near-infrared absorbing gold nanorods. *J Biomed Opt,* 15, 018001.

GUPTA, S., KASS, G. E. N., SZEGEZDI, E. & JOSEPH, B. 2009. The mitochondrial death pathway: a promising therapeutic target in diseases. *Journal of Cellular and Molecular Medicine,* 13, 1004-1033.

HARVEY, D. J. 2011. Analysis of carbohydrates and glycoconjugates by matrix-assisted laser desorption/ionization mass spectrometry: an update for 2007-2008. *Mass Spectrometry Reviews,* 30, 1-100.

HOFFMANN, D., E & STROOBANT, V. 2007. *Mass spectrometry: principles and applications* England, John Wiley & Sons Ltd

HUANG, X., EL-SAYED, I. H., QIAN, W. & EL-SAYED, M. A. 2006. Cancer cell imaging and photothermal therapy in the near-infrared region by using gold nanorods. *Journal of the American Chemical Society,* 128, 2115-2120.

JAIN, P. K., HUANG, X., EL-SAYED, I. H. & EL-SAYED, M. A. 2008. Noble metals on the nanoscale: optical and photothermal properties and some applications in imaging, sensing, biology, and medicine. *Accounts of Chemical Research,* 41, 1578-1586.

KARAS, M. & HILLENKAMP, F. 1988. Laser desorption ionization of proteins with molecular masses exceeding 10 000 daltons [1]. *Analytical Chemistry,* 60, 2299-2301.

KAWAI, N., ITO, A., NAKAHARA, Y., FUTAKUCHI, M., SHIRAI, T., HONDA, H., KOBAYASHI, T. & KOHRI, K. 2005. Anticancer effect of hyperthermia on prostate cancer mediated by magnetite cationic liposomes and immune-response induction in transplanted syngeneic rats. *Prostate,* 64, 373-81.

KRUTCHINSKY, A. N. & CHAIT, B. T. 2002. On the nature of the chemical noise in MALDI mass spectra. *Journal of the American Society for Mass Spectrometry,* 13, 129-134.

LEE, P. J., CHEN, W. B. & GEBLER, J. C. 2004. Qualitative and quantitative analysis of small amine molecules by MALDI-TOF mass spectrometry through charge derivatization. *Analytical Chemistry,* 76, 4888-4893.

LI, J. L., WANG, L., LIU, X. Y., ZHANG, Z. P., GUO, H. C., LIU, W. M. & TANG, S. H. 2009. In vitro cancer cell imaging and therapy using transferrin-conjugated gold nanoparticles. *Cancer Lett,* 274, 319-26.

LOFTSSON, T. & BREWSTER, M. E. 1996. Pharmaceutical applications of cyclodextrins. 1. drug solubilization and stabilization. *Journal of Pharmaceutical Sciences,* 85, 1017-1025.

LOU, X. W., VAN DONGEN, J. L. J., VEKEMANS, J. & MEIJER, E. W. 2009. Matrix suppression and analyte suppression effects of quaternary ammonium salts in matrix-assisted laser desorption/ionization time-of-flight mass spectrometry: an investigation of suppression mechanism. *Rapid Communications in Mass Spectrometry,* 23, 3077-3082.

LU, W., SINGH, A. K., KHAN, S. A., SENAPATI, D., YU, H. & RAY, P. C. 2010. Gold nano-popcorn-based targeted diagnosis, nanotherapy treatment, and in situ monitoring of photothermal therapy response of prostate cancer cells using surface-enhanced raman spectroscopy. *Journal of the American Chemical Society,* 132, 18103-18114.

MANETTA, A., GAMBOA, G., NASSERI, A., PODNOS, Y. D., EMMA, D., DORION, G., RAWLINGS, L., CARPENTER, P. M., BUSTAMANTE, A., PATEL, J. & RIDEOUT, D. 1996. Novel phosphonium salts display in vitro and in vivo cytotoxic activity against human ovarian cancer cell lines. *Gynecologic Oncology,* 60, 203-212.

MANUCHEHRABADI, N., ZHU, L., ATTALURI, A., CAI, H., EDZIAH, R., LALANNE, E., BIEBERICH, C., MA, R. & JOHNSON, A. M. Thermal effect of gold nanorods in implanted prostatic tumors during laser photothermal therapy. ASME 2012 Summer Bioengineering Conference, SBC 2012, 2012. 621-622.

MECHREF, Y., NOVOTNY, M. V. & KRISHNAN, C. 2003. Structural characterization of oligosaccharides using MALDI-TOF/TOF tandem mass spectrometry. *Analytical Chemistry,* 75, 4895-4903.

MEESTERS, R. J. W., VAN KAMPEN, J. J. A., SCHEUER, R. D., VAN DER ENDE, M. E., GRUTERS, R. A. & LUIDER, T. M. 2011. Determination of the antiretroviral drug tenofovir in plasma from HIV-infected adults by ultrafast isotope dilution MALDI-triple quadrupole tandem mass spectrometry. *Journal of Mass Spectrometry,* 46, 282-289.

MILLARD, M., PATHANIA, D., SHABAIK, Y., TAHERI, L., DENG, J. & NEAMATI, N. 2010. Preclinical evaluation of novel triphenylphosphonium salts with broad-spectrum activity. *PLoS ONE,* 5.

MURPHY, M. P., ECHTAY, K. S., BLAIKIE, F. H., ASIN-CAYUELAT, J., COCHEM , H. M., GREEN, K., BUCKINGHAM, J. A., TAYLORT, E. R., HURRELLT, F., HUGHES, G., MIWA, S., COOPER, C. E., SVISTUNENKO, D. A., SMITH, R. A. J. & BRAND, M. D. 2003. Superoxide activates uncoupling proteins by generating carbon-centered radicals and initiating lipid peroxidation: Studies using a mitochondria-targeted spin trap derived from α-phenyl-N-tert-butylnitrone. *Journal of Biological Chemistry,* 278, 48534-48545.

MURPHY, M. P. & SMITH, R. A. J. 2007. Targeting antioxidants to mitochondria by conjugation to lipophilic cations.

PATEL, J., RIDEOUT, D., MCCARTHY, M. R., CALOGEROPOULOU, T., WADWA, K. S. & OSEROFF, A. R. 1994. Antineoplastic activity, synergism, and antagonism of triarylalkylphosphonium salts and their combinations. *Anticancer Research,* 14, 21-28.

PIELES, U., ZURCHER, W., SCHAR, M. & MOSER, H. E. 1993. Matrix-assisted laser desorption ionization time-of-flight mass spectrometry: A

powerful tool for the mass and sequence analysis of natural and modified oligonucleotides. *Nucleic Acids Research,* 21, 3191-3196.

PORTEOUS, C. M., LOGAN, A., EVANS, C., LEDGERWOOD, E. C., MENON, D. K., AIGBIRHIO, F., SMITH, R. A. J. & MURPHY, M. P. 2010. Rapid uptake of lipophilic triphenylphosphonium cations by mitochondria in vivo following intravenous injection: Implications for mitochondria-specific therapies and probes. *Biochimica et Biophysica Acta - General Subjects,* 1800, 1009-1017.

PROMEGA. *Promega UK* [Online]. Available: https://www.promega.co.uk/products/cell-health-and-metabolism/cell-viability-assays/celltiter_glo-luminescent-cell-viability-assay/?activeTab=0.

RIDEOUT, D., BUSTAMANTE, A. & SIUZDAK, G. 1993. Cationic drug analysis using matrix-assisted laser desorption/ionization mass spectrometry: application to influx kinetics, multidrug resistance, and intracellular chemical change. *Proceedings of the National Academy of Sciences of the United States of America,* 90, 10226-10229.

RIDEOUT, D. C., CALOGEROPOULOU, T., JAWORSKI, J. S., DAGNINO R, R. J. & MCCARTHY, M. R. 1989. Phosphonium salts exhibiting selective anti-carcinoma activity in vitro. *Anti-Cancer Drug Design,* 4, 265-280.

ROSS, M. F., KELSO, G. F., BLAIKIE, F. H., JAMES, A. M., COCHEM , H. M., FILIPOVSKA, A., DA ROS, T., HURD, T. R., SMITH, R. A. J. & MURPHY, M. P. 2005. Lipophilic triphenylphosphonium cations as tools in mitochondrial bioenergetics and free radical biology. *Biochemistry (Moscow),* 70, 222-230.

ROSS, M. F., PRIME, T. A., ABAKUMOVA, I., JAMES, A. M., PORTEOUS, C. M., SMITH, R. A. J. & MURPHY, M. P. 2008. Rapid and extensive uptake and activation of hydrophobic triphenylphosphonium cations within cells. *Biochemical Journal,* 411, 633-645.

SEHY, D. W., SHAO, L. E., RIDEOUT, D. & YU, J. 1993. Sensitivity of committed hematopoietic progenitor cells in vitro (BFU-E, CFU-E, CFU-GM) and two human carcinoma cell lines toward rhodamine-123 and phosphonium salt II-41. *Leukemia Research,* 17, 247-253.

SHAO, J., GRIFFIN, R. J., GALANZHA, E. I., KIM, J.-W., KOONCE, N., WEBBER, J., MUSTAFA, T., BIRIS, A. S., NEDOSEKIN, D. A. & ZHAROV, V. P. 2013. Photothermal nanodrugs: potential of TNF-gold nanospheres for cancer theranostics. *Sci. Rep.,* 3.

SHIOJI, K., OYAMA, Y., OKUMA, K. & NAKAGAWA, H. 2010. Synthesis and properties of fluorescence probe for detection of peroxides in mitochondria. *Bioorganic and Medicinal Chemistry Letters,* 20, 3911-3915.

SLENO, L. & VOLMER, D. A. 2005. Some fundamental and technical aspects of the quantitative analysis of pharmaceutical drugs by matrix-assisted laser desorption/ionization mass spectrometry. *Rapid Communications in Mass Spectrometry,* 19, 1928-1936.

SLENO, L. & VOLMER, D. A. 2006. Assessing the properties of internal standards for quantitative matrix-assisted laser desorption/ionization mass spectrometry of small molecules. *Rapid Communications in Mass Spectrometry,* 20, 1517-1524.

SMITH, R. A. J., HARTLEY, R. C., COCHEM , H. M. & MURPHY, M. P. 2012. Mitochondrial pharmacology. *Trends in Pharmacological Sciences,* 33, 341-352.

SMITH, R. A. J., HARTLEY, R. C. & MURPHY, M. P. 2011. Mitochondria-targeted small molecule therapeutics and probes. *Antioxidants and Redox Signaling,* 15, 3021-3038.

SMITH, R. A. J., PORTEOUS, C. M., COULTER, C. V. & MURPHY, M. P. 1999. Selective targeting of an antioxidant to mitochondria. *European Journal of Biochemistry,* 263, 709-716.

SMITH, R. A. J., PORTEOUS, C. M., GANE, A. M. & MURPHY, M. P. 2003. Delivery of bioactive molecules to mitochondria in vivo. *Proceedings of the National Academy of Sciences of the United States of America,* 100, 5407-5412.

SPARBIER, K., SCHUBERT, S., WELLER, U., BOOGEN, C. & KOSTRZEWA, M. 2012. Matrix-Assisted Laser Desorption Ionization-Time of Flight Mass Spectrometry-Based Functional Assay for Rapid Detection of Resistance against beta-Lactam Antibiotics. *Journal of Clinical Microbiology,* 50, 927-937.

ST HLER, K. & MEYER, H. E. 2004. MALDI: More than peptide mass fingerprints. *Current Opinion in Molecular Therapeutics,* 6, 239-248.

STERN, J. M., STANFIELD, J., KABBANI, W., HSIEH, J.-T. & CADEDDU, J. A. 2008. Selective Prostate Cancer Thermal Ablation With Laser Activated Gold Nanoshells. *The Journal of Urology,* 179, 748-753.

SZ JLI, E., FEH R, T. & MEDZIHRADSZKY, K. F. 2008. Investigating the quantitative nature of MALDI-TOF MS. *Molecular and Cellular Proteomics,* 7, 2410-2418.

TANAKA, K., WAKI, H., IDO, Y., AKITA, S., YOSHIDA, Y., YOSHIDA, T. & MATSUO, T. 1988. Protein and polymer analyses up to m/z 100 000 by laser ionization time-of-flight mass spectrometry. *Rapid Communications in Mass Spectrometry,* 2, 151-153.

WANG, J., SEFAH, K., ALTMAN, M. B., CHEN, T., YOU, M., ZHAO, Z., HUANG, C. Z. & TAN, W. 2013. Aptamer-conjugated nanorods for targeted photothermal therapy of prostate cancer stem cells. *Chem Asian J,* 8, 2417-22.

WEISSIG, V. 2005. Targeted drug delivery to mammalian mitochondria in living cells. *Expert Opinion on Drug Delivery,* 2, 89-102.

WEISSIG, V. 2011. Mitochondrial delivery of biologically active molecules. *Pharmaceutical Research,* 28, 2633-2638.

WEISSIG, V., CHENG, S. M. & D'SOUZA, G. G. M. 2004. Mitochondrial pharmaceutics. *Mitochondrion,* 3, 229-244.

WINGERATH, T., KIRSCH, D., SPENGLER, B. & STAHL, W. 1999. Analysis of cyclic and acyclic analogs of retinol, retinol acid, and retinal by laser desorption ionization-, matrix-assisted laser desorption ionization-mass spectrometry, and UV/Vis spectroscopy. *Analytical Biochemistry,* 272, 232-242.

WITTIG, G. 1980. From diyls to ylides to my idyll. *Science,* 210, 600-604.

ZHU, Y. F., LEE, K. L., TANG, K., ALLMAN, S. L., TARANENKO, N. I. & CHEN, C. H. 1995. Revisit of MALDI for small proteins. *Rapid Communications in Mass Spectrometry,* 9, 1315-1320.

Chapter 5.

Investigation of the use of phosphonium-functionalised gold nanoparticles *in vitro* for photothermal therapy applications

5.1 Introduction

AuNPs are known to passively target tumour cells due to their inherent small size and the chaotic nature of tumour blood vessels. It has been demonstrated that "naked" AuNPs with no functionalisation do not target all cell types (Patra *et al.*, 2007). AuNPs can be directed to specific sites by attaching ligands to the surface of the nanoparticles for targeted delivery, examples include antibodies to target a specific tumour marker that is usually overexpressed on tumour cells of interest (El-Sayed *et al.*, 2006, Sokolov *et al.*, 2003, Kirui *et al.*, 2010) and ligands to target specific receptors overexpressed on the surface of tumour cells (Dixit *et al.*, 2006, Chen *et al.*, 2007).

Chemotherapeutic drugs have also been attached to the surface of AuNPs to enhance the cellular uptake and improve the bioavailability of the drug (Gibson *et al.*, 2007, Nadeau *et al.*, 2010, Hwu *et al.*, 2009). Targeting can be improved further to target specific sub-cellular organelles such as the mitochondria; AuNPs have been functionalised with a pro-apoptotic peptide which has shown to amplify apoptotic cell death in HeLa cells by inducing mitochondrial membrane swelling and bursting the membrane (Chen *et al.*, 2013).

The concept of using heat to treat cancer is not new (Field and Bleehen, 1979); both hyperthermia and thermal ablation use heat to kill pathophysiological tissues, the difference is based on the range of heating temperatures. Thermal ablation involves raising the temperature above 50°C and induces cell death by necrosis, whereas hyperthermia is associated with mild increase in temperature between 41-46°C and causes cell death via the apoptotic pathway (Vauthier *et al.*, 2011, Lepock, 2003, Rivera Gil *et al.*, 2010).

The current model of apoptotic hyperthermic cell death indicates that an increase in temperature will result in the activation of pro-caspase-2; caspase-2 can act as an initiator caspase which engages in the mitochondria-dependent apoptotic pathway by inducing the release of cytochrome *c* and other apoptotic proteins (e.g. Bak and Bax) into the cell cytoplasm, subsequently activating other apoptotic proteins leading to mitochondrial membrane damage which is critical for hyperthermic induced apoptotic cell death (Milleron and Bratton, 2007,

175

Aksenova *et al.*, 2013, Guo *et al.*, 2002). Furthermore Caspase-2 has also been suggested to be able to act as an effector caspase (Delgado *et al.*, 2013, He *et al.*, 2004).

The application of thermotherapy in a clinical setting has been limited to unresectable malignant hepatic leison, pelvic, prostate cancer, head and neck tumours (Cherukuri *et al.*, 2010, Baronzio *et al.*, 2009, El-Sayed, 2010). At present the lack of tissue specificity is the primary obstacle in the development of thermotherapy, in addition to killing cancer cells, the heat also spreads to neighbouring healthy tissues causing collateral damage (Cherukuri and Curley, 2010, Diagaradjane *et al.*, 2008, Feng *et al.*, 2009). This lack of specificity has been overcome by using gold based nanomaterials; the use of AuNPs for photothermal therapy (PTT) was first demonstrated by Pistillides and co-workers in 2003 (Pitsillides *et al.*, 2003).

AuNPs have the unique ability of converting absorbed light into heat on a picosecond time domain by electron-phonon and phonon-phonon processes (Link and El-Sayed, 2000). This highly efficient conversion of heat energy from absorbed light led to their investigation for cancer therapeutics (Huang *et al.*, 2008, Huang *et al.*, 2007, Vauthier *et al.*, 2011, Everts, 2007). Several groups have demonstrated elective PTT in cancer cells *in vitro*; Pitsillides and colleagues (Pitsillides *et al.*, 2003) treated lymphocytes with spherical AuNPs (d = 30 nm) conjugated to anti-CD8-R-phycoerythrin and irradiated with short laser pulses (20 ns) at 532 nm. CD8+ T lymphocytes showed an increase in percentage cell death with the increase in number of AuNPs per cell with lowest cell death > 50%, whereas CD8- T lymphocytes exhibited good cell viability greater than 90% under the same conditions. Li and co-workers (Li *et al.*, 2009) treated breast cancer cells (Ks578T) with spherical AuNPs (d = 23 nm) conjugated with transferrin and irradiated with a nanosecond laser at 530 nm. When cells were treated with conjugated AuNPs cell damage were observed at a significant lower laser power of 7 W/cm^2 in comparison to 1600 cm^2 in the absence of AuNPs.

El-Sayed's group (El-Sayed *et al.*, 2006, Huang *et al.*, 2006) treated oral squamous carcinoma cells lines (HOC 3 Clone 8 and HSC 313) and a benign epithelial cell line (HaCaT) with spherical AuNPs (d = 40 nm) conjugated to anti-EGFR antibody and irradiated with a continuous wave (CW) argon laser at 514 nm. The selectivity of this method is demonstrated by the results that carcinoma cells required less than half the laser energy to be killed in comparison to benign cells; 19 W/cm^2 for HOC, 25 W/cm^2 for HSC and 57 W/cm^2 for HaCaT. In addition, no photothermal damage were observed for any of the cell types without AuNP labeling, even at four times the energy required to kill cancer cells labelled with antibody conjugated AuNPs.

The main aim of this chapter was to investigate if AuNPs functionalised with lipophilic phosphonium ligands synthesised previously in chapter 3 can lead to mitochondria specific accumulation and to selectively induce apoptosis of cells by photothermal therapy.

5.2 Materials and Experimental Methods

5.2.1 Reagents

Propidium iodide (PI) Hoechst 33342, gold nanoparticles 5 nm, glutaraldehyde, sodium phosphate dibasic (Na$_2$HPO$_4$), sodium phosphate dibasic, dodecahydrate (Na$_2$HPO$_4$.12H$_2$O) and 1,2-epoxypropane were purchased from Sigma (Gillingham, Dorset, UK). Phenol red free Dulbecco's Modified Eagle Medium (PRF DMEM) was obtained from Invitrogen Life Technologies (Paisley, Renfrewshire, UK) and Caspase-3 activity assay was acquired from Cambridge Bioscience (Bar Hill, Cambridge, UK). Agar low viscosity (LV) resin, agar low viscosity hardener (VH1 & VH2), low viscosity accelerator and 2% osmimum tetraoxide were purchased from Agar Scientific (Stansted, Essex, UK).

5.2.2 Investigating the use of Phosphonium-Functionalised Gold Nanoparticles for Photothermal Therapy

PC3 cells were seeded in a 96 well plate at a density of 10,000 cells/ well and allowed to adhere overnight. Cells were then treated with different concentrations of AuNPs (0-100 mg/mL) and incubated for several hours. For preliminary irradiation experiments, an Olympus IX81 motorised inverted

microscope (Olympus, Southend-on-Sea, UK) with a 100 watt bulb, with varying different wavelength cubes for different length of time (0-30 minutes) was used, after irradiation cells were returned to the incubator and visualised on the following day.

5 nm diameter gold nanoparticles was chosen as a control for experiments, because it has been reported in the literature that AuNPs sizes ≥ 3 nm was able to enter the mitochondria intermembrane space whereas 6 nm AuNPs were not (Salnikov et al., 2007). Thus the cut off point for AuNPs not able to pass through the mitochondrial membrane is somewhere between > 3 and 6 nm. 5 nm were chosen because P-AuNPs synthesised previously in chapter 3 are between 3.0 and 4.9 nm depending on the precursor ligand. If the control of 5 nm were taken-up by the mitochondria, in theory PPTA capped AuNPs (4.9 nm) would also be taken-up by the mitochondria.

For experiments irradiated using a Zeiss Axiovert 200M inverted microscope, laser LSM 510 laser module (Zeiss, Cambridge, UK), PC3 cells were seeded in fluorodish cell culture dish 35 mm (World Precision Instruments, Hitchin, Hertfordshire, UK) at a density of 500,000 cells/dish. Cells were then treated with different concentrations of AuNPs (0-10 μg/mL), incubated for several hours and irradiated, after irradiation cells were returned to the incubator and visualised the next day.

To visualise the cells, the cells were first stained with Hoechst (20μg/mL) and incubated for 30 minutes, prior to analysis PI (10μg/mL) was added. Cells were visualised using an Olympus IX81 motorised inverted microscope (Olympus, Southend-on-Sea, UK). The number of viable, apoptotic and necrotic cells were counted, a total umber of 200 cells were counted from each field of view from 3 independent repeats. The number of viable, apoptotic and necrotic cells are expressed as a percentage of the total number of cells counted. Staistical analyses were then conducted using the method described previously in chapter 2.16.

5.2.3 Investigating the Cellular Uptake of Phosphonium-Functionalised Gold Nanoparticles by Transmission Electron Microscopy

PC3 cells were plated in a 6 well plate at a density of 500,000 cells/ well and allowed to adhere overnight. Cells were then treated with varied concentrations of P-AuNPs (12.5, 25.0, 50.0 mg/mL) and incubated overnight. After incubation, cells were trypsinised and transferred to a microcentrifuge tube and washed with phosphate buffer 0.1 M pH 7.2 for 10 minutes x 2. 0.1 M phosphate buffer 7.2 was prepared by mixing 36 mL of phosphate solution A (0.2 M of $Na_2HPO_4.12H_2O$) with 14 mL phosphate solution B (0.2 M of Na_2HPO_4). Cell pellet were then fixed in 2% glutaraldehyde in phosphate buffer for 1 hour, washed in phosphate buffer 0.1 M pH 7.2 for 10 minutes x 2.

Cells were then fixed in 2% aqueous osmium tetroxide for 1 hour, washed in DIH_2O for 15 minutes x 2 and embedded in 2% agar in DIH_2O at 50°C. Agar pellets were cut into pieces approximately 1 x 1 mm, dehydrated in a series of ethanol and water (25, 50, 70, 90 and 100% x 2, 30 minutes each), ethanol was then replaced with 1,2-epoxypropane for 1 hour, after an hour 1,2-epoxypropane was replaced with 50:50 1,2-epoxypropane: resin overnight. Sample was then transferred to a BEEM capsules and fresh 100% resin was added and incubated overnight at 65°C with caps off. Resin was prepared by mixing 48 mL Agar LV resin, 10 mL VH1, 42 mL VH2 and 2.5 mL accelerator. For a schematic illustration see Figure 5.1.

Samples were taken to Brunel University for sectioning and TEM analysis; samples were sectioned at 100 nm thickness using a PowerTome XL Ultramicrotome (Boeckeler, Tuscon, Arizona, USA). TEM micrographs of AuNPs in cells were obtained on a Jeol JEM-2100F TEM (ETC, Brunel University, Middlesex, UK), set at 100 kV.
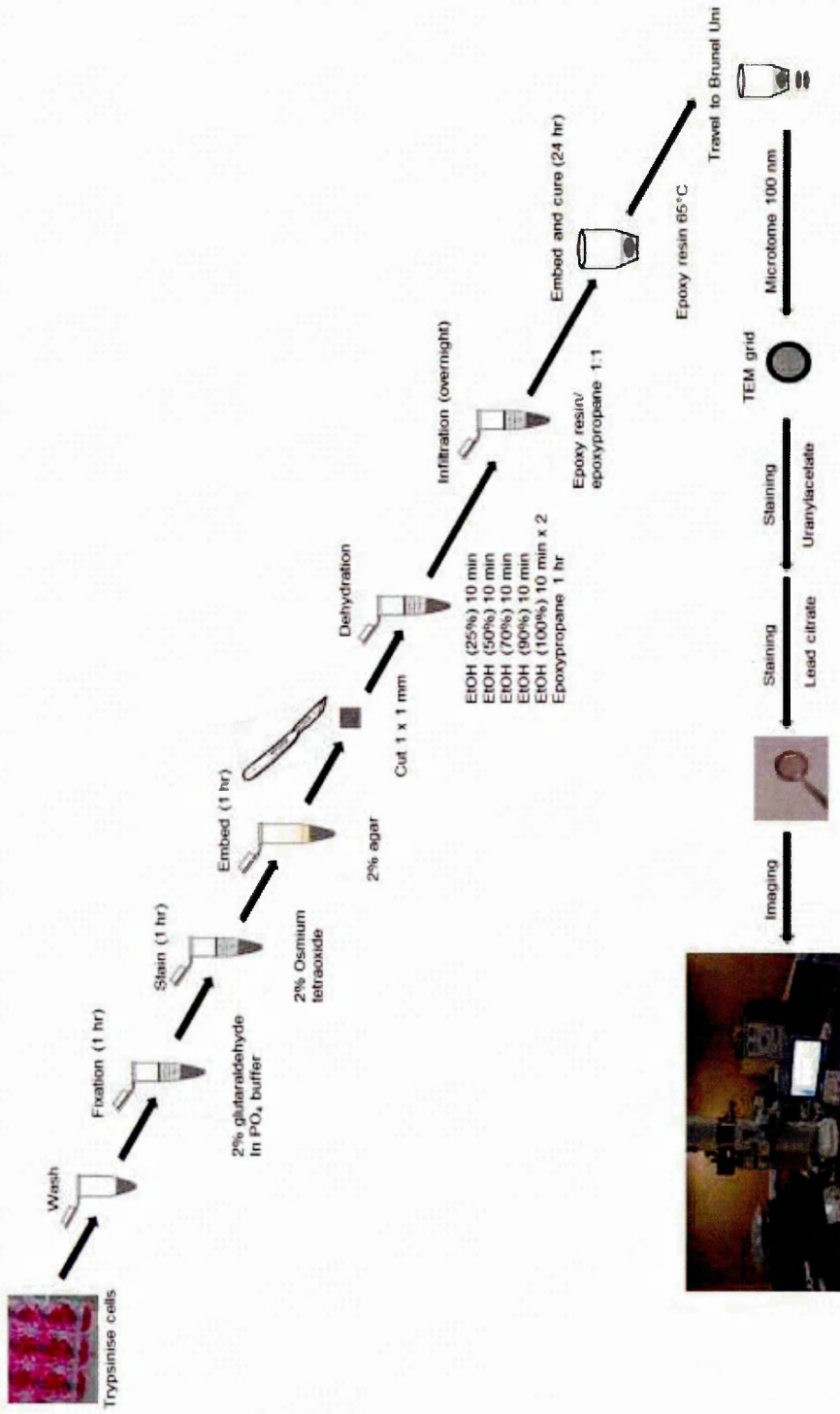
Figure 5.1 Schematic illustration of TEM sample preparation procedure. The samples were fixed in TEM fixative (2% glutaraldehyde), post fixed in 2% osmium tetraoxide, dehydrated, infiltrated and embedded in epoxy resin, sliced into 100 nm thin sections and stained with uranyl acetate and lead citrate (saturated solution) for several minutes.

180

5.2.4 Quantification of the Uptake of Phosphonium-Functionalised Gold Nanoparticles in cells by ICP-MS

PC3 cells were plated in a 6 well plate at a density of 500,000 cells/well and allowed to adhere overnight. Cells were treated with different concentrations of P-AuNPs (12.5, 25.0, 50.0 mg/mL) and incubated overnight. On the subsequent day cells were trypsinised, washed in PBS, fixed in 100% EtOH and sent to MEDAC (Chobham, Surrey, UK) for ICP-MS analysis.

5.3 Results and Discussion

5.3.1 Solubility of Phosphonium-Functionalised Gold Nanoparticles in Biological Media

The biological activity of AuNPs is influenced by many parameters including the particle size, shape, concentration, surface charge and agglomeration state (Pan *et al.*, 2007, Yen *et al.*, 2009). The investigation of the biological effects of AuNPs and their applications in biomedical research is ongoing (Sperling *et al.*, 2008, Arnida *et al.*, 2010, Cobley *et al.*, 2011, Kanaras *et al.*, 2011, Kumar *et al.*, 2013). The size of commercial standard AuNPs (60 nm, National Institute of Standards and Technology reference material 8013) has been shown to increase in size from 61 to 70 nm in the presence of human plasma, indicating that the addition of proteins modifies the surface of the nanoparticles in some way (Montes-Burgos *et al.*, 2010). This alteration may induce changes of the AuNPs properties and thus affect their biological activity in cells.

The freeze-dried P-AuNPs can be re-suspended in water, methanol, ethanol or DMSO. The UV-vis spectra of the solutions after re-suspension in DIH_2O are similar to that of a freshly prepared solution (Figure 3. 9), indicating that the freeze-drying process does not significantly alter the particle size or shape. In contrast when dissolved in complete Dulbecco's modified Eagle's medium (CDMEM), a significant shift in the SPR band from 520 nm to ~560 nm was observed, this suggest that the particle size has been modified. This shift in SPR band was also observed for purchase AuNPs of similar size (5 nm) (Figure 5.4), which indicate that the CDMEM has an effect on AuNPs in general and not just P-AuNPs.

Different cell culture media have been used to investigate the dispersibility of AuNPs; in pure RPMI, strong agglomeration was observed, where as in RPMI containing up to 10% foetal calf serum (FCS) or bovine serum albumin showed the AuNPs remained well dispersed above 1% w/v protein concentration (Mahl *et al.*, 2010).
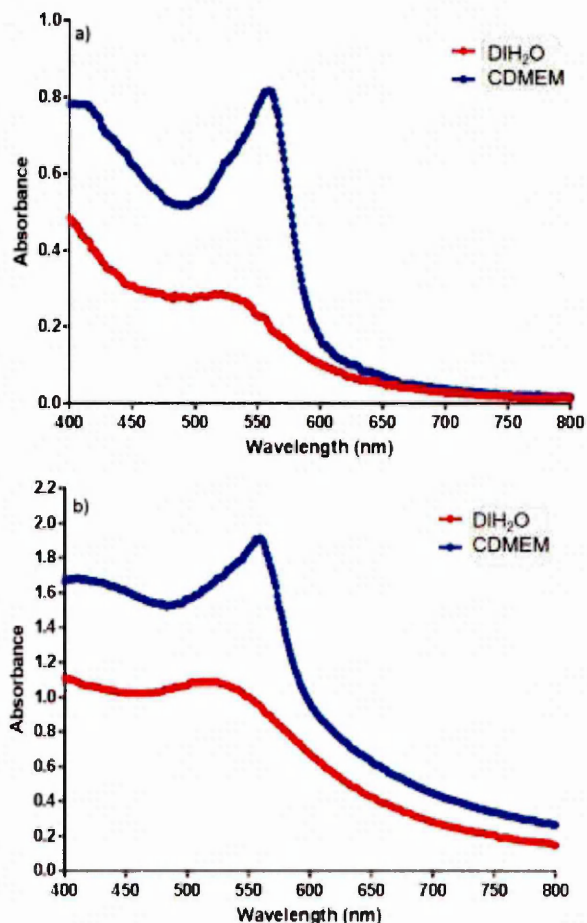
Figure 5.2 Visible spectra of nanoparticles re-suspended in DIH_2O and CDMEM for a) commercial 5nm AuNPs and b) P-AuNPs.

Both nanoparticles exhibited their characteristic SPR band at ~520 nm when dissolved in deionised-water, however when dissolved in CDMEM, their characteristic SPR band shifts to above ~550 nm. It is known that the SPR band of spherical gold nanoparticles shifts from ~ 520 nm to ~ 600 nm as you increase the size from 5 nm to 99 nm (Jain et al., 2007). Therefore the shift in peak observed from 520 nm to 550 nm suggested that the AuNPs has aggregated.

Visible spectra shown in Figure 5.2 suggested that there might be a possible peak at around 400 nm, the origin of this peak has been investigated (Figure 5.3). Studies showed that this peak is due to FCS and does not interfere with the SPR band of the AuNPs.
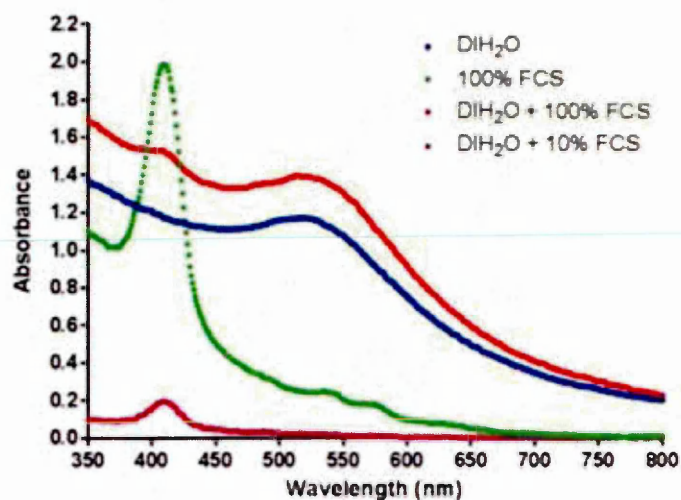
Figure 5.3 Visable spectra of P-AuNPs re-suspended in different solutions, and with different concentration of FCS. The peak at around 400 nm correlates to FCS as the absorbance of this peak increases dramatically as the concentration of FCS increase from 10% to 100%.
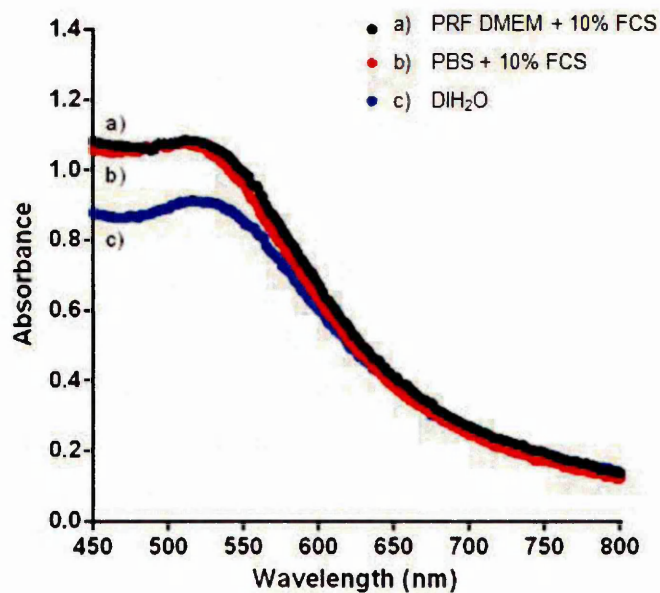
Figure 5.4 Visable spectra of P-AuNPs re-suspended in different biological media; a) phosphate buffered saline plus 10% foetal calf serum, b) phenol red free Dulbecco's modified Eagle medium plus 10% foetal calf serum and c) deionised water.

183

Visible spectra illustrated that P-AuNPs can be dissolved in phenol red free DMEM, as its gives a very similar SPR band profile as observed in deionised water. When P-AuNPs was dissolved in either PBS or phenol red free DMEM it gave very similar SPR profiles as observed in DIH_2O. This indicated that these biological media do not alter the particle size or shape of the AuNPs and are both suitable for re-suspending AuNPs for cell culture studies. Since cells are best cultured in DMEM, it was decided that phenol red free DMEM would be used as the cell culture medium rather than PBS plus 10% FCS for experiments involving AuNPs and cells.

5.3.2 Investigating the Potential of Phosphonium-Functionalised Gold Nanoparticles for Photothermal Therapy Applications

5.3.2.1 Investigating Different Excitation Wavelength of Light

AuNPs tuneable optical properties are due to the phenomenon of SPR, and are sensitive to the size, shape, composition and the dielectric environment (Dreaden *et al.*, 2011, Jain *et al.*, 2008, Kelly *et al.*, 2003, Liz-Marzán, 2004). Theoretically the SPR effect should only occur when a frequency overlaps the SPR band of the AuNPs which subsequently result in local heating of the surrounding environment.

To test this theory, cells have been treated with P-AuNPs and irradiated for the same amount of time with different wavelengths of light by using different filter cubes including yellow filter cube (U-MWIY, 545-580 nm), blue filter cube (U-MWIB, 460-490 nm), narrow green filter cube (U-MNG, 530-550 nm) and wide green filter cube (U-MWG, 510-550 nm) (Figure 5.6). After irradiating the cells with the light they were returned to the incubator for 24 hours prior to analysis by fluorescent microscopy.
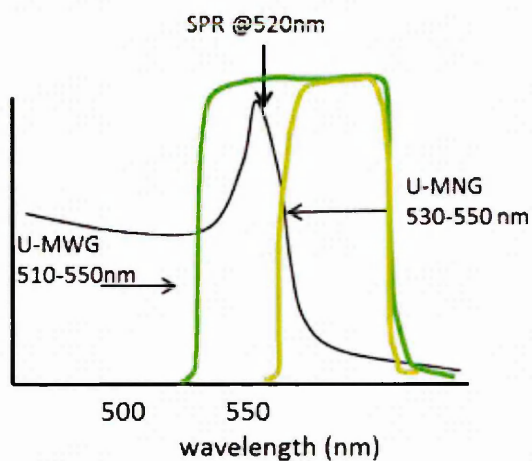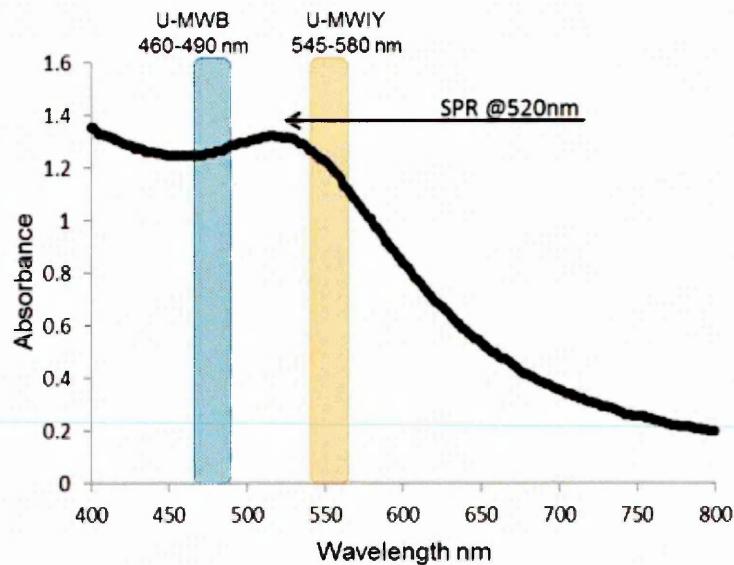
Figure 5.5 Diagram to illustrate different filter block cubes used in the experiment; yellow filter cube (U-MWIY, 545-580 nm), blue filter cube (U-MWB, 460-495 nm), narrow green filter cube (U-MNG, 530-550 nm) and wide green filter cube (U-MWG, 510-550 nm). Only the latter filter cube overlaps the SPR band of P-AuNPs, when cells were irradiated with this filter cube it induces a response in cells.

The result showed that when PC3 cells were treated with P-AuNPs at a concentration non-toxic to cells and irradiated with a light source that does not overlap the SPR band of the AuNPs, the cells have no effect and were alive. When cells were treated with the same dose of P-AuNPs and irradiated with a light source that overlaps the SPR band of the AuNPs (510-550 nm) cells were killed either by apoptosis or necrosis depending on the radiation length of time

185

(Figure 5.6). After 5 minutes irradiation, cells died by apoptosis as shown by typical apoptotic morphology (cell shrinkage and nuclear material condensation), and after 10 minutes irradiation cells died from necrosis as confirmed by the positive staining of PI.
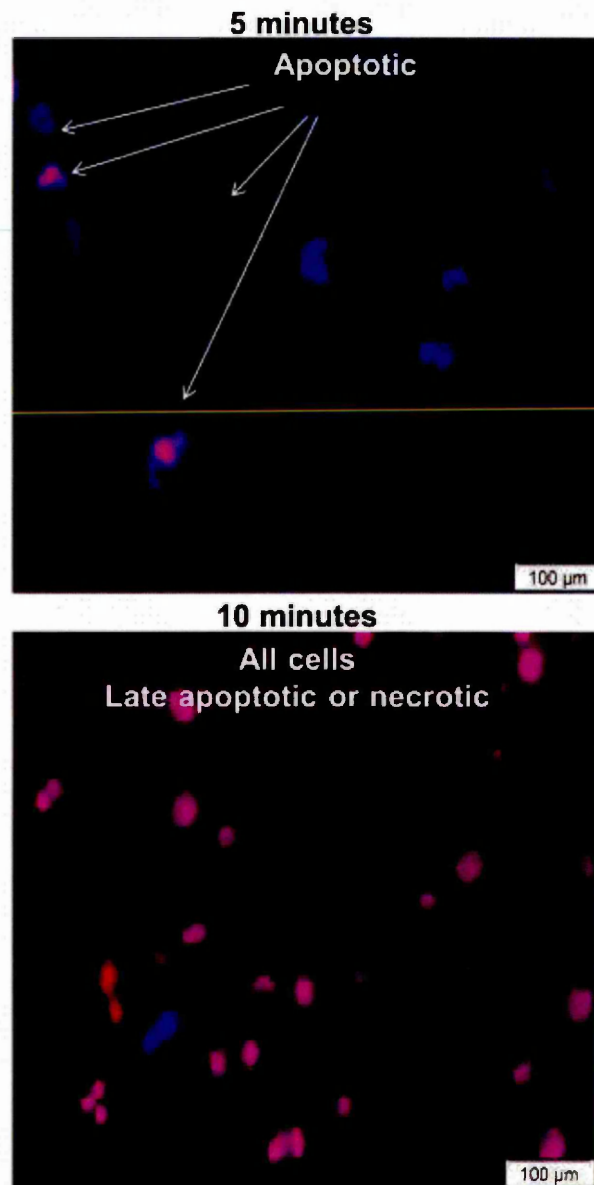
Figure 5.6 Fluorescent microscope images of PC3 cells treated with P-AuNPs 25 mg/mL for 4 hours and irradiated with wide green filter cube (U-MWG, 510-550 nm) for 5 and 10 minutes. At 5 minutes, cells exhibited typical apoptotic morphology, whereas at 10 minuntes, all cells were dead (late apoptosis or necrosis) and the membranes were permeabilised which was confirmed by the positive staining of PI. Images were taken on an 20x objective lens.
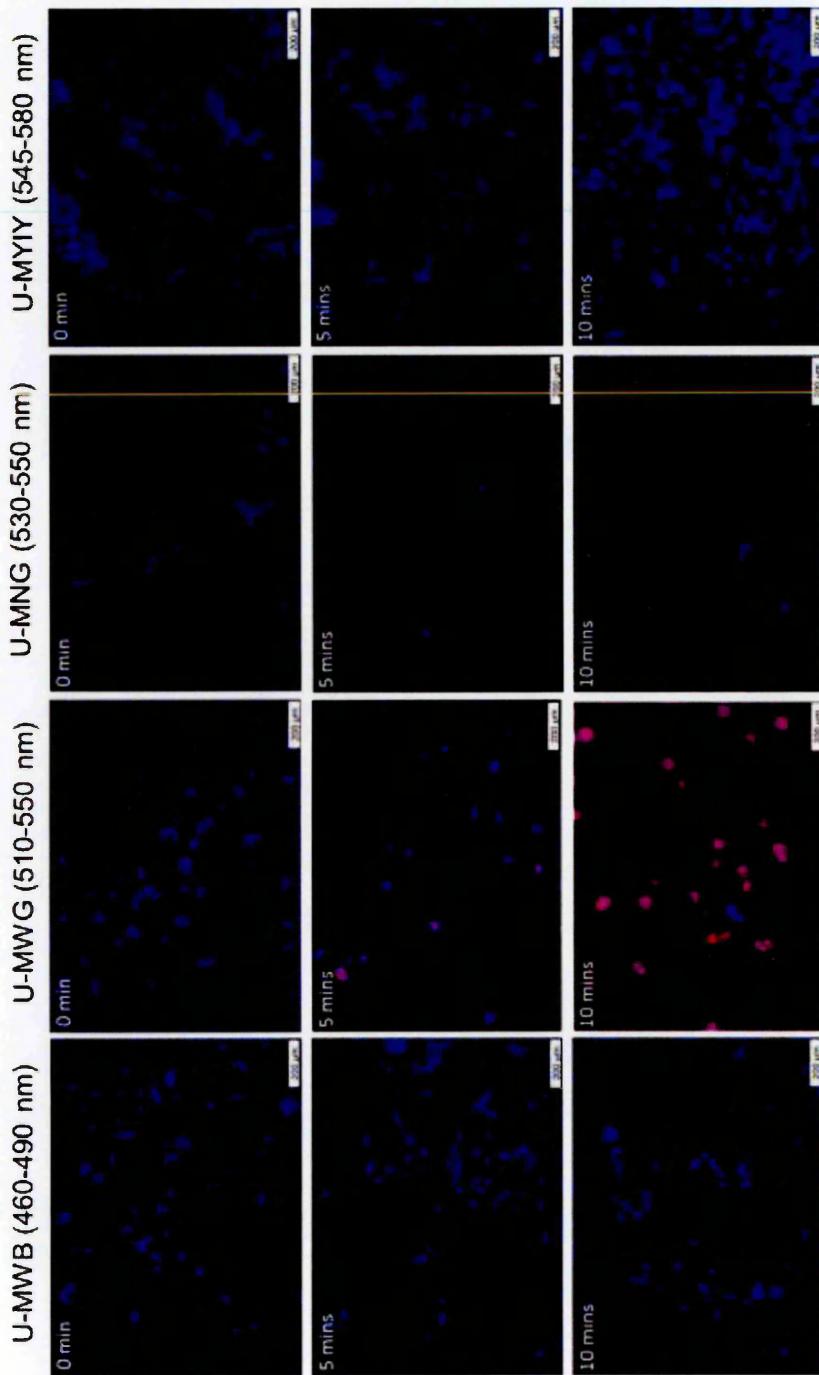
Figure 5.7 Representative fluorescent microscope images of PC3 cells treated with P-AuNPs 25 mg/mL for 4 hours and irradiated with different filter cubes; yellow filter cube (U-MYIY, 545-580 nm), blue filter cube (U-MWB, 460-490 nm), narrow green filter cube (U-MNG, 530-550 nm) and wide green filter cube (U-MWG, 510-550 nm) for varying length of time between 0 and 10 minutes. Cells stained with Hoechst and PI and images were taken on an 10x objective lens.

187

These results illustrated that P-AuNPs are specific to green light excitation (510-550 nm); when cells which were irradiated with yellow (U-MWIY, 545-580 nm), blue (U-MWB, 460-490 nm) and narrow green filter cube (U-MNG, 530-550 nm) cells remain viable. However when irradiated with a light source that overlaps the SPR of the P-AuNPs at 520 nm, cells undergo photothermal effect and result in cell death. Therefore the wide green (U-MWG, 510-550 nm) filter cube was used for future PTT experiments.

5.3.2.2 Preliminary Investigation of the use of Phosphonium-Functionalised Gold Nanoparticles as Photothermal Therapy Agents

Once it had been established that P-AuNPs are specifically activated by green light excitation (U-MWG, 510-550 nm), experiments were conducted to explore the effect of different concentrations of P-AuNPs on cells. PC3 cells were treated with different concentration of P-AuNPs and irradiated with the same wavelength (U-MWG, 510-550 nm) and length of time (5 minutes). The result (Figure 5.8) showed that an increasing in concentration of P-AuNPs resulted in an increase number of dead cells.
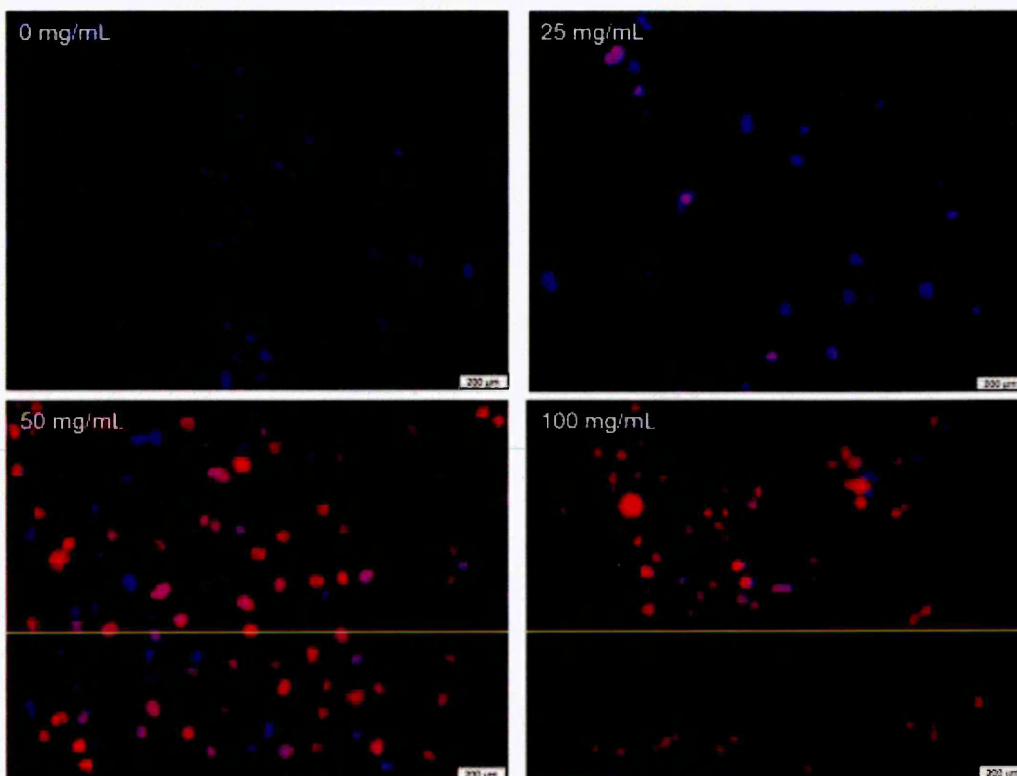
Figure 5.8 Fluorescent microscope images of cells treated with varying concentrations of P-AuPs (0-10 mg/mL) and irradiated with U-MWG, 510-550 nm light for 10 minutes. The number of PI positive cells increases with concentration of P-AuNPs. Cells stained with Hoechst and PI, images were taken on a 10x objective lens.

To confirm that cells undergo apoptosis when treated with P-AuNPs (25 mg/mL) and irradiated for 5 minutes with U-MWG, 510-550 nm light source, caspase-3 activity assay was used. With the addition of P-AuNPs to cells, the percentage of caspase-3 positive cells increased from 6 % (prior to treatment) to ~70% (Figure 5.10). Cells that were caspase 3 positive indicated that they were actively undergoing apoptosis and the results (Figure 5.9) showed that there was an increase in the number of cells that were actively undergoing apoptosis followed by 5 minutes irradiation. Statisitcal analysis (figure 5.10) showed that there is a significant increase of caspase-3 positive cells after the treatment of 25 mg/mL of P-AuNPs followed by 5 minutes irradiation with green light U-MWG 510-550 nm excitation (P = 0.0213).
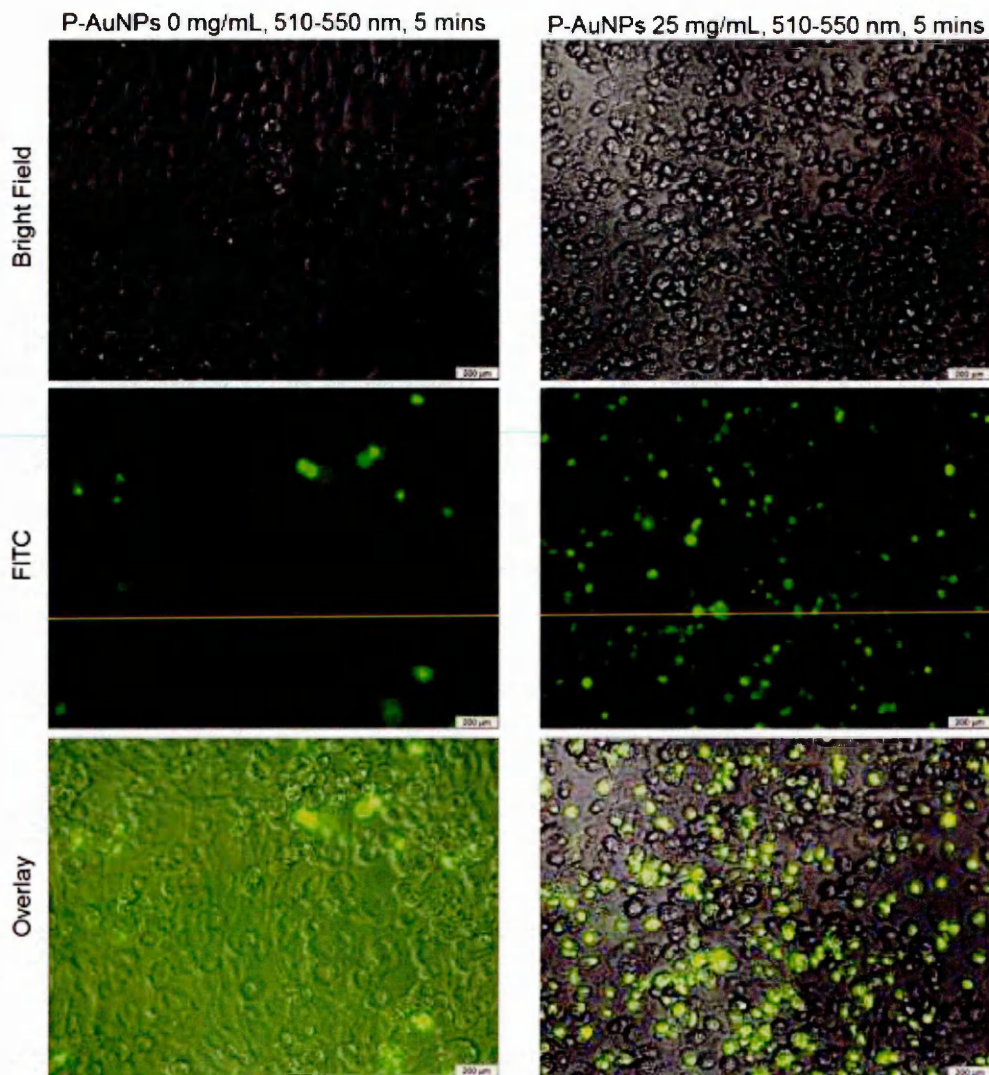
Figure 5.9 Fluorescent microscope images of cells treated with P-AuNPs and irradiated with U-MWG, 510-550 nm light for 5 minutes. Cells were stained with caspase-3 assay; the number of caspase-3 positive cells increases considerably when cells were treated and irradiated. Images were taken on a 10x objective lens.
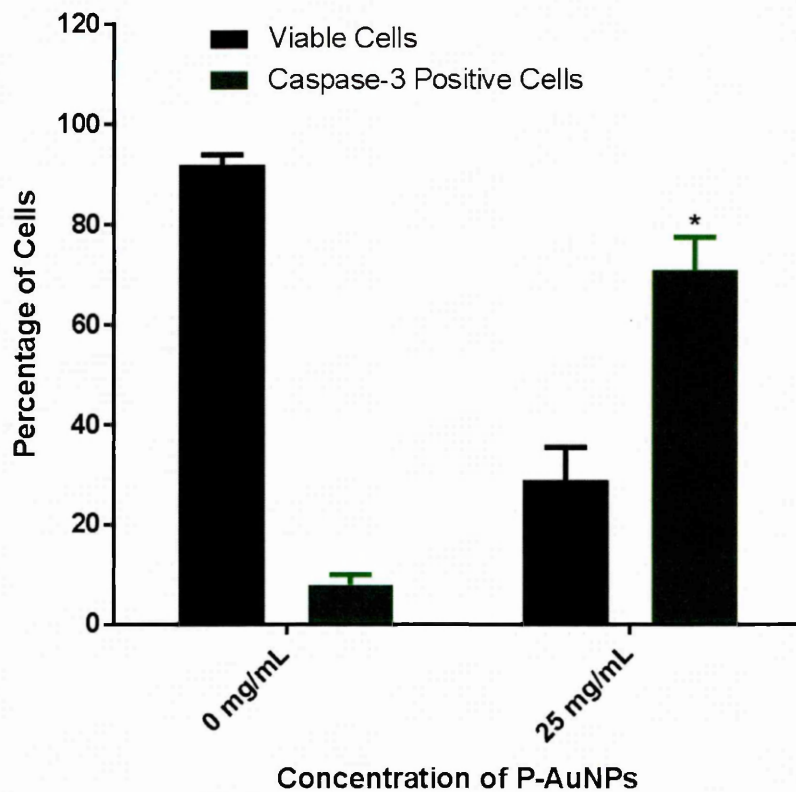
Figure 5.10 Quantitation of PC3 cells treated with 25 mg/mL P-AuNPs and irradiated with U-MWG 510-550 nm light for 5 minutes. Cells were stained with caspase-3 assay. Data is expressed as a percentage of cells (200 cells were count for each reading), for each sample 3 readings were recorded from each triplicate repeats (n=9). * Statisitcal significance between the number of Caspase-3 positive cells $P \leq 0.05$.

In a subsequent experiment, instead of irradiating each well individually, two sample wells were irradiated at the same time in an attempt to increase sample throughput. Interestingly, the result showed a dramatic difference in caspase-3 positive cells within the irradiated area vs non-irradiated area (Figure 5.11). When cells were treated with P-AuNPs at a concentration of 25 mg/mL and irradiated with U-MWG, 510-550 nm light for 5 minutes, cells responded to PTT and apoptosis was observed, furthermore death by apoptosis was confirmed by caspase 3 assay.
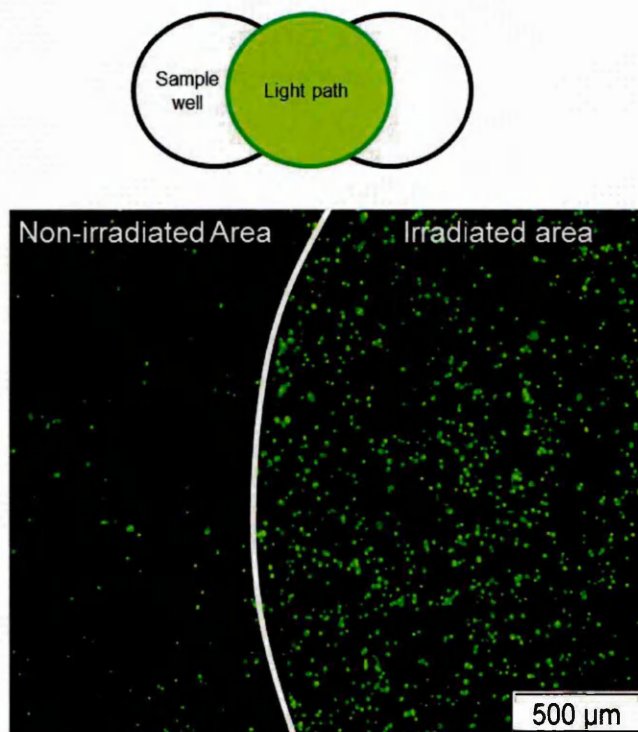
**Figure 5.11** Fluorescent microscope images of cells treated with P-AuPs (25 mg/mL) and irradiated with U-MWG, 510-550 nm light for 5 minutes, cells stained with caspase-3 assay. As shown in the Figure, there are substantial number of cells that are caspase-3 positive within the irradiated area compared to the non-irradiated area. Images were taken on a 4x objective lens.

Preliminary PTT experiments demonstrated that P-AuNPs synthesised responded specifically to an excitation wavelength that overlaps with the SPR band at 520 nm and no PTT effect was observed when cells were irradiated with a light source that did not overlap the SPR band (Figure 5.5). The PTT effect on cells is dependent on the concentration of P-AuNPs; at a concentration of 25 mg/mL cells were alive, with some apoptotic cell death whereas concentrations above 50 mg/mL majority of cells were dead by necrosis. Apoptotic death were observed at a concentration 25 mg/mL P-AuNPs, this was confirmed by caspase 3 assay, which showed that after 5 minutes irradiation, cells were actively undergoing apoptosis.

To confirm the preliminary PTT results, it was important to conduct the experiments using a more controlled system particularly the intensity of the

192

excitation source and the irradiation area, which had to be consistent and regulated across experiments. These parameters were not controllable using the Olympus fluorescent microscope; the Zeiss confocal microscope has the ability to control the laser power and scan size, thereby PTT experiments were investigated using the confocal microscope.

5.3.2.3 Investigating the use of Phosphonium-Functionalised Gold Nanoparticles as Photothermal Therapy Agents by Confocal Microscopy

Before irradiating PC3 cells treated with P-AuNPs, it was crucial to determine the non-toxic dosage of P-AuNPs, to ensure that cell death is a result of hyperthermia rather than from the cytotoxicity of the P-AuNPs. PC3 cells were treated with P-AuNPs at different concentrations for 24 hours, typical images are shown in Figure 5.13. To provide useful quantification data 200 cells were counted and the values of viable, apoptotic and necrotic cells were expressed as a percentage (Figure 5.12).
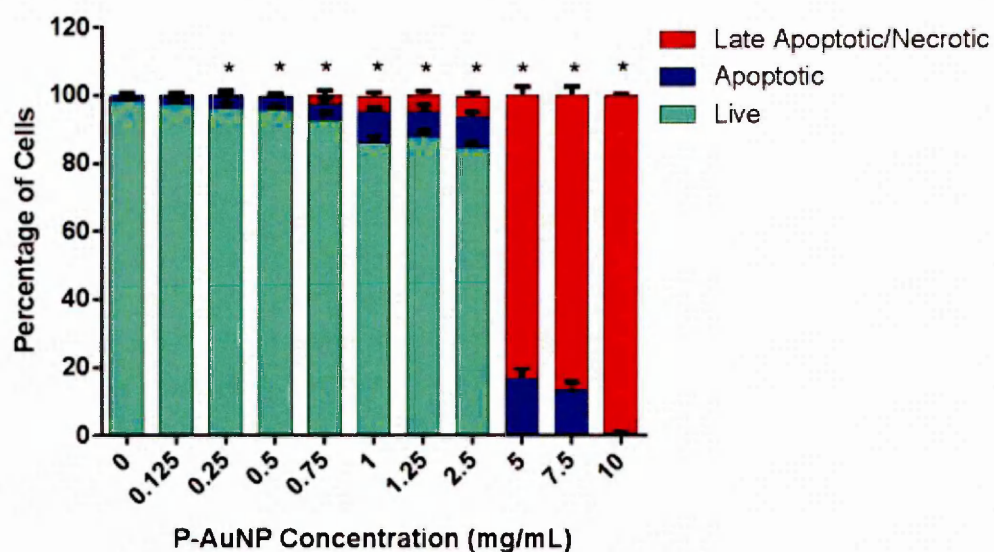
Figure 5.12 PC3 cells were treated with varying different concentrations of P-AuNPs (0-10 mg/mL) for 24 hours. Cells were stained with Hoechst and PI and viewed by fluorescent microscopy. Data is expressed as percentages of cells (200 cells were counted for each reading), for each sample 3 readings were recorded for each of the triplicate repeats (n=9). *Statisitcal significance between the levels of apoptotic cells $P \leq 0.05$.

Staisitical analysis showed that the levels of apoptotic cells in PC3 treated with different concentrations of P-AuNPs increased significantly compared to control: 0.25 mg/mL (P = 0.0017), 0.50 mg/mL (P = 0.0002), 0.75 mg/mL (P = 0.00021), 1.0 mg/mL (P = < 0.0001), 1.25 mg/mL (P = < 0.0001), 2.5 mg/mL (P = < 0.0001), 5.0 mg/mL (P = < 0.0001), 7.5 mg/mL (P = < 0.0001), 10.0 mg/mL (P = < 0.00291).

Results presented above in Figure 5.12 showed that P-AuNPs with a concentration of up to 5.0 mg/mL are relatively non-toxic to cells, with cell viability above 90% and at a P-AuNPs concentration above 5.0 mg/mL the majority of dead cells were necrotic. This observation could also be seen visually as shown below in Figure 5.13, with the number of of PI positive cells increasing with the increase in concentration of P-AuNPs.

P-AuNPs concentration of 1.25 and 2.50 mg/mL were chosen for follow up PTT experiments to determine if the cells would selectively induce apoptosis following green light excitation (U-MWG, 510-550 nm). As a positive control, P-AuNPs concentration of 5.0 mg/mL was used as the toxic dose for comparison purposes.
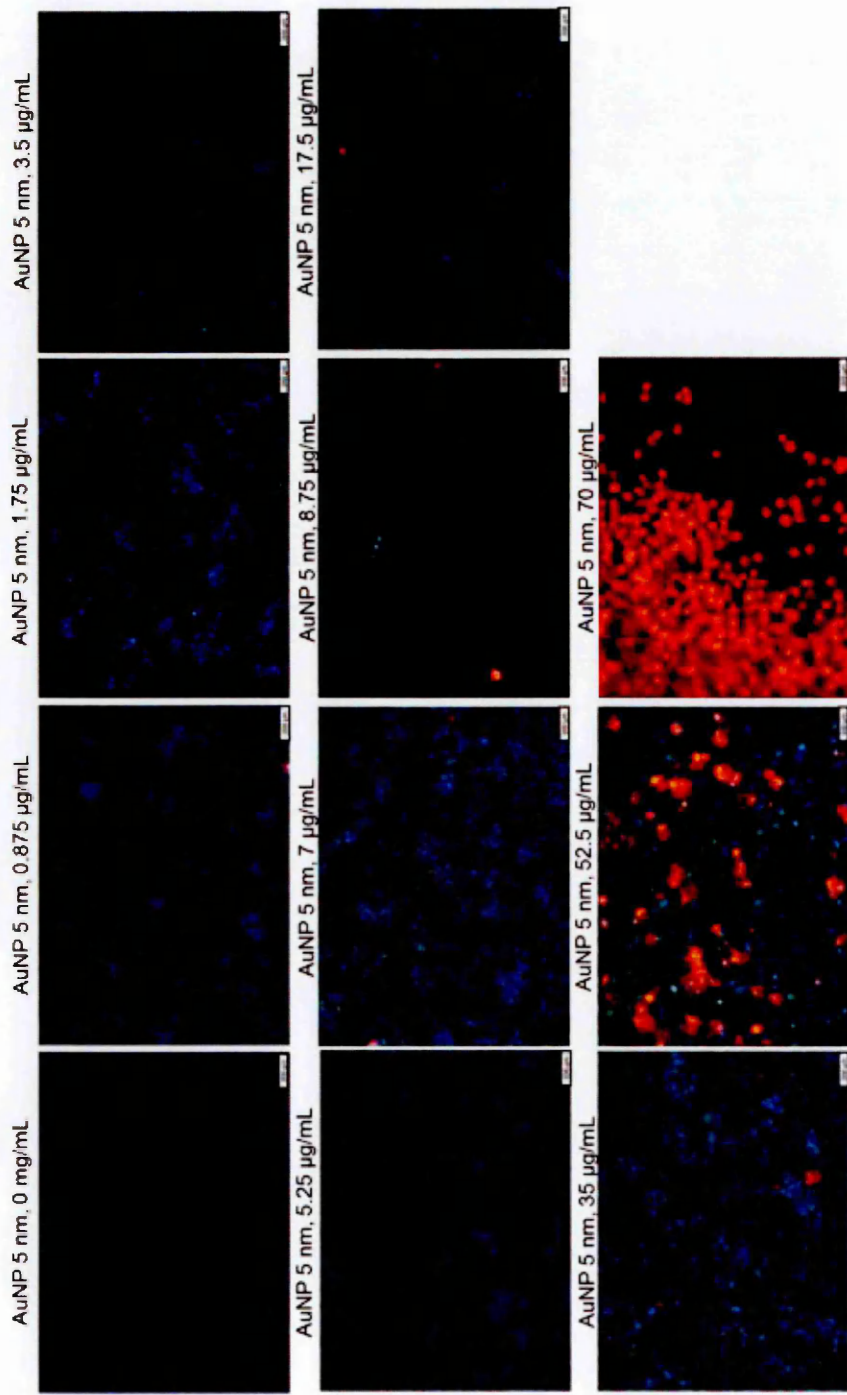
Figure 5.13 Typical fluorescent microscope images of PC3 cells treated with varying different concentration of P-AuNPs (0-10 mg/mL) for 24 hours, number of dead cells increased with the concentration of P-AuNPs. Cells stained with Hoechst and PI, images were taken on a 10x objective lens.

195

In subsequent PTT experiments, P-AuNPs concentration at 1.25 and 2.50 mg/mL were investigated to determine if the cells would selectively induce apoptosis following green light excitation (U-MWG, 510-550 nm). In addition to treating the cells with P-AuNPs for 24 hours, a 6 hour time point was also selected as it has been reported that the cellular uptake of AuNPs reached a plateau after 6 hours incubation with cells (Chithrani *et al.*, 2006).

Overall the results suggested that irradiating PC3 cells followed by a 6 hour treatment of P-AuNPs with varying concentrations between 0-5.0 mg/mL have negligible effect on cells. As shown in Figure 5.14-5.16 when PC3 cells were treated with P-AuNPs (0-5.0 mg/mL) for 6 hours and irradiated between 0-20 minutes, ca 90% of cells remained viable.

In contrast when PC3 wells were treated with P-AuNPs for 24 hours and irradiated for different lengths of time (between 0-20 minutes), the effect of cell death is dependent upon the concentration of P-AuNPs. As the concentration of P-AuNPs increase from 1.25 mg/mL to 5.0 mg/mL the percentage of dead cells also increases (Figure 5.17-5.19). At the highest concentration of 5.0 mg/mL ca 80% of cells were dead, even when not irradiated. This result is in agreement with results obtained previously in Figure 5.12, and this confirmed that P-AuNPs at a concentration of 5.0 mg/mL is cytotoxic to cells after 24 hours incubation. However this dosage is not cytotoxic to cells at a shorter incubation time of 6 hours (Figure 5.16).
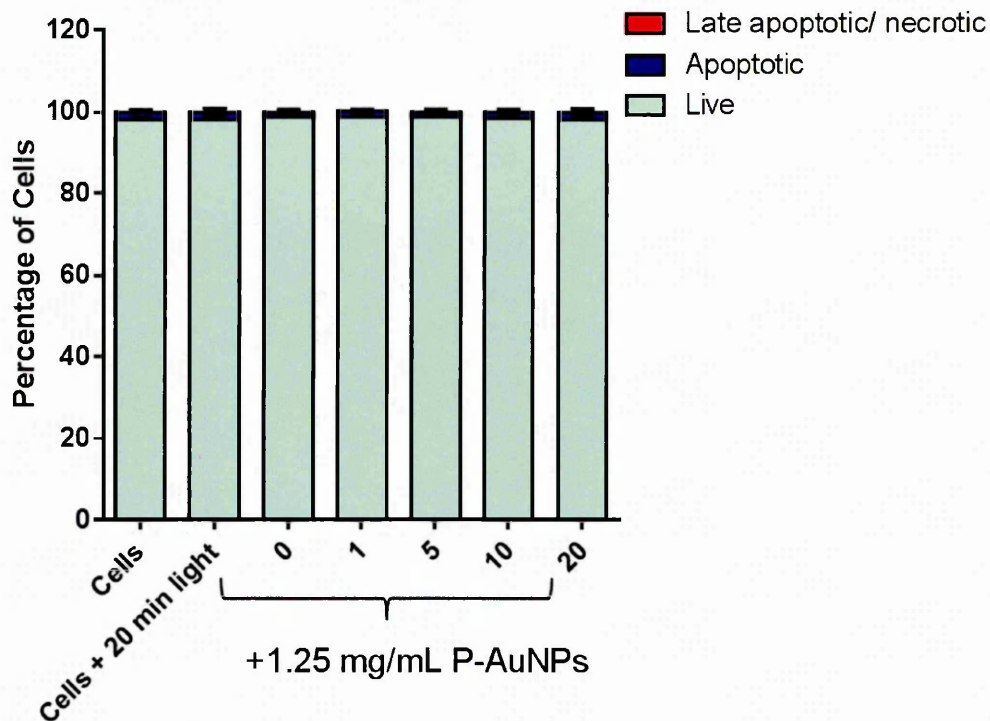
Figure 5.14 Percentage of viable, apoptotic and necrotic cells following a 6 hour treatment with P-AuNPs at a concentration of 1.25 mg/mL and irradiated with a 523 nm laser for varied length of time (0-20 minutes). For each sample 3 repeats were conducted, for each repeat 3 readings were obtained by counting 200 cells per sample (n=9), data expressed as percentage of cells.

Results showed that treating cells with P-AuNPs at a concentration of 1.25 mg/mL for 6 hours is non-cytotoxic to cells (control at 0 min), when irradiated with a laser at 523 nm at the maximum time point of 20 minutes, cells remained unaffected with cell viability above 95%. Statistical analysis showed that when PC3 cells were treated with P-AuNPs at a concentration at 1.25 mg/mL for 6 hours and irradiated for up to 20 minutes with a 532 nm laser has no significant effect on the number of apoptotic cells compared to control ($P = \geq 0.05$).
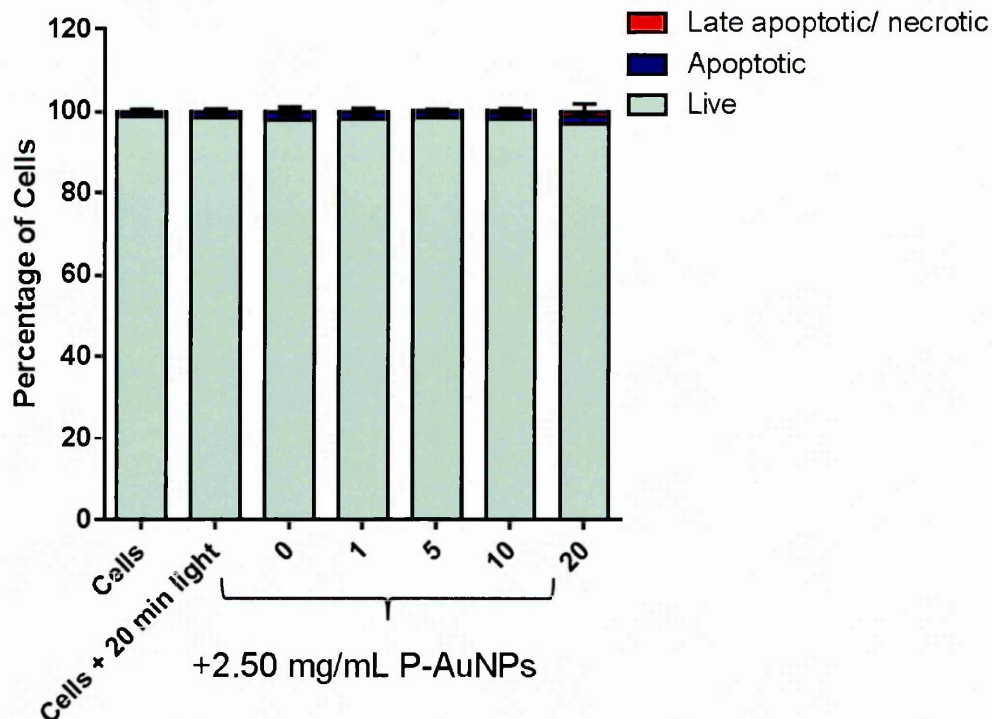
Figure 5.15 Percentage of viable, apoptotic and necrotic cells following a 6 hour treatment with P-AuNPs at a concentration of 2.50 mg/mL and irradiated with a 523 nm laser for varied length of time (0-20 minutes). For each sample 3 repeats were conducted, for each repeat 3 readings were obtained by counting 200 cells per sample, data expressed as a percentage of cells (n=9).

Results showed that treating cells with P-AuNPs at a concentration of 2.50 mg/mL for 6 hours is non-cytotoxic to cells (control at 0 min), when irradiated with a laser at 523 nm at the maximum time point of 20 minutes, cells remained unaffected with cell viability above 95%. Statistical analysis showed that when PC3 cells were treated with P-AuNPs at a concentration of 2.50 mg/mL for 6 hours and irradiated for 20 minutes with a 532 nm laser has no significant effect on the number of apoptotic cells compared to control (P = ≥ 0.05).
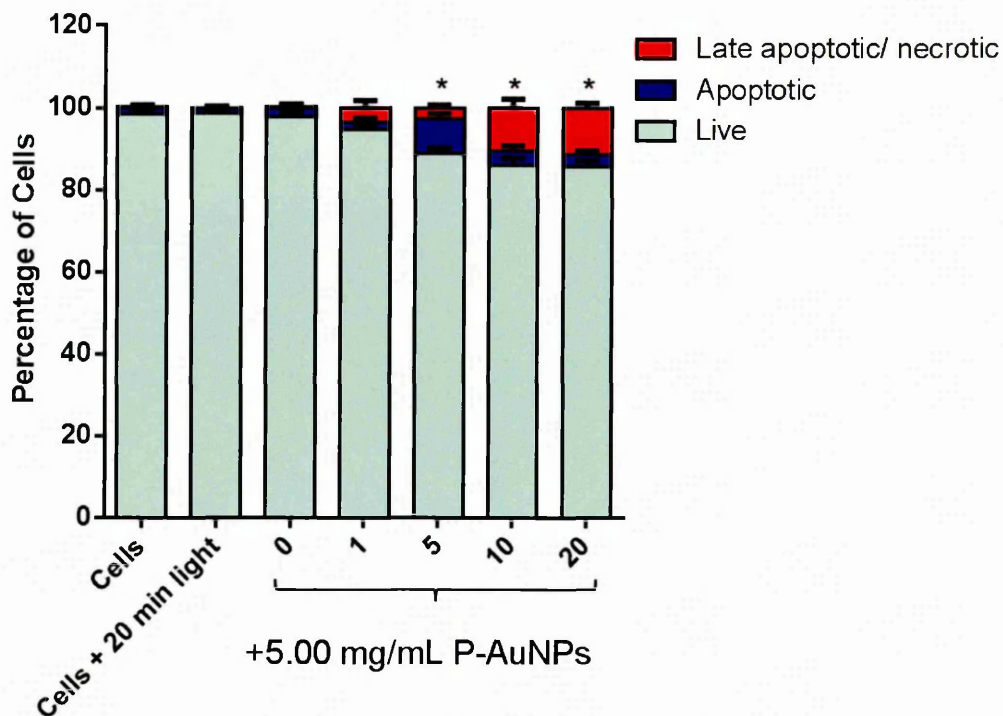
Figure 5.16 Percentage of viable, apoptotic and necrotic cells following a 6 hour treatment with P-AuNPs at a concentration of 5.00 mg/mL and irradiated with a 523 nm laser for varied length of time (0-20 minutes). For each sample 3 repeats were conducted, for each repeat 3 readings were obtained by counting 200 cells per sample, data expressed as percentage of cells (n=9). * Statisitcal significance between the levels of apoptotic cells $P \leq 0.05$.

Results showed that treating cells with P-AuNPs at a concentration of 5.00 mg/mL for 6 hours is non-cytotoxic to cells (control at 0 min), this confirmed that the death of cells following irradiation were due to the effect from the irradiation of cells and not by the cytotoxicity of P-AuNPs. Statistical analysis showed that when PC3 cells were treated at a concentration of 5.00 mg/mL for 6 hours and irradiated for 5, 10 and 20 minutes with a 532 nm laser has an significant effect on the number of apoptotic cells compared to control ($P = > 0.0001$, $P = > 0.0002$ and $P = > 0.0031$ respectively).
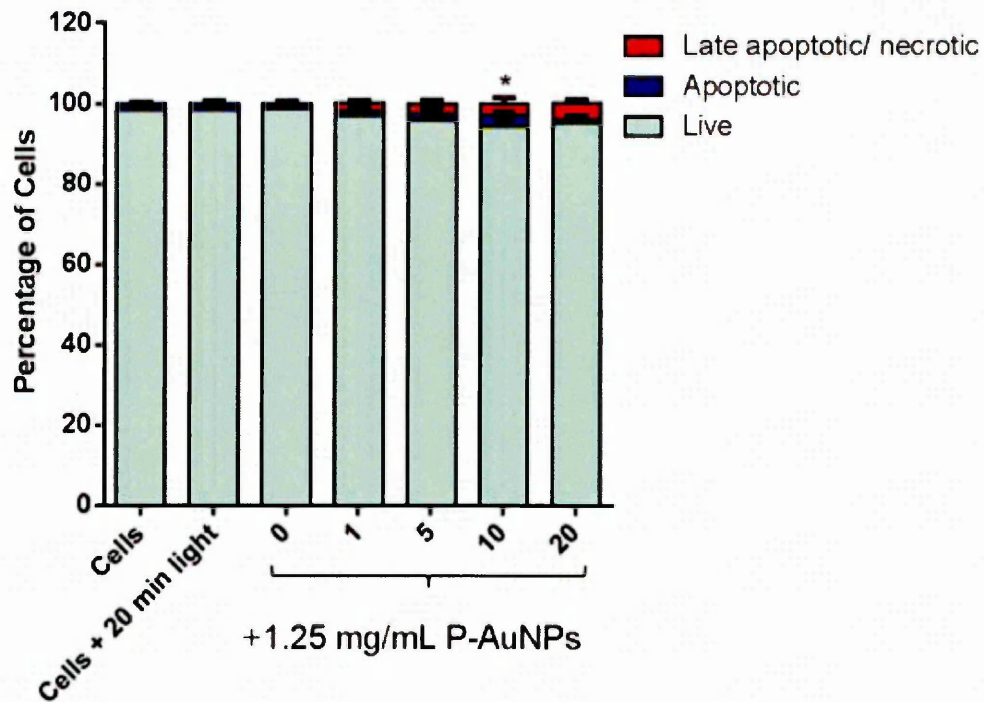
Figure 5.17 Percentage of viable, apoptotic and necrotic cells following a 24 hour treatment with P-AuNPs at a concentration of 1.25 mg/mL and irradiated with a 523 nm laser for varied length of time (0-20 minutes). For each sample 3 repeats were conducted, for each repeat 3 readings were obtained by counting 200 cells per sample, data expressed as percentage of cells (n=9). * Statisitcal significance between the levels of apoptotic cells $P \le 0.05$.

Results showed that treating cells with P-AuNPs at a concentration of 1.25 mg/mL for 24 hours has negligible effect on cells (control at 0 min), this confirmed that the death of cells following irradiation were due to effect from the irradiation of cells and not by the cytotoxicity of P-AuNPs. When cells were irradiated with a laser at 523 nm approximately 10% of cells were dead. Statistical analysis showed that PC3 cells treated at a concentration of 1.25 mg/mL for 24 hours and irradiated for 10 minutes with a 532 nm laser has an significant effect on the number of apoptotic cells compared to control (P = < 0.0005).
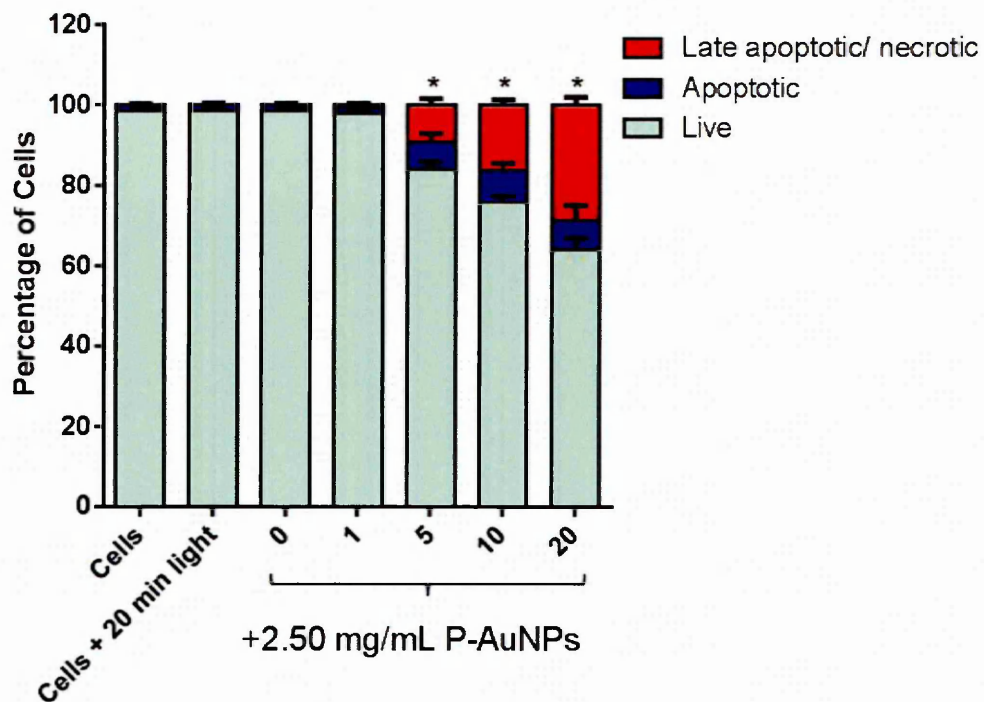
Figure 5.18 Percentage of viable, apoptotic and necrotic cells following a 24 hour treatment with P-AuNPs at a concentration of 2.50 mg/mL and irradiated with a 523 nm laser for varied length of time (0-20 minutes). For each sample 3 repeats were conducted, for each repeat 3 readings were obtained by counting 200 cells per sample, data expressed as percentage of cells (n=9). * Statisitcal significance between the levels of apoptotic cells $P \leq 0.05$.

Results showed that treating cells with P-AuNPs at a concentration of 2.50 mg/mL for 24 hours has negligible effect on cells (control at 0 min) this confirmed that the death of cells following irradiation was due to the effect from the irradiation of cells and not the cytotoxicity of P-AuNPs. Statistical analysis showed that PC3 cells treated at a concentration of 2.50 mg/mL for 24 hours and irradiated for 5, 10 and 20 minutes with a 532 nm laser has an significant effect on the number of apoptotic cells compared to control ($P = < 0.0001$, $P = < 0.0001$ and $P = < 0.0021$ respectively).

The main type of cell death observed was by necrosis, with the number of necrotic cells being dependent on the length of irradiation time. As shown on the graph, the percentage of both apoptotic and necrotic cells increases with irradiation time from 1 to 20 minutes.
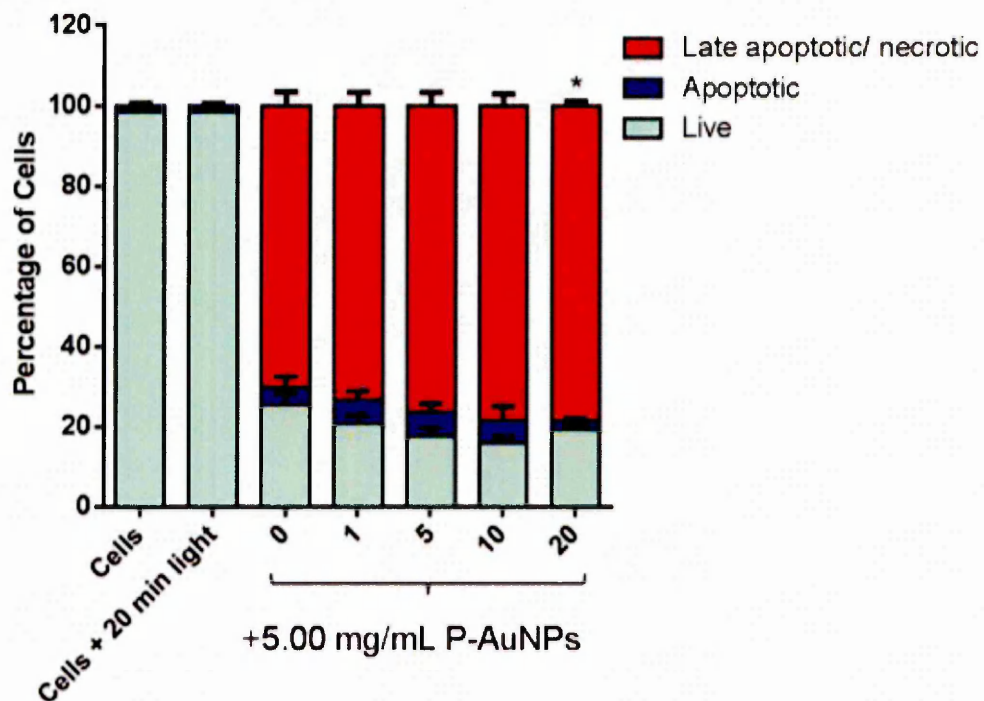

Figure 5.19 Percentage of viable, apoptotic and necrotic cells following a 24 hour treatment with P-AuNPs at a concentration of 5.00 mg/mL and irradiated with a 523 nm laser for varied length of time (0-20 minutes). For each sample 3 repeats were conducted, for each repeat 3 readings were obtained by counting 200 cells per sample, data expressed as percentage of cells (n=9). * Statisitcal significance between the levels of apoptotic cells $P \leq 0.05$.

Results showed that treating cells with P-AuNPs at a concentration of 5.00 mg/mL for 24 hours are cytotoxic to cells (control at 0 min). Following irradiation the percentage of necrotic cells increases from ~60% to 80%. This dosage of P-AuNPs is cytotoxic to cells with and without irradiation. Statistical analysis showed that PC3 cells treated at a concentration of 5.00 mg/mL for 24 hours and irradiated for 20 minutes with a 532 nm laser has an significant effect on the number of apoptotic cells compared to control ($P = 0.0429$).

In subsequent experiments, PC3 cells were treated with the same concentrations of P-AuNPs (0-5.00 mg/mL) with an additional step of removing excess P-AuNPs following the treatment. This was done by replacing the media with fresh media, and the results showed that number of necrotic cells decreased significantly (Figure 5.20 and 5.21).

What was particularly interesting was when PC3 cells were treated with P-AuNPs at a concentration of 5.00 mg/mL for 24 hours with excess P-AuNPs removed, there was an increase in the proportion of apoptotic cells as the irradiation time increases from 0 to 20 minutes (Figure 5.21). In addition, there is a significant difference between treating the cells with same concentration of P-AuNPs for same period of time, with no replacement in media. By replacing the media, the percentage of necrotic cells decreases drastically from ~80% (Figure 5.19) to ~10% (Figure 5.21).

The removal of excess P-AuNPs prior to irradiation could explain the increase in cell viability observed as only cells taken-up the P-AuNPs would exhibit an effect upon irradiation. Higher percentage of necrotic cells were observed in samples without the change of media, this was not surprising since excess P-AuNPs not taken-up by the cells would still respond when irradiated and produce heat and effectively heating cells in the entire well.
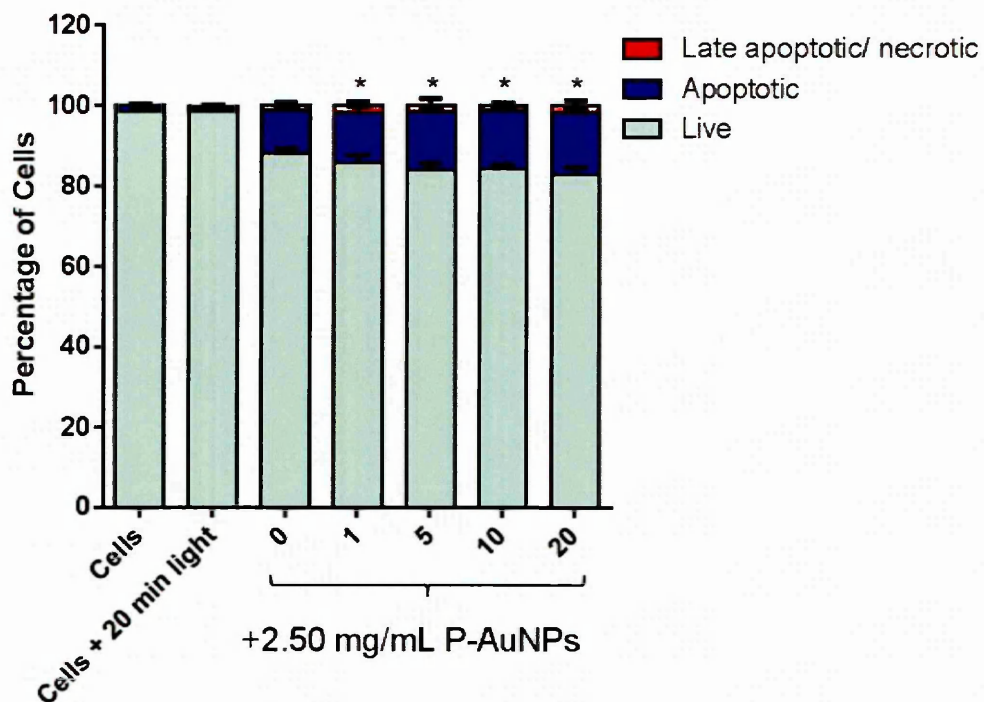
Figure 5.20 Percentage of viable, apoptotic and necrotic cells following a 24 hour treatment with P-AuNPs at a concentration of 2.50 mg/mL, media was removed and replaced with fresh media prior to irradiation with a 523 nm laser for varied length of time (0-20 minutes). For each sample 3 repeats were conducted, for each repeat 3 readings were obtained by counting 200 cells per sample, data expressed as percentage of cells (n=9). *Statisitcal significance between the levels of apoptotic cells $P \leq 0.05$.

Results showed that treating cells with P-AuNPs at a concentration of 2.50 mg/mL for 24 hours, replacing media prior to irradiation has an effect on cells (control at 0 min) with a decrease in cell viability by approximately 10%. Following irradiation even at the longest period of 20 minutes, the percentage of apoptotic cells remained very similar, this suggested that increasing the irradiation time does not have much effect compared to cells with no irradiation. Statistical analysis showed that PC3 cells treated at a concentration of 2.50 mg/mL for 24 hours, replaced with fresh media and irradiated for 1, 5, 10 and 20 minutes with a 532 nm laser has an significant effect on the number of apoptotic cells compared to control (P = 0.014, P = < 0.0001, P = < 0.0001 and P = < 0.0001 respectively).
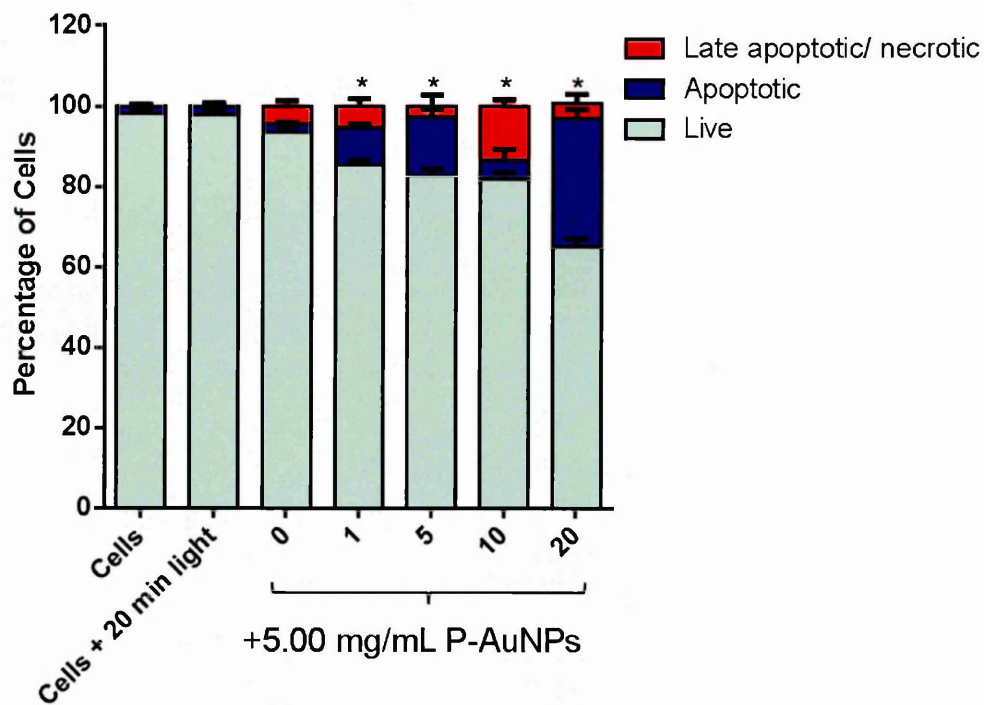
Figure 5.21 Percentage of viable, apoptotic and necrotic cells following a 24 hour treatment with P-AuNPs at a concentration of 5.00 mg/mL, media was removed and replaced with fresh media prior to irradiation with a 523 nm laser for varied length of time (0-20 minutes). For each sample 3 repeats were conducted, and for each repeat 3 readings were obtained by counting 200 cells per sample, data expressed as percentage of cells (n=9). *Statisitcal significance between the levels of apoptotic cells $P \leq 0.05$.

Results showed that treating cells with P-AuNPs at a concentration of 5.00 mg/mL for 24 hours, replacing media prior to irradiation has an effect on cells (control at 0 min) with a decrease in cell viability by approximately 10%. The results showed that the percentage of apoptotic cells increases with irradiation time, as shown above in Figure 5.21. Statistical analysis showed that PC3 cells treated at a concentration of 5.00 mg/mL for 24 hours, replaced with fresh media and irradiated for 1, 5, 10 and 20 minutes with a 532 nm laser has an significant effect on the number of apoptotic cells compared to control ($P = <$ 0.0001, $P = <$ 0.0001, $P = 0.0008$ and $P = <$ 0.0001 respectively).

5.3.3 Investigating the Cellular Uptake of Phosphonium-Functionalised Gold Nanoparticles by Transmission Electron Microscopy

Studying the uptake of nanoparticles in cellular systems is of utmost importance for understanding their biological effects. Detecting their uptake inside cells is challenging owing to their small size and quantity. Electron microscopy is commonly used in nanoparticle research, despite lengthy and complex sample preparation (Mayhew *et al.*, 2009). TEM has been the preferred method for studying the cellular uptake of nanoparticles, and reports have been published for both *in vitro* and *in vivo* accumulation (Nativo *et al.*, 2008, Rothen-Rutishauser *et al.*, 2007, Mühlfeld *et al.*, 2007a, Mühlfeld *et al.*, 2007b, Arnida *et al.*, 2010). Due to the high resolution of electron microscopy TEM analysis can provide invaluable details of the interaction of nanoparticles with cell structures, as well as images of organelles, membrane invaginations and vesicle formation, thus making it feasible to study the mode of uptake of nanoparticles inside cells (Motskin *et al.*, 2009, Nativo *et al.*, 2008, Chithrani, 2010, Chithrani *et al.*, 2006).

To determine whether P-AuNPs are taken-up by cells, PC3 cells have been treated with P-AuNPs (1.25, 2.50 and 5.00 mg/mL) for 24 hours and analysed using TEM. For each sample two 100 nm sections were imaged; one section was analysed as prepared in the department, the other section was stained with saturated solutions of uranyl acetate and lead citrate at Brunel University. In addition to visualising the samples by electron microscopy, elemental analysis was conducted by using energy-dispersive X-ray spectroscopy (EDX).

TEM images confirmed that P-AuNPs are taken-up by PC3 cells; at the lowest concentration of 1.25 mg/mL, P-AuNPs can be seen to be located in vesicles or organelles as shown in Figure 5.24. The P-AuNPs are clearly encapsulated by a membrane with image 5.24 a and c showing a double membrane. Zoomed-in images of Figure 5.24 a, b and c are shown in Figure 5.25, 5.26 and 5.27, respectively along with their corresponding EDX spectrum which confirmed the particles to be gold and thereby confirming the presence of P-AuNPs in the encapsulated vesicle/organelle.

Without any staining, TEM images obtained were clear with dense regions of P-AuNPs easily identified. The dense regions of suspected P-AuNPs were confirmed by EDX analysis which confirmed the presence of gold (AuLλ) and thus confirming the presence of P-AuNPs in cells. In an attempt to obtain better images, with greater sub-cellular structure details particularly the mitochondrion, a section from the same sample was prepared by staining with uranyl acetate and lead citrate, which are routinely used for TEM staining of biological samples (McNeil, 2011).

Staining improved the image contrast significantly, as shown in Figure 5.28 when viewing the cell as a whole more detail could be observed compared to un-stained sample (Figure 5.24). With staining a beautiful TEM image of P-AuNPs inside the mitochondrion was observed, as shown in Figure 5.29, the outer double membrane and cristae can be clearly seen. Several darker, dense black rounded shaped spots inside the cell (Figure 5.28) were originally thought to be the gold nanoparticles, EDX analysis (data not shown) confirmed they were Au negative and osmium positive indicating they are lipid dense organelles and are likely to be peroxisome.

EDX spot analyses were conducted to confirm the presence of P-AuNPs inside the cells (Figure 5.29, 5.31, 5.35, 5.38, 5.41 and 5.43). EDX mapping analyses were conducted on samples to obtain a visual image of the location of Au inside the cell. Unfortunately, when the maps are exported from the software the images are automatically converted to black, the maps are not as clear in black and white as they are in colour. However, what was fascinating with the results was that the density of the map of Au correlates to the overall shape of the AuNPs cluster inside the cell (Figure 5.36 and 5.42).

207
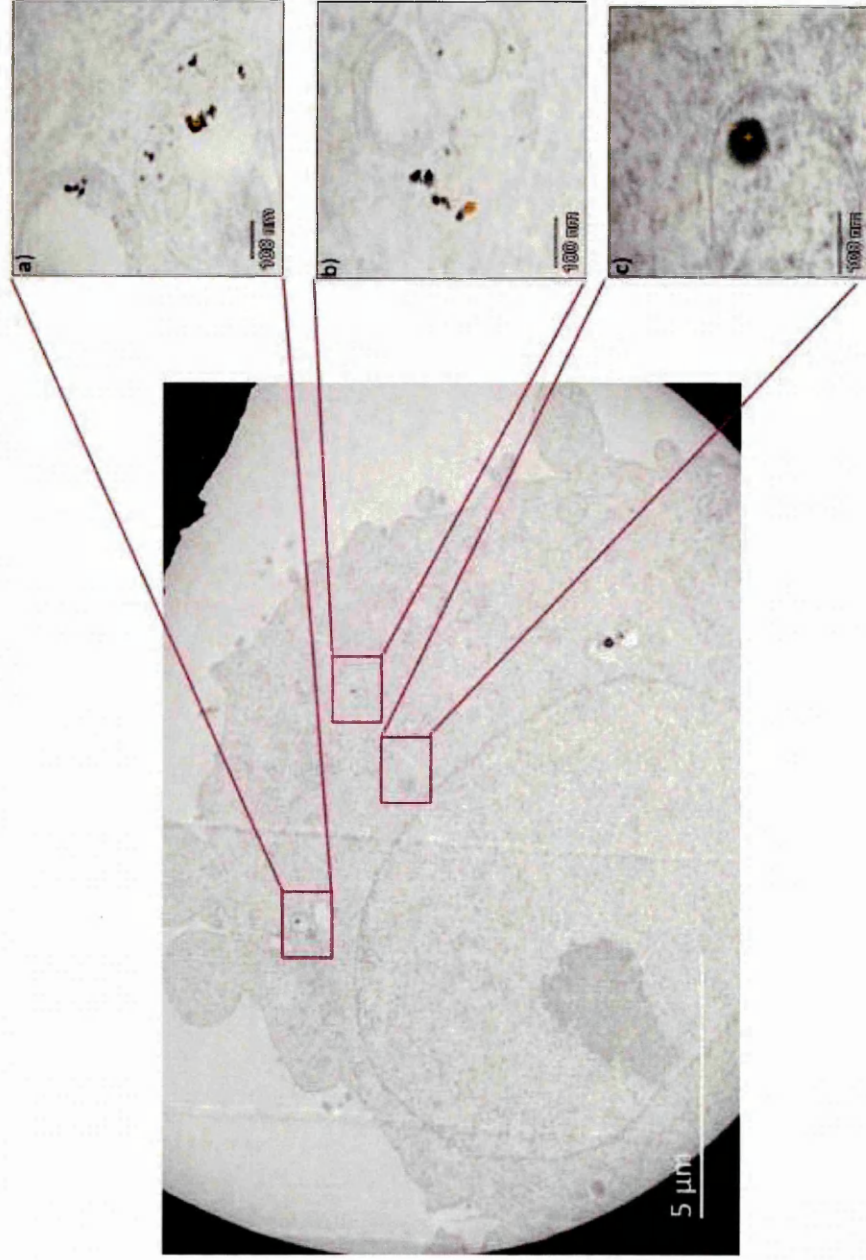
Figure 5.22 TEM image of unstained sample of PC3 cells treated with P-AuNPs 1.25 mg/mL for 24 hours. The zoomed in images showed that P-AuNPs are taken-up by the cells and were contained in vesicles/organelles of some type, as shown by the P-AuNPs encapsulated by single (b) and double membranes (a) and (c).

208
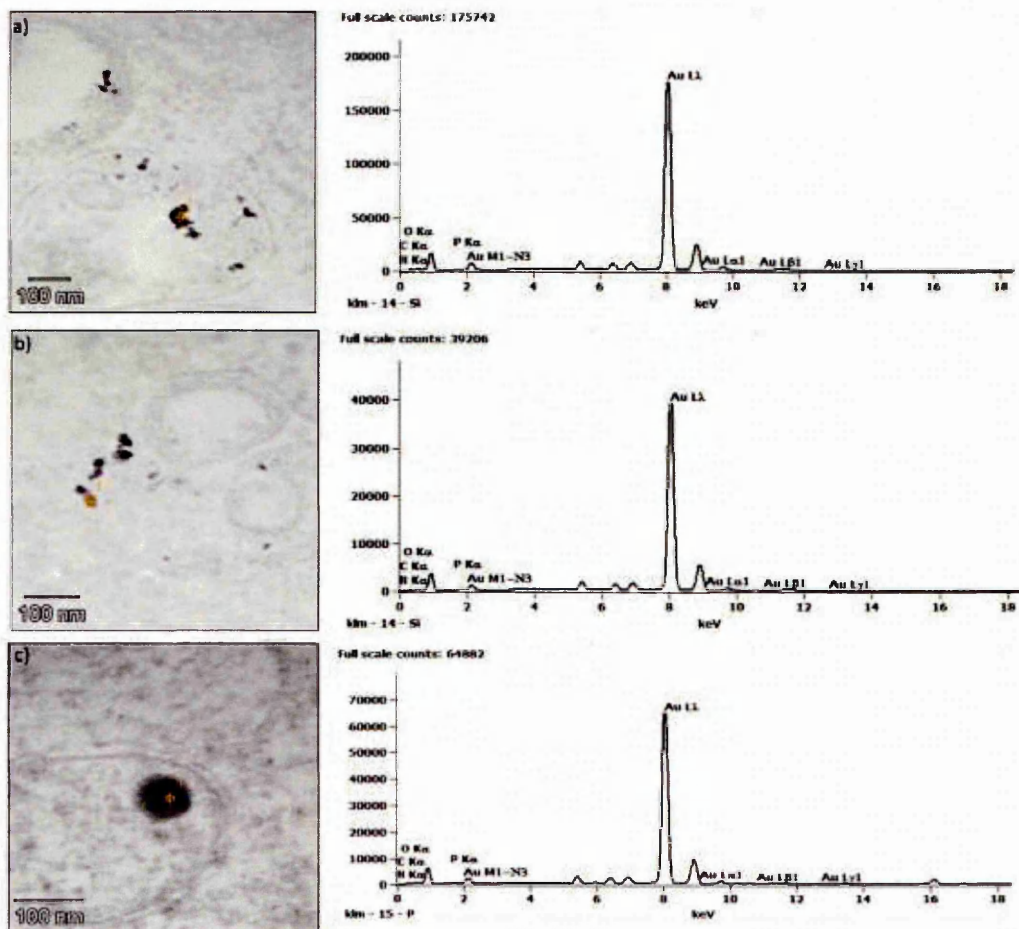
Figure 5.23 TEM images and EDX spectrum of the areas shown Figure 5.21a-c.

Figure 5.23a showed that P-AuNPs are encapsulated around a double membrane, which may not be a mitochondrion as the folded inner membrane was not observed. Figure 5.23b showed that P-AuNPs are encapsulated around a single membrane, which could be a vesicle. Figure 5.23c showed that the P-AuNPs are encapsulated around a double membrane, which could potentially be a mitochondrion, however the folded inner membrane was not identified.

The yellow spots (labelled 1) in Figure 5.23a-c indicated the area analysed by EDX and the corresponding spectrum is shown next to the TEN image. EDX spectrum of unstained sample of PC3 cells treated with P-AuNPs 1.25 mg/mL for 24 hours confirmed the uptake of P-AuNPs inside the cells.

209
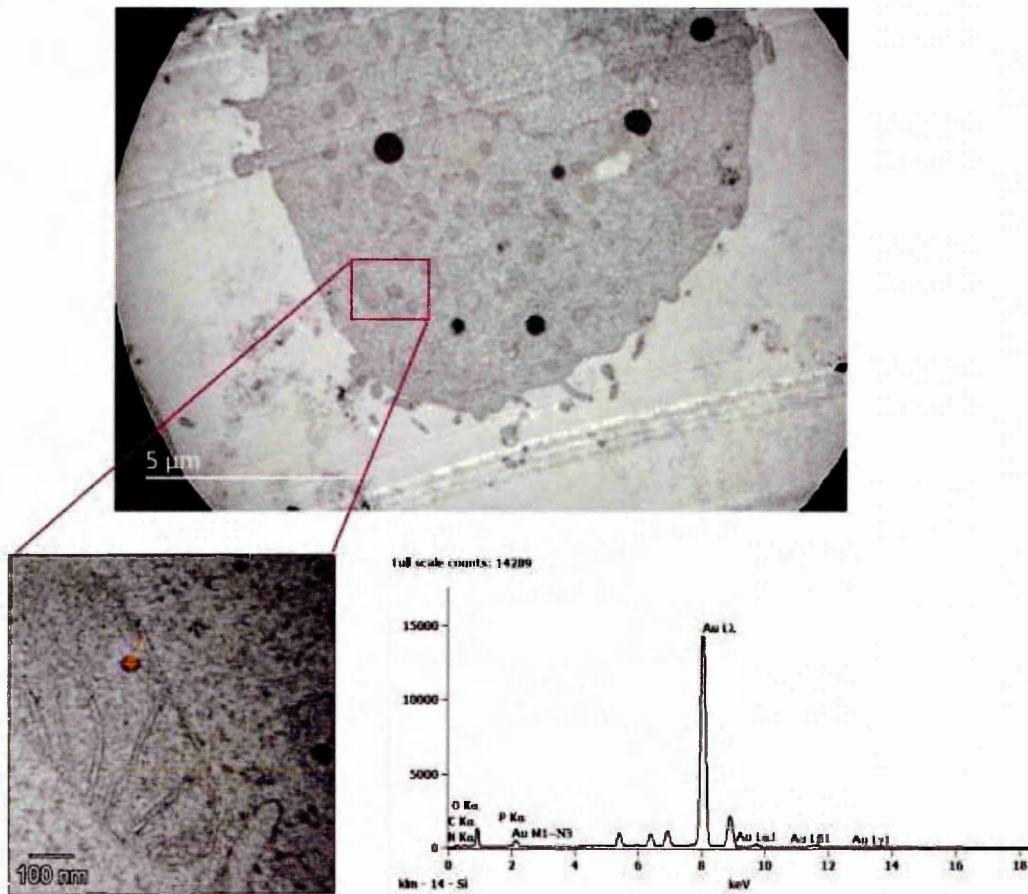
Figure 5.24 TEM image of PC3 cells treated with P-AuNPs 1.25 mg/mL for 24 hours. Sample stained with uranyl acetate and lead citrate. The yellow spot (labelled 1) indicated the area analysed by EDX and the spectrum obtained is shown next to the zoomed-in image.

With staining the mitochondria were readily identified compared to unstained samples. The zoomed-in TEM image showed that P-AuNPs are taken-up by the mitochondrion, as shown by the double membrane and the clear intermembrane. EDX spectrum of stained sample of PC3 cells treated with P-AuNPs 1.25 mg/mL for 24 hours confirmed the presence of P-AuNPs inside the mitochondrion.
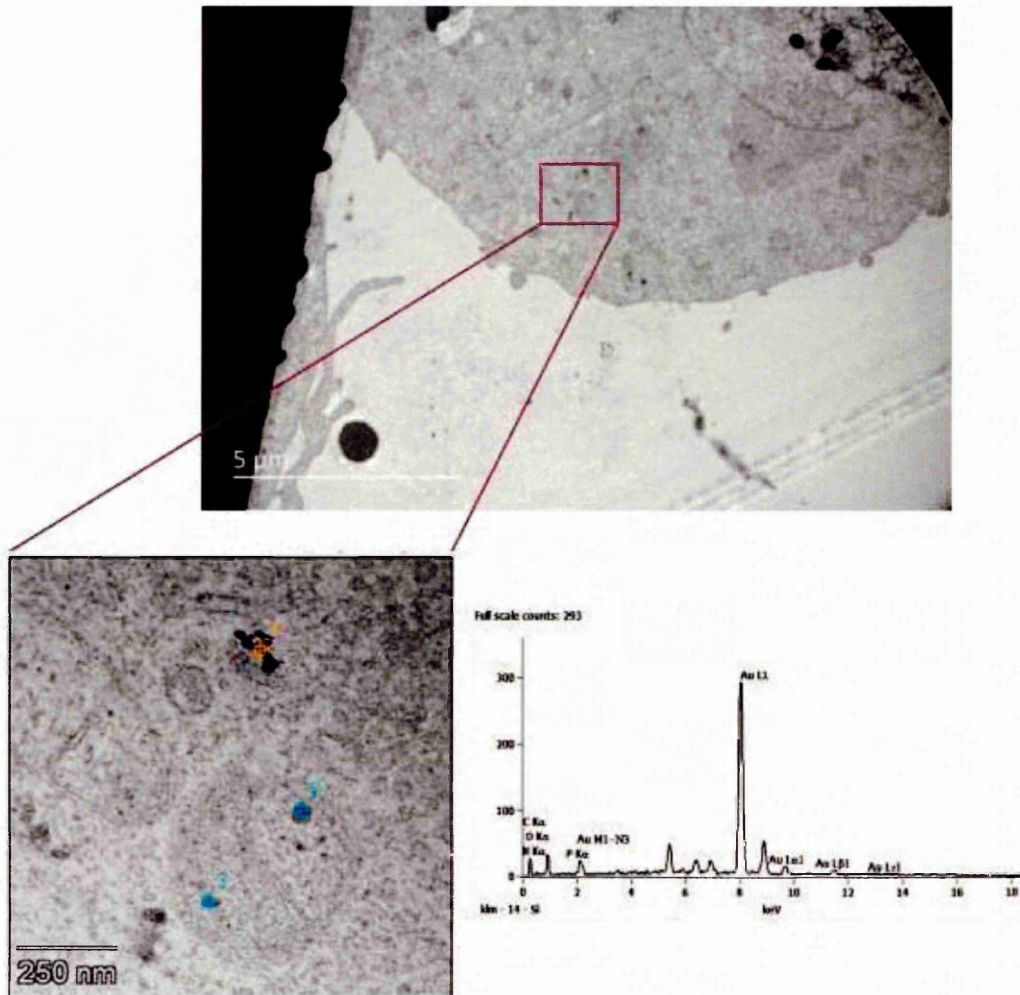
Figure 5.5.25 TEM image of PC3 cells treated with P-AuNPs 1.25 mg/mL for 24 hours, sample stained with uranyl acetate and lead citrate. The blue spots (labelled 2) indicated the area analysed by EDX and the spectrum obtained is shown next to the zoomed-in image.

TEM image showed that P-AuNPs are taken-up by the cells (as shown by electron dense region) in the image and the outline of mitochondria could be observed from the staining. The blue spots (labelled 2 & 3) indicated the area analysed by EDX and the spectrum obtained is shown next to the zoomed-in image.

The image showed two mitochondria have been stained uranyl acetate and lead citrate, with clear inner membrane which can be observed. What was interesting about this particular image was that one mitochondria (red arrow) was sliced

211

vertically across the mitochondrion whereas the other mitochondrion (blue arrow) the mitochondrion is sectioned on the horizontal plane with the double membrane and cristae clearly identifiable. EDX spectrum of stained sample of PC3 cells treated with P-AuNPs 1.25 mg/mL for 24 hours confirmed the presence of P-AuNPs inside the mitochondrion.
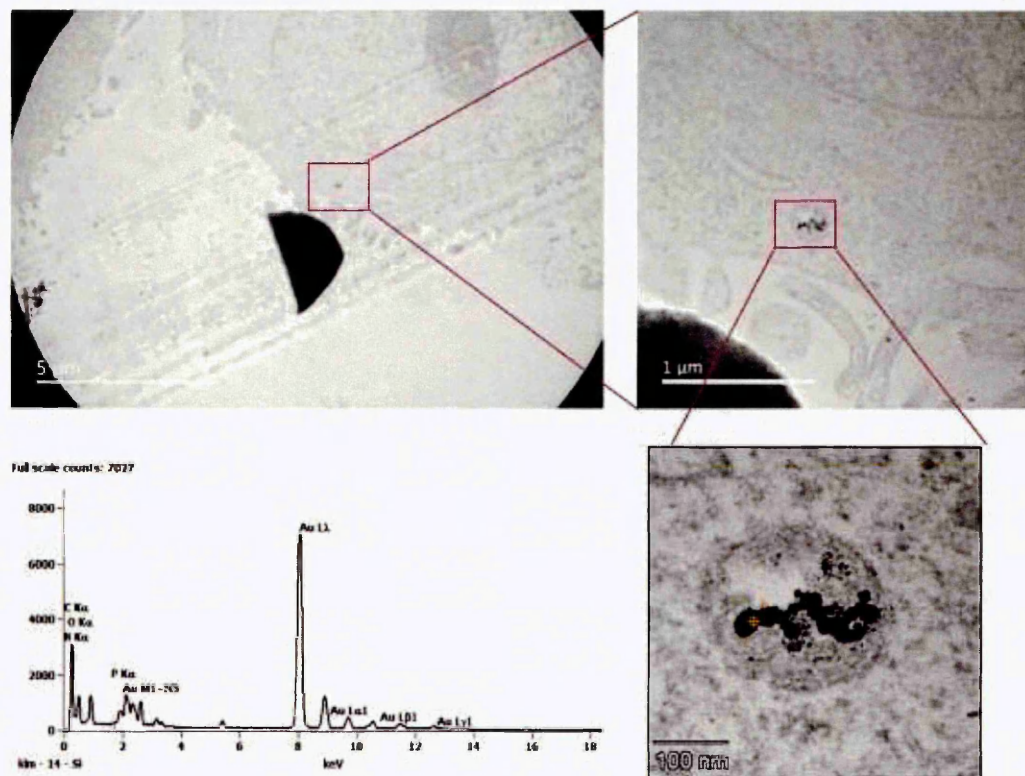
Figure 5.26 TEM image of PC3 cells treated with P-AuNPs 2.50 mg/mL for 24 hours, sample stained with uranyl acetate and lead citrate. The yellow spot (labelled 1) indicated the area analysed by EDX and the spectrum obtained is shown next the TEM image.

TEM image showed that P-AuNPs are encapsulated in vesicle of some form most likely to be endocytosis as vesicle is towards the edge of the cell. The zoomed-in imaged illustrated that P-AuNPs are taken-up by vesicle or organelle of some form as shown by the singe membrane. EDX spectrum confirmed the electron dense particles inside the vesicle/organelle are P-AuNPs.

212

Endocytosis is one of the main pathways for the cellular uptake of nanoparticles; the internalisation mechanism of AuNPs is generally considered to be receptor-mediated endocytosis also called clathrin-dependent endocytosis (Kirchhausen, 2000, Chithrani *et al.*, 2006, Harush-Frenkel *et al.*, 2007). Receptor-mediated endocytosis of nanoparticles occurs through the interactions between ligands on the surface of the nanoparticles and cell membrane receptors and this ligand-receptor property has been exploited to improve the targeting of AuNPs, For example human transferrin has been coated onto the surface of PEGylated AuNPs to target cancer cells that over express transferrin receptors to enhance intracellular delivery of therapeutic agents to the site of solid tumours (Choi *et al.*, 2010).

Figure 5.26 showed that the P-AuNPs are taken-up in cells by vesicles, the size of the diameter of vesicle is approximately 400 nm, this observation is in agreement with Chithrani and colleagues (Chithrani *et al.*, 2009). The authors reported that AuNPs were localized in vesicles with an average diameter of 300-500 nm, and no AuNPs were found in the cytoplasm or nucleus of the cells. To confirm that P-AuNPs are only taken-up in the mitochondria and not in the cytoplasm or nucleus, cell fractionation can be used; one method is to use mitochondria isolation kit as used in chapter 4.3.1.5. This would isolate the mitochondria fraction only, which can subsequently be analysed by TEM.

Furthermore, P-AuNPs were shown to be encapsulated in a vesicle near the edge of the cell which suggested that the P-AuNPs are taken-up by clathrin-dependent endocytosis. Harush-Frenkel and colleagues (Harush-Frenkel *et al.*, 2007) have investigated the endocytosis pathways of negatively- and positively-charged nanoparticles in HeLa cells; the results showed that negatively charged nanoparticles exhibited a lower rate of endocytosis and are not involved in the clathrin-mediated endocytosis pathway, whereas positively charged nanoparticles are internalised rapidly via the clathrin-mediated pathway.
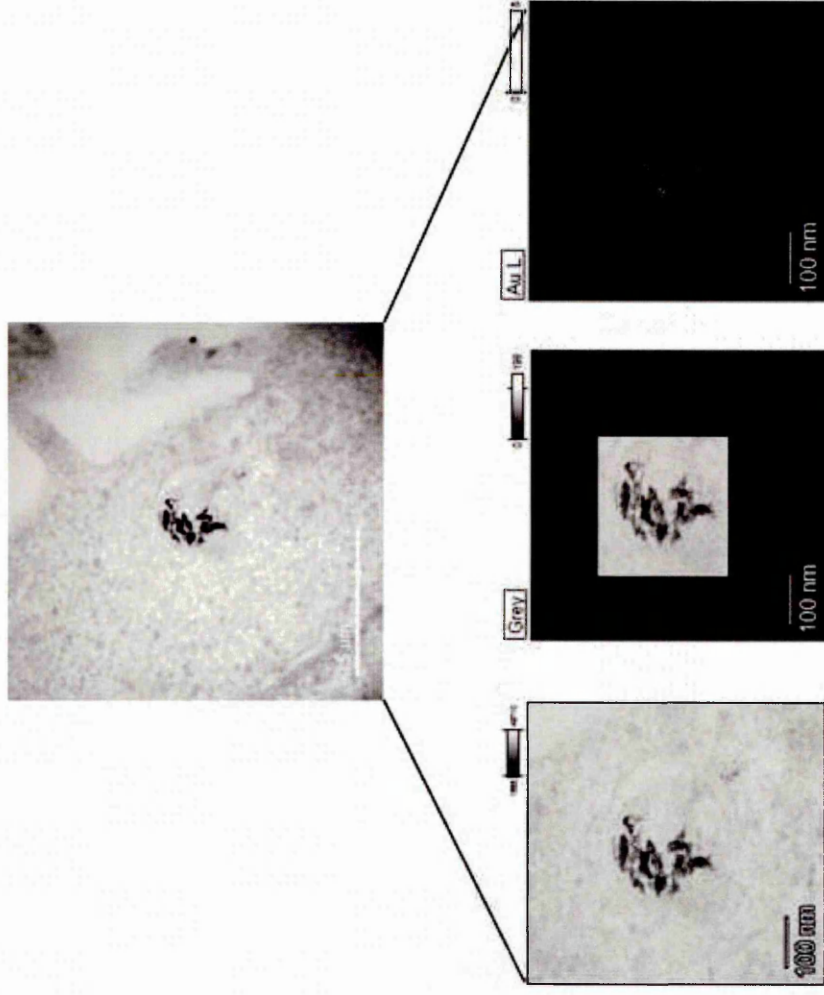
**Figure 5.27** TEM image and EDX mapping analysis of PC3 cells treated with P-AuNPs 25.0 mg/mL for 24 hours, sample stained with uranyl acetate and lead citrate. TEM image showed that P-AuNPs are encapsulated in a single membrane vesicle. EDX mapping confirmed the electron dense parts in the vesicle were P-AuNPs.

214
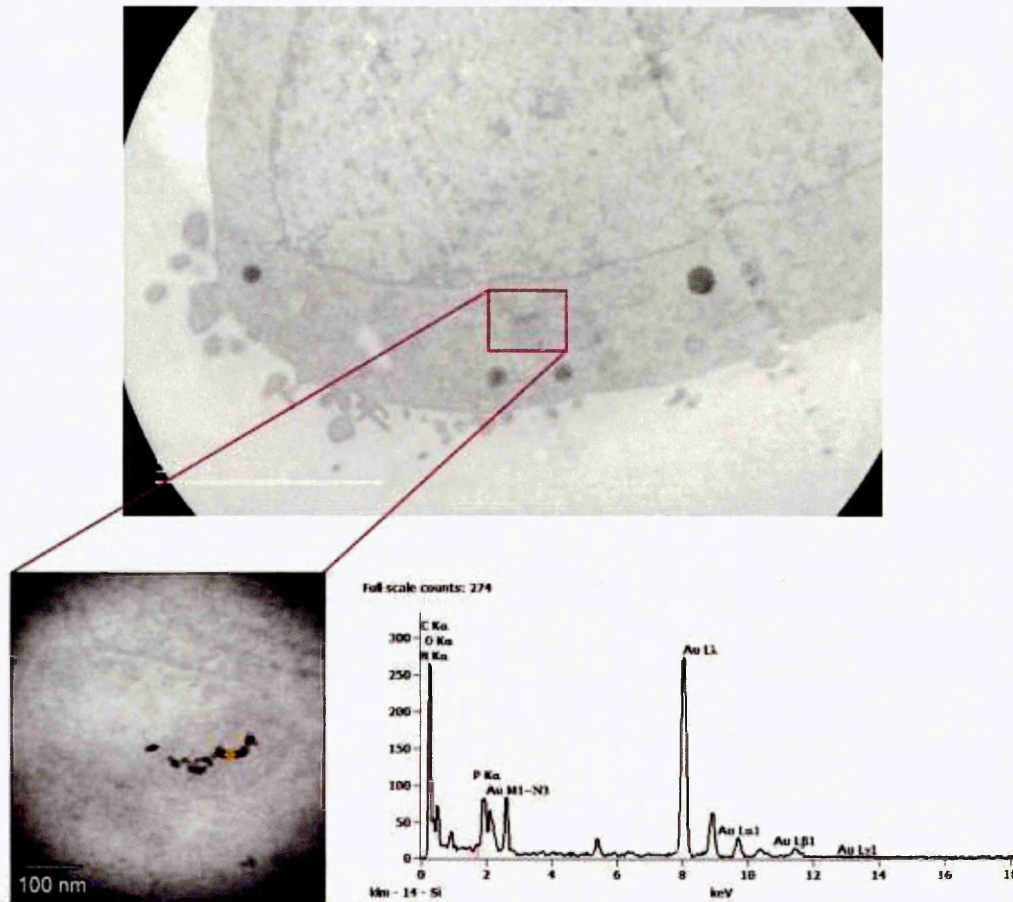
Figure 5.28 TEM image of PC3 cells treated with P-AuNPs 2.50 mg/mL for 24 hours, unstained sample. The yellow spot (labelled 1) indicated the area analysed by EDX and the spectrum obtained is shown next to the TEM image.

TEM image showed that P-AuNPs are taken-up by the mitochondrion, even with no staining the double layer membrane can be identified. EDX spectrum of unstained sample of PC3 cells treated with P-AuNPs 2.5 mg/mL for 24 hours confirmed the electron dense particles inside the vesicle/organelle are P-AuNPs.
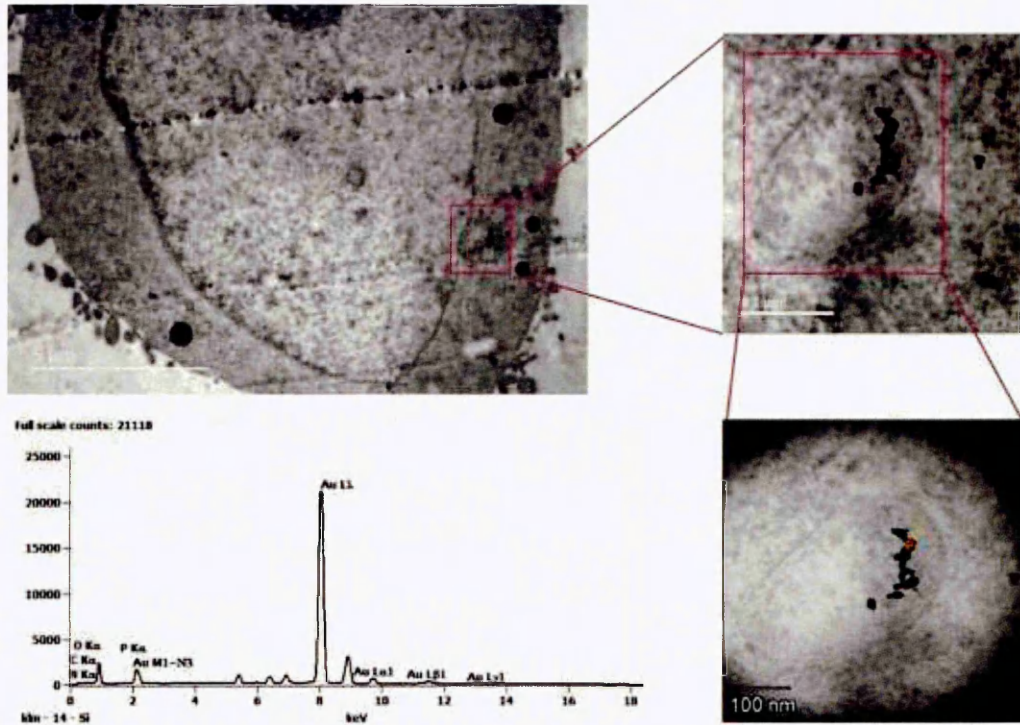
Figure 5.29 TEM image of PC3 cells treated with P-AuNPs 2.50 mg/mL for 24 hours, sample stained with uranyl acetate and lead citrate. The yellow spot (labelled 1) indicated the area analysed by EDX and the spectrum obtained is shown next to the TEM image.

Following staining, the organelles within the cell could be readily identified by the increase in contrast of TEM images. TEM image showws that P-AuNPs are taken-up by the mitochondria, as can be observed from the double membrane in the stained sample. EDX spectrum of the stained sample of PC3 cells treated with P-AuNPs 2.5 mg/mL for 24 hours confirmed the electron dense particles inside the mitochondrion are P-AuNPs.

TEM data confirmed that P-AuNPs are taken-up by the mitochondrion; staining the sample with uranyl acetate and lead citrate provided stronger contrast in the TEM images and enable the organelles and membrane to be readily identified compared to unstained sample. As shown in Figure 5.29 in the sainted sample, the double membrane of the mitochondrion can easily be identified which also support the TEM image obtained previously in Figure 5.28 in the unstained sample, confirming the structure of the mitochondrion.
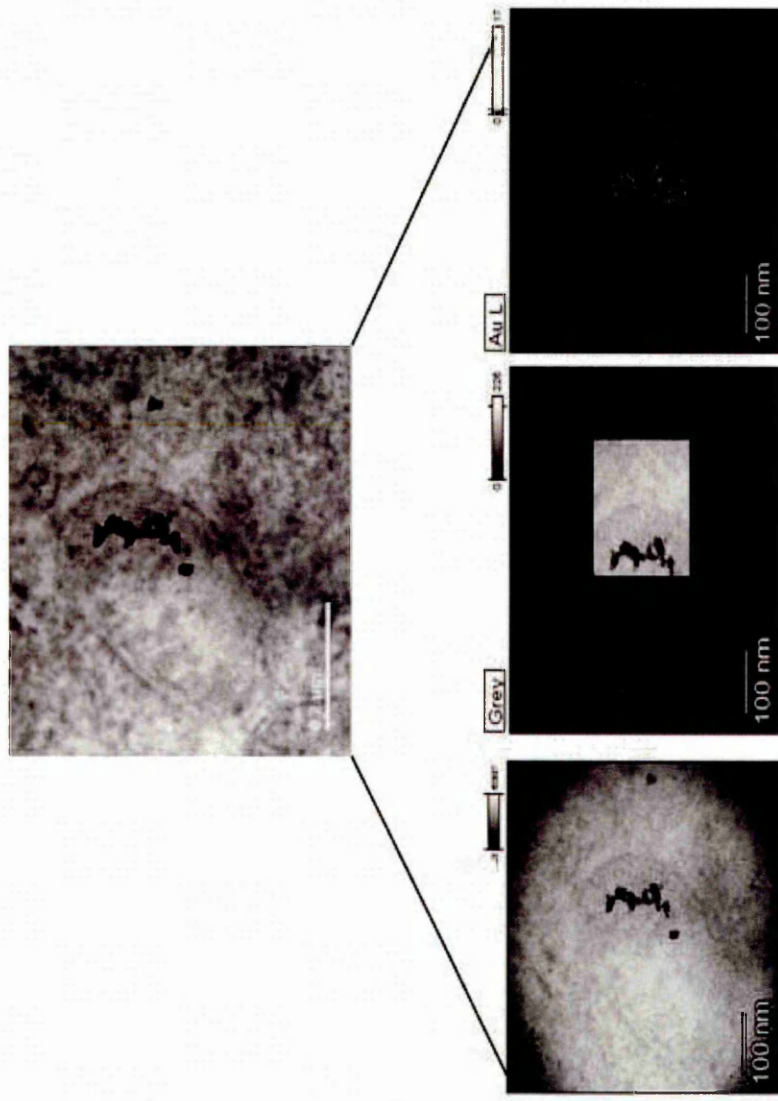
Figure 5.30 TEM image and EDX mapping analysis of PC3 cells treated with P-AuNPs 25.0 mg/mL for 24 hours, sample stained with uranyl acetate and lead citrate. TEM image showed that P-AuNPs are encapsulated in a double membrane vesicle. EDX mapping confirmed the electron dense parts in the mitochondrion are P-AuNPs.

217

Mitochondria have emerged as an attractive pharmacological target for cancer therapeutics (Gupta *et al.*, 2009, Weissig, 2005), several research groups have investigated the use of nanocarriers for mitochondria-specific delivery, these include DQAsomes (D'Souza *et al.*, 2003), liposomes (Boddapati *et al.*, 2010) and solid nanoparticles (Weissig *et al.*, 2007). The most challenging aspect of targeting therapeutic agents to the mitochondrial is that the therapeutic agents must be able to cross the mitochondrial membranes, it has been determined that permeability of the outer mitochondrial membrane to be ≥ 3 and ≤ 6 nm (Salnikov *et al.*, 2007).

TEM images (Figure 5. 28and 5.29) showed that P-AuNPs (mean diameter of 3 nm) were taken-up by the mitochondria these observations are in agreement with the data reported by Salnikov *et al.* 2007 who have illustrated that the outer mitochondrial membrane are not permeable to nanoparticles greater than 6 nm in diameter.
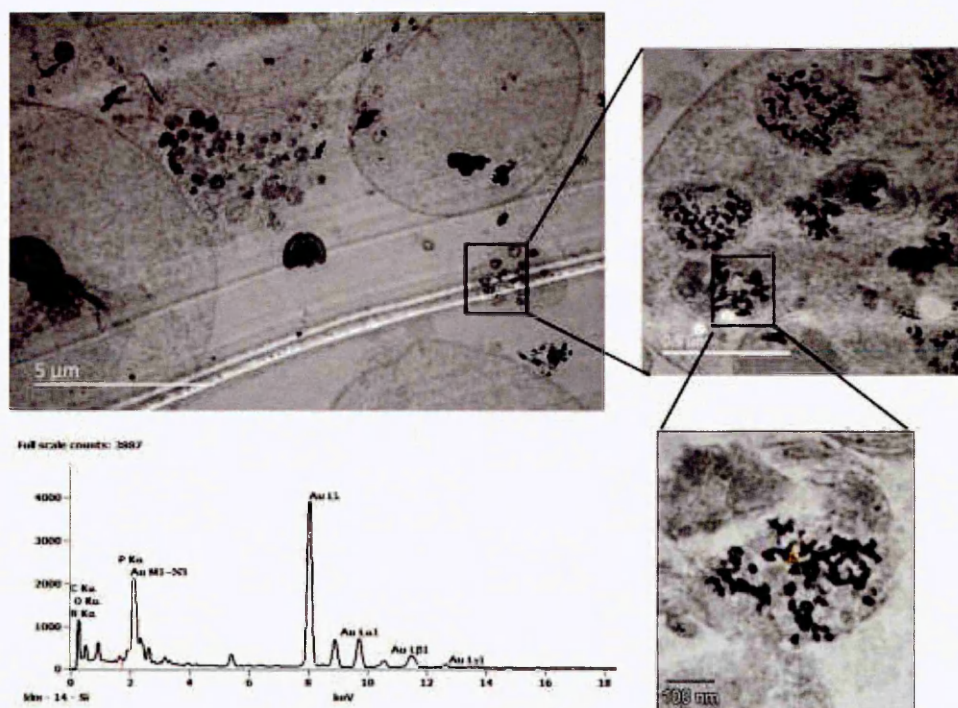
**Figure 5.31** TEM image of PC3 cells treated with P-AuNPs 5.0 mg/mL for 24 hours, sample stained with uranyl acetate and lead citrate. SEM image shows the expansion region in boxed area in the TEM image. The yellow spot (labelled 1) indicated the area analysed by EDX, EDX analysis confirmed the presence of P-AuNPs inside the cell.

At the highest concentration of P-AuNPs at 5.0 mg/mL, the TEM image (Figure 5.31) showed the shrinkage of the cells and cell contents spilling outside the cell. P-AuNPs are contained in several distinct vesicles which appeared to be an apoptotic body, this illustrated that P-AuNPs are cytotoxic to cells at this concentration. This observation is in accord with the results obtained by fluorescent microscopy (Figure 5.15 and Figure 5.21).

Figure 5.31 showed that P-AuNPs have aggregated inside the cells, it has been reported that nanoparticles can aggregate in cell culture media due to the presence of ions and proteins which may cause unexpected results (Maiorano et al., 2010, Rausch et al., 2010). Aggregation occurs when the van der Waals forces between particles are greater than the electrostatic repulsive forces on the nano surface (Derjaguin and Landau, 1993, Lundqvist et al., 2008). It is important to study/understand the aggregation of nanomaterials, as the aggregation of nanoparticles can have an effect on their cellular uptake and cytotoxicity; Albanese and co-workers (Albanese and Chan, 2011) have reported a 25% decrease in uptake of aggregated nanoparticles compared to single and monodisperse nanoparticles in HeLa and A549 cells.

In general, TEM images recorded display 3 trends: 1) the number of nanoaprticles present in cells increases with the concentration of P-AuNPs, 2) P-AuNPs are taken-up by cells, however they are not distributed equally in all the organelles. Zhu and colleagues (Zhu *et al.*, 2008) reported similar observation; within a cell, AuNPs were only observed to be taken-up as one big cluster in one endosome and not the other endosomes. 3) P-AuNPs are taken-up in clusters, this observation has been reported by other research groups (Arnida *et al.*, 2010, Nativo *et al.*, 2008, Liu *et al.*, 2010).

Uptake of single nanoparticles has been observed; Chithrani and colleagues (Chithrani and Chan, 2007) reported single 50 nm transferrin-coated AuNPs are able to enter the cells, while 14 nm transferrin-coated AuNPs were only taken up when clustered in groups with a minimum of 6 particles, indicating that the uptake of nanoparticles (single or clusters) is influenced by the particle size.

5.3.4 Quantification of the Uptake of Phosphonium-Functionalised Gold Nanoparticles in cells by ICP-MS

Quantification of AuNPs in the pure form has been achieved successfully using ICP-MS (Allabashi *et al.*, 2009, Elzey *et al.*, 2012, Helfrich and Bettmer, 2011). The use of ICP-MS for quantifying the uptake of AuNPs in cells has also been investigated (Zhu *et al.*, 2012, Chithrani *et al.*, 2006). In this chapter, ICP-MS has been used to determine the amount of AuNPs in cells, and the results showed that both P-AuNPs and commercial AuNPs (stabilised suspension in citrate buffer) with good uptake (> 70%) observed across all concentrations (Figure 5.32).
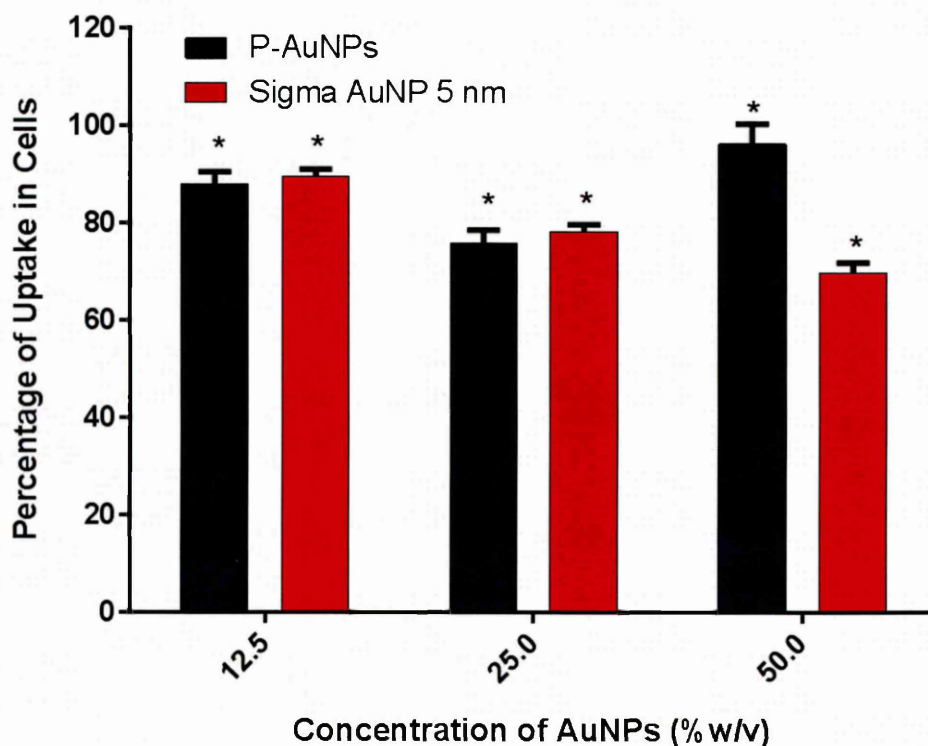
Figure 5.32 ICP-MS data showing the percentage uptake of P-AuNPs and commerical AuNPs in PC3 (n=3). *Statisitcal significance between the levels of apoptotic cells $P \leq 0.05$.

Staisitical analysis showed that the treatment of PC3 treated with P-AuNPs and commercial available AuNPs 5 nm has significantly increased compared to control, assuming there are no uptake at 0 mg/mL. The P value for P-AuNPs and Sigma AuNPs for all 3 concentrations (12.5, 25.0 and 5.0 mg/Ml) is calculated to be $P = 0.0213$,

The uptake of "naked" AuNPs is consistent for all concentrations, this observation is in agreement with Arnida and co-workers (Arnida *et al.*, 2010) who have reported the uptake of plan spherical AuNPs (d = 30 nm) is steady across all concentration tested (0-40 nM) and this saturated uptake may be due to the limited cationic sites available on the cell surface (Wilhelm *et al.*, 2003).

It is difficult to compare data obtained with published studies, due to variations in reporting the data, as reviewed by Lévy and colleagues (Lévy *et al.*, 2010). For example the units of size vary between groups thereby making comparison a tricky and complicated task; Zhu *et al.* (2012) reported the uptake of AuNPs by ICP-MS in terms of pmol, while Arnida *et al.* (2010) reported the uptake of AuNPs by number per cell and Chithrani *et al.* (2006) reported the uptake by number of AuNPs per cell (10^3). The cellular uptake of AuNPs as a function of size have been reported by the number of particles per cell (Chithrani *et al.*, 2006) and pg/cell (Lu *et al.*, 2009). What was interesting was that when Levy *et al.* expressed Chithrani *et al* results in pg/cell instead of the number of particles per cell, the results changes significantly with a plateau observed around 100 nm rather than the reported 50 nm.

Chithrani *et al.* 2006 have used the following equations (equation 1 and 2) to convert the number of gold atoms obtained from ICP-AES measurements to the number of gold nanoparticles. The number of atoms (U) in each volume of gold nanoparticles can be calculated, where D is the diameter of a nanosphere, α refers to the edge of a unit cells which has a vlue of 4.0786 Å on the edge, there are 4 gold atoms per unit cells, M is the measured number of gold atoms from ICP-AES.

$$U = \frac{2}{3}\pi \left(\frac{D}{a}\right)^3 \quad \text{(equation 1)}$$

$$N = \frac{M}{U} \quad \text{(equation 2)}$$

For a sphere nanoparticle, the diameter (D), the number of atoms (U) in each volume of gold nanoparticles can be calculated. Based on these equations, the diameter of PPTS capped AuNPs (3.0 nm) can be substituted in the equation

and the number of gold atoms calculated to be 27,328 gold nanoparticles per cell.

$$U = \frac{2}{3}\pi\left(\frac{3}{a}\right) = 0.3980$$

$$N = \frac{11000}{0.3980} = 27638$$

Arnida *et al.* 2010 investigated the uptake of plain and PEGylated gold nanospheres of different sizes (30, 50 and 90 nm) in PC3 cells, PEGylated nanoparticles showed very little uptake compared to pain AuNPs. The authors reported the uptake of plain 30 nm AuNPs to be between 10,000 to 45,000 gold nanoparticles per cell depending on concentration (1 nM – 10 nM). The results showed that the uptake of AuNPs is concentration dependent: at the lowest concentration at 1 nM the uptake is around 11,000 particles per cell and at the highest concentration at 10 nM the uptake is around 45,000 particles per cell.

ICP-MS data obtained was converted to AuNPs per cell using the equations described above (equation 1 and 2). The number of AuNPs per cell has been calculated to be 27,638, 47,738 and 128,643 for cells treated with P-AuNPs at a concentration of 12.0 mg/mL, 25.0 mg/mL and 50.0 mg/mL respectively. Comparing results obtained in this chapter with results reported by Arnida and colleagues (Arnida et al., 2010) the data showed that plain 30 nm AuNPs (nanomolar concentration) has a higher uptake compared to 3 nm P-AuNPs (millimolar concentration). The ease of synthesis of AuNPs with variety of surface ligands has been exploited by many research groups to enhance their cellular uptake for biomedical applications (described previously in chapter 1.1.3.). It is evident that functionalised AuNPs have better cellular uptake compared to plain AuNPs (Chou et al., 2011, Wang and Thanou, 2010, Wang et al., 2012). The higher uptake observed for 30 nm AuNPs could be due to the different size: Chithrani *et al.* 2006 have investigated the cellular uptake of plain spherical AuNPs of different sizes (10 nm – 100 nm): the results showed that with an increase in size from 10 nm to 50 nm the uptake increases with size, where as increase size from 50 nm to 100 nm the uptake decreases. This demonstrated that the size plays an important role in the cellular uptake of AuNPs in cells.

5.4 Conclusion

Results reported in this chapter demonstrated that P-AuNPs are soluble in biological media which is of great importance for cell biology studies. Initial PTT studies illustrated that P-AuNPs are specific and respond specifically to a wide green excitation source (510-550 nm) which overlaps the SPR band of the P-AuNPs at ~525 nm. Preliminary qualitative data showed promising results that P-AuNPs can selectively induce apoptosis in cells followed by PTT; under the same irradiation conditions cells with a higher concentration of P-AuNPs undergo cell death by necrosis, whereas cells with a lower concentration of P-AuNPs undergo apoptosis. Quantitative analysis of PTT indicated that the percentage of apoptosis cell is actually around a third which is not as high as originally hypothesised.

TEM images showed that P-AuNPs are clustered inside the cells and are not distributed equally amongst all mitochondria, which could explain the small population of apoptotic cells observed from PTT experiments. TEM images suggested that the uptake mode of P-AuNPs is by endocytosis, which is in agreement with other research groups (Chithrani *et al.*, 2006, Nativo *et al.*, 2008).

5.5   References

AKSENOVA, V. I., BYLINO, O. V., ZHIVOTOVSKY, B. D. & LAVRIK, I. N. 2013. Caspase-2: What do we know today? *Molecular Biology,* 47, 165-180.

ALBANESE, A. & CHAN, W. C. W. 2011. Effect of gold nanoparticle aggregation on cell uptake and toxicity. *ACS Nano,* 5, 5478-5489.

ALLABASHI, R., STACH, W., DE LA ESCOSURA-MU IZ, A., LISTE-CALLEJA, L. & MERKO I, A. 2009. ICP-MS: A powerful technique for quantitative determination of gold nanoparticles without previous dissolving. *Journal of Nanoparticle Research,* 11, 2003-2011.

ARNIDA, MALUGIN, A. & GHANDEHARI, H. 2010. Cellular uptake and toxicity of gold nanoparticles in prostate cancer cells: A comparative study of rods and spheres. *Journal of Applied Toxicology,* 30, 212-217.

BARONZIO, G., GRAMAGLIA, A. & FIORENTINI, G. 2009. Current role and future perspectives of hyperthermia for prostate cancer treatment. *In Vivo,* 23, 143-146.

BODDAPATI, S. V., D'SOUZA, G. G. & WEISSIG, V. 2010. Liposomes for drug delivery to mitochondria. *Methods in molecular biology (Clifton, N.J.),* 605, 295-303.

CHEN, W. H., CHEN, J. X., CHENG, H., CHEN, C. S., YANG, J., XU, X. D., WANG, Y., ZHUO, R. X. & ZHANG, X. Z. 2013. A new anti-cancer strategy of damaging mitochondria by pro-apoptotic peptide functionalized gold nanoparticles. *Chemical Communications,* 49, 6403-6405.

CHEN, Y. H., TSAI, C. Y., HUANG, P. Y., CHANG, M. Y., CHENG, P. C., CHOU, C. H., CHEN, D. H., WANG, C. R., SHIAU, A. L. & WU, C. L. 2007. Methotrexate conjugated to gold nanoparticles inhibits tumor growth in a syngeneic lung tumor model. *Molecular Pharmaceutics,* 4, 713-722.

CHERUKURI, P. & CURLEY, S. A. 2010. Use of nanoparticles for targeted, noninvasive thermal destruction of malignant cells. *Methods in molecular biology (Clifton, N.J.),* 624, 359-373.

CHERUKURI, P., GLAZER, E. S. & CURLEYA, S. A. 2010. Targeted hyperthermia using metal nanoparticles. *Advanced Drug Delivery Reviews,* 62, 339-345.

CHITHRANI, B. D. & CHAN, W. C. W. 2007. Elucidating the mechanism of cellular uptake and removal of protein-coated gold nanoparticles of different sizes and shapes. *Nano Letters,* 7, 1542-1550.

CHITHRANI, B. D., GHAZANI, A. A. & CHAN, W. C. W. 2006. Determining the size and shape dependence of gold nanoparticle uptake into mammalian cells. *Nano Letters,* 6, 662-668.

CHITHRANI, B. D., STEWART, J., ALLEN, C. & JAFFRAY, D. A. 2009. Intracellular uptake, transport, and processing of nanostructures in cancer cells. *Nanomedicine: Nanotechnology, Biology, and Medicine,* 5, 118-127.

CHITHRANI, D. B. 2010. Intracellular uptake, transport, and processing of gold nanostructures. *Molecular Membrane Biology,* 27, 299-311.

CHOI, C. H. J., ALABI, C. A., WEBSTER, P. & DAVIS, M. E. 2010. Mechanism of active targeting in solid tumors with transferrin-containing gold nanoparticles. *Proceedings of the National Academy of Sciences of the United States of America,* 107, 1235-1240.

CHOU, L. Y. T., MING, K. & CHAN, W. C. W. 2011. Strategies for the intracellular delivery of nanoparticles. *Chemical Society Reviews,* 40, 233-245.

COBLEY, C. M., CHEN, J., CHO, E. C., WANG, L. V. & XIA, Y. 2011. Gold nanostructures: A class of multifunctional materials for biomedical applications. *Chemical Society Reviews,* 40, 44-56.

D'SOUZA, G. G. M., RAMMOHAN, R., CHENG, S. M., TORCHILIN, V. P. & WEISSIG, V. 2003. DQAsome-mediated delivery of plasmid DNA toward mitochondria in living cells. *Journal of Controlled Release,* 92, 189-197.

DELGADO, M. E., OLSSON, M., LINCOLN, F. A., ZHIVOTOVSKY, B. & REHM, M. 2013. Determining the contributions of caspase-2, caspase-8 and effector caspases to intracellular VDVADase activities during apoptosis initiation and execution. *Biochimica et Biophysica Acta - Molecular Cell Research,* 1833, 2279-2292.

DERJAGUIN, B. & LANDAU, L. 1993. Theory of the stability of strongly charged lyophobic sols and of the adhesion of strongly charged particles in solutions of electrolytes. *Progress in Surface Science,* 43, 30-59.

DIAGARADJANE, P., SHETTY, A., WANG, J. C., ELLIOTT, A. M., SCHWARTZ, J., SHENTU, S., PARK, H. C., DEORUKHKAR, A., STAFFORD, R. J., CHO, S. H., TUNNELL, J. W., HAZLE, J. D. & KRISHNAN, S. 2008. Modulation of in vivo tumor radiation response via gold nanoshell-mediated vascular-focused hyperthermia: Characterizing an integrated antihypoxic and localized vascular disrupting targeting strategy. *Nano Letters,* 8, 1492-1500.

DIXIT, V., VAN DEN BOSSCHE, J., SHERMAN, D. M., THOMPSON, D. H. & ANDRES, R. P. 2006. Synthesis and grafting of thioctic acid-PEG-folate conjugates onto Au nanoparticles for selective targeting of folate receptor-positive tumor cells. *Bioconjugate Chemistry,* 17, 603-609.

DREADEN, E. C., MACKEY, M. A., HUANG, X. H., KANG, B. & EL-SAYED, M. A. 2011. Beating cancer in multiple ways using nanogold. *Chemical Society Reviews,* 40, 3391-3404.

EL-SAYED, I. H. 2010. Nanotechnology in head and neck cancer: The race is on. *Current Oncology Reports,* 12, 121-128.

EL-SAYED, I. H., HUANG, X. & EL-SAYED, M. A. 2006. Selective laser photo-thermal therapy of epithelial carcinoma using anti-EGFR antibody conjugated gold nanoparticles. *Cancer Letters,* 239, 129-135.

ELZEY, S., TSAI, D. H., RABB, S. A., YU, L. L., WINCHESTER, M. R. & HACKLEY, V. A. 2012. Quantification of ligand packing density on gold nanoparticles using ICP-OES. *Analytical and Bioanalytical Chemistry,* 403, 145-149.

EVERTS, M. 2007. Thermal scalpel to target cancer. *Expert Review of Medical Devices,* 4, 131-136.

FENG, Y., FUENTES, D., HAWKINS, A., BASS, J. M. & RYLANDER, M. N. 2009. Optimization and real-time control for laser treatment of heterogeneous soft tissues. *Computer Methods in Applied Mechanics and Engineering,* 198, 1742-1750.

FIELD, S. B. & BLEEHEN, N. M. 1979. Hyperthermia in the treatment of cancer. *Cancer Treatment Reviews,* 6, 63-94.

GIBSON, J. D., KHANAL, B. P. & ZUBAREV, E. R. 2007. Paclitaxel-functionalized gold nanoparticles. *Journal of the American Chemical Society,* 129, 11653-11661.

GUO, Y., SRINIVASULA, S. M., DRUILHE, A., FERNANDES-ALNEMRI, T. & ALNEMRI, E. S. 2002. Caspase-2 induces apoptosis by releasing proapoptotic proteins from mitochondria. *Journal of Biological Chemistry,* 277, 13430-13437.

GUPTA, S., KASS, G. E. N., SZEGEZDI, E. & JOSEPH, B. 2009. The mitochondrial death pathway: a promising therapeutic target in diseases. *Journal of Cellular and Molecular Medicine,* 13, 1004-1033.

HARUSH-FRENKEL, O., DEBOTTON, N., BENITA, S. & ALTSCHULER, Y. 2007. Targeting of nanoparticles to the clathrin-mediated endocytic pathway. *Biochemical and Biophysical Research Communications,* 353, 26-32.

HE, Q., HUANG, Y. & SHEIKH, M. S. 2004. Bax deficiency affects caspase-2 activation during ultraviolet radiation-induced apoptosis. *Oncogene,* 23, 1321-1325.

HELFRICH, A. & BETTMER, J. 2011. Analysis of gold nanoparticles using ICP-MS-based hyphenated and complementary ESI-MS techniques. *International Journal of Mass Spectrometry,* 307, 92-98.

HUANG, X., JAIN, P. K., EL-SAYED, I. H. & EL-SAYED, M. A. 2006. Determination of the minimum temperature required for selective photothermal destruction of cancer cells with the use of immunotargeted gold nanoparticles. *Photochemistry and Photobiology,* 82, 412-417.

HUANG, X., JAIN, P. K., EL-SAYED, I. H. & EL-SAYED, M. A. 2008. Plasmonic photothermal therapy (PPTT) using gold nanoparticles. *Lasers in Medical Science,* 23, 217-228.

HUANG, X. H., JAIN, P. K., EL-SAYED, I. H. & EL-SAYED, M. A. 2007. Gold nanoparticles: interesting optical properties and recent applications in cancer diagnostic and therapy. *Nanomedicine,* 2, 681-693.

HWU, J. R., LIN, Y. S., JOSEPHRAJAN, T., HSU, M. H., CHENG, F. Y., YEH, C. S., SU, W. C. & SHIEH, D. B. 2009. Targeted paclitaxel by conjugation to iron oxide and gold nanoparticles. *Journal of the American Chemical Society,* 131, 66-68.

JAIN, P. K., HUANG, X., EL-SAYED, I. H. & EL-SAYAD, M. A. 2007. Review of some interesting surface plasmon resonance-enhanced properties of noble metal nanoparticles and their applications to biosystems. *Plasmonics,* 2, 107-118.

JAIN, P. K., HUANG, X., EL-SAYED, I. H. & EL-SAYED, M. A. 2008. Noble metals on the nanoscale: optical and photothermal properties and some applications in imaging, sensing, biology, and medicine. *Accounts of Chemical Research,* 41, 1578-1586.

KANARAS, A. G., BARTCZAK, D., SANCHEZ-ELSNER, T., MILLAR, T. M. & MUSKENS, O. L. 2011. Gold Nanoparticles in Biomedical Applications. *In:* PARAK, W. J., YAMAMOTO, K. & OSINSKI, M. (eds.) *Colloidal Quantum Dots/Nanocrystals for Biomedical Applications Vi.*

KELLY, K. L., CORONADO, E., ZHAO, L. L. & SCHATZ, G. C. 2003. The optical properties of metal nanoparticles: The influence of size, shape, and dielectric environment. *Journal of Physical Chemistry B,* 107, 668-677.

KIRCHHAUSEN, T. 2000. Three ways to make a vesicle. *Nature Reviews Molecular Cell Biology,* 1, 187-198.

KIRUI, D. K., REY, D. A. & BATT, C. A. 2010. Gold hybrid nanoparticles for targeted phototherapy and cancer imaging. *Nanotechnology,* 21.

KUMAR, D., SAINI, N., JAIN, N., SAREEN, R. & PANDIT, V. 2013. Gold nanoparticles: an era in bionanotechnology. *Expert Opinion on Drug Delivery,* 10, 397-409.

L VY, R., SHAHEEN, U., CESBRON, Y. & S E, V. 2010. Gold nanoparticles delivery in mammalian live cells: a critical review. *Nano Reviews.*

LEPOCK, J. R. 2003. Cellular effects of hyperthermia: Relevance to the minimum dose for thermal damage. *International Journal of Hyperthermia,* 19, 252-266.

LI, J. L., WANG, L., LIU, X. Y., ZHANG, Z. P., GUO, H. C., LIU, W. M. & TANG, S. H. 2009. In vitro cancer cell imaging and therapy using transferrin-conjugated gold nanoparticles. *Cancer Letters,* 274, 319-326.

LINK, S. & EL-SAYED, M. A. 2000. Shape and size dependence of radiative, non-radiative and photothermal properties of gold nanocrystals. *International Reviews in Physical Chemistry,* 19, 409-453.

LIU, S. Y., LIANG, Z. S., GAO, F., LUO, S. F. & LU, G. Q. 2010. In vitro photothermal study of gold nanoshells functionalized with small targeting peptides to liver cancer cells. *Journal of Materials Science: Materials in Medicine,* 21, 665-674.

LIZ-MARZ N, L. M. 2004. Nanometals: Formation and color. *Materials Today,* 7, 26-31.

LU, F., WU, S. H., HUNG, Y. & MOU, C. Y. 2009. Size effect on cell uptake in well-suspended, uniform mesoporous silica nanoparticles. *Small,* 5, 1408-1413.

LUNDQVIST, M., STIGLER, J., ELIA, G., LYNCH, I., CEDERVALL, T. & DAWSON, K. A. 2008. Nanoparticle size and surface properties determine the protein corona with possible implications for biological impacts. *Proceedings of the National Academy of Sciences of the United States of America,* 105, 14265-14270.

M HLFELD, C., MAYHEW, T. M., GEHR, P. & ROTHEN-RUTISHAUSER, B. 2007a. A novel quantitative method for analyzing the distributions of nanoparticles between different tissue and intracellular compartments. *Journal of Aerosol Medicine: Deposition, Clearance, and Effects in the Lung,* 20, 395-407.

M HLFELD, C., ROTHEN-RUTISHAUSER, B., VANHECKE, D., BLANK, F., GEHR, P. & OCHS, M. 2007b. Visualization and quantitative analysis of nanoparticles in the respiratory tract by transmission electron microscopy. *Particle and Fibre Toxicology,* 4.

MAHL, D., GREULICH, C., MEYER-ZAIKA, W., K LLER, M. & EPPLE, M. 2010. Gold nanoparticles: Dispersibility in biological media and cell-biological effect. *Journal of Materials Chemistry,* 20, 6176-6181.

MAIORANO, G., SABELLA, S., SORCE, B., BRUNETTI, V., MALVINDI, M. A., CINGOLANI, R. & POMPA, P. P. 2010. Effects of cell culture media on the dynamic formation of protein-nanoparticle complexes and influence on the cellular response. *ACS Nano,* 4, 7481-7491.

MAYHEW, T. M., M HLFELD, C., VANHECKE, D. & OCHS, M. 2009. A review of recent methods for efficiently quantifying immunogold and other nanoparticles using TEM sections through cells, tissues and organs. *Annals of Anatomy,* 191, 153-170.

MCNEIL, S. E. 2011. *Characterization of Nanoparticles Intended for Drug Delivery* Humana Press.

MILLERON, R. S. & BRATTON, S. B. 2007. 'Heated' debates in apoptosis. *Cellular and Molecular Life Sciences,* 64, 2329-2333.

MONTES-BURGOS, I., WALCZYK, D., HOLE, P., SMITH, J., LYNCH, I. & DAWSON, K. 2010. Characterisation of nanoparticle size and state prior to nanotoxicological studies. *Journal of Nanoparticle Research,* 12, 47-53.

MOTSKIN, M., WRIGHT, D. M., MULLER, K., KYLE, N., GARD, T. G., PORTER, A. E. & SKEPPER, J. N. 2009. Hydroxyapatite nano and microparticles: Correlation of particle properties with cytotoxicity and biostability. *Biomaterials,* 30, 3307-3317.

NADEAU, J., ZHANG, E. & CHIBLI, H. Enhanced cytotoxicity of doxorubicin conjugated to ultrasmall Au nanoparticles. 2010. 316-319.

NATIVO, P., PRIOR, I. A. & BRUST, M. 2008. Uptake and intracellular fate of surface-modified gold nanoparticles. *ACS Nano,* 2, 1639-1644.

PAN, Y., NEUSS, S., LEIFERT, A., FISCHLER, M., WEN, F., SIMON, U., SCHMID, G., BRANDAU, W. & JAHNEN-DECHENT, W. 2007. Size-dependent cytotoxicity of gold nanoparticles. *Small,* 3, 1941-1949.

PATRA, H. K., BANERJEE, S., CHAUDHURI, U., LAHIRI, P. & DASGUPTA, A. K. 2007. Cell selective response to gold nanoparticles. *Nanomedicine: Nanotechnology, Biology, and Medicine,* 3, 111-119.

PITSILLIDES, C. M., JOE, E. K., WEI, X. B., ANDERSON, R. R. & LIN, C. P. 2003. Selective cell targeting with light-absorbing microparticles and nanoparticles. *Biophysical Journal,* 84, 4023-4032.

RAUSCH, K., REUTER, A., FISCHER, K. & SCHMIDT, M. 2010. Evaluation of nanoparticle aggregation in human blood serum. *Biomacromolecules,* 11, 2836-2839.

RIVERA GIL, P., H HN, D., DEL MERCATO, L. L., SASSE, D. & PARAK, W. J. 2010. Nanopharmacy: Inorganic nanoscale devices as vectors and active compounds. *Pharmacological Research,* 62, 115-125.

ROTHEN-RUTISHAUSER, B., M HLFELD, C., BLANK, F., MUSSO, C. & GEHR, P. 2007. Translocation of particles and inflammatory responses after exposure to fine particles and nanoparticles in an epithelial airway model. *Particle and Fibre Toxicology,* 4.

SALNIKOV, V., LUKY NENKO, Y. O., FREDERICK, C. A., LEDERER, W. J. & LUKY NENKO, V. 2007. Probing the outer mitochondrial membrane in cardiac mitochondria with nanoparticles. *Biophysical Journal,* 92, 1058-1071.

SOKOLOV, K., FOLLEN, M., AARON, J., PAVLOVA, I., MALPICA, A., LOTAN, R. & RICHARDS-KORTUM, R. 2003. Real-time vital optical imaging of precancer using anti-epidermal growth factor receptor antibodies conjugated to gold nanoparticles. *Cancer Research,* 63, 1999-2004.

SPERLING, R. A., RIVERA GIL, P., ZHANG, F., ZANELLA, M. & PARAK, W. J. 2008. Biological applications of gold nanoparticles. *Chemical Society Reviews,* 37, 1896-1908.

VAUTHIER, C., TSAPIS, N. & COUVREUR, P. 2011. Nanoparticles: Heating tumors to death? *Nanomedicine,* 6, 99-109.

WANG, A. Z., LANGER, R. & FAROKHZAD, O. C. 2012. Nanoparticle delivery of cancer drugs.

WANG, M. & THANOU, M. 2010. Targeting nanoparticles to cancer. *Pharmacological Research,* 62, 90-99.

WEISSIG, V. 2005. Targeted drug delivery to mammalian mitochondria in living cells. *Expert Opinion on Drug Delivery,* 2, 89-102.

WEISSIG, V., BODDAPATI, S., JABR, L. & D'SOUZA, G. G. 2007. Mitochondria-specific nanotechnology. *Nanomedicine, 2*, 275-285.

WILHELM, C., BILLOTEY, C., ROGER, J., PONS, J. N., BACRI, J. C. & GAZEAU, F. 2003. Intracellular uptake of anionic superparamagnetic nanoparticles as a function of their surface coating. *Biomaterials, 24*, 1001-1011.

YEN, H. J., HSU, S. H. & TSAI, C. L. 2009. Cytotoxicity and immunological response of gold and silver nanoparticles of different sizes. *Small, 5*, 1553-1561.

ZHU, Z. J., GHOSH, P. S., MIRANDA, O. R., VACHET, R. W. & ROTELLO, V. M. 2008. Multiplexed screening of cellular uptake of gold nanoparticles using laser desorption/ionization mass spectrometry. *Journal of the American Chemical Society, 130*, 14139-14143.

ZHU, Z. J., TANG, R., YEH, Y. C., MIRANDA, O. R., ROTELLO, V. M. & VACHET, R. W. 2012. Determination of the intracellular stability of gold nanoparticle monolayers using mass spectrometry. *Analytical Chemistry, 84*, 4321-4326.

Chapter 6.

Conclusion and future work

6.1 Conclusion and Future Work

The work presented in this thesis demonstrated that triarylphosphoniopropylthiosulfate zwitterions and ω-thioacetylpropyl(triphenyl)-phosphonium salts can be used to prepare cationic, water-soluble AuNPs with mean core sizes in the range of 2.5-5 nm. A number of techniques have been employed to characterise the P-AuNPs including NMR, LDI MS, SIMS, XPS, TGA, ICP-MS, MALDI-MS and TEM. The presence of phosphoniopropylthiolate ligands on the surface of the AuNPs have been supported by NMR, LDI, SIMS and XPS.

Quantitative analysis of P-AuNPs has also been investigated; TGA data indicate there is a high thiol/Au ratio which is in line with ICP-MS data, ICP-MS has been successfully used to quantify the thiol ligand density of AuNPs (Hinterwirth *et al.*, 2013), additional ICP-MS analysis are required in order to obtain more quantitative data regarding the thiol ligand density. To-date the characterisation of intact AuNPs by MALDI-MS has only been reported for Au core sizes of up to 2 nm (Chaki *et al.*, 2008, Yu and Andriola, 2010). The use of MALDI-MS as an additional tool to characterise AuNPs has been challenging and further experiments are required.

TEM results showed all nanoparticles synthesised have a uniform spherical shape, however the PPTA salt produces slightly larger AuNPs and greater particle size distribution in comparison to the corresponding PPTS zwitterion, despite both protecting ligands produces the same Au-S ligation. This observation is consistent with slower or incomplete reaction and is supported by LDI-MS results.

In general the thioacetate salts (PPTA and FPPTA) are more soluble than the corresponding zwitterion, this poor solubility of the zwitterions is possibly due to their structural packing in their lattice obtained from crystallography study. Since thioacetate salts are readily soluble in a range of solvents, they were taken forward for cell culture experiments.

231

Cell viability assay demonstrated that thioacetates are toxic towards PC3 cells at high concentrations and at prolonged incubation time. However, thioacetate salts synthesised in this project are not as cytotoxic compared to other phosphonium compounds reported by Millard et al (2010). The authors investigated the cytotoxicity of numerous phosphonium compounds in several cancer cell lines including PC3 cells utilised in this study. Their most toxic compound has an IC_{50} value of 0.4 μM at 72 hours in PC3 which is approximately ~150 fold more toxic than PPTA.

In contrast in synthesising compounds containing the TPP moiety that are cytotoxic towards the cells like other research groups (Millard *et al.*, 2010, Rideout *et al.*, 1989, Patel *et al.*, 1994, Manetta *et al.*, 1996), thioacetates ligands synthesised in this project are comparatively non-toxic towards cells and can be used as transport vector to deliver AuNPs into the cell for other therapeutic applications such as PTT.

The work presented in chapter 4 demonstrated the successful application of MALDI-MS for the semi-quantification of phosphonium compounds in PC3 cells, follow on work from this could include treating tissues with ligands and analysing by MALDI-MS imaging to obtain useful information regarding the distribution of phosphonium ligands in tissues as well obtaining useful quantification data. The success uses of MALDI-MS imaging of tissues has been reported and reviewed by several groups (Koeniger *et al.*, 2011, Pól *et al.*, 2010, Norris and Caprioli, 2013).

MALDI-MS results also showed that phosphonium ligands (PPTA and FPPTA) are rapidly taken-up by PC3 cells within minutes, an attempt has been made to analyse the uptake of PPTA in the mitochondrial fraction, to compare to uptake of phosphonium ligands inside the mitochondrial versus in the cytosol however the signal from the instruments were extremely weak, future studies in this area could be to isolate the mitochondria fraction by an alternative method such as the protocol published by Wieckowski and colleagues (Wieckowski *et al.*, 2009).

Results from chapter 5 illustrated that P-AuNPs synthesised are soluble in biological media which is of great importance for cell biology studies. Initial PTT studies demonstrated that P-AuNPs are specific and respond only to wide green excitation source (510-550 nm) which overlaps the SPR band of the P-AuNPs at ~525 nm. TEM results confirmed that P-AuNPs synthesised are indeed taken-up in the mitochondria as hypothesised, this observation agrees with the report by Salnikov and colleagues (Salnikov *et al.*, 2007) who have demonstrated that the outer mitochondrial membrane is not permeable to nanoparticles greater than 6 nm in diameter. Due to the nature of the small size of P-AuNPs (< 6 nm) they are able to accumulate inside the mitochondria thus making them feasible for mitochondria targeting applications.

TEM results also showed that P-AuNPs are not taken-up by all mitochondria in cells, which may explain the PTT results why apoptosis death is only around 25% which is lower than originally hypothesised. P-AuNPs are taken-up by small fraction of mitochondria in cells, when exposed with a light source only the cells containing P-AuNPs will result in mitochondrial damage and releasing cytochrome *c* into the cytosol and triggering the caspase cascade, since only a small fraction of mitochondria membrane will burst open, the cells can tolerate minor damages to the mitochondria and thus the results will not be as catastrophic if all P-AuNPs are taken-up by all mitochondria, upon irradiation all mitochondria membranes will burst open, triggering the caspase cascade and inducing apoptosis throughout the entire cell.

In addition, TEM images showed that P-AuNPs awere taken-up in cells in clusters rather than single nanoparticles as originally hypothesised, this might explain the percentage of apoptotic cells from photothermal therapy experiments were lower than hypothesised.. The results suggested that P-AuNPs are taken-up in clusters by the cells and thus only mitochondria containing P-AuNPs will respond to irradiation. Since a small proportion of mitochondria contain P-AuNPs would be affected, the death of small percentage of mitochondria are not enough to be a catastrophic event for the entire cell and may just induce localized autophagy.

The idea that cells can commit suicide by other mechanisms besides apoptosis has gained momentum over the past few years; non-apoptotic forms of programmed cell death include necrosis and autophagy (Lockshin and Zakeri, 2004, Proskuryakov *et al.*, 2003, Edinger and Thompson, 2004). The term autophagy is derived from Greek meaning "eating of self", is credited to de Duve and colleague (Deter and De Duve, 1967), it is a cellular catabolic degradation process which respond to starvation or stress by engulfing damaged proteins and organelles which are then recycled to maintain cellular metabolism (Mathew *et al.*, 2007).

Furthermore autophagy is also the mechanism for the engulfment of apoptosis cells (Qu *et al.*, 2007), which may be feasible explanation to why the percentage of apoptosis observed from PTT studies were lower than expected, as when cells were stained with caspase-3, majority of cells were caspase-3 positive thereby suggesting that cells are actively undergoing apoptosis, however when stained with Hoechst, only minority of cells exhibited apoptotic morphology. If the apoptotic cells were engulfed by autophagy the number of apoptotic cells will thereby decrease which agree with the observations for PTT experiments. To determine if cells are dying through autophagy rather than apoptosis, for future experiments could be to test for autophagy.

The measurement of autophagy has been a topic of intense discussion, with reviews, methods and guidelines available in the literature (Mizushima, 2004, Klionsky *et al.*, 2008, Mizushima *et al.*, 2010). Conventionally, electron microscopy has been the standard approach to detect autophagy by the studying the morphological structures of autophagosomes, however it can be difficult to distinguish autophagic vacuoles from other structures just by examining the morphology. Although TEM is well established method, the main downfalls are that it is quite costly and not readily accessible (Kimmelman, 2011, Mizushima, 2004).

Several newer essays have been based on LC3 (ATG8) which is a general marker for autophagic membranes, this protein cleaved by ATG4 to generate LC3-I, subsequently it is lapidated to give LC3-II (Ichimura *et al.*, 2000), which

can be detected as a faster migrating band by immunoblotting (Mizushima and Yoshimori, 2007). Since LC3-II is incorporated into the inner and outer surfaces of autophagosomes, this localisation can easily be examined by fusing LC3 with green fluorescent protein (GFP) which can be visualised by fluorescent microscopy (Mizushima, 2004). In order to test for autophagy, future analysis could include the detection and confirmation of autophagy using a range of methods including Western-blot analysis, fluorescence microscopy to gain both qualitative and quantitative data and TEM to obtain high resolution images. Confocal microscopy can be used to image autophagy markers, which can be used to visualise ATG/LC3-1, confocal microscopy enables real-time cross section viewing of autophagy forming, and can take Z-stacks of cell to provide a 3 dimensional image of the cell.

In recent years, autophagy has emerged as a mechanism of nanomaterials toxicity (Stern *et al.*, 2012, Li *et al.*, 2010), what is particularly interesting is that iron core and gold shell nanoparticles have been shown to inhibit cell proliferation of oral cancer through mitochondria-mediated autophagy (Wu et al., 2011). With the finding that nanomaterials can cause cell death by autophagy, future work will focus on investigating whether P-AuNPs causes autophagy in cells.

6.2 References

CHAKI, N. K., NEGISHI, Y., TSUNOYAMA, H., SHICHIBU, Y. & TSUKUDA, T. 2008. Ubiquitous 8 and 29 kDa gold:alkanethiolate cluster compounds: Mass-spectrometric determination of molecular formulas and structural implications. *Journal of the American Chemical Society,* 130, 8608-8610.

DETER, R. L. & DE DUVE, C. 1967. Influence of glucagon, an inducer of cellular autophagy, on some physical properties of rat liver lysosomes. *Journal of Cell Biology,* 33, 437-449.

EDINGER, A. L. & THOMPSON, C. B. 2004. Death by design: Apoptosis, necrosis and autophagy. *Current Opinion in Cell Biology,* 16, 663-669.

HINTERWIRTH, H., KAPPEL, S., WAITZ, T., PROHASKA, T., LINDNER, W. & L MMERHOFER, M. 2013. Quantifying thiol ligand density of self-assembled monolayers on gold nanoparticles by inductively coupled plasma-mass spectrometry. *ACS Nano,* 7, 1129-1136.

ICHIMURA, Y., KIRISAKO, T., TAKAO, T., SATOMI, Y., SHIMONISHI, Y., ISHIHARA, N., MIZUSHIMA, N., TANIDA, I., KOMINAMI, E., OHSUMI, M., NODA, T. & OHSUMI, Y. 2000. A ubiquitin-like system mediates protein lipidation. *Nature,* 408, 488-492.

KIMMELMAN, A. C. 2011. The dynamic nature of autophagy in cancer. *Genes and Development,* 25, 1999-2010.

KLIONSKY, D. J., ABELIOVICH, H., AGOSTINIS, P., AGRAWAL, D. K., ALIEV, G., ASKEW, D. S., BABA, M., BAEHRECKE, E. H., BAHR, B. A., BALLABIO, A., BAMBER, B. A., BASSHAM, D. C., BERGAMINI, E., BI, X., BIARD-PIECHACZYK, M., BLUM, J. S., BREDESEN, D. E., BRODSKY, J. L., BRUMELL, J. H., BRUNK, U. T., BURSCH, W., CAMOUGRAND, N., CEBOLLERO, E., CECCONI, F., CHEN, Y., CHIN, L. S., CHOI, A., CHU, C. T., CHUNG, J., CLARKE, P. G. H., CLARK, R. S. B., CLARKE, S. G., CLAV , C., CLEVELAND, J. L., CODOGNO, P., COLOMBO, M. I., COTOMONTES, A., CREGG, J. M., CUERVO, A. M., DEBNATH, J., DEMARCHI, F., DENNIS, P. B., DENNIS, P. A., DERETIC, V., DEVENISH, R. J., DI SANO, F., DICE, J. F., DIFIGLIA, M., DINESH-KUMAR, S., DISTELHORST, C. W., DJAVAHERI-MERGNY, M., DORSEY, F. C., DR GE, W., DRON, M., DUNN JR, W. A., DUSZENKO, M., EISSA, N. T., ELAZAR, Z., ESCLATINE, A., ESKELINEN, E. L., F S S, L., FINLEY, K. D., FUENTES, J. M., FUEYO, J., FUJISAKI, K., GALLIOT, B., GAO, F. B., GEWIRTZ, D. A., GIBSON, S. B., GOHLA, A., GOLDBERG, A. L., GONZALEZ, R., GONZ LEZ-EST VEZ, C., GORSKI, S., GOTTLIEB, R. A., H USSINGER, D., HE, Y. W., HEIDENREICH, K., HILL, J. A., H YER-HANSEN, M., HU, X., HUANG, W. P., IWASAKI, A., J TTEL , M., JACKSON, W. T., JIANG, X., JIN, S., JOHANSEN, T., JUNG, J. U., KADOWAKI, M., KANG, C., KELEKAR, A., KESSEL, D. H., KIEL, J. A. K. W., HONG, P. K., KIMCHI, A., KINSELLA, T. J., KISELYOV, K., KITAMOTO, K., KNECHT, E., et al. 2008. Guidelines for the use and interpretation of assays for monitoring autophagy in higher eukaryotes. *Autophagy,* 4, 151-175.

KOENIGER, S. L., TALATY, N., LUO, Y., READY, D., VOORBACH, M., SEIFERT, T., CEPA, S., FAGERLAND, J. A., BOUSKA, J., BUCK, W., JOHNSON, R. W. & SPANTON, S. 2011. A quantitation method for mass spectrometry imaging. *Rapid Communications in Mass Spectrometry,* 25, 503-510.

LI, J. J., HARTONO, D., ONG, C. N., BAY, B. H. & YUNG, L. Y. L. 2010. Autophagy and oxidative stress associated with gold nanoparticles. *Biomaterials,* 31, 5996-6003.

LOCKSHIN, R. A. & ZAKERI, Z. 2004. Caspase-independent cell death? *Oncogene,* 23, 2766-2773.

MANETTA, A., GAMBOA, G., NASSERI, A., PODNOS, Y. D., EMMA, D., DORION, G., RAWLINGS, L., CARPENTER, P. M., BUSTAMANTE, A., PATEL, J. & RIDEOUT, D. 1996. Novel phosphonium salts display in vitro and in vivo cytotoxic activity against human ovarian cancer cell lines. *Gynecologic Oncology,* 60, 203-212.

MATHEW, R., KARANTZA-WADSWORTH, V. & WHITE, E. 2007. Role of autophagy in cancer. *Nature Reviews Cancer,* 7, 961-967.

MILLARD, M., PATHANIA, D., SHABAIK, Y., TAHERI, L., DENG, J. & NEAMATI, N. 2010. Preclinical evaluation of novel triphenylphosphonium salts with broad-spectrum activity. *PLoS ONE,* 5.

MIZUSHIMA, N. 2004. Methods for monitoring autophagy. *International Journal of Biochemistry and Cell Biology,* 36, 2491-2502.

MIZUSHIMA, N. & YOSHIMORI, T. 2007. How to interpret LC3 immunoblotting. *Autophagy,* 3, 542-545.

MIZUSHIMA, N., YOSHIMORI, T. & LEVINE, B. 2010. Methods in Mammalian Autophagy Research. *Cell,* 140, 313-326.

NORRIS, J. L. & CAPRIOLI, R. M. 2013. Analysis of tissue specimens by matrix-assisted laser desorption/ionization imaging mass spectrometry in biological and clinical research. *Chemical Reviews,* 113, 2309-2342.

P L, J., STROHALM, M., HAVL ČEK, V. & VOLN , M. 2010. Molecular mass spectrometry imaging in biomedical and life science research. *Histochemistry and Cell Biology,* 134, 423-443.

PATEL, J., RIDEOUT, D., MCCARTHY, M. R., CALOGEROPOULOU, T., WADWA, K. S. & OSEROFF, A. R. 1994. Antineoplastic activity, synergism, and antagonism of triarylalkylphosphonium salts and their combinations. *Anticancer Research,* 14, 21-28.

PROSKURYAKOV, S. Y., KONOPLYANNIKOV, A. G. & GABAI, V. L. 2003. Necrosis: A specific form of programmed cell death? *Experimental Cell Research,* 283, 1-16.

QU, X., ZOU, Z., SUN, Q., LUBY-PHELPS, K., CHENG, P., HOGAN, R. N., GILPIN, C. & LEVINE, B. 2007. Autophagy Gene-Dependent Clearance of Apoptotic Cells during Embryonic Development. *Cell,* 128, 931-946.

RIDEOUT, D. C., CALOGEROPOULOU, T., JAWORSKI, J. S., DAGNINO R, R. J. & MCCARTHY, M. R. 1989. Phosphonium salts exhibiting selective anti-carcinoma activity in vitro. *Anti-Cancer Drug Design,* 4, 265-280.

SALNIKOV, V., LUKY NENKO, Y. O., FREDERICK, C. A., LEDERER, W. J. & LUKY NENKO, V. 2007. Probing the outer mitochondrial membrane in cardiac mitochondria with nanoparticles. *Biophysical Journal,* 92, 1058-1071.

STERN, S. T., ADISESHAIAH, P. P. & CRIST, R. M. 2012. Autophagy and lysosomal dysfunction as emerging mechanisms of nanomaterial toxicity. *Particle and Fibre Toxicology,* 9.

WIECKOWSKI, M. R. M. R., GIORGI, C., LEBIEDZINSKA, M., DUSZYNSKI, J. & PINTON, P. 2009. Isolation of mitochondria-associated membranes and mitochondria from animal tissues and cells. *Nature Protocols,* 4, 1582-1590.

WU, Y. N., YANG, L. X., SHI, X. Y., LI, I. C., BIAZIK, J. M., RATINAC, K. R., CHEN, D. H., THORDARSON, P., SHIEH, D. B. & BRAET, F. 2011. The selective growth inhibition of oral cancer by iron core-gold shell nanoparticles through mitochondria-mediated autophagy. *Biomaterials,* 32, 4565-4573.

YU, L. & ANDRIOLA, A. 2010. Quantitative gold nanoparticle analysis methods: A review. *Talanta,* 82, 869-875.

Chapter 7.

Associated work

7.1 Publications

- Ju-Nam, Y., **Chen, Y.-S.,** Ojeda, JJ., Allen, DW., Cross, NA., Gardiner, P., and Bricklebank. N. (2012) Water soluble gold nanoparticles stabilised with cationic phosphonium thiolate ligand. *RSC Advsnces* **2** (27) 10345-10351.

7.2 Poster Presentations

- **Chen., Y.-S.,** Cross, NA., and Bricklebank. N. (2012) Phosphonium-functionalised gold nanoparticles as novel transport vectors for mitochondrial targeting therapeutics. Colloids and Nanomedicine, Amsterdam, Netherlands.

- **Chen., Y.-S.,** Cross, NA., Allen., DW., and Bricklebank. N. (2012) Gold nanoparticles functionalised with lipophilic phosphonium ligands as novel delivery vectors for targeting mitochondria: potential cancer therapeutics. Targeting Mitochondria, Berlin, Germany.

7.3 Conferences Attended

- Mass Spectrometry Showcase Day (Jul 2011), Sheffield Hallam University, UK.
- North of England Cell Biology Forum (Sep 2011), the University of Sheffield, UK.
- Sheffield Cytometry Users Meeting (Oct 2011), The University of Sheffield, UK.
- Manchester Mass Spectrometry Symposium (Dec 2011), the University of Manchester, UK.

7.4 Appendices

Appendix 1 Crystal data and structure refinement for FPPTS.

Compound	FPPTS (7)
Empirical formula	$C_{21}H_{18}F_3O_3PS_2$
Formula weight	470.44
Crystal system	Triclinic
Space group	$P-1$
a / Å	9.4169(13)
b / Å	15.279(3)
c / Å	16.090(3)
β / °	77.619(10)
Volume / Å^3	2099.2(6)
Z	4
D_{calc} / Mg m^3	1.489
Absorption coefficient / mm^{-1}	0.377
$F(000)$	968
Crystal	Slab; colourless
Crystal size / mm^3	0.20 × 0.20 × 0.04
θ range for data collection / °	2.98 – 27.48
Reflections collected	40825
Independent reflections	9403 [R_{int} = 0.1243]
Completeness to θ = 27.48°	97.7 %
Max. and min. transmission	0.9851 and 0.9284
Data / restraints / parameters	9403 / 9 / 554
Goodness-of-fit on F^2	1.035
Final R indices [$F^2 > 2\sigma(F^2)$]	$R1$ = 0.0830, $wR2$ = 0.1670
R indices (all data)	$R1$ = 0.1834, $wR2$ = 0.2039
Largest diff. peak and hole	0.464 and −0.456 e Å^{-3}

Appendix 2 Crystal data and structure refinement for FPPTA

Compound	FPPTA (8)
Empirical formula	$C_{23}H_{23}BrF_3O_2PS$
Formula weight	531.35
Crystal system	Monoclinic
Space group	$P21/c$
a / Å	14.8827(3)
b / Å	31.9320(5)
c / Å	10.6385(2)
β / °	108.9170(10)
Volume / Å^3	4782.71(15)
Z	8
D_{calc} / Mg m^3	1.476
Absorption coefficient / mm^{-1}	1.914
$F(000)$	2160
Crystal	Block; Colourless
Crystal size / mm^3	$0.20 \times 0.17 \times 0.17$
θ range for data collection / °	$2.91 - 25.00°$
Reflections collected	73742
Independent reflections	$[R_{int} = 0.1243]$
Completeness to θ = 25.00°	99.8 %
Max. and min. transmission	0.7368 and 0.7008
Data / restraints / parameters	8401 / 8 / 573
Goodness-of-fit on F^2	1.029
Final R indices [$F^2 > 2\sigma(F^2)$]	$R1 = 0.0760$, $wR2 = 0.1978$
R indices (all data)	$R1 = 0.0933$, $wR2 = 0.2113$
Largest diff. peak and hole	1.824 and -2.589 e Å^{-3}